



The
University
Of
Sheffield.

Synthesis and Properties of Stimuli-Responsive Ionic Nanogels Prepared via RAFT Dispersion Polymerisation

Marissa Daniela Morales Moctezuma

A thesis submitted in partial fulfilment of the requirements for the degree of

Doctor of Philosophy

The University of Sheffield

Faculty of Science

Department of Chemistry

September 2020

AUTHOR'S DECLARATION

The work described in this thesis was carried out at the University of Sheffield under the supervision of Dr. Sebastian G. Spain between September 2017 and September 2020 and has not been submitted, either wholly or in part, for this or any other degree. All work is the original work of the author, except where acknowledged.

Signature: _____

Marissa Daniela Morales Moctezuma

September 2020

ABSTRACT

Stimuli-responsive nanogels are of increasing interest in a variety of biomedical applications and therefore various synthetic approaches have been established to prepare these nanomaterials. However, some of these techniques can include the use of surfactants or highly toxic organic solvents whose presence could be detrimental for intended biomaterials. Previous work has established the use of reversible addition-fragmentation chain-transfer (RAFT) dispersion aqueous polymerisation as a versatile approach to preparing nanogels with controlled composition, architecture, and functionality under environmentally-friendly conditions. Although the nanogel formation *via* this approach is well-understood, only a few studies have developed temperature-responsive nanogels and no thorough studies are available on the synthesis of nanogels from only weak polyelectrolytes, which are relevant pH-sensitive nanomaterials. This thesis comprises fundamental studies on the synthesis and properties of two classes of stimuli-responsive ionic nanogels prepared by RAFT dispersion polymerisation. Studies were developed to prepare ionic nanogels from an anionic polyelectrolyte poly(acrylic acid) (PAA) or a cationic polyelectrolyte poly(2-(dimethylamino)ethyl methacrylate) (PDMAEMA)-based macromolecular chain-transfer agents (macro-CTAs). The chain extension of the macro-CTAs with *N*-isopropylacrylamide (NIPAM) and *N,N'*-methylenebisacrylamide (BIS) produced thermo-responsive ionic nanogels in a one-pot synthesis. In both cases, the effects of the systematic variation of the core-forming PNIPAM/BIS block and the shell-stabiliser polyelectrolyte block on the physicochemical properties of the nanogels were determined mainly by DLS and TEM analyses. Irrespective of their composition, the two classes of nanogels were capable to respond to varying degrees of temperature, pH, and salt addition. Additionally, the effects of synthesis cosolvent composition (water-ethanol) on the properties of the anionic nanogels was particularly investigated for nanogels with the same PNIPAM/BIS composition. Studies suggest that the addition of ethanol for the copolymerisation not only affects the nanogel particle formation but also their size, tacticity and thus the volume phase transition temperature (VPTT) of nanogels with similar composition. In the case of the cationic nanogels, the use of acetate buffer for the synthesis of a PDMAEMA macro-CTA caused the simultaneous polymerisation and hydrolysis of the monomer, thus forming a polyampholyte composed mainly of PDMAEMA and minorly of poly(methacrylic acid) (PMAA). Regardless of the polyampholyte nature of the macro-CTA, results showed that the use of an acetate buffer allowed the preparation of pH- and temperature-sensitive nanogels with controlled size.

Keywords: Nanogels, stimuli-responsive, RAFT dispersion polymerisation, PISA.

Dedicated to my beloved family

ACKNOWLEDGEMENTS

The completion of the present work would not have been possible without the immense support of the following people. First, I would like to express my sincerest gratitude to my supervisor Dr Seb Spain, who kindly took me back after the bumpy start of my PhD journey. His invaluable knowledge, ideas and support made this project possible. Additionally, I am particularly grateful for his weekly support for thesis work and mental wellbeing amidst a pandemic.

I would like to thank the “Consejo Nacional de Ciencia y Tecnología” (CONACYT) for the financial support provided that allowed me to pursue and finish my postgraduate studies from the MSc to the PhD.

I am extremely grateful to everyone in the Chemistry Department at the University of Sheffield who provided their friendly assistance and training when it was needed. Thank you also to Dr Svet Tzokov (MBB department) for patiently training me to use the TEM facilities. I would also like to thank Dr Joey Shepherd (School of Clinical Dentistry) for the help provided for the microbiological tests, even though what was planned could not be finished. I am also incredibly grateful to Dr Edyta Niezabitowska and Dr Tom McDonald at the University of Liverpool for their assistance in the characterisation of the anionic nanogels by AF4.

I would like to thank the past members of the Spain group: Kat, Dom, Jas, and Rheanna for the support provided at the beginning of my PhD, and the present members of the Spain group: Anna, Sam, Josh and Ellen for making the end of my PhD more enjoyable. A special thanks to Emma, who particularly guided me in the lab. Thanks also to Tom for his assistance in the rheology measurements. I am also incredibly grateful to Laila, who patiently helped me with my chemistry questions. Thank you also to the members of the Armes group that provided their assistance when needed.

“Agradezco infinitamente a mi familia por siempre estar y brindarme su apoyo para cumplir mis metas, no hubiera podido terminar esta etapa sin ustedes: papá, mamá, Karla, Migue, Pau, Mariana y nana. Soy la más afortunada por tenerlos en mi vida. A todos mis amigos en México, agradezco nuestra amistad a la distancia, estoy segura de que prevalecerá por muchos años más. A los amigos que conocí en Sheffield, muchísimas gracias por hacerme sentir en casa.”

Last but not least, I am so grateful to Adam, who has been my rock during the PhD. Words will never express how lucky I am to have you in my life.

PUBLICATIONS

Publications derived from the work in this thesis

“The effects of cononsolvents on the synthesis of responsive particles *via* polymerisation-induced self-assembly” Marissa D. Morales Moctezuma, Sebastian G. Spain. Unpublished work.

“Insights into the internal structures of nanogels using a versatile asymmetric-flow field-flow fractionation method” Edyta Niezabitowska, Adam R. Town, Bassem Sabagh, Marissa D. Morales Moctezuma, Victoria R. Kearns, Sebastian G. Spain, Steve P. Rannard and Tom O. McDonald. *Nanoscale Adv.*, **2**, 4713-4721 (2020).

PRESENTATIONS

Oral presentations at conferences

“Stimuli-responsive nanogels with controlled size and architecture” Rapid fire oral presentation. RSC Biomaterials Chemistry Conference at the University of Liverpool, UK. (January 2019)

“Multi-responsive nanogels for biomedical applications” Oral presentation. RSC Biomaterials Chemistry Conference at the University of Manchester, UK. (January 2020)

Poster presentations at conferences

“Stimuli-responsive nanogels with controlled size and architecture” Poster presentation. RSC Biomaterials Chemistry Conference at the University of Liverpool, UK. (January 2019)

“Effects of cononsolvency on the synthesis of pH and temperature responsive nanogels *via* RAFT aqueous dispersion polymerisation” Poster presentation. Macro group Young Researchers Meeting (YRM) at the University of Kent, UK. (July 2019)

“Effects of cononsolvency on the synthesis of pH and temperature responsive nanogels *via* RAFT aqueous dispersion polymerisation” Poster presentation. Women in Chemistry: Conference and Careers Event at the University of Nottingham, UK (March 2020)

Conferences attended

Sheffield Colloid Researchers' Meeting. (April 2018)

Macro Group UK Young Researchers Meeting (YRM) RCSI Dublin. (July 2018)

Macro Group UK Young Researchers Meeting (YRM) Virtual conference. (June 2020)

CONTENTS

Abstract	iii
Acknowledgements	v
Abbreviations	ix
List of figures.....	xiv
List of tables	xix
List of schemes	xx
List of equations.....	xxi
Chapter 1. General introduction	1
1.1. The relevance of nanogels in biomedical applications	2
1.2. Stimuli-responsive polymers for designing smart nanogels.....	3
1.2.1. Physical Stimuli.....	4
1.2.2. Chemical stimuli.....	6
1.2.3. Biological stimuli	ix
1.3. Preparation methods of nanogels.....	10
1.3.1. Nanogel preparation from radical polymerisation	13
1.4. Fundamentals of RAFT polymerisation	16
1.4.1. The mechanism of RAFT polymerisation	16
1.4.2. Guidelines for the design of CTAs	18
1.5. The use of RAFT polymerisation to prepare nanogels	21
1.5.1. Preparation of nanogels by RAFT-mediated dispersion polymerisation.....	22
1.6. Concluding remarks	29
1.7. Thesis aims.....	30
1.8. References.....	31
Chapter 2. Anionic nanogels: The effects of cononsolvents on their synthesis and properties	43
2.1. Chapter outlook	44
2.2. Introduction.....	45
2.3. Results and discussion	49
2.3.1. Synthesis and characterisation of PAA macro-CTAs	49
2.3.2. Synthesis of PAA- <i>b</i> -P(NIPAM- <i>st</i> -BIS) nanogels by RAFT aqueous dispersion.....	53
2.3.3. Synthesis of PAA- <i>b</i> -P(NIPAM- <i>st</i> -BIS) nanogels by RAFT dispersion in cononsolvents ...	62
2.3.4. Insights into the internal structure of the anionic nanogels	71
2.3.5. Synthesis and characterisation of PAA _{<i>x</i>} - <i>b</i> -PNIPAM _{<i>y</i>} diblock copolymers.....	75
2.4. Conclusions	89

2.5. Experimental	91
2.6. Characterisation.....	95
2.7. References.....	99
Appendix A.....	106
Chapter 3. Anionic nanogels: Effects of synthesis variables on their stimuli-responsive behaviour	119
3.1. Chapter outlook	120
3.2. Introduction.....	121
3.3. Results and discussion	124
3.3.1. The temperature dependent deswelling behavior of the anionic nanogels	124
3.3.2. The pH-responsive behavior of the anionic nanogels	137
3.3.3. The response of nanogels to metal-ions	142
3.4. Conclusions	148
3.5. Materials and methods	150
3.6. References.....	151
Appendix B.....	155
Chapter 4. Cationic nanogels: Synthesis and properties.....	157
4.1. Chapter outlook	158
4.2. Introduction.....	159
4.3. Results and discussion	161
4.3.1. Synthesis and characterisation of PDMAEMA-based macro-CTAs.....	161
4.3.2. Synthesis and properties of P(DMAEMA- <i>co</i> -MAA)- <i>b</i> -PNIPAM copolymers.....	168
4.3.3. Synthesis of P(DMAEMA- <i>co</i> -MAA)- <i>b</i> - P(NIPAM- <i>st</i> -BIS) nanogels	175
4.3.4. The temperature behaviour of cationic nanogels	181
4.3.5. The pH responsive behavior of the cationic nanogels	184
4.3.6. Effect of solution ionic strength on the properties of cationic nanogels.....	186
4.4. Conclusions	188
4.5. Experimental	190
4.6. Characterisation.....	193
4.7. References.....	195
Appendix C.....	199
Chapter 5. Concluding remarks and future work	205
5.1. Concluding remarks.....	206
5.2. Future work.....	208
5.3. References.....	210

ABBREVIATIONS

AA	Acrylic acid
ACVA	4,4'-Azobis(4-cyanopentanoic acid)
AF4	Asymmetric-flow field-flow fractionation
AIBN	2,2'-Azobis(2-methylpropionitrile)
ATR	Attenuated total reflectance
ATRP	Atom transfer radical polymerisation
BIS	<i>N,N'</i> -methylenebisacrylamide
CDCl ₃	Deuterated chloroform
CECPA	4-((((2-carboxyethyl)thio)carbonothioyl)thio)-4-cyanopentanoic acid
CMC	Critical micelle concentration
CRP	Controlled radical polymerisation
CTA	Chain-transfer agent
D ₂ O	Deuterium oxide
DAAM	Diacetone acrylamide
DDS	Drug delivery system
DEAM	<i>N,N</i> -diethylacrylamide
DEGMA	Di(ethylene glycol) methyl ether methacrylate
DI water	Deionised water
DLS	Dynamic light scattering
DMAEMA	2-(dimethylamino)ethyl methacrylate
DMAPS	3-dimethyl(methacryloyloxyethyl) ammonium propanesulfonate
DMEA	Dimethylethanolamine
DMSO-d ₆	Deuterated dimethylsulfoxide
DP	Degree of polymerisation
DPBS	Dulbecco's phosphate-buffered saline
DTT	Dithiolthreitol
FT-IR	Fourier-transform infrared spectroscopy
GPC	Gel permeation chromatography
GSH	Glutathione
HEMP	2-(hydroxyethylthiocarbonothioylthio)-2-methylpropanoic acid
HPMA	2-hydroxypropyl methacrylate
IUPAC	International Union of Pure and Applied Chemistry
LAMs	"Less activated" monomers

LCST	Lower critical solution temperature
MAA	Methacrylic acid
Macro-CTA	Macromolecular chain-transfer agent
MALS	Multi-angle light scattering
MAMs	"More activated" monomers
MEA	2-methoxyethyl acrylate
MMA	Methyl methacrylate
MSD	Multi-size distribution
NIPAM	<i>N</i> -isopropylacrylamide
NIR	Near infrared light
NMEP	<i>N</i> -(2-methacryloyloxy)ethylpyrrolidone
NMP	Nitroxide mediated polymerisation
NMR	Nuclear magnetic resonance
O/W	Oil-in-water
OEGAs	Oligo(ethylene glycol) acrylates
OEGMAs	Oligo(ethylene glycol) methacrylates
P4VP	Poly(4-vinylpyridine)
PAA	Poly(acrylic acid)
PAMPSA	Poly(2-acrylamido-2-methylpropane sulfonic acid)
PASP	Poly(aspartic acid)
PDEAEMA	Poly((2-diethylamino)ethyl methacrylate)
PDEAM	Poly(<i>N,N</i> -diethylacrylamide)
PDI	Polydispersity index as determined by DLS
PDMA	Poly(<i>N,N</i> -dimethylacrylamide)
PDMAEMA	Poly(2-dimethylamino)ethyl methacrylate)
PDMAPS	Poly(<i>N,N'</i> -dimethyl(methacryloylethyl) ammonium propanesulfonate)
PDS	Pyridyl disulfide
PEG	Poly(ethylene glycol)
PEGMA	Poly(ethylene glycol)methyl ether methacrylate
PEO	Poly(ethylene oxide)
PISA	Polymerisation-induced self-assembly
PLGA	Poly(L-glutamic acid)
PLH	Poly(L-histidine)
PMMA	Poly(methyl methacrylate)
PNIPAM	Poly(<i>N</i> -isopropyl acrylamide)
POEGMAs	Poly(oligo(ethylene glycol) methacrylate)s

PRINT	Particle replication in nonwetting templates
PVCL	Poly(<i>N</i> -vinylcaprolactam)
PVPA	Poly(vinylphosphonic acid)
PVPBA	Poly(vinylphenyl boronic acid)
RAFT	Reversible addition-fragmentation chain-transfer
RDRP	Reversible deactivation radical polymerisation
SANS	Small-angle neutron scattering
SAXS	Small-angle X-ray scattering
TEM	Transmission electron microscopy
TEMPO	2,2,6,6-Tetramethylpiperidine-1-oxyl
TMS	Trimethylsilyldiazomethane
UCST	Upper critical solution temperature
UV-vis	Ultraviolet-visible
VPTT	Volume phase transition temperature
W/O	Water-in-oil
Y(OTf) ₃	Yttrium trifluoromethanesulfonate

SYMBOLS

α	Deswelling ratio
a_0	Area of the hydrophilic block
C_{tr}	Chain transfer constant
δ	Chemical shift
D	Hydrodynamic diameter at a given temperature
D_b	Hydrodynamic diameter of a shrunk nanogel (bottom temperature)
D_h	Average hydrodynamic particle diameter
D_t	Hydrodynamic diameter of a swollen nanogel (top temperature)
D_{TEM}	Average particle diameter as determined by TEM studies
ΔG	Change in Gibbs free energy
ΔH	Change in enthalpy
ΔS	Change in entropy
ϵ_r	Dielectric constant
G'	Storage modulus
G''	Loss modulus
I	Intensity of scattered light
K_{app}	Apparent kinetic rate constant of polymerisation
$k_{add}, k_{-\beta}, k_{addP}$	Addition rate coefficients
$k_{-add}, k_{\beta}, k_{-addP}$	Fragmentation rate coefficients
λ	Wavelength
l_c	Length of the hydrophobic block
μ	Solution ionic strength
m	Meso diads
M	Molar mass of a micelle
M_{CTA}	Molar mass of chain transfer agent
$M_{i=1,2, \text{ or } 3}$	Molar mass of a monomer
\bar{M}_n	Number-average molar mass
M_o	Molar mass of the polymer backbone
\bar{M}_w	Weight-average molar mass
\bar{M}_w / \bar{M}_n	Dispersity as estimated by GPC studies
N_A	Avogadro's number
N_{agg}	Average number of polymer chains per particle

\emptyset	Polymer volume fraction
p	Packing parameter
ρ	Shape factor
r	Racemic diad
R_h	Average hydrodynamic radius
R_g	Radius of gyration
σ	Slope of the phase transition
S_{agg}	Average number of copolymer chains per unit surface area
T_{cp}	Cloud point temperature
T_{gel}	Macroscopic gelation temperature
v	Volume of the hydrophobic block
$\bar{\nu}$	Wavenumber
ω	Halfway point between the swollen and shrunk state average size
χ	Fractional monomer conversion
X_e	Ethanol mole fraction
ζ	Zeta-potential

LIST OF FIGURES

1.1: Main classification of external stimuli: physical, chemical, or biological.	3
1.2: Examples of the structure of physical stimuli responsive polymers/functional groups.	4
1.3: Schematic representation of phase diagrams showing the behaviour of polymers in solution according to temperature and polymer volume fraction (ϕ).	5
1.4: Examples of structures of chemical stimuli responsive polymers/functional groups.	7
1.5: Structures of (a) poly(acrylic acid) and (b) poly((2-dimethylamino)ethyl methacrylate).....	ix
1.6: Schematic illustration showing the main strategies for nanogel preparation.	10
1.7: Chemical structures of the main classes of RAFT CTAs according to their Z-group.....	16
1.8: The proposed mechanism of RAFT polymerisation by Moad <i>et al.</i> ¹⁴⁸	17
1.9: The reversible addition-fragmentation chain-transfer process	18
1.10: Guidelines for the selection of suitable Z and R groups of CTAs for the RAFT polymerisation of various monomers.	20
1.11: The schematic representation of RAFT dispersion polymerisation showing some of the possible morphologies of the nano-objects obtained by <i>in situ</i> self-assembly of diblock copolymers.....	22
1.12: Water-miscible monomers used in aqueous dispersion PISA.	23
1.13: Macro-CTAs and schematic representation of the RAFT precipitation polymerisation process of NIPAM.	24
1.14: Macro-CTAs and the formation of ethylene glycol-based core-shell nanogels <i>via</i> RAFT dispersion polymerisation.	25
1.15: Schematic of the volume phase transition mechanism of P(MEA- <i>co</i> -PEGA)/PDMA and PNIPAM/PDMA core-shell nanogels upon heating.	26
1.16: Schematic illustration for the synthesis of carbohydrate-based nanogels and their degradation in the acidic environment.	27
1.17: (A) RAFT dispersion polymerisation of NIPAM for the synthesis of block copolymers and (B) crosslinked nanogels	28
1.18: Synthesis of UCST-type thermosensitive nanogels by RAFT PISA	28
2.1: The schematic representation of the effects of the synthesis cononsolvent composition on the size of a range of anionic nanogels prepared <i>via</i> RAFT dispersion polymerisation.	44
2.2: A schematic of the RAFT aqueous dispersion polymerisation for nanogel formation.....	45
2.3: Kinetic study of the RAFT ethanolic polymerisation of AA using HEMP as CTA.	50
2.4: Molar mass determination during the RAFT polymerisation of AA.	50
2.5: THF GPC chromatograms of the series of PAA macro-CTAs after methylation with TMS-diazomethane.	52

2.6: Schematic representation of RAFT-mediated PISA showing the progression of polymer nano-object morphologies.....	53
2.7: Size determination of the $A_{52}N_yB_3$ nanogels synthesised in water.....	56
2.8: TEM micrographs of the $A_{52}N_yB_3$ nanogels synthesised in water.	58
2.9: Size determination of the $A_{84}N_yB_3$ nanogels synthesised in water.	60
2.10: Digital photographs of the $A_{52}N_yB_3-X_e$ crude nanogel dispersions	63
2.11: Size determination of the $A_{52}N_{100}B_3-X_e$	65
2.12: Size determination of the $A_{52}N_{200}B_3-X_e$	67
2.13: Cartoons showing (a) the effect of the ethanol mole fraction composition on the size of the nanogels and (b) the hypothesised fusion of nanogel particles.	68
2.14: Size determination of the $A_{52}N_{300}B_3-X_e$ nanogels.....	69
2.15: TEM micrographs of nanogels synthesised in mixtures of water and ethanol showing the effect of the crosslinker density and the DP of the stabiliser block on the morphology of nanogels.	70
2.16: AF4-MALS-DLS analysis of $A_{52}N_yB_z-X_e$ nanogels.....	72
2.17: Cartoons showing (a) a nanogel with denser inner core compared to the outer shell (b) a nanogel with apparently more homogeneous internal crosslinking density.	73
2.18: Stacked 1H NMR spectra recorded in D_2O of purified $A_{37}N_{199}-X_e$ diblock copolymers.	77
2.19: Stacked 1H NMR spectra recorded in D_2O of purified PNIPAM- X_e homopolymers synthesised by free radical polymerisation.	79
2.20: Digital photograph of the crude $A_{37}N_{199}-0$ copolymer at 70 and 20 °C.....	80
2.21: Turbidimetry experiments of $A_{37}N_y-0$ diblock copolymers in aqueous solution at pH 7.....	82
2.22: Turbidimetry experiments of $A_{37}N_{199}-X_e$ diblock copolymers in aqueous solution at pH 7.....	83
2.23: Turbidimetry experiments of $A_{37}N_{199}-X_e$ diblock copolymers at pH 7 in the ethanol mole fraction these were synthesised.....	84
2.24: (a) Turbidimetry experiments and (b) DMF GPC chromatograms of PHEA $_{42}$ - <i>b</i> -PNIPAM $_{200}$ diblock copolymers.	85
2.25: Size determination studies for the self-assembly of the $A_{37}N_{199}-0.06$ with temperature.	86
2.26: Size determination of the aggregate structures of $A_{37}N_{199}-X_e$ copolymers.	88
2.27: The cross-flow profile over time chosen for the separation of the nanogel particles.....	98
2A.1: 1H NMR spectrum of recrystallised HEMP CTA.	106
2A.2: ^{13}C NMR spectrum of recrystallized HEMP CTA.	106
2A.3: 1H NMR spectrum of PAA $_{37}$ macro-CTA before purification	107
2A.4: 1H NMR spectrum of PAA $_{52}$ macro-CTA before purification	107
2A.5: 1H NMR spectrum of PAA $_{84}$ macro-CTA before purification	108
2A.6: 1H NMR spectrum of PAA $_{37}$ macro-CTA after purification.....	108

2A.7: ^1H NMR spectrum of PAA ₅₂ macro-CTA after purification.....	109
2A.8: ^1H NMR spectrum of PAA ₈₄ macro-CTA after purification.....	109
2A.9: The effect of adding the crosslinker at different times (t) during the polymerisation on the properties of A ₅₂ N ₂₀₀ B ₃ -0.04 nanogels.....	110
2A.10: Digital photograph of the crude mixture when the polymerisation was attempted without any pH adjustment.	111
2A.11: Size distributions obtained from DLS of the A ₅₂ N _y B ₃ nanogels synthesised in water.	112
2A.12: Acid titration curves of (a) PAA ₅₂ and (b) PAA ₈₄ at 10 mg mL ⁻¹ aqueous solution.	112
2A.13: Kinetic study of the RAFT dispersion polymerisation of NIPAM by chain extension of PAA ₃₇ as macro-CTA.	113
2A.14: Stacked ^1H NMR spectra recorded in D ₂ O of purified A ₃₇ N ₃₀₂ -X _e diblock copolymers.	113
2A.15: Stacked ^1H NMR spectra recorded in D ₂ O of purified A ₈₄ N ₂₀₂ -X _e diblock copolymers.	114
2A.16: Stacked ^1H NMR spectra recorded in D ₂ O of purified A ₈₄ N ₃₀₃ -X _e diblock copolymers.....	114
2A.17: Characterisation of PNIPAM-X _e synthesised by free radical polymerisation.....	115
2A.18: Turbidimetry experiments of PNIPAM-HEMP homopolymers in aqueous solution.	115
2A.19: Turbidimetry experiments of A ₃₇ N _y -X _e diblock copolymers in aqueous solution at pH 7....	115
2A.20: Turbidimetry experiments of A ₈₄ N _y -X _e diblock copolymers in aqueous solution at pH 7... 116	116
2A.21: Stacked ^1H NMR spectra recorded in D ₂ O of PHEA ₄₂ -b-PNIPAM _y synthesised in either water or water-ethanol mixtures.....	117
2A.22: Size determination studies of the self-assembly of A ₃₇ N _y -X _e copolymers.....	117
2A.23: Size determination studies of the self-assembly of A ₈₄ N _y -X _e copolymers.....	118
3.1: A schematic of the stimuli-responsive behaviour of A _x N _y B _z anionic nanogels.	120
3.2: (a) Cartoon showing the temperature-dependent deswelling behaviour of PNIPAM and (b) the chemical structure of PNIPAM showing the hydrogen bonding with water.....	121
3.3: Cartoon showing the effect of temperature on the hydrodynamic size of the A _x N _y B _z nanogels below and above the volume phase temperature transition (VPTT).	124
3.4: DLS analysis on the hysteresis of the A ₅₂ N ₁₈₁ B ₃ -0 nanogel.....	125
3.5: DLS analysis of the A ₅₂ N _y B ₃ -0 nanogels.....	126
3.6: Deswelling behaviour of the A ₅₂ N _y B ₃ -0 nanogels.....	127
3.7: DLS analysis of the (♦) A ₅₂ N ₁₈₁ B ₃ -0 and (●) A ₈₄ N ₁₆₅ B ₃ -0 nanogels.....	128
3.8: Deswelling behaviour of the (♦) A ₅₂ N ₁₈₁ B ₃ -0 and (●) A ₈₄ N ₁₆₅ B ₃ -0 nanogels.....	129
3.9: DLS analysis of the A ₅₂ N ₂₀₀ B ₃ -X _e nanogels synthesised in cononsolvents.	130
3.10: Deswelling behaviour of the A ₅₂ N ₂₀₀ B ₃ -X _e nanogels.	131
3.11: DLS analysis of the A ₅₂ N ₁₈₄ B ₃ -0.12 nanogel at different temperatures.	133

3.12: DLS analysis of the $A_{52}N_{200}B_z-0.05$ nanogels.....	134
3.13: Deswelling behaviour of the $A_{52}N_{200}B_z-0.05$ nanogels.....	135
3.14: DLS analysis of the (\blacklozenge) $A_{52}N_{197}B_3-0.05$ and (\bullet) $A_{84}N_{181}B_3-0.05$ nanogels.....	136
3.15: Cartoon showing the effect of pH value on the hydrodynamic size of the $A_xN_yB_z$ nanogels at neutral and acidic pH.....	137
3.16: Effect of the pH on the deswelling behaviour of the (a) $A_{52}N_{181}B_3-0$ and (b) $A_{52}N_{197}B_3-0.05$ nanogels.....	138
3.17: Effect of the pH on the deswelling behaviour of the (a) $A_{84}N_{165}B_3-0$ and (b) $A_{84}N_{181}B_3-0.05$ nanogels.....	139
3.18: Effect of the pH on the ζ -potential of (a) $A_{52}N_{181}B_3-0$ and (b) $A_{52}N_{197}B_3-0.05$ nanogels.....	140
3.19: Effect of the pH on the ζ -potential of (a) $A_{52}N_{182}B_5-0.05$ and (b) $A_{52}N_{292}B_5-0.05$ nanogels..	141
3.20: Effect of the pH on the ζ -potential of the $A_{84}N_{181}B_3-0.05$ nanogel.	141
3.21: DLS studies on the addition of NaCl and $CaCl_2$ to (a) $A_{52}N_{181}B_3-0$ and (b) $A_{52}N_{197}B_3-0.05$ nanogels.....	142
3.22: Images showing the macroscopic gelation of $A_{52}N_{181}B_3-0.11$ nanogel (1% w/w) injected into PBS (pH 7.4) with $CaCl_2$	144
3.23: Images showing the macroscopic gelation of $A_{52}N_{181}B_3-0.11$ nanogel (9.7% w/w, \sim pH 7) with varying $CaCl_2$ concentrations.	145
3.24: Cartoon showing the coordination of Ca^{2+} with carboxylate groups at high pH from the shell of the nanogels.	146
3.25: Temperature-dependence of G' and G'' for nanogel dispersions with and without $CaCl_2$ at different nanogel concentrations.	147
3.26: Temperature-dependence of G' and G'' for nanogel dispersions at 5% w/w with different $CaCl_2$ concentrations.	147
3B.1: DLS analysis of the $A_{52}N_{100}B_3-X_e$ nanogels synthesised in consolvents.....	155
3B.2: DLS analysis of the $A_{52}N_{300}B_3-X_e$ nanogels synthesised in consolvents.....	155
3B.3: Size determination of the $A_{52}N_{200}B_z-0.05$ nanogels	156
4.2: The conversion of DMAEMA with time for a targeted DP of 62	163
4.3: Kinetic studies of the RAFT polymerisation of DMAEMA and MAA as determined by 1H NMR spectroscopy.....	164
4.4: Aqueous GPC chromatograms of the series of DM_x macro-CTAs.	166
4.5: Acid titration curve of the DM_{57} macro-CTA.	166
4.6: Turbidimetry experiments at different pH of the (a) DM_{57} and (b) DM_{87} macro-CTAs in aqueous solution.	167
4.7: The synthesis and characterisation of $DM_{57}N_y$ copolymers.....	168
4.8: Turbidimetry experiments of purified DM_xN_y diblock copolymers in acetate buffer	170

4.9: Turbidimetry experiments of purified DM_xN_y diblock copolymers in salt-free aqueous solutions at pH 7.	171
4.10: MSD size determination studies of the self-assembled $DM_{54}N_y$ diblock copolymers in (a) acetate buffer (1 M, pH 5.2) at 50 °C and (b) DI water at pH 7 and 62.5 °C	173
4.11: MSD size determination studies of the self-assembled $DM_{87}N_y$ diblock copolymers in (a) acetate buffer (1 M, pH 5.2) at 50 °C and (b) DI water at pH 7 and 62.5 °C	174
4.12: Size determination of the $DM_{57}N_yB_3$ nanogels.	177
4.13: Enlargement of TEM micrographs of the $DM_{57}N_yB_3$ nanogels.	178
4.14: Size determination of the $DM_{87}N_{123}B_3$ and $DM_{57}N_{110}B_3$ nanogels.	179
4.15: Size determination of the $DM_{87}N_{214}B_3$ and $DM_{57}N_{187}B_3$ nanogels.	180
4.16: DLS studies on the deswelling behaviour of $DM_{57}N_yB_3$ nanogels.	181
4.17: Effect of the copolymer concentration on the cloud point of DM_{57} copolymer at pH 8.9.	182
4.18: DLS studies on the deswelling behaviour of $DM_{87}N_yB_3$ nanogels.	183
4.19: DLS studies on the deswelling behaviour of $DM_{54}N_{252}B_3$ nanogel with pH.	184
4.20: Effect of the pH on the ζ -potential of the (a) $DM_{57}N_{110}B_3$ and (b) $DM_{57}N_{265}B_3$ nanogels.	185
4.21: DLS studies on the effect of dispersions ionic strength of $DM_{57}B_{265}B_3$ nanogel	187
4.22: DLS studies on the addition of NaCl and CaCl ₂ to $DM_{57}N_{265}B_3$ nanogel.	187
4C.1: ¹ H NMR spectrum of commercially available CECPA CTA.	199
4C.2: ¹³ C NMR spectrum of commercially available CECPA CTA.	199
4C.3: The conversion of DMAEMA with time for target DP of 126.	200
4C.4: Kinetic studies of the RAFT polymerisation of DMAEMA and MAA as determined by ¹ H NMR spectroscopy.	201
4C.5: ¹ H NMR study for the determination of the DMAEMA conversion and its degradation into dimethylethanolamine for the target composition of [DMAEMA]:[CECPA]:[ACVA] of 60:1:0.1 at 25% w/w.	201
4C.6: ¹ H NMR study for the determination of the DMAEMA conversion and its degradation into dimethylethanolamine for the target composition of [DMAEMA]:[CECPA]:[ACVA] of 124:1:0.1 at 25% w/w.	202
4C.7: ¹ H NMR spectrum of purified DM_{57} for the determination of the macro-CTA DP.	202
4C.8: ¹ H NMR spectrum of purified DM_{87} for the determination of the macro-CTA DP.	203
4C.9: Size distributions obtained from DLS of the $DM_{57}N_yB_3$ nanogels.	203
4C.10: Effect of the pH on the ζ -potential of the $DM_{57}N_{187}B_3$ nanogel.	204
5.1: Citotoxicity of $DM_{57}N_{187}B_3$ nanogel tested against (a) <i>P. aeruginosa</i> and (b) <i>S. Aureus</i> bacteria.	209

LIST OF TABLES

1.1: Covalent crosslinking reactions for nanogel formation from polymer precursors.	12
1.2: Heterogeneous techniques to obtain micro- and nanoparticles. ^{131–133}	14
2.1: Summary of the synthesis and properties of the PAA _x macro-CTAs.....	51
2.2: Summary of the synthesis and properties of A _x N _y B _z nanogels.....	55
2.3: Summary of the synthesis and properties of A _x N _y B _z -X _e nanogels synthesised by RAFT dispersion polymerisation in water/ethanol mixtures.	63
2.4: Summary of the mode values obtained from AF4-MALS-DLS.....	74
2.5: Summary of the synthesis and properties of A _x N _y -X _e diblock copolymers.	76
2.6: Summary of the ζ -potential values of the A ₃₇ N ₁₉₉ -X _e copolymers at different temperatures.	87
2A.1: Summary of the optimisation parameters for the synthesis of A _x N _y B _z nanogels synthesised by RAFT dispersion polymerisation.	111
2A.2: Summary of the synthesis and properties of PHEA ₄₂ - <i>b</i> -PNIPAM _y copolymers synthesised by RAFT dispersion polymerisation in either water or water/ethanol mixtures.	116
4.1: Summary of the synthesis and properties of DM _x macro-CTAs.....	165
4.2: Summary of the results of the synthesis and properties of DM _x N _y copolymer.....	169
4.3: Summary of the synthesis and properties of the DM _x N _y B _z nanogels.	175

LIST OF SCHEMES

2.1: The synthesis of PAA _x <i>via</i> RAFT ethanolic polymerisation using HEMP as RAFT agent.	49
2.2: The synthesis of PAA _x - <i>b</i> -P(NIPAM- <i>st</i> -BIS) _{y,z} nanogels <i>via</i> RAFT aqueous dispersion polymerisation.....	54
2.3: Synthesis of PAA _x - <i>b</i> -PNIPAM _y diblock copolymers using RAFT dispersion polymerisation. .	75
4.1: The synthesis of P(DMAEMA- <i>co</i> -MAA) _x macro-CTA by RAFT aqueous solution polymerisation using CECPA as RAFT agent.	162
4.2: The synthesis of P(DMAEMA- <i>co</i> -MAA) _x - <i>b</i> -P(NIPAM- <i>st</i> -BIS) _{y,z} nanogels <i>via</i> RAFT aqueous dispersion polymerisation.	175

LIST OF EQUATIONS

1.1: The Gibbs free energy.....	5
1.2: The degree of polymerisation by RAFT polymerisation	18
1.3: Theoretical number-average molar mass.....	18
1.4: The packing parameter.....	22
2.1: Number of polymer chains aggregated per particle	65
2.2: Molar mass of a micelle	66
2.3: Average-number of copolymer chains per unit surface area.....	66
3.1: The Boltzmann sigmoidal equation for VPTT determination.....	125
3.2: The extent of nanogel deswelling.....	127
3.3: The normalisation of the hydrodynamic diameter with temperature	127

This page intentionally left blank

CHAPTER 1

General introduction

1.1. The relevance of nanogels in biomedical applications

Numerous approaches toward using nanomaterials in a wide range of biomedical applications have been developed over the past decades. Particular interest has been given to developing nanomaterials for minimally invasive medical procedures, where injectable matrices and therapeutic carriers are of utmost interest in medicine.^{1,2} Among the most promising nanomaterials that have been investigated, nanogels have emerged as novel platforms for numerous biomedical applications including gene³ and drug delivery,⁴ biosensors,^{5,6} imaging⁷ and tissue engineering.⁸ Nanogels, owing their name to their nanometric size, are polymeric networks that are chemically or physically crosslinked into a three-dimensional structure that prevents their dissolution in aqueous conditions.^{9,10} Similar to hydrogels, nanogels have a high water content and swellability due to their hydrophilic or amphiphilic character.¹¹ This feature is the most promising for drug delivery, since drugs can potentially be entrapped or encapsulated within their structure.¹² In terms of size, nanogels are recognised as gel nanoparticles with a diameter in the range of 1 to 100 nm,¹³ however some studies include nanogels for drug delivery with greater diameter (<200 nm). This is because spherical particles that are 100-200 nm in size, have a prolonged circulation time since these are big enough to prevent uptake by the liver yet small enough to be filtrated through the spleen.¹⁴ Regarding their shape, nanogels can have different structures such as a solid sphere,¹⁵ rod-like,¹⁶ core-shell,¹⁷⁻¹⁹ or core-shell-corona,²⁰ this is primarily related to the synthetic methodology followed, and will be discussed in detail in Section 1.3.

Several polymers can be used to form nanogels, their formation can be from natural or synthetic polymers or by a combination of both. Natural polymers include polysaccharides such as chitosan,^{21,22} dextran,²³⁻²⁵ hyaluronic acid,²⁶⁻²⁹ and heparin.³⁰⁻³² Advantages of using polymers from natural sources is that these are biodegradable and biocompatible. However, the use of synthetic polymers as building blocks offers better control over the structure, mechanical strength and tailored chemical or biological response to stimuli.³³ The production of materials that are able to change their properties as a response to specific stimuli is of particular interest. Hence, special attention has been given to the fabrication of stimuli-responsive or “smart” nanogels, since these are fast-responsive soft nanoparticles able to act, for instance, as site-specific drug/gene delivery vehicles.⁴ Additionally, stimuli-responsive nanogels can be designed for sensing and imaging applications by incorporating inorganic nanoparticles such as gold, silver, or iron oxide in their structure.³⁴ Hence, according to the specific targeted application, smart nanogels can be designed from the early synthetic stages to potentially exhibit a desired response to one or more stimuli of

different nature. In terms of designing stimuli-responsive nanogels, there are two main criteria that will be covered next: (1) the choice of polymers that can integrate a nanogel based on their sensitivity to specific stimuli, and (2) the size or structure that nanogels can have based on synthetic routes and chemical composition.

1.2. Stimuli-responsive polymers for designing smart nanogels

A variety of stimuli-responsive polymers can be used as building blocks for the preparation of nanogels, where the sensitivity to particular stimuli is given by the functional groups within the polymer chain or by inorganic nanoparticles (e.g. plasmonic, magnetic and carbonaceous materials).^{34,35} Stimuli can trigger a physical or chemical change in the properties of these smart materials, and the intensity of the stimulus usually determines the extent of response in the polymer structure.³⁵ Throughout the years, different types of stimuli have been investigated resulting in a further classification according to the nature of the stimuli: physical, chemical, or biological (Figure 1.1).^{36,37}

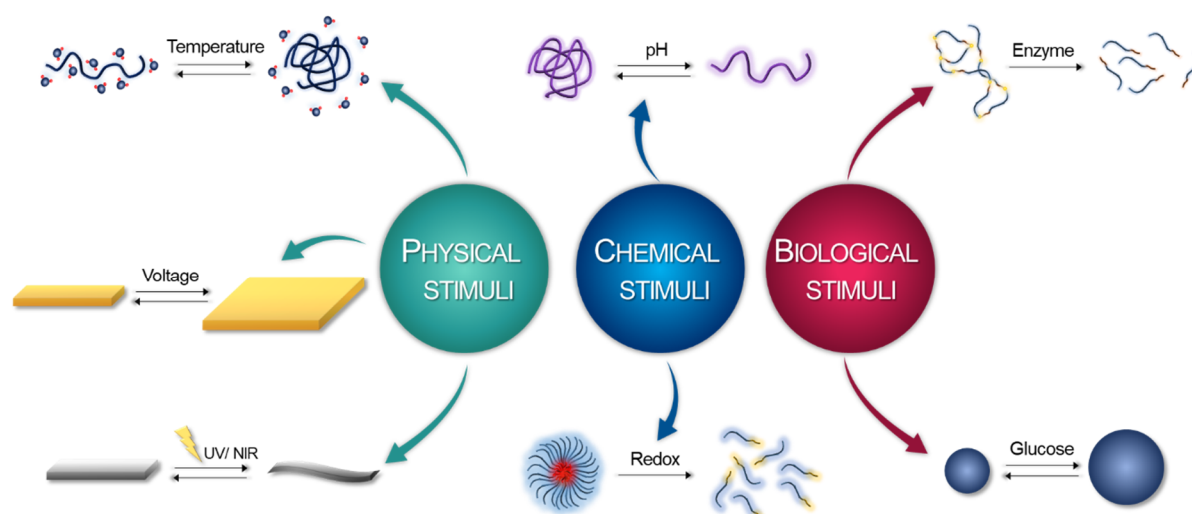


Figure 1.1: Main classification of external stimuli: physical, chemical, or biological.

Physical stimuli: Temperature (solubility changes according to chain dynamics of secondary interactions); Electro-responsive (Change of size by application of an electric current due to coulomb interactions or migration of ions); Light-responsive (Deformation of material caused by a beam of light, molecules respond towards wavelengths from the infrared to the ultraviolet range). **Chemical stimuli:** pH (Collapsed to extended state due to ionisation); Redox (Disassembling of particles due to changes in the oxidation states of molecules). **Biological stimuli:** Glucose (Glucose oxidase catalyse the conversion of glucose into gluconic acid which triggers conformational changes); Enzyme (rupture by biocatalytic action of an enzyme on the receptor attached groups).

1.2.1. Physical Stimuli

Physical stimuli-responsive polymers modify their chain dynamics when a stimulus is applied.³⁶ Stimuli such as temperature,³⁸ electric³⁹ or magnetic⁴⁰ fields, intensity of light,⁴¹ and ultrasound⁴² are among the most studied for biomedical applications since their response can easily be controlled externally. In temperature-responsive polymers, solubility phase changes of the polymer are observed at a lower or upper critical solution temperature (LCST or UCST), where the hydrophobic-hydrophilic interactions between polymer and solvent are altered by temperature variations.³⁷ Among the most studied thermoresponsive polymers are (Figure 1.2): the (i) *N*-alkyl-substituted polyacrylamides such as poly(*N*-isopropylacrylamide) (PNIPAM)^{43,44} and poly(*N,N*-diethylacrylamide) (PDEAM),⁴⁵ (ii) poly(*N*-vinyl lactams) such as poly(*N*-vinylcaprolactam) (PVCL),⁴⁶ (iii) poly(oligo(ethylene glycol) methacrylate)s (POEGMAs),⁴⁷ and (iv) zwitterionic polymers such as poly(*N,N'*-dimethyl(methacryloyl)ethyl ammonium propanesulfonate) (PDMAPS).⁴⁸

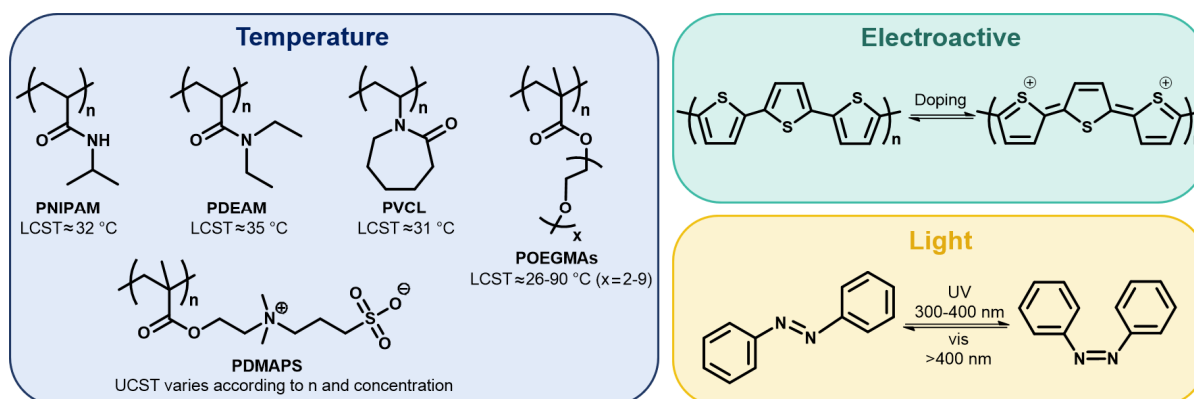


Figure 1.2: Examples of the structure of physical stimuli responsive polymers/functional groups. The most common temperature sensitive polymers. Electroactive-sensitive: polythiophene-based polymers. Light-sensitive: Azobenzene derivatives moiety.

In electro-responsive polymers, changes in shape (swelling, shrinking or bending) are caused by the presence of electric fields. In these materials, migration of electrons/ions under an electric field produce changes in the conductivity due to the presence of conjugated chains that contain alternating single and double bonds.³⁹ Among the most used electroactive polymers are the polythiophene derivatives (Figure 1.2).⁴⁹ In light-sensitive polymers, phase transitions are caused upon exposure to light, at wavelengths between the ultraviolet, visible or near-infrared regions.³⁷ One of the most of common light-sensitive moieties used in biomedical applications are the azobenzene derivatives (Figure 1.2), which undergo reversible cis-trans isomerisation under UV-vis light.⁵⁰

1.2.1.1. Temperature-responsive polymers

As previously stated, temperature-sensitive polymers are those that undergo an abrupt phase separation at a critical temperature. If the phase separation occurs at a high temperature, it is known as a lower critical solution temperature (LCST) whilst the opposite behaviour is referred as an upper critical solution temperature (UCST).⁵¹ Hence, LCST and UCST are the minimum and maximum points, respectively, of the coexistence curve of the phase diagram (Figure 1.3). Any other temperature upon which a phase transition occurs is known as cloud point temperature (T_{cp}), and it is given at any polymer concentration on the curve.⁵² As shown in Figure 1.3a, below the LCST the polymer assumes a coil conformation (i.e. it is soluble) but above the LCST the polymer changes to a globular conformation (two-phase region).⁵³ Contrary to this, a polymer with an UCST is soluble above its critical temperature, and the polymer becomes insoluble below the UCST (Figure 1.3b).

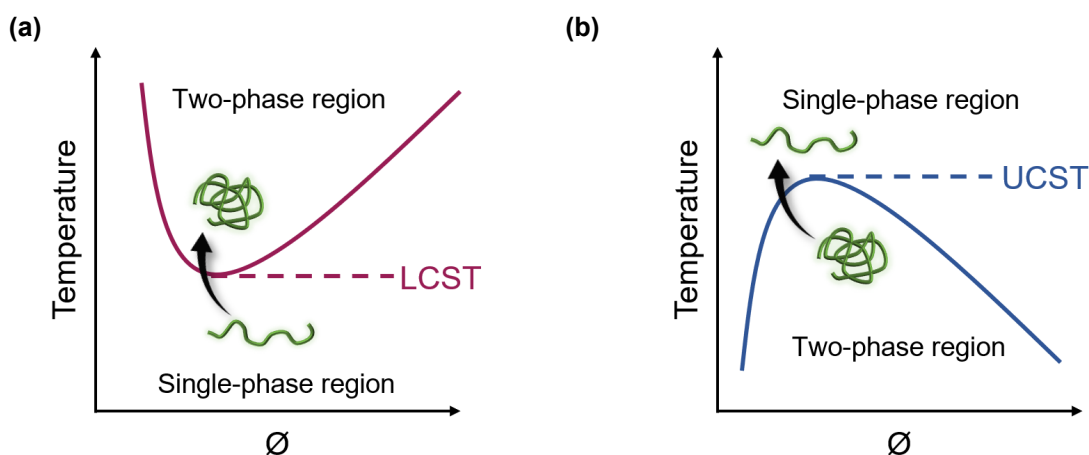


Figure 1.3: Schematic representation of phase diagrams showing the behaviour of polymers in solution according to temperature and polymer volume fraction (\emptyset). (a) Lower critical solution temperature (LCST) behaviour and (b) upper critical solution temperature (UCST) behaviour.

The abrupt change in solubility is related to an energetic balance derived from the hydrogen bonding between polymer chains and solvent molecules. In terms of thermodynamics, this is given by the change in free energy (ΔG) in the Gibbs equation (Equation 1.1), where ΔH is the change in enthalpy, ΔS is the change in entropy and T is the temperature.

$$\Delta G = \Delta H - T \Delta S \quad \text{Equation 1.1}$$

For polymers that display an LCST in water, the ΔH of mixing is negative below the LCST since the favourable hydrogen bonding between polymer chains and water molecules results in a

lower enthalpy and the release of heat (i.e. exothermic process). Besides, the ΔS contribution is also negative since water loses entropy as a result of the hydration of the polymer (i.e. unfavourable entropy of mixing due to the specificity of hydrogen bonding and strict bonding angles). By increasing the temperature above the LCST, the hydrogen bonding is weakened (i.e. lower enthalpy of mixing) and since free water molecules have higher entropy, the polymer chains get dehydrated to minimise their contact with water leading to a globular conformation (i.e. hydrophobic effect) which leads to a positive ΔG of mixing.⁵² Since the change in entropy outweighs the change in enthalpy the LCST phase transition is known as an entropy-driven process. Among the most studied polymers showing LCST to design nanogels are PNIPAM,^{54,55} PDEAM,⁵⁶ PVCL,⁵⁷ and poly(2-dimethylamino)ethyl methacrylate) (PDMAEMA).⁵⁸

In the case of polymers displaying an UCST in water, another enthalpic parameter is considered namely as ΔH of supramolecular association of polymer chains. These inter- and intra-polymer interactions can be either by hydrogen or electrostatic bonding. Above the UCST, these interactions are broken upon dissolution and the hydrogen bonding between water and polymer chains is favourable. Upon cooling, the polymer coil dehydrates leading to phase separation in an enthalpy-driven process.^{48,53} UCST-type polymers such as PDMAPS has been used previously to prepare zwitterionic nanogels.⁵⁹

1.2.2. Chemical stimuli

In the case of chemically responsive polymers, molecular interactions between specific molecules/ions and the polymer functional groups govern the changes in the polymer structure when a stimulus is applied.³⁷ Stimuli such as pH, redox potential, ionic strength, and type of solvent are the most representative chemical triggers. Redox-responsive polymers are those with functional groups sensitive to reduction or oxidation stimuli that triggers changes in their oxidation state. Among the most investigated moieties for redox-sensitive nanogels systems are the disulfide^{30,60-63} and diselenide⁶⁴⁻⁶⁶ bonds (Figure 1.4 redox a, and b). These types of bonds are promising for drug delivery applications since the nanogel structure can be dissociated upon contact with a reducing agent such as glutathione (GSH) an abundant molecule found in body cells. Other types of redox-responsive moieties that have been investigated for biomedical applications are ferrocene^{67,68} and tetramethylpiperidine-1-oxyl (TEMPO)⁶⁹ (Figure 1.4 redox c, and d).

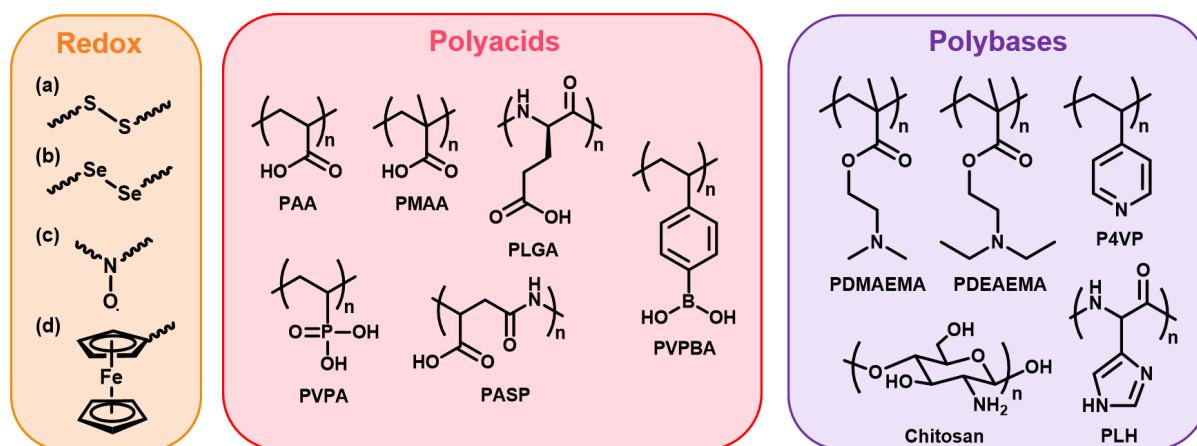


Figure 1.4: Examples of structures of chemical stimuli responsive polymers/functional groups. Redox-sensitive: (a) disulfide, (b) diselenide, (c) TEMPO, and (d) ferrocene moieties. pH-responsive polymers respectively divided into polyacids and polybases.

Polymers that are pH-sensitive have ionisable functional groups capable of donating or accepting protons. Upon ionisation, electrostatic repulsion leads to conformational changes in the polymer chain from compact to extended states.⁷⁰ According to the nature of the charge, pH-responsive polymers are divided into weak polyacids or polybases (Figure 1.4). Examples of polyacids that have been used to obtain nanogels are (i) carboxylic acid-containing polymers such as poly(acrylic acid) (PAA)^{71–73} and poly(methacrylic acid) (PMAA),^{74–76} (ii) amino acid-containing polymers like poly(aspartic acid) (PASP)^{77,78} and poly(L-glutamic acid) (PLGA),^{79,80} (iii) boronic acid polymers such as poly(vinylphenyl boronic acid) (PVPBA)^{81,82} and (iv) phosphoric acid-containing polymers like poly(vinylphosphonic acid) (PVPA).⁸³ Examples of polybases consist of (i) polymers with tertiary amine groups such as poly((2-dimethylamino)ethyl methacrylate) (PDMAEMA)^{58,84–86} and poly((2-diethylamino)ethyl methacrylate) (PDEAEMA),^{87–89} (ii) pyridine derivatives like poly(4-vinylpyridine) (P4VP),⁹⁰ (iii) natural polymers like chitosan^{21,22,91} and (iv) amino acids such as poly(L-histidine)(PLH).^{92,93}

1.2.2.1. pH-Responsive polymers

A fundamental parameter in designing nanomaterials for many biomedical applications, especially for drug/gene delivery, is pH since the physiological pH can vary greatly in the human body. The most representative example of this variation is the pH throughout the gastrointestinal tract, which fluctuates from pH 1 to 3.5 in the stomach, from 6 to 7.5 in the small intestine, and colonic pH can vary between pH 5 to 8.⁹⁴ Additionally, certain pathologies can trigger changes in the pH environment such as metabolic acidosis caused by diseases like diabetes, infections, renal failure, inflammation, and cancer.⁹⁵ As a consequence, a great deal of pH-sensitive polymers have been investigated to potentially treat or diagnose these type of diseases. Therefore, to understand the structure and dynamics of pH-responsive polymers is of utmost importance for developing new biomaterials.

As briefly explained before, pH-responsive polymers have functional groups able to accept or donate protons in response to variations in pH when dissolved in a polar solvent (usually water). These acidic or basic groups in the polymer chains behave similarly to small molecules; nonetheless, the neighbouring groups are adjacent to each other hindering full ionisation (i.e. weak polyelectrolytes).⁹⁶ Unlike weak polyelectrolytes, strong polyelectrolytes completely dissociate almost independently of the pH; hence, these are considered as pH-insensitive polymers. Upon ionisation, weak polyelectrolytes give ionic polymeric chains that expand due to the electrostatic self-repulsion, which increases the hydrodynamic volume of the polymer (i.e. extended coil structure). Contrary to this, the polymer chains attain a compact configuration when unionised due to hydrophobic interactions and hydrogen bonding.⁹⁷ Hence, the polymer conformation relies on the degree of ionisation which is greatly affected by the solution pH, ionic strength and temperature.

Polyacids, such as PAA, produce negatively charged polyanions (conjugate base of the polyacid) when increasing the pH due to their tendency of donating protons (Figure 1.5a). Conversely, polybases, like PDMAEMA, give positively charged polycations (conjugate acid of the polybases) when decreasing the pH as they tend to accept protons (Figure 1.5b). In the case of PAA, the carboxylic groups are protonated at low pH, where the hydrophobic interactions dominate decreasing the polymer volume. As the pH increases, carboxylate groups are formed from the deprotonation of the carboxylic acid groups thus generating a charge density in the polyanion, which ultimately increases the volume of the polymer due to charge repulsion between

neighbouring carboxylate groups. On the other hand, the amine groups in PDMAEMA are ionised at low pH (i.e. extended coil), and at high pH values these groups become unionised (i.e. tight coil). The chain configuration in polyelectrolytes can be thus considered as a function of the pH and the pK_a of the polymer, and like small molecules, the pK_a can be determined from the titration curve.⁹⁸

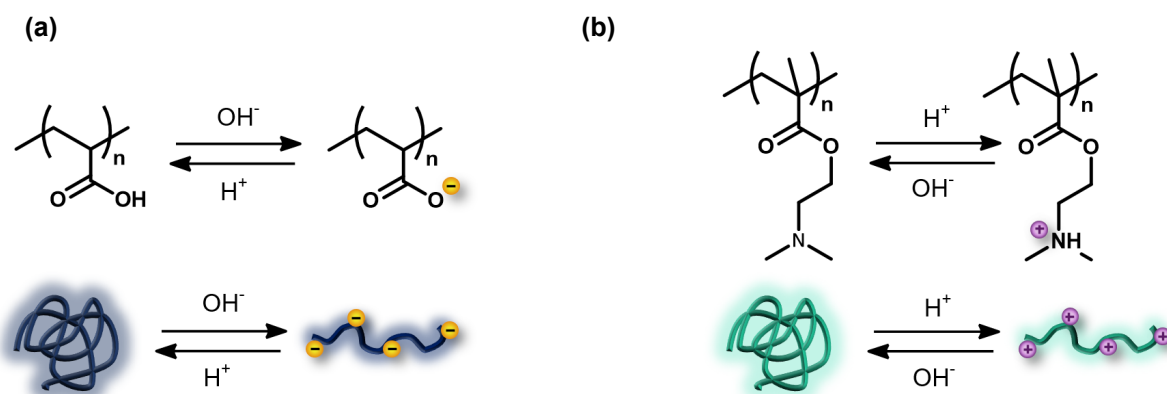


Figure 1.5: Structures of (a) poly(acrylic acid) and (b) poly((2-dimethylamino)ethyl methacrylate) and the schematic illustration of their conformational configuration.

1.2.3. Biological stimuli

The third classification to cover includes polymers that exhibit a response to biomolecules that are found in living systems such as glucose, specific enzymes, protein receptors and inflammation-related metabolites.^{99,100} For example, enzyme-responsive polymers used to design nanomaterials include those that target enzymes like glycosidases, which degrade polysaccharides like chitosan and dextrin.³⁶ Another representative example is the design of glucose-responsive nanogels, which are promising due to a targeted insulin delivery. In these systems, insulin is released due to changes in volume according to variations in the pH. The pH is lowered when glucose oxidase (GOx) oxidises glucose into gluconic acid and hydrogen peroxide leading to swelling of the system.¹⁰¹

1.3. Preparation methods of nanogels

Various approaches can be followed to prepare nanogels (Figure 1.6). These can be divided into four main strategies: (i) physical self-assembly of polymers, (ii) chemical crosslinking of preformed polymers, (iii) polymerisation of monomers in an heterogeneous phase, and (iv) template-assisted nanofabrication techniques.¹⁰²

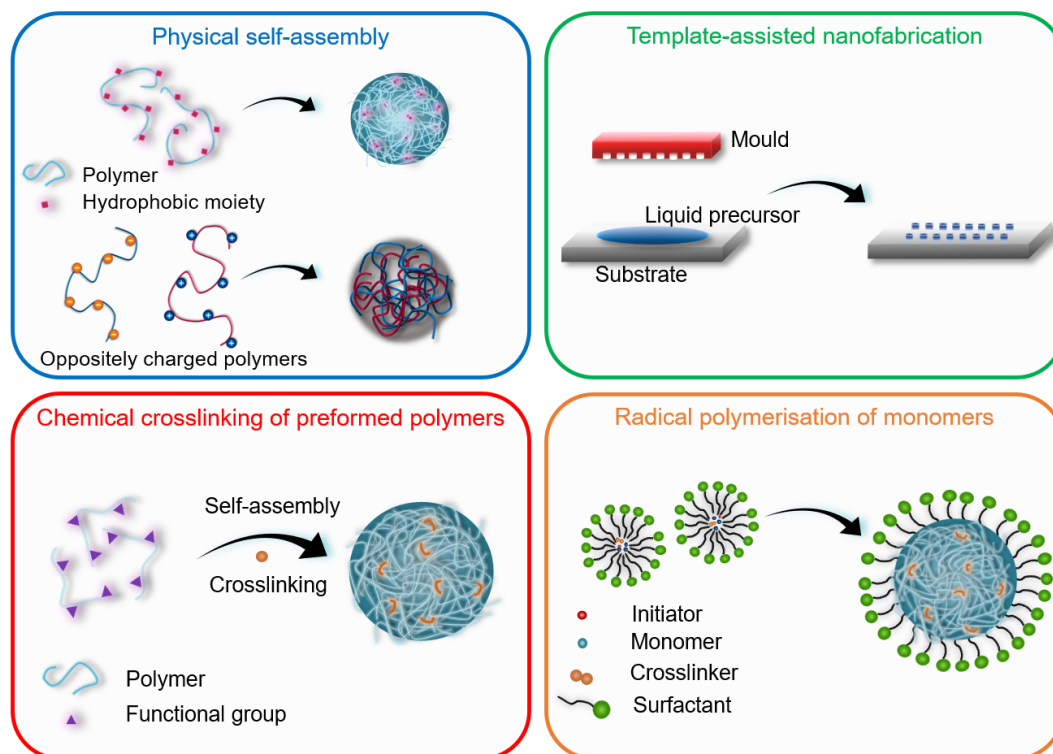


Figure 1.6: Schematic illustration showing the main strategies for nanogel preparation. (Adapted from Ref 102).

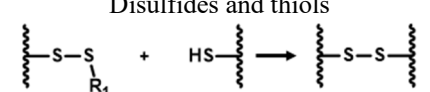
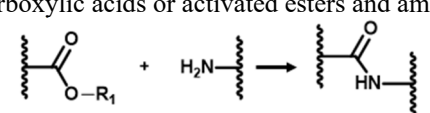
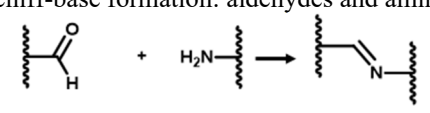
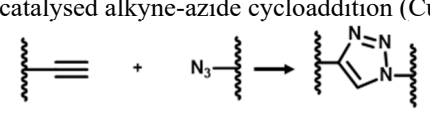
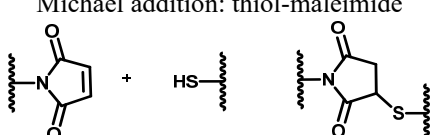
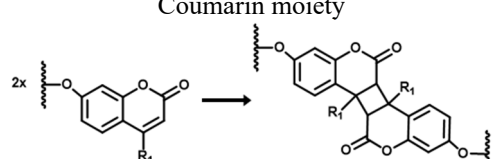
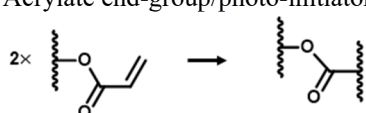
The preparation of nanogels by physical self-assembly is normally carried out in water and involves the aggregation of hydrophilic or amphiphilic polymer chains. In this case, the nanogel is essentially formed *via* physical crosslinking by association or complexation of the polymer chains by non-covalent forces such as ionic interactions (e.g. oppositely charged polymers), hydrogen bonding, hydrophobic interactions, or Van der Waals forces.¹⁰² Due to their weak association, the nanogel formation and its size depends on the composition and concentration of the polymer, temperature, pH and ionic strength.¹⁰³ The most representative example of nanogel formation *via* weak interactions is the polysaccharide-based nanogels, where the hydrophilic polymer chains (e.g. mannan, pullulan or chitosan) are modified with hydrophobic moieties (e.g. cholesterol, cholic or deoxycholic acid) and the structure is crosslinked by formation of hydrophobic domains (Figure 1.6).^{104–106} In the literature, it can be found that variety of synthetic

polymers have also been used to produce physically crosslinked nanogels with a micellar structure. In this case, amphiphilic block copolymers with two or more blocks are designed to self-assemble at certain conditions into a range of structures.¹⁰⁷ The disadvantage of non-covalent interactions in physically crosslinked nanogels is that they are relatively weak; therefore, nanogels may exhibit low mechanical properties and poor stability for certain biomedical applications.¹⁰⁸ Hence, most of the research has focussed on developing nanomaterials with covalently crosslinked networks and as such it will be further discussed.

Template-assisted nanofabrication of polymeric particles is another approach to produce nanogels. This technique is based on a “top-down” approach by using an imprint lithography technique named particle replication in nonwetting templates (PRINT).¹⁰⁹ In this technique, a fluoropolymer with low surface energy is applied to the master template and is then photochemically crosslinked to give a replica mould that is non-wetting to organic liquids. The precursor solution (organic liquid) containing monomer(s) and catalyst then fills the mould cavities by capillary action, and once the polymerisation takes place the monodisperse nanoparticles are harvested. Gratton and co-workers¹¹⁰ showed that PEG-based nanogels with encapsulated drugs can be harvested by this technique with a good control over the composition, shape and size of the particles. There is scarce literature on nanogels produced by PRINT; however, it could represent a versatile and innovative method to synthesise particles with monodisperse size. A drawback of this method is the use of catalysts with unknown toxicity in the synthesis, which may hinder their health-related applications such as drug delivery.

The other two approaches to produce nanogels are based in the formation of covalent bonds by chemical reactions in solution. Incorporation of covalent crosslinking increases the colloidal stability of nanogels in comparison to those that are physically crosslinked.¹⁰⁸ The formation of chemically crosslinked nanogels is classified into two methods. The crosslinking from (i) preformed polymers with reactive functionalities or (ii) *via* radical polymerisation of comonomers. The former method involves a crosslinking reaction of polymer precursors (normally amphiphilic) to lock a self-assembled structure, while the latter involves the radical polymerisation of monomers, and it will be reviewed in Section 1.3.1. The crosslinking from polymer assemblies is achieved by formation of covalent bonds between reactive functional groups on the polymer chains and in some cases with the aid of another reactive molecule (e.g. photo-initiator or a crosslinker).¹⁰⁸ Table 1.1 shows the most representative coupling strategies to produce nanogels from preformed polymers, which involve chemistries such as thiol-disulfide exchange, amide crosslinking, click chemistry, and photo-induced crosslinking.

Table 1.1: Covalent crosslinking reactions for nanogel formation from polymer precursors.

Reactions	References	Reacting groups
Thiol-disulfide exchange reaction	111–117	Disulfides and thiols 
Amide-based crosslinking	77,118,119	Carboxylic acids or activated esters and amines 
Imine-based crosslinking	120	Schiff-base formation: aldehydes and amines 
Click chemistry	121	Cu(I) catalysed alkyne-azide cycloaddition (CuAAC) 
Pseudo-click reaction	122	Michael addition: thiol-maleimide 
Photo-induced crosslinking	123,124 125–127	Coumarin moiety  Acrylate end-group/photo-initiator 

The nanogel formation from covalent bonding of polymer assemblies have been exploited by several research groups. For example, the Thayumanavan group have explored extensively the formation of redox responsive disulfide bonds through thiol-disulfide exchange reactions of pyridyl disulfide (PDS) with dithiolthreitol (DTT).^{111–117} Overall, the crosslinking occurs between PDS moieties and the thiols generated from the cleavage of the disulfide bond of PDS with DTT, where the disulfide bonds are formed by displacement of one sulfur by the deprotonated free thiol (i.e. thiolate anion). Another interesting crosslinking strategy followed by the same group is the amidation of activated esters with diamino molecules (crosslinker), which contained labile moieties in their structure such as disulfide (redox-cleavable)¹¹⁸ and ketal (acid-cleavable).¹¹⁹

Thus, representing an opportunity to introduce other stimuli-responsive functionalities into a nanogel structure. Imine linkages have also been explored as labile groups under weakly acidic conditions by the Yang group.^{120,128,129} They explored the formation of imine bonds to give an amphiphilic protein-polymer conjugate nanogel, that was crosslinked by a Schiff-base reaction between the amino groups from the lysine residues of urokinase protein and benzaldehyde bifunctional PEG.¹²⁰

The use of copper-catalysed click chemistry has also been used to synthesise nanogels by crosslinking azides with alkynes without producing by-products in contrast to the methods mentioned above.¹²¹ However, the use of copper might be detrimental for biomedical applications if its removal is deficient. Hence, the use of metal-free click strategies has also been explored for nanogel formation. An example of this is the formation of thioether bonds by using a thiol-maleimide Michael addition in a copper-free approach under mild reaction conditions.¹²² Alternatively, photo-induced crosslinking is also used to produce stable nanogels and it is considered a “green” technique as no by-products are produced. In this case, polymers are functionalised with photo-activable groups such as vinylic units or photo-dimerisable units like coumarin. For instance, nanoassemblies have been photo-crosslinked with acrylate end-groups with the aid of a photo-initiator.^{125–127} Conversely, a photo-switchable nanogel can be prepared by using coumarin moieties as photo-crosslinker under UV irradiation without the addition of an initiator.^{123,124} The crosslinking photo-switchability is given by the reversible photo-dimerisation of coumarin side groups ($\lambda > 310$ nm) and photo-cleavage of cyclobutene bridges ($\lambda < 260$ nm).

1.3.1. Nanogel preparation from radical polymerisation

Nanogel formation *via* polymerisation of monomers is classified into a (1) free radical or (2) living/controlled radical polymerisation (CRP).¹³⁰ In both techniques, the reaction is normally performed in a heterogeneous system (usually two-phases) and involves the simultaneous polymerisation of vinylic monomer(s) and a crosslinker (bi- or multi-functional monomer). To produce submicron-size gels, a confined nanoscale space is usually needed for the *in situ* reaction of comonomer(s) which in turn promotes intraparticle crosslinking rather than interparticle crosslinking (i.e. macroscopic gelation). Templating methods include (inverse) emulsion, (inverse) miniemulsion, dispersion or precipitation polymerisation, where the choice of the process depends mainly on the nature of the monomers.¹¹ Due to the numerous reports of micro- and nanogels made using free radical polymerisation, a brief overview of the main synthetic methodologies is presented in Table 1.2 and details on CRP methods will later be covered.

Table 1.2: Heterogeneous techniques to obtain micro- and nanoparticles.^{131–133}

Polymerisation technique	Main features
Conventional emulsion (oil-in-water O/W)	<ul style="list-style-type: none"> ◦ Monomer is immiscible (or scarcely miscible) in the continuous phase (water). ◦ Initiator is soluble in the continuous phase. ◦ Surfactant is needed to stabilise the particles (1-3% w/v). ◦ Monomer droplets are formed by mechanical stirring (1 to 100 μm in size) and thermodynamically stabilised by surfactant molecules (concentration above the critical micellar concentration (CMC)). ◦ Particles formed by homogeneous or micellar nucleation.
Inverse emulsion (water-in-oil W/O)	<ul style="list-style-type: none"> ◦ Inverse of an O/W emulsion, the continuous phase is an organic solvent and the dispersed phase is water (W/O). ◦ Hydrophilic monomers are dispersed in an oil/organic phase. ◦ Initiator is soluble in the continuous phase (hydrophobic initiator). ◦ Surfactants used are normally steric and non-ionic.
Microemulsion	<ul style="list-style-type: none"> ◦ Monomer droplets are thermodynamically stabilised by high amounts of surfactant (10% w/v) ◦ A water-insoluble co-stabiliser (e.g. alcohols such as hexanol) is often used as co-surfactant. ◦ Particles formed by droplet nucleation (10 to 100 nm in size).
Miniemulsion	<ul style="list-style-type: none"> ◦ The monomer droplets are stabilised by the surfactant (Surfactant concentration \leq CMC) and a co-stabiliser (e.g. long-chain alkenes or alcohols for O/W systems and salts or sugars for inverse miniemulsions). ◦ Monomer droplets are broken into smaller droplets by application of high shear stress such as ultrasonication or high-pressure homogenisation (50 to 500 nm in size). ◦ Absence of micelles due to a low surfactant concentration. Hence, reaction occurs in the monomer-swollen micelles (i.e. droplet nucleation).
Precipitation	<ul style="list-style-type: none"> ◦ Homogeneous mixture before initiation (i.e. comonomers and initiator are soluble in the organic solvent). ◦ Formed particles do not swell in the medium (i.e. insoluble) ◦ Polymerisation occurs in the reaction medium and the crosslinker “isolate” particles. ◦ Particles with irregular shape and high polydispersities are formed due to their growth mechanism.
Dispersion	<ul style="list-style-type: none"> ◦ Similar to a precipitation polymerisation, but a stabiliser is added in addition to the comonomers, and initiator. ◦ During polymerisation, the formed polymer becomes insoluble and is stabilised by a colloidal stabiliser.

While emulsion or precipitation polymerisation has been utilised for the synthesis of microgels,^{134–136} different adaptations of an emulsion polymerisation process have been explored to prepare even smaller and more uniformly crosslinked nanogels, e.g. semicontinuous starved-feed emulsion polymerisation.¹³⁷ By using a conventional emulsion or precipitation

polymerisation, inhomogeneous structures (i.e. core-shell) are likely to be formed if there are differences in reactivity ratios and variations between the hydrophobicity/hydrophilicity of the monomers and crosslinker, which ultimately affects the diffusion mechanism of growing oligomers between phases.^{130,135} A way to overcome the inhomogeneous crosslinking when using these templating techniques is by conferring a higher control over the radical polymerisation, e.g. by using a controlled radical polymerisation (CRP). The most effective CRP techniques include atom transfer radical polymerisation (ATRP), nitroxide mediated polymerisation (NMP), and reversible addition-fragmentation chain-transfer (RAFT) polymerisation.¹³⁸ The belief that a more uniform crosslinked structure can be formed by CRP methods is because of the dynamic equilibrium between propagating (active) chains and dormant species that ultimately allows the preparation of polymers with controlled molar mass, narrow dispersity ($\bar{M}_w/\bar{M}_n < 1.5$) and with good end-group fidelity than those prepared by conventional free radical methods.¹³⁹ Additionally, a uniform distribution of crosslinks could also be achieved by using an inverse emulsion due to better solvency conditions of the comonomers and a different locus of polymerisation (i.e. monomer droplets).¹³⁵ This is mainly because most of the comonomers used for nanogel preparation contain hydrophilic groups, e.g. -OH, -CONH-, -CONH₂, -SO₃H.¹² Hence, inverse mini- or microemulsion polymerisations are the most frequently used techniques to produce nanogels.¹³³ However, a drawback of these approaches is the requirement of surfactants that are hard to remove, and in some cases the use of organic solvents and catalysts (frequently used in ATRP) could affect the biocompatibility of nanogels.¹⁴⁰ As a way to avoid the use of surfactants and exploit the features of CRP methods, nanogel formation using RAFT polymerisation has emerged as a versatile way to prepare nanogels *via* polymerisation-induced self-assembly (PISA) in an aqueous medium.¹⁴¹ Details of RAFT polymerisation will be described next followed by the fundamentals of the *in situ* self-assembly of block copolymers.

1.4. Fundamentals of RAFT polymerisation

RAFT is a reversible deactivation radical polymerisation (RDRP)¹⁴² that allows the synthesis of polymers of controlled molar mass with narrow dispersity ($\bar{M}_w/\bar{M}_n < 1.2$), high end-group fidelity and with the ability for continued chain growth (i.e. block copolymers).^{143–146} Analogous to a conventional free radical polymerisation, a large variety of vinylic monomers with different functionalities (e.g. -OH, -NR₂, -COOH, -CONR₂, -SO₃H) under a range of conditions can be polymerised *via* RAFT polymerisation. The main feature of RAFT polymerisation is the addition of an addition-fragmentation chain-transfer agent (CTA) usually a thiocarbonylthio compound which can include four different main classes: dithioesters (Z=alkyl or aryl), trithiocarbonates (Z=SR'), xanthates (Z=OR') and dithiocarbamates (Z=NR'R'') (Figure 1.7). General details on the design of CTAs for specific monomers will be covered in Section 1.4.2.

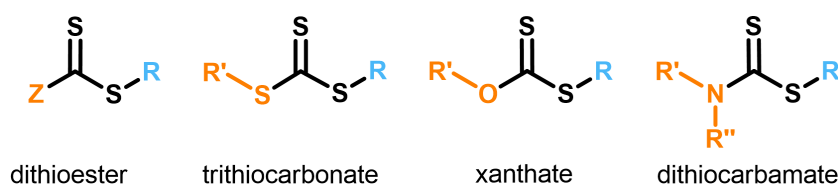


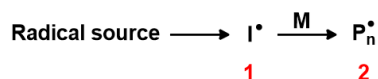
Figure 1.7: Chemical structures of the main classes of RAFT CTAs according to their Z-group.

1.4.1. The mechanism of RAFT polymerisation

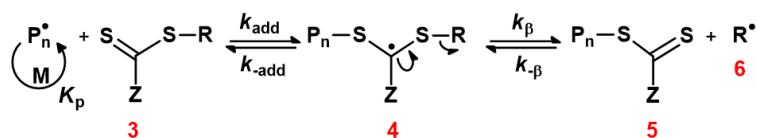
Analogous to a free radical polymerisation, RAFT polymerisation involves steps such as initiation and termination, the main difference being a series of addition-fragmentation equilibria that mediate propagation (Figure 1.8). In the initiation stage, free radicals (1) are generated by decomposition of an initiator, e.g. by thermal decomposition of diazo compounds or peroxides.¹⁴⁷ These newly formed radicals initiate the polymerisation by reacting with monomer (M), thus giving a propagating radical (2). Then, the propagating radical (2) reacts with the RAFT CTA (3) leading to the formation of an unstable intermediate radical (4) that fragments into a new radical (6) and a deactivated polymeric thiocarbonylthio compound (5) (i.e. macromolecular CTA or macro-CTA) in a dormant state. This expelled radical (6) is the free radical leaving group that enables the reinitiation of polymerisation. In the next step, more monomer reacts with this radical to form a new propagating polymer radical (7), which then adds to the dormant macro-CTA (5). Similar to the previous dynamic equilibrium, another unstable intermediate radical is formed (8)

which fragments into one active macro-radical and one dormant macro-CTA. This main equilibrium between the active polymeric radicals (2 and 7) and the dormant macro-CTA chains must be rapid with respect to propagation to control the monomer addition per polymer chain. In this way, each chain has an equal chance to grow during polymerisation, thus producing polymers with controlled molar mass and narrow dispersity.¹⁴⁸

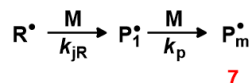
Initiation



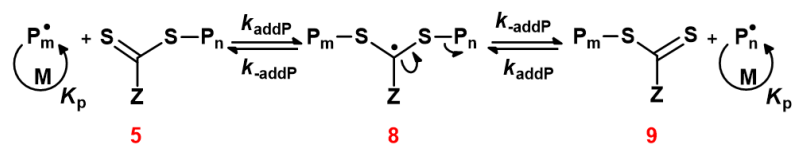
Reversible chain transfer



Reinitiation



Chain equilibrium



Termination



Figure 1.8: The proposed mechanism of RAFT polymerisation by Moad *et al.*¹⁴⁸

At the end of the polymerisation, it is expected that the vast majority of the resulting polymer chains have the R- and S=C(Z)S- functionalities as the α and ω end-groups, respectively. However, some other products, sometimes in negligible proportion, are formed due to the radical nature of the polymerisation, e.g. chains with an initiator fragment instead of the R-group at the α-end, and dead chains without the thiocarbonylthio end-group at the ω-end.¹⁴⁹ To maximise the number of dormant species with the R- and S=C(Z)S-groups, a higher concentration of CTA than initiator is required as well as using RAFT CTA with a large chain-transfer constant.¹⁵⁰ Inevitably, termination events will occur when two active propagating radicals react to give dead polymer chains, even if the initiator concentration is minimised. In order to retain high “livingness” for further chain extension by another monomer, reactions are sometimes stopped prior full monomer conversion. In this way, it is ensured that most of the polymer chains retain the RAFT CTA end-groups.

To determine the average degree of polymerisation two assumptions are typically made. Firstly, that the CTA is consumed within the first few percent of monomer conversion and secondly the number of polymer chains due to initiator decomposition is small. Hence, it can be assumed that the number of polymer chains is equal to the number of CTA molecules and therefore the average degree of polymerisation is given by:¹⁵⁰

$$DP = \frac{\chi [M]_0}{[CTA]_0} \quad \text{Equation 1.2}$$

Where, χ is the fractional monomer conversion, and $[M]_0$ and $[CTA]_0$ are the initial concentrations of the monomer and RAFT CTA, respectively. As consequence, a theoretical number-average molar mass can be easily calculated with Equation 1.3, where M_i and M_{CTA} are the molar masses of the monomer and CTA, respectively.

$$\bar{M}_{n,theo} = M_{CTA} + \frac{M_i \chi [M]_0}{[CTA]_0} = M_{CTA} + M_i \times DP \quad \text{Equation 1.3}$$

1.4.2. Guidelines for the design of CTAs

As previously explained, a sequence of reversible addition-fragmentation equilibria is achieved by means of a CTA. Overall, the chain-transfer process involves the exchange of end-group functionalities (i.e. $S=C(Z)S-$ and $R-$) between dormant chains and propagating radicals that only differ in molar mass (Figure 1.9).¹⁴³ The efficiency of this exchange determines the “living” character on the polymerisation.¹⁴⁵

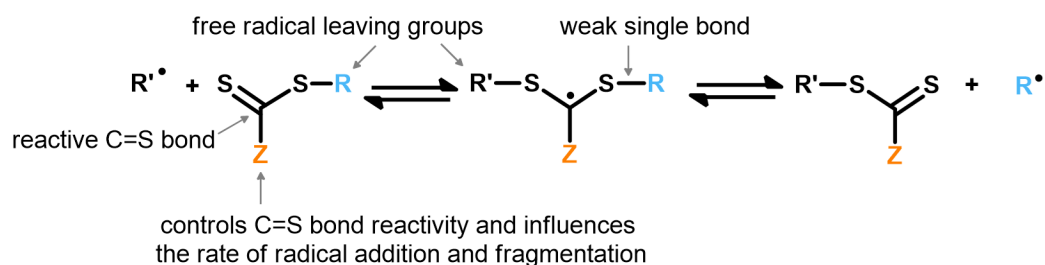


Figure 1.9: The reversible addition-fragmentation chain-transfer process, where $R \bullet$ and $R' \bullet$ are both the propagating radicals. Adapted from Ref 151,152.

The two distinctive Z and R groups of the RAFT CTA ($S=C(Z)S-R$) are key to achieve good control over the polymerisation. On one hand, the R group should be a good free radical leaving group in comparison to the growing polymeric chain and as an expelled radical, R^\bullet , should have the ability to reinitiate polymerisation.¹⁴⁶ On the other hand, the Z group strongly influences the stability of the intermediate radical and affects the reactivity of the C=S bond.¹⁴⁵

For a successful RAFT process, it is key to select a suitable CTA for the monomer(s) being polymerised. General guidelines for the selection of thiocarbonylthio RAFT agents have been reported before and is summarised in Figure 1.10.^{148,151-153} The CTA structure can be modified by changing the R- and Z-groups to tailor their reactivity. The design of the Z-group mainly depends on the monomer being polymerised and the reaction conditions.¹⁵³ According to the reactivity of the monomer, the rate of radical addition (k_{add} , $k_{-β}$, k_{addP}) can be modified by manipulation of the Z-group. Monomers can broadly be considered as either “more activated” monomers (MAMs) (i.e. double bond conjugated to an aromatic ring, a carbonyl or a nitrile group) or as “less activated” monomers (LAMs) (i.e. double bond adjacent to oxygen, nitrogen, halogen, sulfur lone pairs or saturated carbons).^{149,153} In general, MAMs (e.g. methacrylates, acrylamides, etc.) produce more stable propagating radicals due to resonance stabilisation, i.e. they are less reactive in radical addition (lower k_{add}). Consequently they need a more active Z-group that favours radical addition on the C=S double bond and that facilitates the stabilisation of the intermediate radical.¹⁴⁹ Among the most active CTAs, dithiobenzoates (Z=phenyl) and trithiocarbonates give better results for polymerisation of MAMs. Contrarily, LAMs (e.g. *N*-vinylamides or vinyl esters) are highly reactive in radical addition (higher k_{add}) and less active Z-groups are needed to favour the fragmentation of the propagating radical.¹⁴⁹ In this case, the lone pair of electrons on xanthates or dithiocarbamates plays an important role in the deactivation of the C=S double bond towards radical addition, thus promoting propagation and the destabilisation of the radical intermediate. Hence, the presence of electron-withdrawing groups on the Z-group affects the chain-transfer constant (C_{tr}) and the reactivity of the C=S double bond. In general, the effect of varying Z decreases the rate of addition and increases the fragmentation rate in the series shown in Figure 1.10 from left to right. The choice of the R-group is dictated by a balance between radical stability and steric effects, since it has to form a stable radical after fragmentation that is reactive enough to reinitiate polymerisation.¹⁵³ Polar (i.e. electron-withdrawing groups) and steric effects (i.e. bulky groups) are important factors in determining the leaving-group ability of R. In general, the effect of varying R decreases the rate of addition and the fragmentation rate in the series showed in Figure 1.10 from left to right.

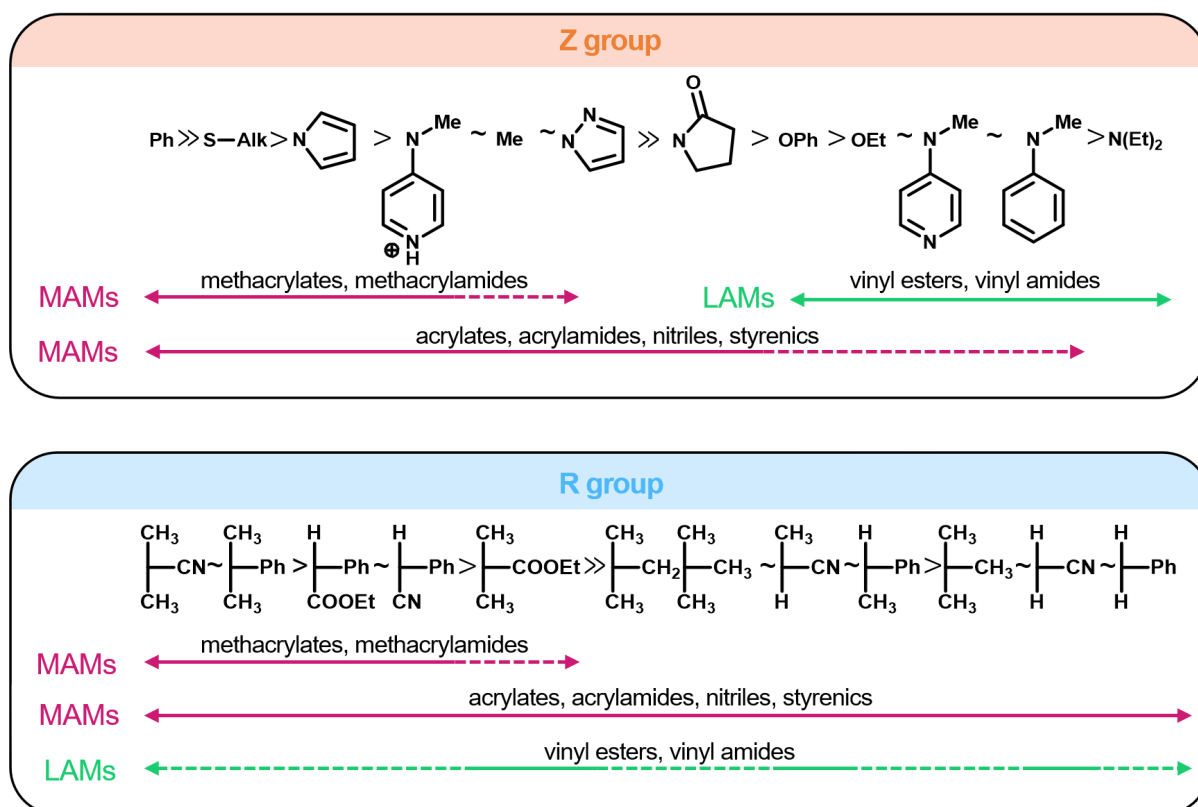


Figure 1.10: Guidelines for the selection of suitable Z and R groups of CTAs for the RAFT polymerisation of various monomers. Solid lines indicate that a good control can be achieved, whilst dashed lines indicate partial control (Adapted from Ref 153).

To finish this section, it is important to emphasise that as the popularity of RAFT polymers for biomedical application has increased, as have the concerns of potential toxicity attributable to the RAFT CTA.¹⁵⁴ In vitro studies of the toxicity of RAFT polymers has demonstrated that they can possess low toxicity to cells, depending on the RAFT end group used in their preparation (e.g. trithiocarbonates).¹⁵⁵ However, if necessary the thiocarbonylthio group can easily be modified by simple reactions, e.g. thermolysis, radical induced reduction, nucleophilic replacement and nucleophilic removal.¹⁵⁶

1.5. The use of RAFT polymerisation to prepare nanogels

As mentioned previously, submicron-gels can either be obtained from preformed polymers by further coupling reactions or they can be prepared from direct polymerisation of comonomers. Due to the versatility of RAFT polymerisation, these two main strategies have been explored in the preparation of nanogels, as it has been previously reported.¹⁴¹ However, the majority of literature examples are based on direct RAFT copolymerisation of monomer(s) and crosslinker due to the mild reaction conditions and tolerance to a variety of functionalities. These reports showed that the RAFT-mediated nanogel formation can be conducted either in heterogeneous or homogeneous systems. Interestingly, in a homogeneous system only soluble branched polymers were reported and were termed also as nanogels. As is the case of Taton and Poly¹⁵⁷⁻¹⁵⁹ who have investigated the synthesis of branched polymers of acrylic acid, acrylamide or vinyl acetate using a xanthate RAFT CTA. It is arguable that these soluble branched polymers should be considered nanogels since their properties differ from those synthesised under heterogeneous conditions (i.e. size dispersity and different crosslinking density). Besides, they could resemble more the properties of dendritic nanocarriers.¹⁶⁰ Nevertheless, it is worth mentioning that this is facile one-pot technique to obtain nanosized materials that fit into the broad definition of a gel. In the case of RAFT-mediated polymerisation in heterogeneous systems, inverse miniemulsion and precipitation/dispersion are the main methodologies used for the preparation of nanogels.¹⁴¹ Generalities of these techniques were already covered in Section 1.3.1. A great drawback of inverse miniemulsion, is the use of surfactants and oils during the synthesis of nanogels as explored by Schork *et al.*¹⁶¹ Although the use of surfactants can be avoided by using amphiphilic diblock copolymers, as shown by Matyjaszewski and co-workers for the synthesis of hollow nanogels *via* miniemulsion ATRP.¹⁶² A lack of control over the size distribution of the particles was observed, besides of producing nanoparticles with diameters within the range of 200-300 nm. Additionally, miniemulsion polymerisation faces several constraints for scalability such as sonication at large scale and effective purification methods of materials intended for use in bioapplications.¹⁶³ Conversely, aqueous dispersion polymerisation *via* RAFT allows the synthesis of block copolymer nano-objects with controlled size, morphology, and composition at high solids contents.¹⁶⁴ As a result, this approach has been explored for the synthesis of crosslinked particles, as it will be next reviewed.

1.5.1. Preparation of nanogels by RAFT-mediated dispersion polymerisation

In a typical RAFT dispersion polymerisation, a soluble polymer (i.e. macro-CTA) is chain extended by an also initially soluble monomer. During polymerisation, the growing chain loses solubility and eventually becomes insoluble at some critical degree of polymerisation, this drives to the *in situ* self-assembly of the diblock copolymer into self-stabilised nano-objects (Figure 1.11). In principle, the solvophilic macro-CTA enables further chain extension by the soluble monomer and stabilises the chain growth of the solvophobic block, thus avoiding macroscopic precipitation.

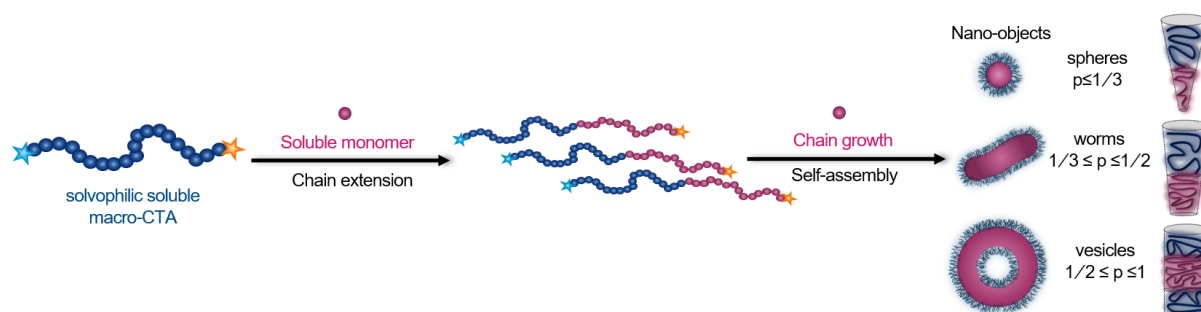


Figure 1.11: The schematic representation of RAFT dispersion polymerisation showing some of the possible morphologies of the nano-objects obtained by *in situ* self-assembly of diblock copolymers. (Adapted from Ref 165).

According to the relative volume fraction of the blocks, the morphology of the nano-objects differs due to a different packing geometry of the copolymer chains, which is defined in terms of the packing parameter (p).¹⁶⁶ Overall, the packing parameter depends on the area of the hydrophilic block (a_0), the volume of the hydrophobic chains (v) and the maximum length the hydrophobic chains can assume (l_c), as Equation 1.4 shows:

$$p = \frac{v}{a_0 l_c} \quad \text{Equation 1.4}$$

For instance, an amphiphilic diblock copolymer will assemble into a spherical micelle when $p \leq 1/3$. So, if the area of the hydrophilic block is maintained constant, a variety of morphologies of higher-order can be formed by increasing the length of the hydrophobic block as shown in Figure 1.11. The process in which aggregates of multiple morphologies can be prepared *via* polymerisation has been coined polymerisation-induced self-assembly (PISA).¹⁶⁷ The PISA strategy has been subject of multiple reviews, in which recent advances and techniques can be found in more depth than in this work.^{164,168–173}

An inherent pre-requisite of using water as dispersing medium in a RAFT aqueous dispersion PISA is that the water-miscible monomer must generate a water-insoluble core-forming block during the reaction.¹⁷⁴ Hence, only a few monomer/polymer pairs can meet such requirements. Examples of vinyl monomers include (Figure 1.12): 2-hydroxypropyl methacrylate (HPMA),¹⁷⁵⁻¹⁷⁷ diacetone acrylamide (DAAM),¹⁷⁸⁻¹⁸⁰ *N,N*-diethylacrylamide (DEAM),⁵⁶ 2-methoxyethyl acrylate (MEA),^{181,182} *N*-isopropylacrylamide (NIPAM),¹⁸³⁻¹⁸⁵ di(ethylene glycol) methyl ether methacrylate (DEGMA)¹⁸⁶ and *N*-(2-methacryloyloxy)ethylpyrrolidone (NMEP).¹⁸⁷

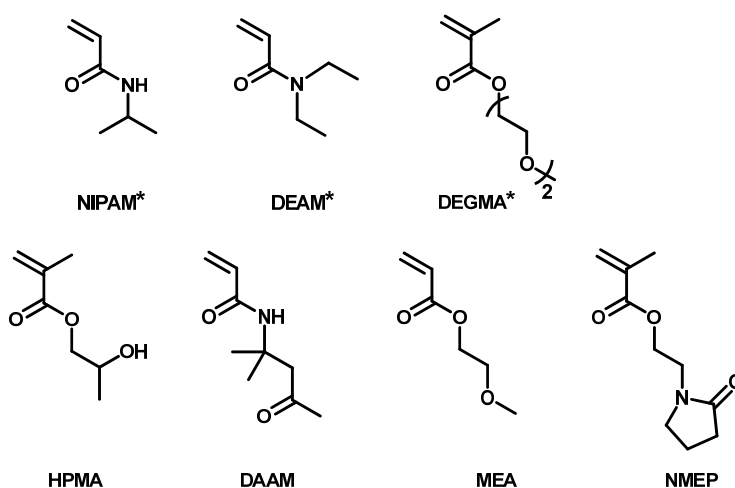


Figure 1.12: Water-miscible monomers used in aqueous dispersion PISA.
*Monomers that exhibit a thermoresponse in water.

Monomers such as NIPAM, DEAM and some monomers with pendant oligo(ethylene glycol) substituents⁴⁷ are capable of polymerisation using aqueous dispersion RAFT-mediated PISA due to their weak hydrophobic character of the corresponding homopolymer with temperature-dependent solubility.^{169,188} The use of RAFT-mediated PISA to prepare nanogels was first reported by An *et al.*,¹⁸³ who prepared a series of poly(*N,N'*-dimethylacrylamide) (PDMA) macro-CTAs as mediators for the polymerisation of NIPAM and *N,N'*-methylenebisacrylamide (BIS) as crosslinker (Figure 1.13). During the polymerisation, PNIPAM becomes insoluble once a critical DP is reached thus driving self-assembly. This occurs due to the polymerisation temperature of 70 °C that is above the LCST of PNIPAM in water (~31-35 °C).^{43,44} By using a crosslinker during the synthesis, the self-assembled structure is locked in this configuration preventing dissolution below the corresponding LCST of the thermoresponsive polymer, in this case, of PNIPAM. Since the work of An *et al.*,¹⁸³ this aqueous PISA strategy has been established as a facile route to produce crosslinked particles in a green solvent (i.e. water) without the use of surfactants that are difficult to remove completely. It is worth mentioning that nanogel formation *via* this technique is a sequential strategy that presumably gives diblock copolymer particles, that

are composed of a hydrophilic shell-forming block[‡] and a core crosslinked block.

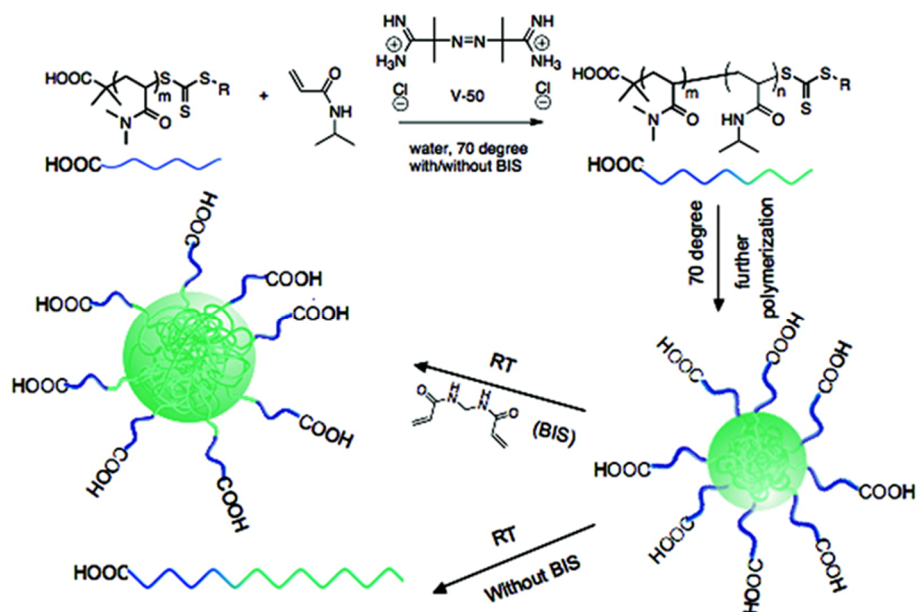


Figure 1.13: Macro-CTAs and schematic representation of the RAFT precipitation polymerisation process of NIPAM. Reprinted with permission from REF 183, Copyright © 2007, American Chemical Society.

The use of temperature-sensitive monomers other than NIPAM has been subject of more recent studies for nanogel preparation *via* RAFT PISA. For instance, Charleux *et al.*^{189,190} prepared nanogels from poly(ethylene oxide)-*b*-poly(*N,N*-dimethylacrylamide) (PEO-*b*-PDMA) macroCTAs with DEAM thermo-responsive monomer and BIS. Overall, they found that the size of the nanogels is affected greatly by the length of the macro-CTA, and by the crosslinker and monomer concentration. Additionally, they showed that the core of the nanogels was able to swell and deswell reversibly in response to changes in temperature.

Diacetone acrylamide (DAAM) has been investigated for nanogel preparation *via* self-assembly of the water-insoluble PDAAM block. Wang *et al.*¹⁸⁰ prepared PDMA-*b*-PDAAM copolymers with and without crosslinker to form nano-objects with a lamellar morphology. Overall finding a temperature-dependent morphological transition from lamellae to worms and spheres at 10 °C after a prolonged time (100 h) for particles with 1 mol% of crosslinker due to interfacial plasticization of some PDAAM units at the PDMA/PDAAM interface. No morphological transitions were observed for greater crosslinker concentrations (2-2.5 mol%) due to the reduced mobility of the hydrophobic block with higher crosslinking density.¹⁸⁰

^{‡‡}The use of an amphiphilic macro-CTAs has also been reported; however, nanogels with broad size distributions are prepared.¹⁸³

Another well-known example of polymers that display a LCST in water are methacrylates with ethylene glycol units as side chains, which response can be tailored by the number of side chain units or by copolymerisation with monomers that have different number of side chains of ethylene glycol. Shen *et al.*¹⁸⁶ evaluated the use of a PEG-derived macro-CTAs for chain extension with monomers based on oligo(ethylene glycol) methacrylates (OEGMAs) such as DEGMA and poly(ethylene glycol)methyl ether methacrylate (PEGMA) and a small amount of poly(ethylene glycol) dimethacrylate as crosslinker (Figure 1.14). Although they reported the synthesis of nanogels with low dispersities and tuneable composition, certain limitations were found. One was related to the low water-solubility of DEGMA monomer in water (2% w/v), which limits the solids content of the dispersion. Furthermore, a broad temperature phase transition was observed, which was attributed a steric effect due to the size of the comonomers.

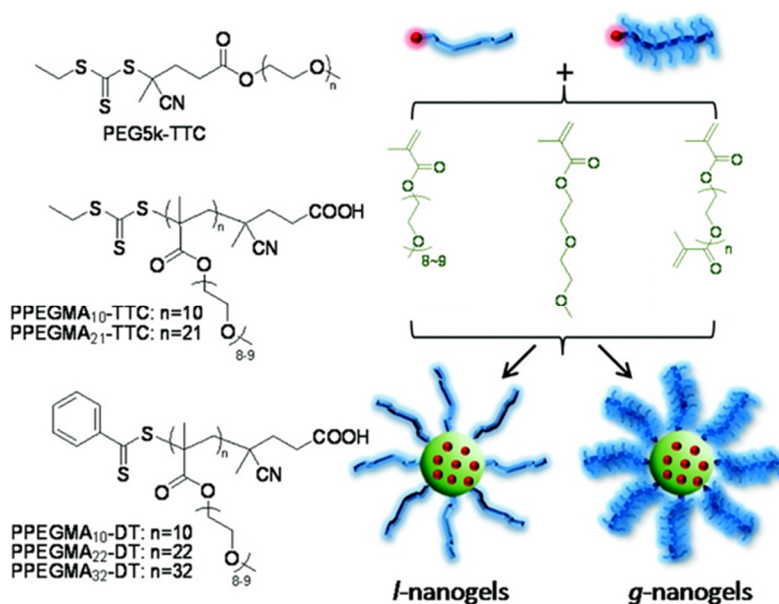


Figure 1.14: Macro-CTAs and the formation of ethylene glycol-based core-shell nanogels *via* RAFT dispersion polymerisation. Reprinted with permission from REF 186, Copyright © 2011, American Chemical Society.

To circumvent the steric effect on the temperature phase transition, Liu *et al.*¹⁸² used PDMA as shell stabiliser macro-CTA instead of PEG-derived macro-CTAs to statistically copolymerise MEA with poly(ethylene glycol)methyl ether acrylate with and without crosslinker. By using MEA, higher solids contents could be targeted with good control over the RAFT process. However, the nanogels displayed an unexpected linear size change upon heating. In another study, the same leading authors attributed the linear volume phase transition to a continuous dehydration of the C=O groups in the P(MEA-*co*-PEGA)/PDMA nanogel core.¹⁸⁴ On the contrary, PNIPAM nanogels exhibit a sharp phase transition due to a cooperative inter- and intramolecular hydrogen bonding (Figure 1.15).

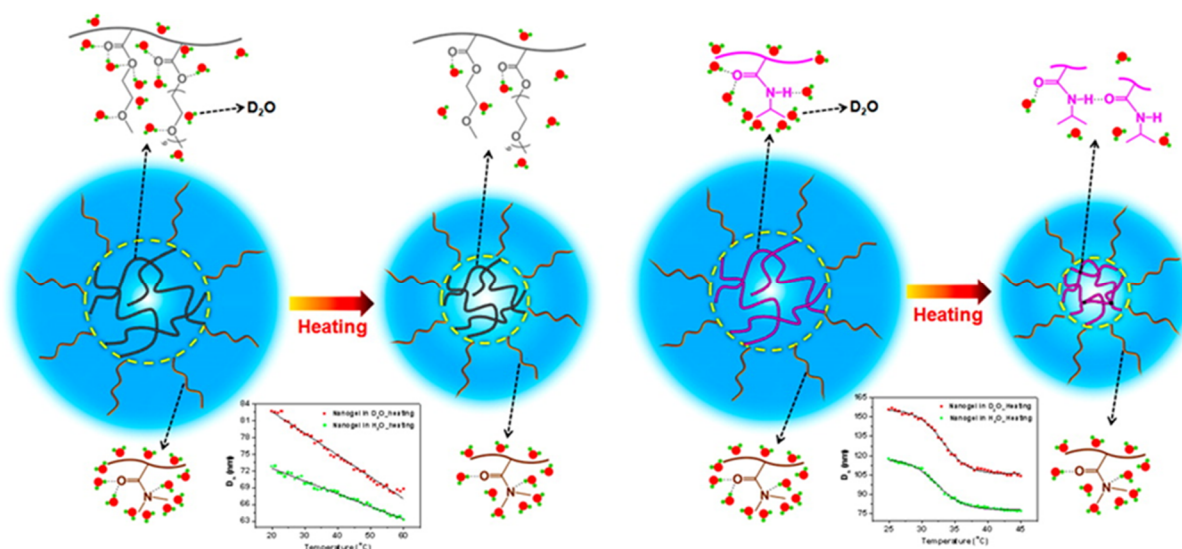


Figure 1.15: Schematic of the volume phase transition mechanism of P(MEA-*co*-PEGA)/PDMA and PNIPAM/PDMA core-shell nanogels upon heating. Reprinted with permission from REF 184, Copyright © 2014, American Chemical Society.

Another thermoresponsive monomer that has been investigated for the production of nanogels *via* aqueous dispersion RAFT-mediated PISA is *N,N'*-dimethylaminoethyl methacrylate (DMAEMA). Yao and Tao¹⁹¹ used an amphiphilic PEG macro-CTA to stabilise the chain growth of PDMAEMA. They showed that the nature of the initiator has an effect on the stability of the nanogels during polymerisation, where a hydrophobic initiator can interfere with the hydrophobic core thus producing unstable micelles. In contrast, a more hydrophilic initiator with a longer half-life yielded more stable nanogels with smaller size.

As previously mentioned, to use water as dispersing medium in RAFT-mediated PISA requires the components to be water soluble for a controlled polymerisation. Hence, a limited number of monomers and CTAs can be used to produce nanogels. To overcome this limitation, some authors have explored the addition of small quantities of organic solvents to water as a way to include various hydrophobic components or to achieve a better control over the polymerisation. For instance, the group of Narain has employed a mixture of water and 2-propanol to produce a series of nonionic (Figure 1.16)¹⁹² and ionic carbohydrate-based nanogels¹⁹³ and (ethylene glycol)-based nanogels,^{194,195} and a mixture of water and dioxane to produce carbohydrate-based cationic nanogels.¹⁹⁶ For the production of these different nanogels, they used a CTA with a dithiobenzoate Z-group, which has a better solubility in organic solvents than in water. Besides, in a previous study they showed that the synthesis of ionisable monomers in water produced polymers with broad polydispersities due to the hydrolysis of the dithioester group.¹⁹⁷

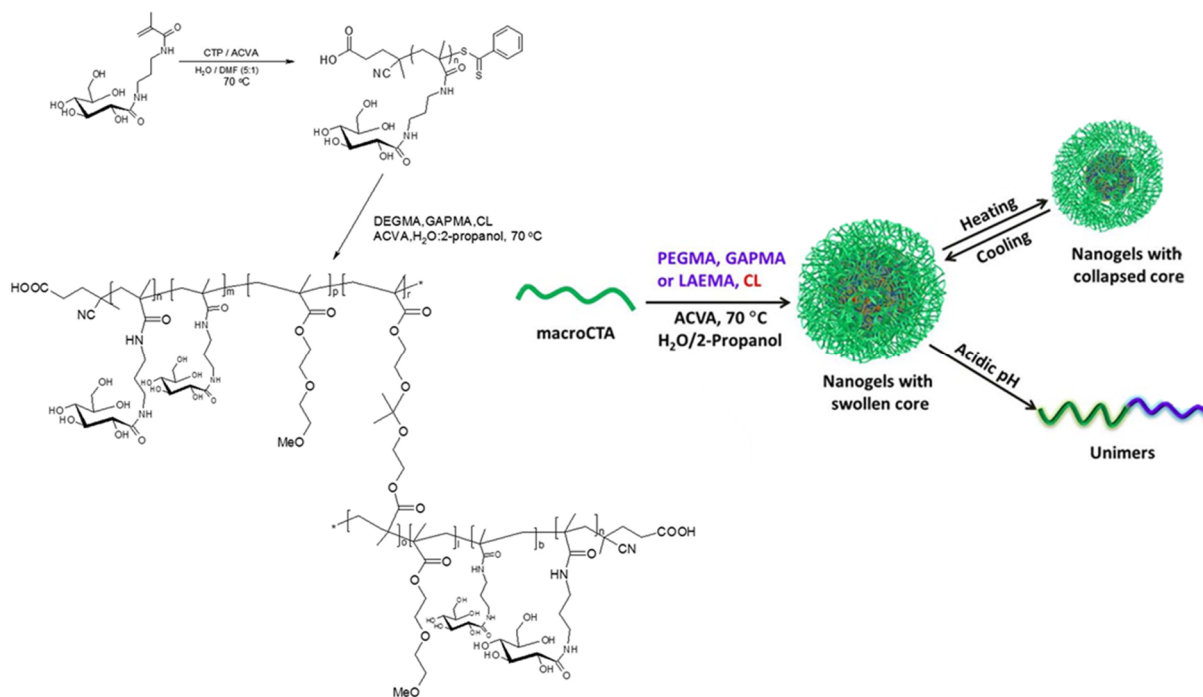


Figure 1.16: Schematic illustration for the synthesis of carbohydrate-based nanogels and their degradation in the acidic environment. Reprinted with permission from REF 192, Copyright © 2012, American Chemical Society.

The group of An has explored the synthesis nanogels *via* RAFT dispersion polymerisation using a mixture of water and different alcohols.^{55,198,199} For instance, they investigated the use of a water-ethanol mixture as a strategy to incorporate hydrophobic comonomers during the copolymerisation of NIPAM and a crosslinker to form nanogels with a crosslinked core (Figure 1.17).⁵⁵ Thus, showing the possibility of expanding the library of nanogels with different compositions and functionalities that were inaccessible by RAFT aqueous dispersion polymerisation. Moreover, they also showed that the nanogel formation by dispersion polymerisation of acrylamide was feasible when using a mixture of water and *tert*-butanol, which is not possible to achieve in just water due to polymer solubility.¹⁹⁸ This occurs because polyacrylamide is not a thermoresponsive polymer which means that it does not precipitate out and self-assemble at a critical DP during polymerisation in water; however, it can become less soluble in mixtures of water and alcohols, thus allowing nanogel formation.

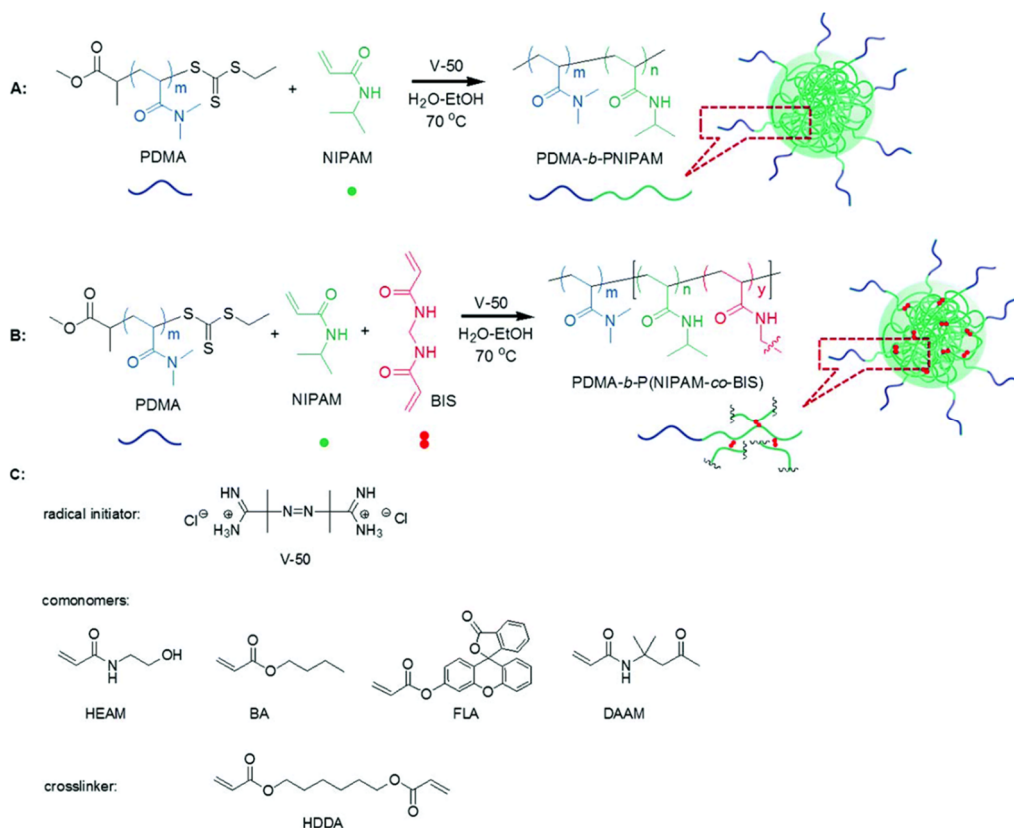


Figure 1.17: (A) RAFT dispersion polymerisation of NIPAM for the synthesis of block copolymers and (B) crosslinked nanogels, and (C) structures of comonomers and crosslinker used for copolymerisation with NIPAM. Reproduced from REF 55 with permission from The Royal Society of Chemistry.

The use of water-organic solvent mixtures was also reported by Fu *et al.*,⁵⁹ who used this strategy to prepare nanogels with a zwitterionic UCST core (Figure 1.18). It is well-known that PDMAPS has a greater solubility in water at high temperatures; as a consequence, it is not possible to produce nanogels of PDMAPS in water by RAFT-mediated PISA. However, the immiscibility of PDMAPS in ethanol or THF and water thus enables the synthesis of nanogels *via* a self-assembly approach.

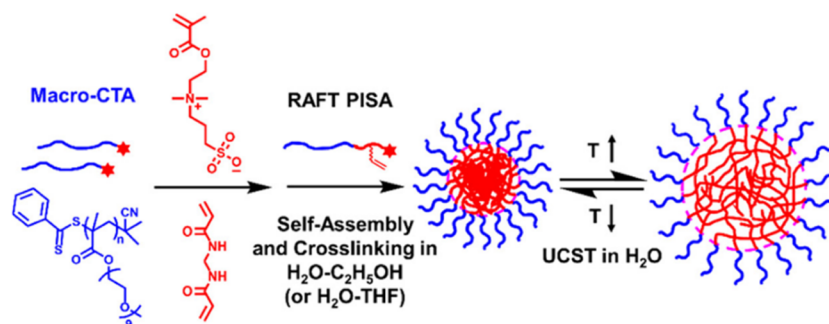


Figure 1.18: Synthesis of UCST-type thermosensitive nanogels by RAFT PISA in Water-Ethanol or -THF Mixtures and schematic illustration of thermally induced reversible swelling and shrinking of nanogels in water. Reprinted with permission from REF 59, Copyright © 2017, American Chemical Society.

1.6. Concluding remarks

Despite the numerous approaches that can be followed to produce stimuli-responsive nanogels, it is of increasing importance to finely control the composition, architecture, and functionality of these materials for intended applications in biomedicine. Among the most promising strategies for the synthesis of nanogels in a dispersed aqueous media without the addition of surfactants or toxic organic solvents, RAFT-mediated PISA has proven to be a novel and facile approach that meets such requirements. Besides, factors like size and shape, functionality and stimuli sensitivity may be easily tuned by modulating parameters such as monomer(s) composition and block(s) length. However, the monomer selection is limited to those that are water soluble and which polymer becomes less soluble with increasing temperature, e.g. NIPAM/PNIPAM. The use of mixtures of water and alcohol as dispersing medium is an emerging direction to include hydrophobic components (e.g. fluorescent monomers)⁵⁵ into PNIPAM-based nanogels during synthesis. However, more studies are needed to evaluate the effects of using binary mixtures of solvents in a polymerisation-induced self-assembly, especially in the case of polymers which solubility is affected by such solvent mixtures such as in the case of PNIPAM.²⁰⁰ Indeed, a remarkable progress has already been achieved majorly for the preparation of temperature-responsive nanogels by RAFT dispersion polymerisation; however, the area is still at an early stage and there is plenty of room for improvement. In particular, the preparation of nanogels from pH-responsive macro-CTAs such as weak polyelectrolytes, which have scarcely been prepared *via* RAFT dispersion polymerisation.

1.7. Thesis aims

Overall, the present work aims to study the synthesis and properties of stimuli-responsive ionic nanogels prepared from polyelectrolytes using a RAFT dispersion polymerisation approach. Two classes of polyelectrolytes are proposed to be used separately as shell-stabiliser blocks for the *in situ* synthesis of ionic nanogels. Both sets of nanogels are to be composed also of poly(*N*-isopropylacrylamide) (PNIPAM) to provide temperature-sensitivity to the nanogel core and of *N,N'*-methylenebisacrylamide (BIS) as crosslinker to lock in the self-assembled structure during polymerisation. Acrylic acid (AA) and 2-(dimethylamino)ethyl methacrylate (DMAEMA) are evaluated to prepare anionic and cationic polyelectrolytes, respectively. The use of weak polyelectrolytes as macro-CTAs is proposed with the intention to provide pH-sensitivity to the nanogels.

To assess the influence of the monomer composition on the size, morphology and stimuli-responsive behaviour of both classes of nanogels, a systematic variation of the core-forming PNIPAM/BIS block and the shell-stabiliser polyelectrolyte block (PAA or PDMAEMA) is thoroughly investigated by dynamic light scattering (DLS), transmission electron microscopy (TEM), and ζ -potential measurements. The internal structure of the anionic nanogels is characterised by asymmetrical-flow field flow fractionation (AF4).

As a particular objective, a thorough investigation of the effects of synthesis cononsolvent composition on the properties of the anionic nanogels is conducted to better understand the addition of ethanol as minor solvent with water during the RAFT polymerisation-induced self-assembly (PISA) of NIPAM. A series of diblock copolymers is prepared alongside the nanogels to further characterise these soluble materials by more precise techniques such as ^1H nuclear magnetic resonance (NMR) and UV-vis spectroscopic analyses.

The work presented in this thesis has the potential to provide insights into the synthesis and properties of pH- and temperature-responsive ionic nanogels with controlled size and compositions. In addition, it can offer a potential route to prepare crosslinked nanomaterials for biomedical applications through a facile polymerisation approach without the use of highly toxic solvents or surfactants.

1.8. References

1. Kretlow, J. D., Klouda, L. & Mikos, A. G. Injectable matrices and scaffolds for drug delivery in tissue engineering. *Advanced Drug Delivery Reviews* vol. 59 263–273 (2007).
2. Prasad, M. *et al.* Nanotherapeutics: An insight into healthcare and multi-dimensional applications in medical sector of the modern world. *Biomed. Pharmacother.* **97**, 1521–1537 (2018).
3. Kandil, R. & Merkel, O. M. Recent progress of polymeric nanogels for gene delivery. *Curr. Opin. Colloid Interface Sci.* **39**, 11–23 (2019).
4. Chacko, R. T., Ventura, J., Zhuang, J. & Thayumanavan, S. Polymer nanogels: A versatile nanoscopic drug delivery platform. *Adv. Drug Deliv. Rev.* **64**, 836–851 (2012).
5. Riedinger, A. *et al.* ‘Nanohybrids’ based on pH-responsive hydrogels and inorganic nanoparticles for drug delivery and sensor applications. *Nano Lett.* **11**, 3136–3141 (2011).
6. Zhou, S. *et al.* Facile fabrication of dextran-based fluorescent nanogels as potential glucose sensors. *Chem. Commun.* **49**, 9473–9475 (2013).
7. Maya, S. *et al.* Smart stimuli sensitive nanogels in cancer drug delivery and imaging: A review. *Curr. Pharm. Des.* **19**, 7203–7218 (2013).
8. Sivashanmugam, A., Arun Kumar, R., Vishnu Priya, M., Nair, S. V. & Jayakumar, R. An overview of injectable polymeric hydrogels for tissue engineering. *Eur. Polym. J.* **72**, 543–565 (2015).
9. Zhang, H., Zhai, Y., Wang, J. & Zhai, G. New progress and prospects: The application of nanogel in drug delivery. *Mater. Sci. Eng. C* **60**, 560–568 (2016).
10. Jalili, N. A., Jaiswal, M. K., Peak, C. W., Cross, L. M. & Gaharwar, A. K. Injectable nanoengineered stimuli-responsive hydrogels for on-demand and localized therapeutic delivery. *Nanoscale* **9**, 15379–15389 (2017).
11. Khoee, S. & Asadi, H. Nanogels: Chemical approaches to preparation. in *Encyclopedia of Biomedical Polymers and Polymeric Biomaterials* 5266–5293 (2016).
12. Sharmin, E. Chapter 3: Medical applications of nanogels. in *Nanogels for Biomedical Applications* 29–31 (RSC Smart Materials, 2018).
13. Alemán, J. V. *et al.* Definitions of terms relating to the structure and processing of sols, gels, networks, and inorganic-organic hybrid materials (IUPAC Recommendations 2007). *Pure Appl. Chem.* **79**, (2007).
14. Petros, R. A. & Desimone, J. M. Strategies in the design of nanoparticles for therapeutic applications. *Nat. Rev. Drug Discov.* **9**, 615–627 (2010).
15. Kokufuta, E., Ogawa, K., Doi, R., Kikuchi, R. & Farinato, R. S. Geometrical characteristics of polyelectrolyte nanogel particles and their polyelectrolyte complexes studied by dynamic and static light scattering. *J. Phys. Chem. B* **111**, 8634–8640 (2007).
16. Lakouraj, M. M., Mojerlou, F. & Zare, E. N. Nanogel and superparamagnetic nanocomposite based on sodium alginate for sorption of heavy metal ions. *Carbohydr. Polym.* **106**, 34–41 (2014).
17. Blackburn, W. H. & Lyon, L. A. Size-controlled synthesis of monodisperse core/shell nanogels. *Colloid Polym. Sci.* **286**, 563–569 (2008).

18. Wu, W., Shen, J., Banerjee, P. & Zhou, S. Core-shell hybrid nanogels for integration of optical temperature-sensing, targeted tumor cell imaging, and combined chemo-photothermal treatment. *Biomaterials* **31**, 7555–7566 (2010).
19. Picos-Corrales, L. A. *et al.* Core-shell nanogels by RAFT crosslinking polymerization: Synthesis and characterization. *J. Polym. Sci. Part A Polym. Chem.* **50**, 4277–4287 (2012).
20. Lu, A., Moatsou, D., Hands-Portman, I., Longbottom, D. A. & O'Reilly, R. K. Recyclable L-proline functional nanoreactors with temperature-tuned activity based on core-shell nanogels. *ACS Macro Lett.* **3**, 1235–1239 (2014).
21. Wu, W., Shen, J., Banerjee, P. & Zhou, S. Chitosan-based responsive hybrid nanogels for integration of optical pH-sensing, tumor cell imaging and controlled drug delivery. *Biomaterials* **31**, 8371–8381 (2010).
22. Artech Pujana, M., Pérez-Álvarez, L., Cesteros Iturbe, L. C. & Katime, I. Biodegradable chitosan nanogels crosslinked with genipin. *Carbohydr. Polym.* **94**, 836–842 (2013).
23. Oh, J. K., Siegwart, D. J. & Matyjaszewski, K. Synthesis and biodegradation of nanogels as delivery carriers for carbohydrate drugs. *Biomacromolecules* **8**, 3326–3331 (2007).
24. Daoud-Mahammed, S. *et al.* Cyclodextrin and polysaccharide-based nanogels: Entrapment of two hydrophobic molecules, benzophenone and tamoxifen. *Biomacromolecules* **10**, 547–554 (2009).
25. Wu, Z., Zhang, X., Guo, H., Li, C. & Yu, D. An injectable and glucose-sensitive nanogel for controlled insulin release. *J. Mater. Chem.* **22**, 22788–22796 (2012).
26. Lee, H., Mok, H., Lee, S., Oh, Y. K. & Park, T. G. Target-specific intracellular delivery of siRNA using degradable hyaluronic acid nanogels. *J. Control. Release* **119**, 245–252 (2007).
27. Bencherif, S. A., Washburn, N. R. & Matyjaszewski, K. Synthesis by AGET ATRP of degradable nanogel precursors for *in situ* formation of nanostructured hyaluronic acid hydrogel. *Biomacromolecules* **10**, 2499–2507 (2009).
28. Wei, X., Senanayake, T. H., Warren, G. & Vinogradov, S. V. Hyaluronic acid-based nanogel–drug conjugates with enhanced anticancer activity designed for the targeting of CD44-positive and drug-resistant tumors. *Bioconjug. Chem.* **24**, 658–668 (2013).
29. Yang, C. *et al.* Hyaluronic acid nanogels with enzyme-sensitive crosslinking group for drug delivery. *J. Control. Release* **205**, 206–217 (2015).
30. Bae, K. H., Mok, H. & Park, T. G. Synthesis, characterization, and intracellular delivery of reducible heparin nanogels for apoptotic cell death. *Biomaterials* **29**, 3376–3383 (2008).
31. Hoon, J., Young, J., Ki, Y., Hee, M. & Dong, K. Intracellular delivery and anti-cancer effect of self-assembled heparin-pluronic nanogels with RNase A. *J. Control. Release* **147**, 420–427 (2010).
32. Nguyen, D. H., Hoon Choi, J., Ki Joung, Y. & Dong Park, K. Disulfide-crosslinked heparin-pluronic nanogels as a redox-sensitive nanocarrier for intracellular protein delivery. *J. Bioact. Compat. Polym.* **26**, 287–300 (2011).
33. Bhatia, S. Natural Polymers vs Synthetic Polymer. in *Natural Polymer Drug Delivery Systems* 95-118 (Springer International Publishing, 2016).
34. Molina, M. *et al.* Stimuli-responsive nanogel composites and their application in nanomedicine. *Chem. Soc. Rev.* **44**, 6161–6186 (2015).
35. Schattling, P., Jochum, F. D. & Theato, P. Multi-stimuli responsive polymers-the all-in-one talents. *Polym. Chem.* **5**, 25–36 (2014).

-
36. Cabane, E., Zhang, X., Langowska, K., Palivan, C. G. & Meier, W. Stimuli-responsive polymers and their applications in nanomedicine. *Biointerphases* vol. 7 1–27 (2012).
 37. Ganesh, V. A., Baji, A. & Ramakrishna, S. RSC Advances Smart functional polymers – A new route towards creating a sustainable environment. *RSC Adv.* **4**, 53352–53364 (2014).
 38. Schmaljohann, D. Thermo- and pH-responsive polymers in drug delivery. *Advanced Drug Delivery Reviews* vol. 58 1655–1670 (2006).
 39. Wang, T. *et al.* Electroactive polymers for sensing. *Interface Focus* **6**, 20160026 (2016).
 40. Filipcsei, G., Csetneki, I., Szilágyi, A. & Zrínyi, M. Magnetic field-responsive smart polymer composites. *Advances in Polymer Science* vol. 206 137–189 (2007).
 41. Timko, B. P. & Kohane, D. S. Prospects for near-infrared technology in remotely triggered drug delivery. *Expert Opin. Drug Deliv.* **11**, 1681–1685 (2014).
 42. Schroeder, A., Kost, J. & Barenholz, Y. Ultrasound, liposomes, and drug delivery: Principles for using ultrasound to control the release of drugs from liposomes. *Chemistry and Physics of Lipids* vol. 162 1–16 (2009).
 43. Heskins, M. & Guillet, J. E. Solution Properties of Poly(*N*-isopropylacrylamide). *J. Macromol. Sci. Part A-Chem.* **2**, 1441–1455 (1968).
 44. Schild, H. G. & Tirrell, D. A. Microcalorimetric detection of lower critical solution temperatures in aqueous polymer solutions. *J. Phys. Chem.* **94**, 4352–4356 (1990).
 45. Idziak, I., Avoce, D., Lessard, D., Gravel, D. & Zhu, X. X. Thermosensitivity of aqueous solutions of Poly(*N,N*-diethylacrylamide). *Macromolecules* **32**, 1260–1263 (1999).
 46. Kirsh, Y. E., Yanul, N. A. & Popkov, Y. M. Temperature behavior of thermo-responsive poly(*N*-vinylcaprolactam) and poly(*N*-isopropylmethacrylamide) in aqueous solutions involving organic solutes. *Eur. Polym. J.* **38**, 403–406 (2002).
 47. Badi, N. Non-linear PEG-based thermoresponsive polymer systems. *Prog. Polym. Sci.* **66**, 54–79 (2017).
 48. Niskanen, J. & Tenhu, H. How to manipulate the upper critical solution temperature (UCST) *Polym. Chem.* **8**, 220–232 (2017).
 49. Palza, H., Zapata, P. A. & Angulo-Pineda, C. Electroactive smart polymers for biomedical applications. *Materials (Basel)*. **12**, 277 (2019).
 50. Bertrand, O. & Gohy, J. F. Photo-responsive polymers: Synthesis and applications. *Polym. Chem.* **8**, 52–73 (2017).
 51. Ward, M. A. & Georgiou, T. K. Thermoresponsive polymers for biomedical applications. *Polymers (Basel)*. **3**, 1215–1242 (2011).
 52. Zhang, Q., Weber, C., Schubert, U. S. & Hoogenboom, R. Thermoresponsive polymers with lower critical solution temperature: From fundamental aspects and measuring techniques to recommended turbidimetry conditions. *Mater. Horizons* **4**, 109–116 (2017).
 53. Hoogenboom, R. Chapter 2: Temperature-responsive polymers: Properties, synthesis and applications. in *Smart Polymers and their Applications* (Eds. Aguilar, M. R. & San Román, J.) 15-44 (Woodhead Publishing Limited, 2014).
 54. Kuckling, D., Vo, C. D. & Wohlrab, S. E. Preparation of nanogels with temperature-responsive core and pH-responsive arms by photo-crosslinking. *Langmuir* **18**, 4263–4269 (2002).
-

-
55. Xu, Y., Li, Y., Cao, X., Chen, Q. & An, Z. Versatile RAFT dispersion polymerization in cononsolvents for the synthesis of thermoresponsive nanogels with controlled composition, functionality and architecture. *Polym. Chem.* **5**, 6244–6255 (2014).
 56. Grazon, C., Rieger, J., Sanson, N. & Charleux, B. Study of poly(*N,N*-diethylacrylamide) nanogel formation by aqueous dispersion polymerization of *N,N*-diethylacrylamide in the presence of poly(ethylene oxide)-*b*-poly(*N,N*-dimethylacrylamide) amphiphilic macromolecular RAFT agents. *Soft Matter* **7**, 3482–3490 (2011).
 57. Macchione, M. A. *et al.* Poly(*N*-vinylcaprolactam) nanogels with antiviral behavior against HIV-1 infection. *Sci. Rep.* **9**, 1–10 (2019).
 58. Cao, Z., Zhou, X. & Wang, G. Selective release of hydrophobic and hydrophilic cargos from multistimuli-responsive nanogels. *ACS Appl. Mater. Interfaces* **8**, 28888–28896 (2016).
 59. Fu, W. *et al.* UCST-type thermosensitive hairy nanogels synthesized by RAFT polymerization-induced self-assembly. *ACS Macro Lett.* **6**, 127–133 (2017).
 60. Zhang, L., Liu, W., Lin, L., Chen, D. & Stenzel, M. H. Degradable disulfide core-crosslinked micelles as a drug delivery system prepared from vinyl functionalized nucleosides *via* the RAFT process. *Biomacromolecules* **9**, 3321–3331 (2008).
 61. Tian, Y., Bian, S. & Yang, W. A redox-labile poly(oligo(ethylene glycol)methacrylate)-based nanogel with tunable thermosensitivity for drug delivery. *Polym. Chem.* **7**, 1913–1921 (2016).
 62. Li, X. *et al.* Redox/temperature responsive nonionic nanogel and photonic crystal hydrogel: Comparison between *N,N'*-Bis(acryloyl)cystamine and *N,N'*-methylenebisacrylamide. *Polymer (Guildf)*. **137**, 112–121 (2018).
 63. You, Y. Z., Manickam, D. S., Zhou, Q. H. & Oupický, D. Reducible poly(2–dimethylaminoethyl methacrylate): Synthesis, cytotoxicity, and gene delivery activity. *J. Control. Release* **122**, 217–225 (2007).
 64. Li, C. *et al.* PEGylated poly(diselenide-phosphate) nanogel as efficient self-delivery nanomedicine for cancer therapy. *Polym. Chem.* **6**, 6498–6508 (2015).
 65. Tian, Y. *et al.* Near-infrared light-responsive nanogels with diselenide–crosslinkers for on-demand degradation and triggered drug release. *Part. Part. Syst. Charact.* **32**, 547–551 (2015).
 66. Zhai, S., Hu, X., Hu, Y., Wu, B. & Xing, D. Visible light-induced crosslinking and physiological stabilization of diselenide-rich nanoparticles for redox-responsive drug release and combination chemotherapy. *Biomaterials* **121**, 41–54 (2017).
 67. Nagel, B., Warsinke, A. & Katterle, M. Enzyme activity control by responsive redoxpolymers. *Langmuir* **23**, 6807–6811 (2007).
 68. Mazurowski, M. *et al.* Redox-responsive polymer brushes grafted from polystyrene nanoparticles by means of surface initiated atom transfer radical polymerization. *Macromolecules* **45**, 8970–8981 (2012).
 69. Zhang, J. *et al.* A simple mechanical agitation method to fabricate chitin nanogels directly from chitin solution and subsequent surface modification. *J. Mater. Chem. B* **7**, 2226–2232 (2019).
 70. Schattling, P., Jochum, F. D. & Theato, P. Multi-stimuli responsive polymers – The all-in-one talents. *Polym. Chem.* **5**, 25–36 (2014).
 71. Ulański, P., Kadlubowski, S. & Rosiak, J. M. Synthesis of poly(acrylic acid) nanogels by preparative pulse radiolysis. *Radiat. Phys. Chem.* **63**, 533–537 (2002).
-

-
72. Park, J. S., Yang, H. N., Woo, D. G., Jeon, S. Y. & Park, K. H. Poly(*N*-isopropylacrylamide-*co*-acrylic acid) nanogels for tracing and delivering genes to human mesenchymal stem cells. *Biomaterials* **34**, 8819–8834 (2013).
 73. Chen, Y. *et al.* Hybrid Fe₃O₄-poly(acrylic acid) nanogels for theranostic cancer treatment. *J. Biomed. Nanotechnol.* **11**, 771–779 (2015).
 74. Liu, T. *et al.* The use of poly(methacrylic acid) nanogel to control the release of amoxicillin with lower cytotoxicity. *Mater. Sci. Eng. C* **43**, 622–629 (2014).
 75. Chen, T. *et al.* Design and in vitro evaluation of a novel poly(methacrylic acid)/metronidazole antibacterial nanogel as an oral dosage form. *Colloids Surfaces B Biointerfaces* **118**, 65–71 (2014).
 76. Zhong, J. X., Clegg, J. R., Ander, E. W. & Peppas, N. A. Tunable poly(methacrylic acid-*co*-acrylamide) nanoparticles through inverse emulsion polymerization. *J. Biomed. Mater. Res. Part A* **106**, 1677–1686 (2018).
 77. Park, C. W., Yang, H. M., Lee, H. J. & Kim, J. D. Core-shell nanogel of PEG-poly(aspartic acid) and its pH-responsive release of RH-insulin. *Soft Matter* **9**, 1781–1788 (2013).
 78. Sim, T. *et al.* Development of pH-sensitive nanogels for cancer treatment using crosslinked poly(aspartic acid-graft-imidazole)-*block*-poly(ethylene glycol). *J. Appl. Polym. Sci.* **135**, 46268 (2018).
 79. Ding, J. *et al.* pH and dual redox responsive nanogel based on poly(L-glutamic acid) as potential intracellular drug carrier. *J. Control. Release* **152**, e11–e13 (2011).
 80. Yan, S. *et al.* Templated fabrication of pH-responsive poly(L-glutamic acid) based nanogels *via* surface-grafting and macromolecular crosslinking. *RSC Adv.* **7**, 14888–14901 (2017).
 81. Wu, W., Mitra, N., Yan, E. C. Y. & Zhou, S. Multifunctional hybrid nanogel for integration of optical glucose sensing and self-regulated insulin release at physiological pH. *ACS Nano* **4**, 4831–4839 (2010).
 82. Lacík, I. *et al.* SEC analysis of poly(acrylic acid) and poly(methacrylic acid). *Macromol. Chem. Phys.* **216**, 23–37 (2015).
 83. Sengel, S. B. & Sahiner, N. Poly(vinyl phosphonic acid) nanogels with tailored properties and their use for biomedical and environmental applications. *Eur. Polym. J.* **75**, 264–275 (2016).
 84. Felberg, L. E. *et al.* Structural transition of nanogel star polymers with pH by controlling PEGMA interactions with acid or base copolymers. *Mol. Phys.* **114**, 3221–3231 (2016).
 85. Brannigan, R. P. & Khutoryanskiy, V. V. Synthesis and evaluation of mucoadhesive acryloyl-quaternized PDMAEMA nanogels for ocular drug delivery. *Colloids Surfaces B Biointerfaces* **155**, 538–543 (2017).
 86. Hajebi, S., Abdollahi, A., Roghani-Mamaqani, H. & Salami-Kalajahi, M. Hybrid and hollow Poly(*N,N*-dimethylaminoethyl methacrylate) nanogels as stimuli-responsive carriers for controlled release of doxorubicin. *Polymer (Guildf)*. **180**, 121716 (2019).
 87. Oishi, M., Hayashi, H., Itaka, K., Kataoka, K. & Nagasaki, Y. pH-Responsive PEGylated nanogels as targetable and low invasive endosomolytic agents to induce the enhanced transfection efficiency of nonviral gene vectors. *Colloid Polym. Sci.* **285**, 1055–1060 (2007).
 88. Aguirre, G., Ramos, J. & Forcada, J. Advanced design of t and pH dual-responsive PDEAEMA-PVCL core-shell nanogels for siRNA delivery. *J. Polym. Sci. Part A Polym. Chem.* **54**, 3203–3217 (2016).
-

-
89. Pikabea, A., Ramos, J., Papachristos, N., Stamopoulos, D. & Forcada, J. Synthesis and characterization of PDEAEMA-based magneto-nanogels: Preliminary results on the biocompatibility with cells of human peripheral blood. *J. Polym. Sci. Part A Polym. Chem.* **54**, 1479–1494 (2016).
 90. Sahiner, N., Ozay, O. & Aktas, N. 4-Vinylpyridine-based smart nanoparticles with *N*-isopropylacrylamide, 2-hydroxyethyl methacrylate, acrylic acid, and methacrylic acid for potential biomedical applications. *Curr. Nanosci.* **7**, 453–462 (2011).
 91. Pujana, M. A., Pérez-Álvarez, L., Iturbe, L. C. C. & Katime, I. Water dispersible pH-responsive chitosan nanogels modified with biocompatible crosslinking-agents. *Polym.* **53**, 3107–3116 (2012).
 92. Lee, E. S. *et al.* Super pH-sensitive multifunctional polymeric micelle for tumor pH specific TAT exposure and multidrug resistance. *J. Control. Release* **129**, 228–236 (2008).
 93. Bilalis, P. *et al.* Preparation of hybrid triple-stimuli responsive nanogels based on poly(L-histidine). *J. Polym. Sci. Part A Polym. Chem.* **54**, 1278–1288 (2016).
 94. Koziolok, M. *et al.* Investigation of pH and temperature profiles in the GI tract of fasted human subjects using the Intellicap® System. *J. Pharm. Sci.* **104**, 2855–2863 (2015).
 95. Bhagavan, N. V. & Ha, C.E. Chapter 37: Water, electrolytes, and acid–base balance. in *Essentials of Medical Biochemistry* 701–713 (Elsevier, 2015).
 96. Nová, L., Uhlík, F. & Košovan, P. Local pH and effective pK_a of weak polyelectrolytes-insights from computer simulations. *Phys. Chem. Chem. Phys.* **19**, 14376–14387 (2017).
 97. Visakh, P. M. Chapter 1: Polyelectrolyte: Thermodynamics and rheology. in *Polyelectrolytes* 1–17 (Springer, 2014).
 98. Reyes-Ortega, F. Chapter 3: pH-responsive polymers: properties, synthesis and applications. in *Smart Polymers and their Applications* (eds. Aguilar, M. R. & San Román, J.) 45–92 (Elsevier, 2014).
 99. Priya James, H., John, R., Alex, A. & Anoop, K. R. Smart polymers for the controlled delivery of drugs – A concise overview. *Acta Pharm. Sin. B* **4**, 120–127 (2014).
 100. Roy, D., Cambre, J. N. & Sumerlin, B. S. Future perspectives and recent advances in stimuli-responsive materials. *Progress in Polymer Science* **35** 278–301 (2010).
 101. Webber, M. J. & Anderson, D. G. Smart approaches to glucose-responsive drug delivery. *Journal of Drug Targeting* vol. 23 651–655 (2015).
 102. Ansuja Pulickal, M., Uthaman, S., Cho, C.S. & Park, I.-K. Chapter 11: Injectable nanogels in drug delivery. in *Nanogels for Biomedical Applications*, 181–209 (RSC Smart Materials, 2017).
 103. Yallapu, M. M., Jaggi, M. & Chauhan, S. C. Design and engineering of nanogels for cancer treatment. *Drug Discov. Today* **16**, 457–463 (2011).
 104. Akiyoshi, K., Deguchi, S., Moriguchi, N., Yamaguchi, S. & Sunamoto, J. Self-aggregates of hydrophobized polysaccharides in water. Formation and Characteristics of Nanoparticles. *Macromolecules* **26**, 3062–3068 (1993).
 105. Akiyama, Y., Fujiwara, T., Takeda, S. I., Izumi, Y. & Nishijima, S. Preparation of stimuli-responsive protein nanogel by quantum-ray irradiation. *Colloid Polym. Sci.* **285**, 801–807 (2007).
 106. Quiñones, J. P., Peniche, H. & Peniche, C. Chitosan based self-assembled nanoparticles in drug delivery. *Polymers (Basel)*. **10**, 235 (2018).
-

-
107. Hrubý, M., Filippov, S. K. & Štěpánek, P. Chapter 8: Biomedical application of block copolymers. in *Macromolecular Self-assembly* (eds. Billon, L. & Borisov, O.) 231–250 (John Wiley & Sons, Inc., 2016).
 108. Zhang, X., Malhotra, S., Molina, M. & Haag, R. Micro- and nanogels with labile crosslinks-from synthesis to biomedical applications. *Chem. Soc. Rev.* **44**, 1948–1973 (2015).
 109. Rolland, J. P. *et al.* Direct fabrication and harvesting of monodisperse, shape-specific nanobiomaterials. *J. Am. Chem. Soc.* **127**, 10096–10100 (2005).
 110. Gratton, S. E. A. *et al.* Nanofabricated particles for engineered drug therapies: A preliminary biodistribution study of PRINT™ nanoparticles. *J. Control. Release* **121**, 10–18 (2007).
 111. Ghosh, S., Basu, S. & Thayumanavan, S. Simultaneous and reversible functionalization of copolymers for biological applications. *Macromolecules* **39**, 5595–5597 (2006).
 112. Ryu, J. H. *et al.* Self-crosslinked polymer nanogels: A versatile nanoscopic drug delivery platform. *J. Am. Chem. Soc.* **132**, 17227–17235 (2010).
 113. González-Toro, D. C., Ryu, J. H., Chacko, R. T., Zhuang, J. & Thayumanavan, S. Concurrent binding and delivery of proteins and lipophilic small molecules using polymeric nanogels. *J. Am. Chem. Soc.* **134**, 6964–6967 (2012).
 114. Li, L., Raghupathi, K., Yuan, C. & Thayumanavan, S. Surface charge generation in nanogels for activated cellular uptake at tumor-relevant pH. *Chem. Sci.* **4**, 3654–3660 (2013).
 115. Raghupathi, K., Li, L., Ventura, J., Jennings, M. & Thayumanavan, S. pH-responsive soft nanoclusters with size and charge variation features. *Polym. Chem.* **5**, 1737–1742 (2014).
 116. Ventura, J. *et al.* Reactive Self-assembly of polymers and proteins to reversibly silence a killer protein. *Biomacromolecules* **16**, 3161–3171 (2015).
 117. Jiang, Z., Cui, W., Mager, J. & Thayumanavan, S. Postfunctionalization of noncationic RNA-polymer complexes for RNA Delivery. *Ind. Eng. Chem. Res.* **58**, 6982–6991 (2019).
 118. Zhuang, J., Jiwanich, S., Deepak, V. D. & Thayumanavan, S. Facile preparation of nanogels using activated ester containing polymers. *ACS Macro Lett.* **1**, 175–179 (2012).
 119. Liu, B. & Thayumanavan, S. Substituent effects on the pH sensitivity of acetals and ketals and their correlation with encapsulation stability in polymeric nanogels. *J. Am. Chem. Soc.* **139**, 2306–2317 (2017).
 120. Tan, H. *et al.* PEG-urokinase nanogels with enhanced stability and controllable bioactivity. *Soft Matter* **8**, 2644–2650 (2012).
 121. Cao, X. T., Showkat, A. M. & Lim, K. T. Synthesis of nanogels of poly(ϵ -caprolactone)-*b*-poly(glycidyl methacrylate) by click chemistry in direct preparation. *Eur. Polym. J.* **68**, 267–277 (2015).
 122. Aktan, B., Chambre, L., Sanyal, R. & Sanyal, A. “Clickable” nanogels *via* thermally driven self-assembly of polymers: Facile access to targeted imaging platforms using thiol–maleimide conjugation. *Biomacromolecules* **18**, 490–497 (2017).
 123. He, J., Tong, X. & Zhao, Y. Photoresponsive nanogels based on photocontrollable crosslinks. *Macromolecules* **42**, 4845–4852 (2009).
 124. Lu, D. *et al.* Triply responsive coumarin-based microgels with remarkably large photo-switchable swelling. *Polym. Chem.* **10**, 2516–2526 (2019).
-

-
125. Choi, W. Il, Tae, G. & Kim, Y. H. One pot, single phase synthesis of thermo-sensitive nanocarriers by photo-crosslinking of a diacrylated pluronic. *J. Mater. Chem.* **18**, 2769–2774 (2008).
 126. Wang, Y. C. *et al.* Engineering nanoscopic hydrogels *via* photo-crosslinking salt-induced polymer assembly for targeted drug delivery. *Chem. Commun.* **46**, 3520–3522 (2010).
 127. Chen, W., Hou, Y., Tu, Z., Gao, L. & Haag, R. pH-degradable PVA-based nanogels *via* photo-crosslinking of thermo-preinduced nanoaggregates for controlled drug delivery. *J. Control. Release* **259**, 160–167 (2017).
 128. Zhao, L. *et al.* Synthesis of composite microgel capsules by ultrasonic spray combined with *in situ* crosslinking. *Soft Matter* **7**, 6144–6150 (2011).
 129. Cui, W. *et al.* pH gradient difference around ischemic brain tissue can serve as a trigger for delivering polyethylene glycol-conjugated urokinase nanogels. *J. Control. Release* **225**, 53–63 (2016).
 130. Sanson, N. & Rieger, J. Synthesis of nanogels/microgels by conventional and controlled radical crosslinking copolymerization. *Polym. Chem.* **1**, 965–977 (2010).
 131. Arshady, R. Suspension, emulsion, and dispersion polymerization: A methodological survey. *Colloid Polym. Sci.* **270**, 717–732 (1992).
 132. Anderson, C. D. & Daniels, E. S. *Emulsion Polymerisation and Applications of Latex.* (Rapra Review Reports, 2002).
 133. Kar, M. *et al.* Chapter 12: Responsive nanogels for anti-cancer therapy. in *Nanogels for Biomedical Applications* (eds. Vashist, A., Kaushik, A. K., Ahmad, S. & Nair, M.) 210–260 (RS, 2018).
 134. Antonietti, M., Bremser, W. & Schmidt, M. Microgels: model polymers for the crosslinked state. *Macromolecules* **23**, 3796–3805 (1990).
 135. Saunders, B. R. *et al.* Microgels: From responsive polymer colloids to biomaterials. *Adv. Colloid Interface Sci.* **147–148**, 251–262 (2009).
 136. Pich, A. & Richtering, W. Chapter 1: Microgels by precipitation polymerization: Synthesis, characterization, and functionalization. in *Chemical Design of Responsive Microgels* 1–37 (Springer, 2010).
 137. Milani, A. H. *et al.* Synthesis of polyacid nanogels: pH-responsive sub-100 nm particles for functionalisation and fluorescent hydrogel assembly. *Soft Matter* (2017).
 138. Matyjaszewski, K. & Spanswick, J. Controlled/living radical polymerization. *Mater. Today* **8**, 26–33 (2005).
 139. Jung, K. O. *et al.* Biodegradable nanogels prepared by atom transfer radical polymerization as potential drug delivery carriers: Synthesis, biodegradation, *in vitro* release, and bioconjugation. *J. Am. Chem. Soc.* **129**, 5939–5945 (2007).
 140. Pamfil, D. & Vasile, C. Chapter 4: Nanogels of Natural Polymers. in *Polymer Gels: Perspectives and Applications* (eds. Thakur, V. K., Thakur, M. K. & Voicu, S. I.) 71–110 (Springer, 2018).
 141. An, Z., Qiu, Q. & Liu, G. Synthesis of architecturally well-defined nanogels *via* RAFT polymerization for potential bioapplications. *Chem. Commun.* **47**, 12424–12440 (2011).
 142. Jenkins, A. D., Jones, R. G. & Moad, G. Terminology for reversible-deactivation radical polymerization previously called ‘controlled’ radical or ‘living’ radical polymerization (IUPAC Recommendations 2010). *Pure Appl. Chem.* **82**, 483–491 (2009).
-

-
143. Chiefari, J. *et al.* Living Free-Radical Polymerization by Reversible Addition-Fragmentation Chain-Transfer: The RAFT process. *Macromolecules* **31**, 5559–5562 (1998).
 144. Mayadunne, R. T. A. *et al.* Living Polymers by the use of trithiocarbonates as Reversible Addition-Fragmentation Chain-Transfer (RAFT) agents: ABA triblock copolymers by radical polymerization in two Steps. *Macromolecules* **33**, 243–245 (2000).
 145. Chiefari, J. *et al.* Thiocarbonylthio compounds (SC(Z)S–R) in free radical polymerization with Reversible Addition-Fragmentation Chain-Transfer (RAFT polymerization). Effect of the activating group Z. 2273–2283 (2003).
 146. Chong, Y. K. *et al.* Thiocarbonylthio compounds [SC(Ph)S–R] in free radical polymerization with Reversible Addition-Fragmentation Chain-Transfer (RAFT Polymerization). Role of the free-radical leaving group (R). *Macromolecules* **36**, 2256–2272 (2003).
 147. Creton, C. 50th Anniversary perspective: Networks and Gels: Soft but dynamic and tough. *Macromolecules* vol. 50 8297–8316 (2017).
 148. Moad, G., Rizzardo, E. & Thang, S. H. Living radical polymerization by the RAFT process. *Aust. J. Chem.* **58**, 379–410 (2005).
 149. Perrier, S. 50th Anniversary Perspective: RAFT Polymerization – A User Guide. *Macromolecules* **50**, 7433–7447 (2017).
 150. Odian, G. Principles of Polymerization. *Princ. Polym. Wiley sons* (2004).
 151. Moad, G., Rizzardo, E. & Thang, S. H. Living Radical Polymerization by the RAFT Process – A first update. *Aust. J. Chem.* **59**, 669–692 (2006).
 152. Moad, G., Rizzardo, E. & Thang, S. H. Radical Addition-Fragmentation chemistry in polymer synthesis. *Polymer (Guildf)*. **49**, 1079–1131 (2008).
 153. Keddie, D. J., Moad, G., Rizzardo, E. & Thang, S. H. RAFT agent design and synthesis. *Macromolecules* **45**, 5321–5342 (2012).
 154. Fairbanks, B. D., Gunatillake, P. A. & Meagher, L. Biomedical applications of polymers derived by Reversible Addition-Fragmentation chain-Transfer (RAFT). *Adv. Drug Deliv. Rev.* **91**, 141–152 (2015).
 155. Pissuwan, D., Boyer, C., Gunasekaran, K., Davis, T. P. & Bulmus, V. *In vitro* cytotoxicity of RAFT polymers. *Biomacromolecules* **11**, 412–420 (2010).
 156. Willcock, H. & O’Reilly, R. K. End group removal and modification of RAFT polymers. *Polym. Chem.* **1**, 149–157 (2010).
 157. Taton, D. *et al.* Water soluble polymeric nanogels by xanthate-mediated radical crosslinking copolymerisation. *Chem. Commun.* 1953 (2006).
 158. Poly, J., Wilson, D. J., Destarac, M. & Taton, D. A comprehensive investigation into “controlled/living” chain growth crosslinking copolymerization including a back to basics modeling. *J. Polym. Sci. Part A Polym. Chem.* **47**, 5313–5327 (2009).
 159. Poly, J. *et al.* Nanogels Based on Poly(vinyl acetate) for the preparation of patterned porous films. *Langmuir* **27**, 4290–4295 (2011).
 160. Kurniasih, I. N., Keilitz, J. & Haag, R. Dendritic nanocarriers based on hyperbranched polymers. *Chem. Soc. Rev.* **44**, 4145–4164 (2015).
-

-
161. Qi, G., Jones, C. W. & Schork, F. J. RAFT Inverse miniemulsion polymerization of acrylamide. *Macromol. Rapid Commun.* **28**, 1010–1016 (2007).
 162. Li, W., Matyjaszewski, K., Albrecht, K. & Möller, M. Reactive surfactants for polymeric nanocapsules *via* interfacially confined miniemulsion ATRP. *Macromolecules* **42**, 8228–8233 (2009).
 163. Asua, J. M. Challenges for industrialization of miniemulsion polymerization. *Prog. Polym. Sci.* **39**, 1797–1826 (2014).
 164. Canning, S. L., Smith, G. N. & Armes, S. P. A Critical appraisal of RAFT-mediated Polymerization-Induced Self-Assembly. *Macromolecules* **49**, 1985–2001 (2016).
 165. Blanazs, A., Armes, S. P. & Ryan, A. J. Self-Assembled block copolymer aggregates: From micelles to vesicles and their biological applications. *Macromol. Rapid Commun.* **30**, 267–277 (2009).
 166. Israelachvili, J. N. Chapter 20: Soft and biological structures. in *Intermolecular and Surface Forces* 535–576 (Elsevier, 2011).
 167. Wan, W.M., Hong, C.Y. & Pan, C.Y. One-pot synthesis of nanomaterials *via* RAFT Polymerization Induced Self-Assembly and morphology transition. *Chem. Commun.* 5883–5885 (2009).
 168. Charleux, B., Delaitre, G., Rieger, J. & D’Agosto, F. Polymerization-Induced Self-Assembly: from soluble macromolecules to block copolymer nano-objects in one step. *Macromolecules* **45**, 6753–6765 (2012).
 169. Warren, N. J. & Armes, S. P. Polymerization-Induced Self-Assembly of block copolymer nano-objects *via* RAFT aqueous dispersion polymerization. *J. Am. Chem. Soc.* **136**, 10174–10185 (2014).
 170. Derry, M. J., Fielding, L. A. & Armes, S. P. Polymerization-Induced Self-Assembly of block copolymer nanoparticles *via* RAFT non-aqueous dispersion polymerization. *Prog. Polym. Sci.* **52**, 1–18 (2016).
 171. Penfold, N. J. W., Yeow, J., Boyer, C. & Armes, S. P. Emerging trends in Polymerization-Induced Self-Assembly. *ACS Macro Lett.* **8**, 1029–1054 (2019).
 172. Zhang, W.J., Hong, C.Y. & Pan, C.Y. Polymerization-Induced Self-Assembly of functionalized block copolymer nanoparticles and their application in drug delivery. *Macromol. Rapid Commun.* **40**, 1800279 (2019).
 173. D’Agosto, F., Rieger, J. & Lansalot, M. RAFT-mediated Polymerization-Induced Self-Assembly. *Angew. Chemie Int. Ed.* **59**, 8368–8392 (2020).
 174. Wang, X. & An, Z. New Insights into RAFT dispersion Polymerization-Induced Self-Assembly: from monomer library, morphological control, and stability to driving forces. *Macromol. Rapid Commun.* **40**, 1800325 (2019).
 175. Blanazs, A., Madsen, J., Battaglia, G., Ryan, A. J. & Armes, S. P. Mechanistic insights for block copolymer morphologies: How do worms form vesicles? *J. Am. Chem. Soc.* **133**, 16581–16587 (2011).
 176. Blanazs, A., Ryan, A. J. & Armes, S. P. Predictive phase diagrams for RAFT aqueous dispersion polymerization: Effect of block copolymer composition, molecular weight, and copolymer concentration. *Macromolecules* **45**, 5099–5107 (2012).
 177. Warren, N. J., Mykhaylyk, O. O., Mahmood, D., Ryan, A. J. & Armes, S. P. RAFT aqueous dispersion polymerization yields poly(ethylene glycol)-based diblock copolymer nano-objects with predictable single phase morphologies. *J. Am. Chem. Soc.* **136**, 1023–1033 (2014).
-

-
178. Zhou, W., Qu, Q., Xu, Y. & An, Z. Aqueous Polymerization-Induced Self-Assembly for the Synthesis of ketone-functionalized nano-objects with low polydispersity. *ACS Macro Lett.* **4**, 495-499 (2015).
179. Byard, S. J., Williams, M., McKenzie, B. E., Blanz, A. & Armes, S. P. Preparation and crosslinking of all-acrylamide diblock copolymer nano-objects *via* Polymerization-Induced Self-Assembly in aqueous solution. *Macromolecules* **50**, 1482–1493 (2017).
180. Wang, X., Zhou, J., Lv, X., Zhang, B. & An, Z. Temperature-induced morphological transitions of poly(dimethylacrylamide)–poly(diacetone acrylamide) block copolymer lamellae synthesized *via* aqueous Polymerization-Induced Self-Assembly. *Macromolecules* **50**, 7222–7232 (2017).
181. Liu, G., Qiu, Q., Shen, W. & An, Z. Aqueous dispersion polymerization of 2-methoxyethyl acrylate for the synthesis of biocompatible nanoparticles using a hydrophilic raft polymer and a redox initiator. *Macromolecules* **44**, 5237–5245 (2011).
182. Liu, G., Qiu, Q. & An, Z. Development of thermosensitive copolymers of poly(2-methoxyethyl acrylate-co-poly(ethylene glycol) methyl ether acrylate) and their nanogels synthesized by RAFT dispersion polymerization in water. *Polym. Chem.* **3**, 504–513 (2012).
183. An, Z. *et al.* Facile raft precipitation polymerization for the microwave-assisted synthesis of well-defined, double hydrophilic block copolymers and nanostructured hydrogels. *J. Am. Chem. Soc.* **129**, 14493–14499 (2007).
184. Hou, L., Ma, K., An, Z. & Wu, P. Exploring the volume phase transition behavior of POEGA- and PNIPAM-based core-shell nanogels from Infrared-Spectral insights. *Macromolecules* **47**, 1144-1154 (2014).
185. Figg, C. A. *et al.* Polymerization-Induced Thermal Self-Assembly (PITSA). *Chem. Sci.* **6**, 1230–1236 (2015).
186. Shen, W. *et al.* Biocompatible, antifouling, and thermosensitive core-shell nanogels synthesized by RAFT aqueous dispersion polymerization. *Macromolecules* **44**, 2524–2530 (2011).
187. Cunningham, V. J., Derry, M. J., Fielding, L. A., Musa, O. M. & Armes, S. P. RAFT aqueous dispersion polymerization of N-(2-(methacryloyloxy)ethyl)pyrrolidone: A convenient low viscosity route to high molecular weight water-soluble copolymers. *Macromolecules* **49**, 4520-4533 (2016).
188. Gurnani, P. & Perrier, S. Controlled radical polymerization in dispersed systems for biological applications. *Prog. Polym. Sci.* **102**, 101209 (2020).
189. Rieger, J., Gazon, C., Charleux, B., Alaimo, D. & Jérôme, C. Pegylated thermally responsive block copolymer micelles and nanogels *via in situ* RAFT aqueous dispersion polymerization. *J. Polym. Sci. Part A Polym. Chem.* **47**, 2373–2390 (2009).
190. Gazon, C., Rieger, J., Sanson, N. & Charleux, B. Study of poly(*N,N*-diethylacrylamide) nanogel formation by aqueous dispersion polymerization of *N,N*-diethylacrylamide in the presence of poly(ethylene oxide)-*b*-poly(*N,N*-dimethylacrylamide) amphiphilic macromolecular RAFT agents. *Soft Matter* **7**, 3482–3490 (2011).
191. Yan, L. & Tao, W. One-step synthesis of pegylated cationic nanogels of poly(*N,N'*-dimethylaminoethyl methacrylate) in aqueous solution *via* self-stabilizing micelles using an amphiphilic macroRAFT agent. *Polymer (Guildf)*. **51**, 2161–2167 (2010).
192. Ahmed, M. & Narain, R. Intracellular delivery of DNA and enzyme in active form using degradable carbohydrate-based nanogels. *Mol. Pharm.* **9**, 3160–3170 (2012).
193. Narain, R., Wang, Y., Ahmed, M., Lai, B. F. L. & Kizhakkedathu, J. N. Blood components interactions to ionic and nonionic glyconanogels. *Biomacromolecules* **16**, 2990–2997 (2015).
-

-
194. Bhuchar, N., Sunasee, R., Ishihara, K., Thundat, T. & Narain, R. Degradable thermoresponsive nanogels for protein encapsulation and controlled release. *Bioconjug. Chem.* **23**, 75–83 (2012).
 195. Kotsuchibashi, Y. & Narain, R. Dual-temperature and pH responsive (ethylene glycol)-based nanogels *via* structural design. *Polym. Chem.* **5**, 3061–3070 (2014).
 196. Sunasee, R., Wattanaarsakit, P., Ahmed, M., Lollmahomed, F. B. & Narain, R. Biodegradable and nontoxic nanogels as nonviral gene delivery systems. *Bioconjug. Chem.* **23**, 1925–1933 (2012).
 197. Singhsa, P., Manuspiya, H. & Narain, R. Study of the RAFT homopolymerization and copolymerization of N-[3-(dimethylamino)propyl]methacrylamide hydrochloride and evaluation of the cytotoxicity of the resulting homo- and copolymers. *Polym. Chem.* **8**, 4140–4151 (2017).
 198. Ma, K., Xu, Y. & An, Z. Templateless synthesis of polyacrylamide-based nanogels *via* RAFT dispersion polymerization. *Macromol. Rapid Commun.* **36**, 566–570 (2015).
 199. Li, Y. *et al.* Formation of multidomain hydrogels *via* thermally induced assembly of PISA-generated triblock terpolymer nanogels. *Macromolecules* **49**, 3038–3048 (2016).
 200. Crowther, H. M. & Vincent, B. Swelling behavior of poly(*N*-isopropylacrylamide) microgel particles in alcoholic solutions. *Colloid Polym. Sci.* **276**, 46–51 (1998).

CHAPTER 2

Anionic nanogels:
The effects of cononsolvents on
their synthesis and properties

2.1. Chapter outlook

In this chapter, RAFT dispersion polymerisation is utilised for the preparation of poly(acrylic acid)-*block*-poly(*N*-isopropylacrylamide-*stat*-*N,N'*-methylenebisacrylamide) (PAA-*b*-P(NIPAM-*st*-BIS)) anionic nanogels. An evaluation of the effects of synthesising PNIPAM nanogels in either water or water-ethanol mixtures is presented as this approach is thought to affect the solvency of the growing PNIPAM chains and thus can influence the critical chain length for the self-assembly. Additionally, the effects of the length of the shell-stabiliser block (PAA_x) and of the core-forming block of NIPAM and BIS on the size and morphology of the nanogels is investigated for the synthesis of nanogels in either water or consolvents. An in-depth analysis of a series of uncrosslinked PAA-*b*-PNIPAM diblock copolymers is also presented by more precise techniques, as a way to elucidate the effects of the synthesis in consolvents on the properties of these materials.

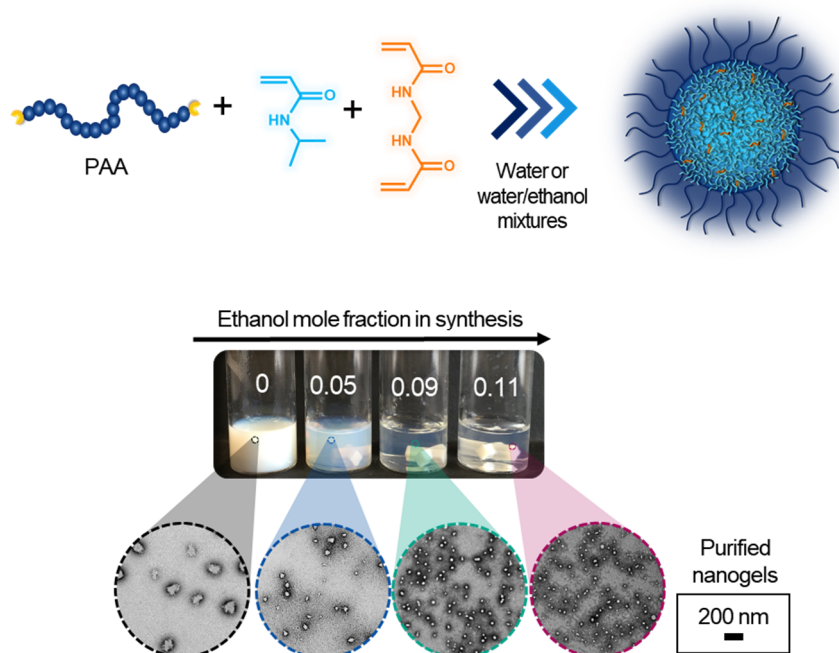


Figure 2.1: The schematic representation of the effects of the synthesis con solvent composition on the size of a range of anionic nanogels prepared *via* RAFT dispersion polymerisation.

2.2. Introduction

The use of RAFT dispersion polymerisation for the synthesis of nanogels has proven to be advantageous over other techniques since these can be prepared from monomers with various functionalities under mild reaction conditions at relatively high solids content.¹ Particularly, the use of water as a dispersing medium is attractive as a way to avoid the use of potentially toxic solvents in the production of materials for intended biomedical applications. Besides, the nanogel formation by RAFT dispersion polymerisation is achieved in a surfactant-free process due to the compartmentalised reaction, in which the insoluble growing chains are stabilised by a hydrophilic macro-CTA. Indeed, the constraint of this approach is that the choice of monomers is limited to those that are inherently water-soluble and which growing chains become less soluble during polymerisation, e.g. monomers with polar and nonpolar moieties. Polymers with a temperature-dependent solubility can meet these requirements, which explains the growing interest in the synthesis of temperature-sensitive nanogels using this approach.^{2–7} Monomers such as *N,N'*-diethylacrylamide (DEAM),^{3,4} *N*-isopropylacrylamide (NIPAM),^{2,8–10} oligo(ethylene glycol) methacrylates (OEGMAs),⁵ oligo(ethylene glycol) acrylates (OEGAs),^{9,11} and 2-(dimethylamino)ethyl methacrylate (DMAEMA)¹² have been used to prepare nanogels *via* aqueous RAFT-mediated PISA. During polymerisation, these polymers become less soluble when a critical chain length is reached due to the reaction temperature being higher than their lower critical solution temperature (LCST). This then induces the precipitation of hydrophobic particle nuclei, where the polymerisation continues (Figure 2.2). For successful particle formation, the water-soluble macro-CTA must provide colloidal stability during the nanogel formation and must mediate the polymerisation of a vinyl monomer and a crosslinker (bifunctional monomer).¹³ Hence the assumption that these nanogels possess a hydrophobic core and a hydrophilic shell. The morphology and size of the nanogels *via* RAFT-mediated PISA thus depends on numerous parameters such as the type of RAFT agent and crosslinker used, the DP of the macro-CTA, and the molar ratios of crosslinker to macro-CTA and of monomer to macro-CTA.¹⁴

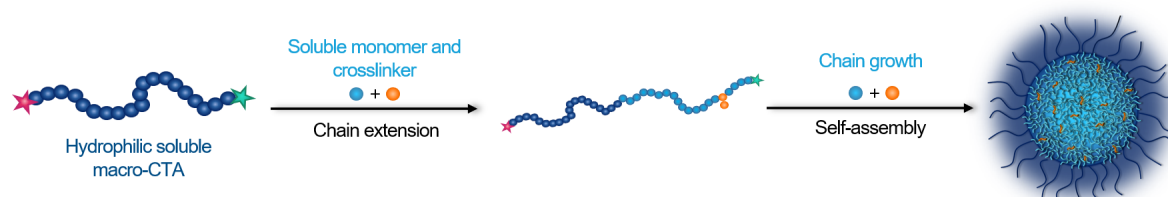


Figure 2.2: A schematic of the RAFT aqueous dispersion polymerisation for nanogel formation.

To expand the applicability of RAFT aqueous dispersion polymerisation to produce nanogels, researchers have explored the addition of another solvent to water to either include hydrophobic components (e.g. additional monomers) into the nanogel structure or to promote the immiscibility of growing chains during polymerisation. For obvious reasons, water is chosen as the major solvent and organic solvents with relative low toxicity such as 2-propanol,^{15–18} ethanol,^{19–21} or *tert*-butanol²² are used as the minor solvents, which ultimately can be easily removed by dialysis against water. For instance, the group of Narain has reported the use of a mixture of water and 2-propanol to produce a series of carbohydrate-based nanogels,^{15,18} and (ethylene glycol)-based nanogels^{16,17} using a CTA with a dithiobenzoate end-group. This water/2-propanol mixture increases the control over the chain extension due to an enhanced solubility of the end-group functionality and minimisation of the hydrolysis of the dithioester group.²³ Another example is the use of alcohols as cononsolvent pair with water, which can be used to decrease the solubility of the growing chains during polymerisation which in turn enhances the driving force for the *in situ* self-assembly.²⁴ Overall, the phenomenon of cononsolvency refers to a polymer being soluble in pure water and another good solvent (e.g. an alcohol) but insoluble in mixtures of these two at a certain concentration range.²⁵ Hence, nanogels that do not exhibit a temperature-dependent solubility, such as polyacrylamide-core nanogels, can be synthesised *via* a dispersion process in cononsolvents due to the reduction of the solvency of the growing polymer which drives to microphase separation.²² In the case of temperature-sensitive nanogels, a reduced solvency of polymers in cononsolvents can shift the critical solution temperature of polymers that exhibit an UCST or a LCST.^{26,27} For instance, the zwitterionic monomer 3-dimethyl(methacryloyloxyethyl) ammonium propanesulfonate (DMAPS), which exhibits an UCST in water, has been used for nanogel preparation in a mixture of water and ethanol.¹⁹ The suppression of the UCST allowed the formation of nanogels with a core of PDMAPS, which it is not feasible in only water due to an increase solubility of PDMAPS in water with high temperature. In the case of polymers with an LCST, PNIPAM has been subject of investigation to form nanogels in cononsolvents.^{20,21} For example, Xu *et al.*²⁰ used a mixture of water and ethanol to allow the incorporation of hydrophobic comonomers into nanogels, which is inaccessible for RAFT dispersion polymerisation in water. Thus proving that the addition of a cononsolvent can increase the solvation of hydrophobic components without disturbing the dispersion polymerisation process.²⁴ Interestingly, in all these studies only one cononsolvent composition was analysed for the synthesis of nanogels without studying the effect of the cononsolvents on the self-assembly. To this end, the cononsolvent composition was herein investigated for nanogel formation *via* a RAFT dispersion approach. PNIPAM was selected as the

thermoresponsive polymer since it has been widely investigated for biomedical applications due to its sharp LCST ($\sim 31\text{--}35\text{ }^{\circ}\text{C}$)^{28,29} near body temperature in aqueous media.^{30–36}

The cononsolvency of PNIPAM in water and organic solvents such as ethanol,^{20,37–39} methanol,^{26,40–42} THF,⁴³ DMSO,^{44,45} and acetone^{46,47} has been formerly reported. However, all of these studies synthesised the PNIPAM-based materials first and then dissolved them in con solvent mixtures as a way to investigate the thermodynamic behaviour between the polymer chains and solvent molecules at given compositions and temperatures. In the literature, Biswas *et al.*⁴⁸ have investigated the effect of the RAFT synthesis of PNIPAM in the presence of yttrium trifluoromethanesulfonate ($\text{Y}(\text{OTf})_3$) as a Lewis acid in mixtures of methanol and water. They observed a change in the tacticity and thus in the cloud point temperature of the polymers according to the composition of the con solvents in which they were synthesised. Moreover, Wang *et al.*⁴⁹ observed a change but only in the morphology and mechanical properties of random copolymers of *N*-ethylacrylamide and NIPAM synthesised in different compositions of water and methanol but by free-radical polymerisation. In the case of diblock copolymers synthesised by RAFT polymerisation, only Xu *et al.*²⁰ have investigated the chain extension of a poly(*N,N*-dimethylacrylamide) (PDMA) macro-CTA by NIPAM in con solvents. Overall, they observed that mixes of water with more polar solvents such as ethanol and methanol produced copolymers with lower dispersity than those synthesised in 2-propanol.

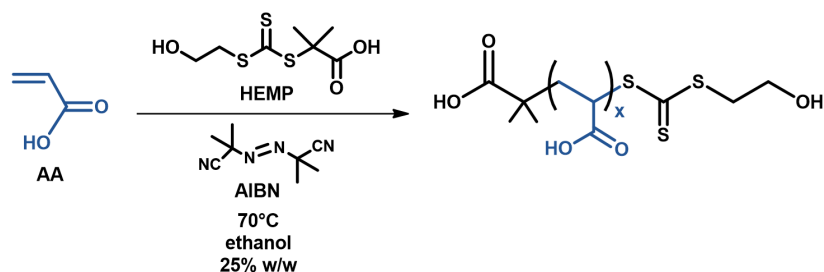
Despite the insights that these studies provide, a better understanding of the effect of the con solvent composition on the *in situ* self-assembly of PNIPAM is needed to assess if the dispersing medium has an effect on the final properties of nanogels synthesised *via* RAFT dispersion polymerisation. It is hypothesised that during PISA, the critical chain length at which PNIPAM becomes hydrophobic is altered depending on the alcohol molar fraction used in the synthesis, consequently affecting the final size of the growing chains. To test this hypothesis, poly(acrylic acid) was chosen as the hydrophilic stabiliser macro-CTA due to its sensitivity to pH and ionic strength. In this way, a multi-responsive nanogel may be obtained. In the literature, the potential biomedical use of PAA-*co*-PNIPAM hydrogels and microgels has been widely been reported before.^{50,51} However, these materials have been mainly obtained by free-radical and emulsion polymerisation, which involves exhaustive purification processes to remove possible surfactant contamination.^{32,52–54} Liu *et al.*⁸ firstly reported the synthesis of PAA-*b*-PNIPAM crosslinked nanogels by an aqueous RAFT-mediated PISA method using KPS/ K_2CO_3 and at a low solids content (2% w/w). Overall, showing that these nanogels are sensitive to pH and temperature.

This chapter aims to show the synthesis of a series of PAA-*b*-P(NIPAM-*st*-BIS) nanogels using a RAFT-mediated PISA process. Prior to assessing the effect of the cononsolvents during the dispersion polymerisation, nanogels were synthesised in water and the effect of parameters such as the DP of the macro-CTA, and the molar ratios of monomer to macro-CTA and of macro-CTA to crosslinker on the size and morphology of the nanogels was investigated. Then, the cononsolvency strategy was used to produce nanogels in various water-ethanol compositions to assess its effect on the properties of the nanogels. Finally, the RAFT dispersion polymerisation of NIPAM in cononsolvents was investigated in the absence of the crosslinker to obtain diblock copolymers as a way to verify if there were changes in the properties of these materials.

2.3. Results and discussion

2.3.1. Synthesis and characterisation of PAA macro-CTAs

The first step to produce nanogels by a RAFT process was the synthesis of an appropriate hydrophilic macro-CTA. To this purpose, a suitable chain-transfer agent (CTA) must be selected for the polymerisation of acrylic acid (AA). In RAFT polymerisation, acrylic acid is considered a “more activated” monomer (MAM) since its vinyl group is conjugated to a carbonyl group hence its polymerisation requires a CTA with a Z-group that favours the radical addition on the C=S. Previous studies showed that the use of trithiocarbonates as CTAs offers good control of the polymerisation of AA in protic solvents.^{55–59} Besides, trithiocarbonates CTAs exhibit a lower susceptibility to hydrolysis than dithiobenzoate CTAs,^{60,61} thus making them better candidates for the production of nanogels in water. Hence, a trithiocarbonate-based RAFT agent was prepared for the polymerisation of AA, which has a (2-hydroxyethyl)thio Z-group and a 2-methylpropanoic acid R-group. Scheme 2.1 shows the reaction scheme for the synthesis of PAA using 2-(hydroxyethylthiocarbonothioylthio)-2-methylpropanoic acid (HEMP) as CTA.



Scheme 2.1: The synthesis of PAA_x via RAFT ethanolic polymerisation using HEMP as RAFT agent.

A kinetic study of the polymerisation was conducted to assess the overall control of the polymerisation when using HEMP as CTA. The kinetic data was derived from ¹H nuclear magnetic resonance (NMR) spectroscopy analyses after quenching each aliquot taken from the reaction mixture at regular intervals. Figure 2.3 shows the conversion versus time curve and the semi-logarithmic plot. AA monomer conversion of more than 90% was achieved within 5 h when using 2,2'-Azobis(2-methylpropionitrile) (AIBN) as the initiator ([HEMP]/[AIBN]=10/1) at 70°C with a targeted degree of polymerisation (DP) of 60. An initial linear semi-logarithmic trend was observed for the first 3 h of reaction ($K_{app}=1.6 \times 10^{-4} \text{ s}^{-1}$) which indicates pseudo-first-order kinetics with respect to the monomer (i.e. steady-state conditions). No induction period was observed at the evaluated reaction conditions. A non-steady state was reached after 80% of AA conversion

where the polymerisation rate clearly decreased, this is observed as the deviation from the initial linearity in the semi-logarithm plot (Figure 2.3). The polymerisation rate became slower at this point probably due to a decrease in the concentration of the active propagating species which can be related to termination or side reactions.⁶²

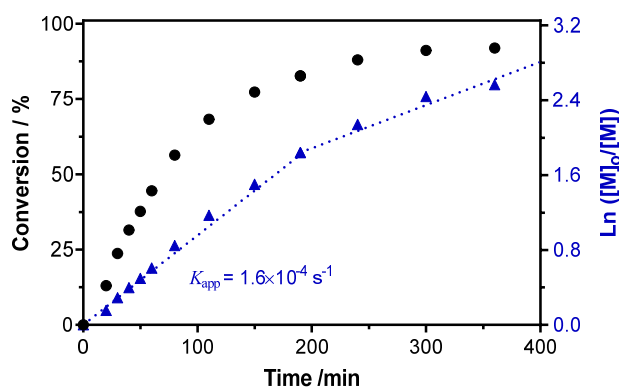


Figure 2.3: Kinetic study of the RAFT ethanolic polymerisation of AA using HEMP as CTA. AA conversion vs time curve (●) and the semi-logarithmic plot of AA conversion over time (▲) for the synthesis of a PAA₆₀ using AIBN ([HEMP]/[AIBN]=10/1) at 70 °C and 25% w/w. (.....) Linear fit for initial steady-state ($R^2=0.99$).

Gel permeation chromatography (GPC) in DMF *versus* near-monodisperse poly(methyl methacrylate) (PMMA) standards was used to monitor the evolution of the molar mass during the polymerisation of AA. To enable analysis in DMF, each PAA sample was methylated using excess (trimethylsilyl)diazomethane (TMS) prior to analysis.^{63,64} The evolution of the molar mass with conversion after esterification of PAA to poly(methyl acrylate) (PMA) is observed in the chromatograms (Figure 2.4a). Figure 2.4b shows a linear increase in \bar{M}_n with AA conversion with relatively low dispersities ($\bar{M}_w/\bar{M}_n < 1.30$), however the \bar{M}_n values determined by GPC do not match the theoretical values and are far from these. An incomplete esterification of PAA could have caused higher retention times due to interactions of the polar groups with the column.

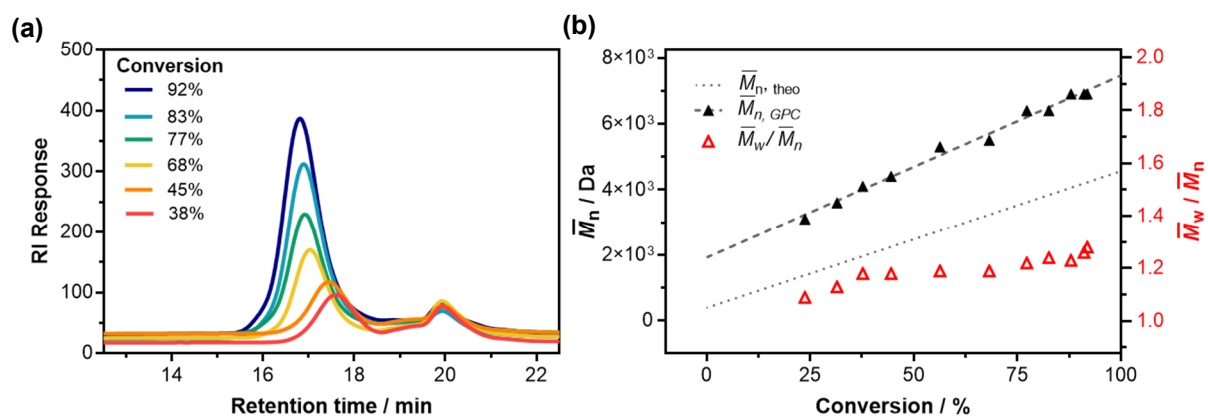


Figure 2.4: Molar mass determination during the RAFT polymerisation of AA. (a) GPC chromatograms (RI signal response vs retention time) of the PAA (methylated to PMA) kinetic samples as function of the AA conversion (b) Evolution of \bar{M}_n (▲) and \bar{M}_w/\bar{M}_n (Δ) vs conversion. (GPC: DMF 0.1% LiBr eluent, vs PMMA standards). (---) Linear fit \bar{M}_n (theo) ($R^2=0.99$) (.....) Linear fit \bar{M}_n (GPC) ($R^2=0.99$).

A series of PAA homopolymers was prepared targeting different DPs to use as macro-CTAs for further chain extension by NIPAM and *N,N'*-methylenebisacrylamide (BIS) as crosslinker to assess the effect of the DP of the macro-CTA on the nanogel formation. Since the chain extension by monomer addition requires that the macro-CTA has good end group fidelity and a “living” character the polymerisation should be stopped at relatively low conversions (i.e. around 80%).⁶⁵ Table 2.1 summarises the data for the synthesis of PAA macro-CTAs and their molar mass characterisation after purification. The number-average DP of the macro-CTAs was estimated using ¹H NMR spectroscopy by end-group analysis of the methylene proton signals corresponding to the CTA and the polymer backbone (See Appendix A, Figure 2A.6-8 for spectra).

Table 2.1: Summary of the synthesis and properties of the PAA_x macro-CTAs.^a

[AA]/[HEMP]	[HEMP]/[AIBN]	Conversion ^b %	Number- average DP ^c	$\bar{M}_{n,theo}$ ^d kDa	$\bar{M}_{n,GPC}$ ^e kDa	\bar{M}_w/\bar{M}_n ^e
61/1	10/1	66	37	3.4	3.8	1.20
60/1	5/1	78	52	4.7	4.7	1.19
118/1	5/1	72	84	7.5	7.1	1.25

^aGeneral reaction conditions: solids content 25% w/w and 70 °C. ^bDetermined by ¹H NMR spectroscopy using the ratio of the sum of vinyl proton integrals and the polymer backbone (See Appendix A, Figure 2A.3-5 for spectra). ^cCalculated from the end group analysis of the methylene proton signals corresponding to the CTA and the polymer backbone as judged by ¹H NMR spectroscopy (See Appendix A, Figure 2A.6-8 for spectra) DP=Area per proton of backbone/area per proton of end-groups. ^dCalculated using the $\bar{M}_n = M_{CTA} + nM_1$ Equation 1.3, where M_{CTA} is the molar mass of the end groups, n the number-average DP as determined by ¹H NMR analyses and M_1 is the molecular mass of the esterified AA repeating unit. ^eDetermined by GPC after esterification of the purified PAA macro-CTAs. (GPC: THF containing 4% v/v acetic acid and 0.025% w/v BHT, calibrated with near-monodisperse PMMA standards).

Unlike the molar mass determination of the kinetic samples performed in DMF as eluent, THF containing acetic acid (4% v/v) was used as the GPC eluent for the determination of the molar mass of the PAA macro-CTAs. This was used as a way to minimise interactions between the esterified PAA sample and the column. In the literature is reported that a good molar mass determination by GPC of PAA after methylation is obtained by using an aqueous eluent (0.1 M Na₂HPO₄ at pH=9) since hydrogen bonding interactions are reduced, although reliable results can be obtained also using THF for linear PAA synthesised by RAFT polymerisation.⁶³ Figure 2.5 shows the GPC chromatograms of the macro-CTAs, which are monomodal and narrow. Moreover, it was noted that the molar masses of the esterified PAA macro-CTAs determined by GPC in THF more closely matched the theoretical values than those measured by GPC in DMF. The dispersity of the macro-CTAs used in this work is reasonably low ($\bar{M}_w/\bar{M}_n < 1.25$) as expected for RAFT polymers, even after esterification. The synthesised macro-CTAs were further investigated for the RAFT dispersion polymerisation of NIPAM and BIS in either water or water/ethanol mixtures.

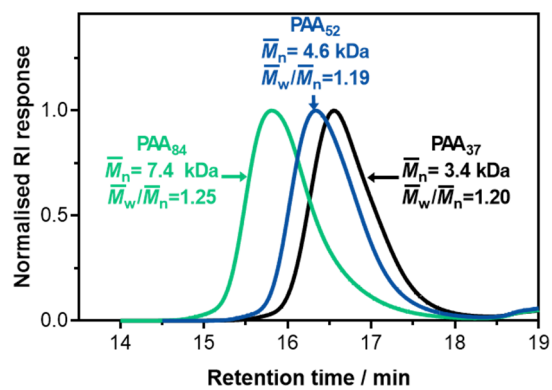


Figure 2.5: THF GPC chromatograms of the series of PAA macro-CTAs after methylation with TMS-diazomethane. (GPC: THF containing 4% v/v acetic acid, 0.025% w/v BHT, calibrated with near-monodisperse PMMA standards).

2.3.2. Synthesis of PAA-*b*-P(NIPAM-*st*-BIS) nanogels by RAFT aqueous dispersion

In a typical RAFT-mediated PISA in dispersion, a solvophilic macro-CTA is chain extended by a second soluble monomer. During chain growth, the second block loses solubility and at some critical DP self-assembles forming spherical micelles first.⁶⁶ As polymerisation progresses, the reorganisation of the block copolymer chains and interparticle collisions can lead to the evolution of the morphology of the nano-object with increasing DP of the solvophobic block (Figure 2.6).⁶⁷ When using temperature-sensitive monomers, such as NIPAM, the *in situ* self-assembly polymerisation is driven by temperature.

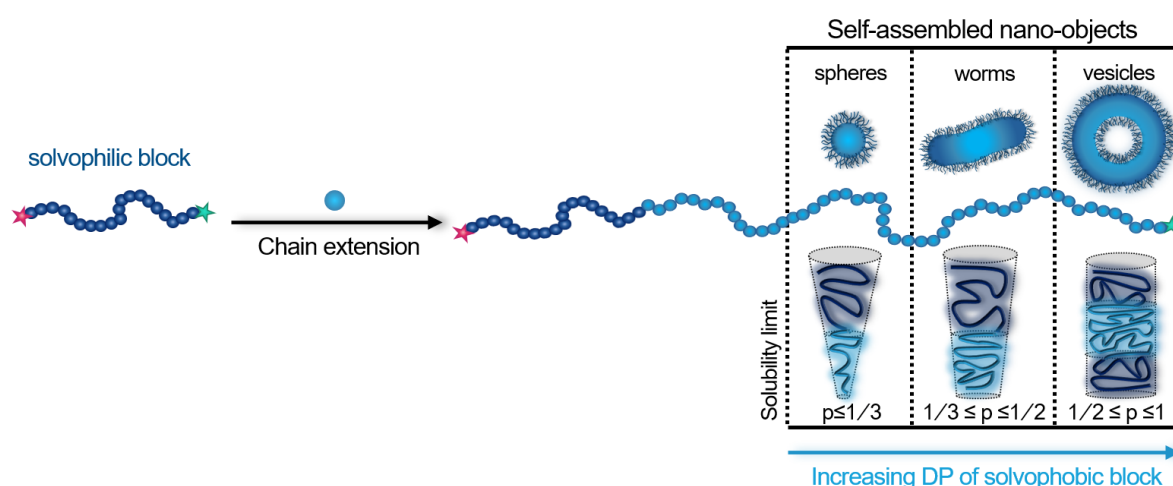
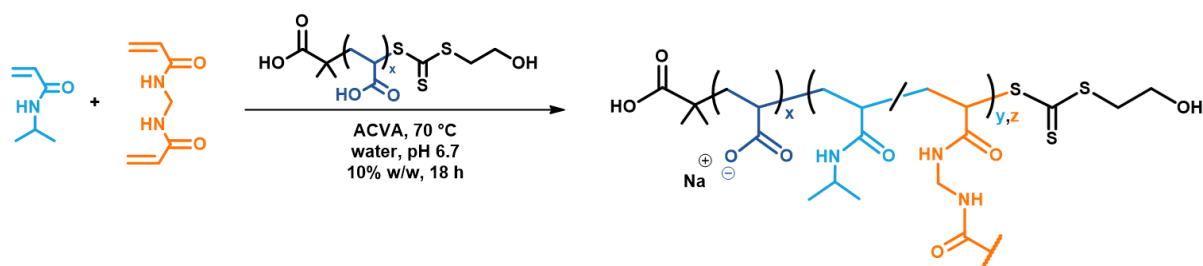


Figure 2.6: Schematic representation of RAFT-mediated PISA showing the progression of polymer nano-object morphologies.

The preparation of nanogels using a PISA synthesis follows the same self-assembly process; however, the presence of the crosslinker from early stages of polymerisation can prevent the reorganisation of the chains and inhibit the formation of higher-order morphologies.^{68,69} Even though the crosslinking can be performed after polymerisation by further coupling reactions of functional groups to ensure higher-order morphologies,⁶⁸ most of the literature based on RAFT-mediated PISA follows the addition of a bifunctional monomer from the beginning of the reaction to prepare nanogels.^{2-12,15-22} Thus, the chain extension of the PAA_x macro-CTAs with NIPAM and BIS was attempted in one-step, and this approach was followed in all the nanogel syntheses presented herein. However, a brief investigation on the addition of crosslinker at specific times can be found in the Appendix A (Figure 2A.9).

Details of the optimisation of the synthesis of nanogels can be found too in the Appendix A (Table 2A.1), where the effects of the type of initiator, pH, and solids content on the synthesis of crosslinked particles *via* RAFT dispersion aqueous polymerisation is presented. Overall, it was found that 4,4'-azobis(4-cyanopentanoic acid) (ACVA) was a better initiator for the synthesis of defined particles than a low-temperature free radical initiator, and that the pH of the solution had to be adjusted to obtain crosslinked nanoparticles with uniform size distributions. For example, when the polymerisation was attempted without any pH adjustment (at pH \approx 2.7 which was the pH of all the reagents in aqueous solution), the growing polymer chains precipitated out of solution during the reaction (Appendix A, Figure 2A.10). This could have meant that the PAA₅₂ did not stabilise the formation of a PNIPAM core-forming block, even though PAA was soluble before reaction at such low pH. The pK_a of PAA₅₂-HEMP was determined to be 5.8 by potentiometric titration (Appendix A, Figure 2A.12). Hence, PAA₅₂ was substantially protonated (>99%) at a pH of 2.7 and it had likely reduced solubility, which considerably decreased upon chain extension with NIPAM. By adjusting the pH to a mildly acidic pH of 4.3 (3% of the AA units deprotonated) the reaction was feasible; however, some small aggregates were observed in the suspension probably due to insufficient deprotonation of the carboxylic acid groups to stabilise the formation of nanoparticles. Hence, to ensure electrostatic stabilisation for particle formation provided by the carboxylate groups, a pH between 6.6–7 was selected due to the high deprotonation of AA units (86–94%). A higher pH was not considered since it has been reported that in alkaline pH a loss in the control over the polymerisation can be observed caused by hydrolysis of the trithiocarbonate RAFT end groups⁷⁰ and/or the pH affecting the nucleation mechanism.⁵⁸

Once the optimum solution pH was found for the synthesis of nanogel particles in water (Scheme 2.2), parameters such as the composition of the core forming block (NIPAM and BIS concentration), and the chain length of the stabiliser shell block (the DP of PAA) were adjusted to investigate the effect that these had on the size and morphology of the nanogels. Each reaction was performed at 10% w/w solids content in water at 70 °C.



Scheme 2.2: The synthesis of PAA_x-*b*-P(NIPAM-*st*-BIS)_{y,z} nanogels *via* RAFT aqueous dispersion polymerisation. Note: Under the reaction conditions, PAA is seemingly \approx 89% deprotonated.

The reactions were stopped after approximately 18 hours to ensure a high monomer conversion. The monomer conversion was estimated by gravimetric analysis using a moisture analyser that gave a dried solids content of the reaction crude mixture heated up to 190 °C. On average, the monomer conversion in these reactions was around 83%. The full list of the properties of the nanogels synthesised in only water can be found in Table 2.2 and these results will be discussed in detail in Section 2.3.2.1 and 2.3.2.2. For clarity, a notation is utilised to describe the nanogels monomer composition. Thus A, N, and B symbolise acrylic acid (AA), *N*-isopropyl acrylamide (NIPAM) and *N,N'*-methylenebisacrylamide (BIS), respectively. Thus $A_xN_yB_z$ symbolises $PAA_x-b-P(NIPAM-st-BIS)_{y,z}$ where x,y and z represents the average-number DP of each monomer component.

Table 2.2: Summary of the synthesis and properties of $A_xN_yB_z$ nanogels.

Target composition [PAA _x]:[NIPAM]:[BIS] ^a		Conversion ^b %	PNIPAM DP _{theo} ^c	$\bar{M}_{n,theo}$ ^d kDa	D_h / nm (PDI) ^e	ζ - Potential ^f mV
x=52	[1]:[100]:[3]	74	74	12.8	80 (0.11)	-41
	[1]:[200]:[3]	90	181	24.9	231 (0.08)	-34
	[1]:[300]:[3]	84	252	33.0	483 (0.06)	-29
	[1]:[300]:[5]	gel	/	/	/	/
x=84	[1]:[100]:[3]	82	82	16.0	104 (0.10)	-37
	[1]:[200]:[3]	83	165	25.4	297 (0.04)	-43

^aGeneral reaction conditions: Targeted [PAA_x]/[ACVA]=5, solids content 10% w/w, 70 °C for 18 hours.

^bGravimetric determination by moisture analysis of solids content against predicted solids content.

^cEstimated using Equation 1.2 for the equivalent of a diblock copolymer without crosslinker. ^dCalculated by $\bar{M}_n = M_{CTA} + xM_1 + yM_2 + zM_3$, where M_{CTA} is the molar mass of the CTA end groups, x, y and z are the DPs of PAA, NIPAM, and BIS respectively and M_1 , M_2 and M_3 is the molar mass of the corresponding monomer unit. ^eDLS data obtained from 0.1% w/w nanogels dispersions in DI water at pH 7 and 25 °C. ^f ζ -potential measurements for 0.1% w/w nanogels dispersions in DI water with 1 mM KCl as a background electrolyte at pH 7 and 25 °C.

2.3.2.1. The effect of the DP of the core-forming block on the size of nanogels

The chain extension of the PAA₅₂ macro-CTA with varying ratios of NIPAM was conducted to investigate how the DP of PNIPAM affected the size and morphology of nanogels. By targeting a PNIPAM DP of 100, 200 and 300, three nanogel dispersions were synthesised in water at a fixed molar ratio of crosslinker to PAA₅₂ of 3:1. During polymerisation, a transition from a homogeneous to heterogeneous solution was observed at around 7 min when targeting a PNIPAM DP of 200 and 300. This indicated the self-assembly of the growing chains due to a reaction temperature higher than the LCST of PNIPAM. After quenching the reaction, the mean PNIPAM DP was determined by monomer conversion from gravimetric analysis. It was noted that the A₅₂N₁₈₁B₃ and A₅₂N₂₅₂B₃ reaction mixtures remained as turbid dispersions, which suggested the crosslinking of the PNIPAM core, whilst the A₅₂N₇₄B₃ remained as a relatively transparent dispersion (Figure 2.7a). Since the colour of the crude mixture solutions varied according to the DP of PNIPAM. It is suggested that particles of small size were obtained for the nanogel A₅₂N₇₄B₃, and larger particles were seemingly produced for the larger PNIPAM DPs of 181 and 252, as the solutions look opaque. This is because the intensity of the scattered light is proportional to the size of the particle and the solution concentration with larger particles scattering more light than smaller particles.

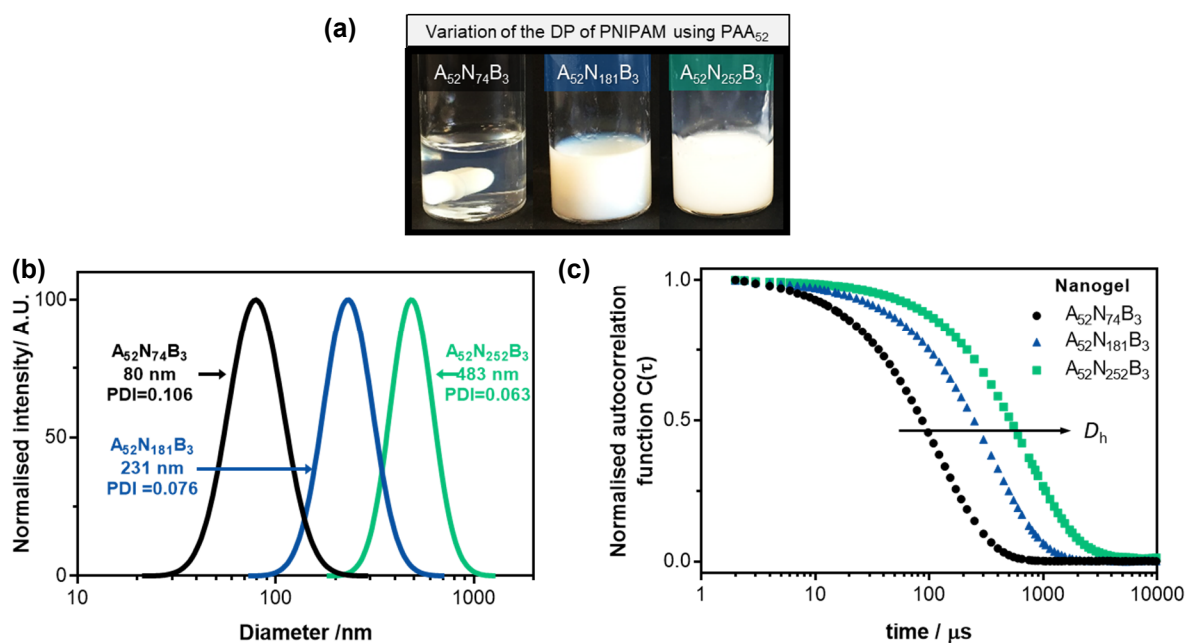


Figure 2.7: Size determination of the A₅₂N_yB₃ nanogels synthesised in water. (a) Digital photograph of the crude nanogel dispersions at 10% w/w and room temperature. (b) Intensity average log-normal size distribution curves (n=4) and (c) their respective autocorrelation functions with time at 25 °C from DLS. Data obtained from 0.1% w/w nanogel dispersions in DI water at neutral pH.

After purification of the nanogels by dialysis against DI water, the difference in the average size was confirmed by dynamic light scattering (DLS) and transmission electron microscopy (TEM) studies. The average hydrodynamic particle diameter (D_h) of the purified nanogel dispersions was determined by DLS first at a constant temperature of 25 °C and at neutral pH. The lognormal size distributions and the autocorrelation curves are shown in Figure 2.7b,c respectively. As judged by DLS, the greater the DP of PNIPAM the larger the D_h of the crosslinked particles, e.g. the D_h increased from 80 nm for the A₅₂N₇₄B₃ nanogel to 483 nm for the A₅₂N₂₅₂B₃ nanogel. Although the A₅₂N₂₅₂B₃ nanogel could be considered as a microgel due to their micrometric size range, in this thesis all the synthesised crosslinked particles are referred to as nanogels to simplify comparison.[†]

It was also noted all of the intensity size distributions have low dispersity (PDI<0.11), which is an indicator that the highly negatively charged PAA₅₂ offered good control and stabilisation over the nanogel formation. From the correlogram, it is clearly observed that the correlation of the signal decays quicker for the smaller particles ($y=74$) than those with greater size ($y=252$) (Figure 2.7c). The particle sizes are shown in a lognormal plot in Figure 2.7b. However, examples of size distributions by intensity, volume, and number of this series of nanogels is presented in the Appendix A (Figure 2A.11), where it can be observed that the D_h size by intensity, volume and number was similar, and that the average size distributions were monomodal. It is noteworthy that DLS is biased toward larger particles; therefore, the presence of small particles and/or unimers for the bigger nanogels are not likely be detected by DLS but it can potentially be determined by small-angle X-ray scattering (SAXS) or by asymmetric-flow field-flow fractionation (AF4) with multi-angle light scattering (MALS).

In agreement with the size determined by DLS, it was observed that the particle size gradually increased with the volume fraction of PNIPAM as judged by the TEM micrographs (Figure 2.8). However, it is noticeable that the average diameter as determined by TEM (D_{TEM}) is smaller than the size by DLS. For example, the A₅₂N₁₈₁B₃ had a D_h of 231 nm and an average D_{TEM} of 102±16 nm (2 times smaller). This is because DLS analysis gives the intensity-average particle size, and bigger particles scatter light much more strongly than smaller particles, since the intensity of scattered light is proportional to the sixth power of the diameter of the particles ($I \propto D^6$).⁷³ Besides, as oppose to TEM, the size determined by DLS considers the outer shell that is

[†]In the literature, examples of “nanogels” with a size range between 200-500 nm have been previously reported.^{36,71,72}

supposedly uncrosslinked, and highly negatively charged at pH 7 (e.g. -41 mV for $A_{52}N_{74}B_3$ as shown in Table 2.2) in which the charge repulsion from the carboxylate groups makes the dangling chains being predominantly extended.^{59,74} In the case of TEM, the number-average size of particle with finite width is determined from nanogel samples dried under high vacuum conditions in comparison to DLS determination where the nanogel chains are solvated.

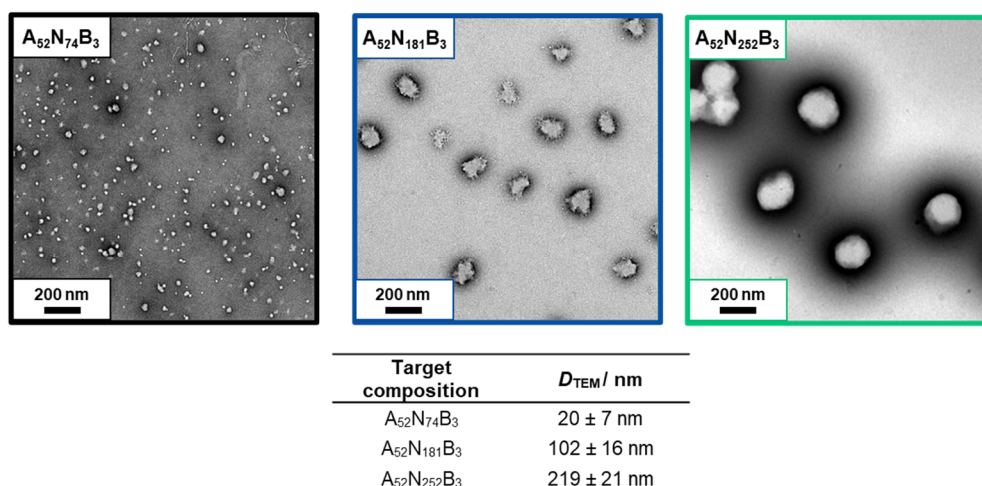


Figure 2.8: TEM micrographs of the $A_{52}N_yB_3$ nanogels synthesised in water. Nanogel samples (0.1% w/w) were stained with phosphotungstic acid (0.75% w/v, pH 7.2).

It was also noted that the nanogels had a semi-spherical shape despite the increasing volume fraction of PNIPAM. As previously described, in a typical PISA dispersion, higher-order morphologies might be formed with increasing DP of the solvophobic block. However, since the crosslinker was added from the beginning of the reaction, the reorganisation of the growing chains may have been prevented, leading to kinetically trapped micellar spheres. As proved by Figg *et al.*,⁶⁸ a range of morphologies (e.g. micelles, worms and vesicles) can be obtained with increasing volume fractions of PNIPAM using aqueous dispersion RAFT-mediated PISA. Nevertheless, an immediate crosslinking reaction of a small fraction of acrylic acid with diamine at 70 °C must be performed after polymerisation to prevent the dissolution of the copolymer chains at ambient temperature.⁶⁸ Another accountable reason for the formation of only spheres rather than high-order morphologies is due to the use of a highly negatively charged macro-CTA. The presence of charged groups in the solvophilic block is believed to reduce the packing parameter⁷⁵ hence producing spheres at higher volume fractions of the solvophobic block.⁷⁶ However, it can also be observed that the $A_{52}N_{181}B_3$ and $A_{52}N_{252}B_3$ nanogels have an irregular shape, which can also suggest the fusion of the growing micellar aggregates during polymerisation due to inter-particle crosslinking, thus creating nanogels with larger sizes.

An increase in the crosslink density was also explored as a way to assess the effect on the particle size when targeting a PNIPAM DP of 300. However, a molar ratio of PAA₅₂ to BIS of 1:5 at 10% w/w led to macroscopic gelation, which is probably due to a higher probability of particle-particle interaction resulting in inter-particle crosslinking. This can potentially be prevented by lowering the solids content from 10% w/w; however, this was not confirmed in the present work.

2.3.2.2. The effect of the DP of the shell-stabiliser block on the size of the nanogels

Since the length of the solvophilic block affects the size and stability of nanogels during polymerisation,^{3,5,20} the formation of nanogels using the PAA macro-CTA with a number-average DP of 84 was investigated with varying PNIPAM DPs. Two nanogel compositions were targeted with a PNIPAM DP of 100 and 200 at a fixed BIS concentration in aqueous solution. Upon polymerisation, phase separation occurred, and the solutions became cloudy, which suggested the self-assembly of the amphiphilic growing chains. Figure 2.9a shows the A₈₄N₈₂B₃ and A₈₄N₁₆₅B₃ nanogel reaction mixtures, which stayed as turbid dispersions at ambient temperature.

Previously, it has been reported that an insufficient PNIPAM block length can inhibit the self-assembly and thus the nanogel formation when using a PDMA macro-CTA with similar block length than the solvophobic block.²⁰ In the present case, nanogels were formed when using PAA₈₄ as a stabiliser block and a target PNIPAM DP of 100, which means that the growing PNIPAM chains reached a critical degree of polymerisation and aggregated in solution, thus allowing particle formation. In Figure 2.9b and c is shown the size measurements by DLS, where a gradual increase on the hydrodynamic diameter was observed with increasing volume fraction of the core-forming block. For instance, an increasing D_h was observed from 104 nm for A₈₄N₈₂B₃ to 297 nm for A₈₄N₁₆₅B₃. In both cases, the intensity size distributions were narrow (PDI<0.10), which is in agreement with TEM size analyses (Figure 2.9d). It is observed in the TEM micrographs that kinetically trapped spheres were produced when using PAA₈₄ and no high-order morphologies were obtained. This is due to the effects of the highly charged stabiliser block on the packing parameter and the constrained chain growth due to early crosslinking.

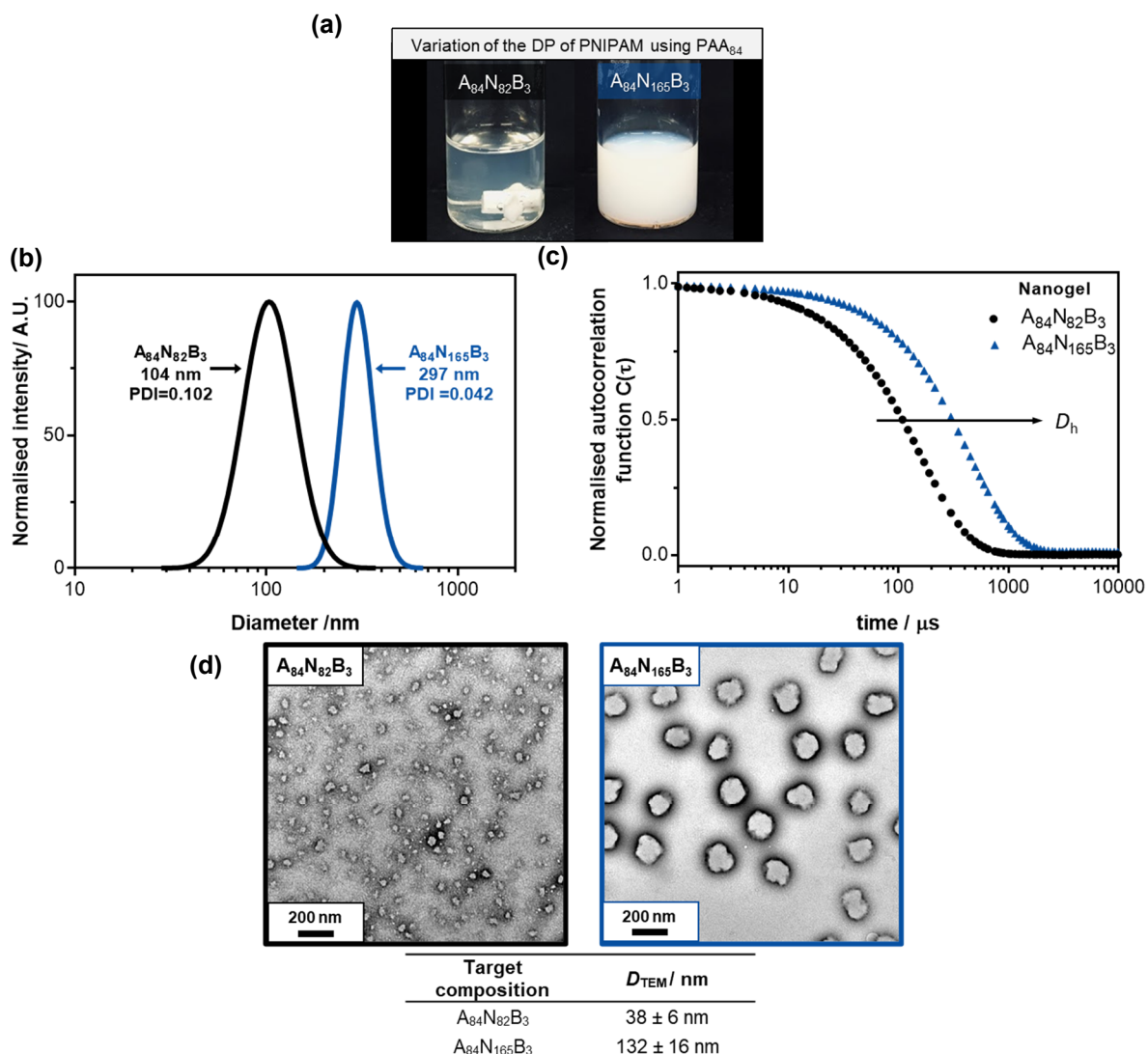


Figure 2.9: Size determination of the A₈₄N_yB₃ nanogels synthesised in water. (a) Digital photograph of the A₈₄N_yB₃ crude nanogel dispersions at 10% w/w and ambient temperature. (b) Intensity average lognormal size distribution curves (n=4) and (c) their respective autocorrelation function with time at 25 °C, and (d) TEM micrographs of the nanogels. Data obtained from 0.1% w/w nanogels dispersions in DI water at neutral pH. Nanogel samples were stained with phosphotungstic acid (0.75% w/v, pH 7.2).

When comparing these synthesised nanogels with those produced with a shorter solvophilic block, it is observed that nanogels with a longer solvophilic block had a greater size and were more uniform in shape than those synthesised using a PAA with a DP of 52 and a similar target PNIPAM DP. For example, the A₅₂N₁₈₁B₃ nanogel had a D_h of 231 nm (PDI=0.076), whilst the A₈₄N₁₆₅B₃ nanogel had a D_h of 297 nm (PDI=0.042) (The morphology of the nanogels can be observed in the TEM micrographs). Hence, it can be suggested that changes in the packing parameter due to the length of the solvophilic block can subtly affect the nanogel shape when using PAA as shell-stabiliser. By using PAA₅₂ as macro-CTA, the critical block copolymer DP for the self-assembly should have been lower than the critical solubility limit of the PAA₈₄-based

nanogels. Thus, resulting in an earlier particle nucleation, which in turn is reflected in a more constrained chain growth due to earlier self-assembly than when using a macro-CTA with a larger solvophilic block.

So far, it has been shown the effect of the main parameters that can affect the nanogel formation using a RAFT dispersion polymerisation in only water. These results then served as a reference point for the synthesis of nanogels in cononsolvents as it will be shown in Section 2.3.3. As described earlier, the addition of another solvent to RAFT aqueous dispersion polymerisation has been used to either include hydrophobic components into the nanogel structure^{19,20} or to promote the immiscibility of growing chains during polymerisation.^{15-18,22} To test the effects of cononsolvency of PNIPAM during nanogel formation, a range of water-ethanol compositions were assessed in the synthesis.

2.3.3. Synthesis of PAA-*b*-P(NIPAM-*st*-BIS) nanogels by RAFT dispersion in cononsolvents

As previously stated, the phenomenon of cononsolvency of PNIPAM refers to the polymer being soluble in pure water and an alcohol but insoluble in mixtures of these two at specific compositions, where the LCST varies according to the mole fraction of the cononsolvents.²⁵ It is believed that the addition of an alcohol as cononsolvent pair with water decreases the solubility of the growing PNIPAM chains during polymerisation and thus enhances the driving force for the *in situ* self-assembly.²⁴ Hence, the cononsolvent composition used during polymerisation of NIPAM should affect the final properties of the nanogels. To assess this hypothesis, a series of nanogels was synthesised following the synthetic methodology reported in Scheme 2.2 but with the addition of ethanol to water at various mole ratios. The effect of the cononsolvent composition on the chain extension of PAA_x macro-CTAs with NIPAM and BIS was studied by targeting a range of core-forming DPs. Details of the optimisation of the synthesis of nanogels in cononsolvents can be found too in the Appendix A (Table 2A.1). However, the most representative results can be found in Table 2.3, where the full list of the properties of the nanogels synthesised in cononsolvents is presented. These results will be discussed separately below.

It was observed that after polymerisation, the colour of the reaction mixtures not only transitioned according to the target DP of PNIPAM but also changed according to the ethanol mole fraction (X_e) used in the synthesis. Considering the nanogels synthesised using PAA₅₂ as an example, the reaction mixtures for a target PNIPAM DP of 100 remained as translucent dispersions after polymerisation, whilst the mixtures with a target DP of 200 and 300 were turbid dispersions in water and at low ethanol mole fractions (Figure 2.10). As more ethanol was used in the synthesis, the more translucent the dispersions became (i.e. apparently smaller particle size). It is noteworthy to mention that since the refractive index of binary solutions of water and ethanol differs from water alone, this visual comparison is not exactly precise but merely indicative. For simplicity, a similar nanogel notation is utilised henceforth ($A_xN_yB_z-X_e$) where X_e represents the mole fraction of ethanol used in the synthesis of the nanogels.

Table 2.3: Summary of the synthesis and properties of $A_xN_yB_z-X_e$ nanogels synthesised by RAFT dispersion polymerisation in water/ethanol mixtures.^a

Target composition [PAA _x]:[NIPAM]:[BIS]		Ethanol mole fraction (X_e) ^b	Conversion ^c %	$DP_{,theo}$ ^d	$\bar{M}_{n,theo}$ ^e kDa	D_h/nm (PDI) ^f	ζ -Potential ^g mV
x=52	[1]:[100]:[3]	0.05	99	99	15.7	56 (0.11)	-30
	[1]:[100]:[3]	0.09	79	79	13.4	55 (0.21)	-33
	[1]:[100]:[3]	0.11	100	100	15.8	67 (0.25)	-29
	[1]:[200]:[3]	0.05	98	197	26.7	159 (0.05)	-31
	[1]:[200]:[3]	0.09	100	200	27.1	97 (0.18)	-34
	[1]:[200]:[3]	0.12	92	184	25.3	90 (0.22)	-23
	[1]:[200]:[5]	0.05	91	182	25.0	150 (0.08)	-38
	[1]:[200]:[7]	0.05	83	167	23.3	139 (0.07)	-42
	[1]:[300]:[3]	0.10	86	259	33.8	203 (0.11)	-18
	[1]:[300]:[5]	0.05	97	292	37.8	244 (0.06)	-29
	[1]:[300]:[5]	0.11	94	281	36.6	162 (0.06)	-35
	[1]:[300]:[7]	0.12	87	260	34.5	110 (0.12)	-40
x=84	[1]:[100]:[3]	0.04	85	85	16.4	93 (0.11)	-46
	[1]:[200]:[3]	0.05	90	181	27.2	173 (0.07)	-34
	[1]:[200]:[5]	0.06	89	178	26.9	140 (0.08)	-35
	[1]:[200]:[7]	0.06	85	169	25.9	133 (0.05)	-45
	[1]:[300]:[3]	0.11	88	261	36.3	180 (0.16)	-33
	[1]:[300]:[5]	0.12	95	284	38.9	175 (0.04)	-40
	[1]:[300]:[7]	0.12	93	280	38.4	158 (0.06)	-45

^aGeneral reaction conditions: Targeted $[PAA_x]/[ACVA]=5$, solids content 10% w/w, 70 °C for 18 h.

^bSolvent mixture of H₂O-ethanol, where X_e is the ethanol mole fraction used in the synthesis.

^cGravimetric determination by moisture analysis of solids content against predicted solids content.

^dEstimated using Equation 1.2 for the equivalent of a diblock copolymer without crosslinker. ^eCalculated using $\bar{M}_n = M_{CTA} + xM_1 + yM_2 + zM_3$, where M_{CTA} is the molar mass of the CTA end groups, x, y and z are the DPs of PAA, NIPAM, and BIS respectively and M_1 , M_2 and M_3 is the molar mass of the corresponding monomer unit. ^fDLS data obtained from 0.1% w/w nanogels dispersions in DI water at neutral pH and 25 °C. ^g ζ -potential measurements for 0.1% w/w nanogels dispersions in DI water with a 1 mM KCl background electrolyte at pH 7 and 25 °C.

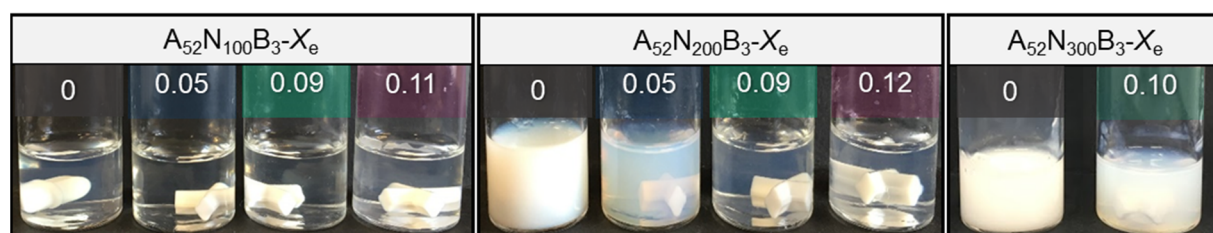


Figure 2.10: Digital photographs of the $A_{52}N_yB_3-X_e$ crude nanogel dispersions, where $y=100, 200$ or 300 at 10% w/w and ambient temperature. The numbers on the vials represents the mole fraction of ethanol (X_e) used in synthesis.

After the removal of ethanol by dialysis against DI water, the particle size of the nanogels in only water was studied by DLS and TEM. Overall, it was observed the particle size decreased as more ethanol was used in the dispersion polymerisation up to a particular X_e where a possible loss

of the control over the polymerisation led to greater size polydispersities. This will be discussed below according to the increasing volume fraction of PNIPAM in the nanogels.

Considering first the nanogels synthesised with PAA₅₂ and the shorter target of the PNIPAM solvophobic block ($y=100$) as an example, Figure 2.11a and b shows the lognormal size distribution and the autocorrelation curves respectively of the nanogels synthesised in either water or mixtures of cononsolvents. Overall, the D_h gradually decreased from 80 nm to 55 nm as more ethanol was added in the synthesis up to the $X_e=0.09$. From the correlogram, it is observed that the correlation of the signal decays later for the bigger particles (A₅₂N₇₄B₃-0) than those with smaller size (A₅₂N₇₉B₃-0.09) (Figure 2.11b). In agreement with DLS, D_{TEM} is greater for the nanogels synthesised in water than those synthesised in small additions of ethanol (Figure 2.11d). For example, the A₅₂N₇₄B₃-0 had a D_{TEM} of 20 ± 7 nm, whilst the A₅₂N₇₉B₃-0.09 had smaller D_{TEM} of 15 ± 5 nm. Interestingly, all the A₅₂N₁₀₀B₃- X_e nanogels had a semi-spherical shape and no high-order morphologies were observed, except for the A₅₂N₁₀₀B₃-0.11 nanogel, where some bigger particles were present as well as some enlarged structures suggesting inter-particle crosslinking during the PISA process. The presence of such inter-crosslinked particles would explain the skew in the D_h of the A₅₂N₁₀₀B₃-0.11 nanogel and the broadening in the hydrodynamic size distribution (PDI=0.25).

As hypothesised, the addition of ethanol to the RAFT aqueous dispersion polymerisation, has an effect during chain growth, thus affecting the final size of the nanogel particles. It is suggested that the critical DP at which PNIPAM became hydrophobic was altered depending on the alcohol mole fraction used in the synthesis, thus affecting the nucleation mechanism. Previously, it has been shown that a reduction of the repulsive electrostatic forces between neighbouring copolymer chains in mixtures of ethanol and water leads to the aggregation of more copolymer chains into the micelles (i.e. bigger particles are obtained).^{77,78} This is due to the lower dielectric constant (ϵ_r) in water/ethanol mixtures (e.g. for $X_e=0.09$ $\epsilon_r\sim 51$ at 70 °C)[‡] than in only water (for $X_e=0$ $\epsilon_r\sim 64$ at 70 °C).⁷⁹ However, this was not observed for the synthesised nanogels since at the tested conditions nanogels with small size were obtained with increasing X_e . This suggests a major effect of the reduced solvency of the growing PNIPAM chains on the particle size, rather than the contribution of the dielectric constant in water/ethanol mixtures on the charge repulsion between the anionic stabiliser chains.

[‡]Data calculated from the extrapolation of the dielectric constant values vs ethanol wt.% of ethanol/water mixtures at 60 and 80 °C as reported in REF 79.

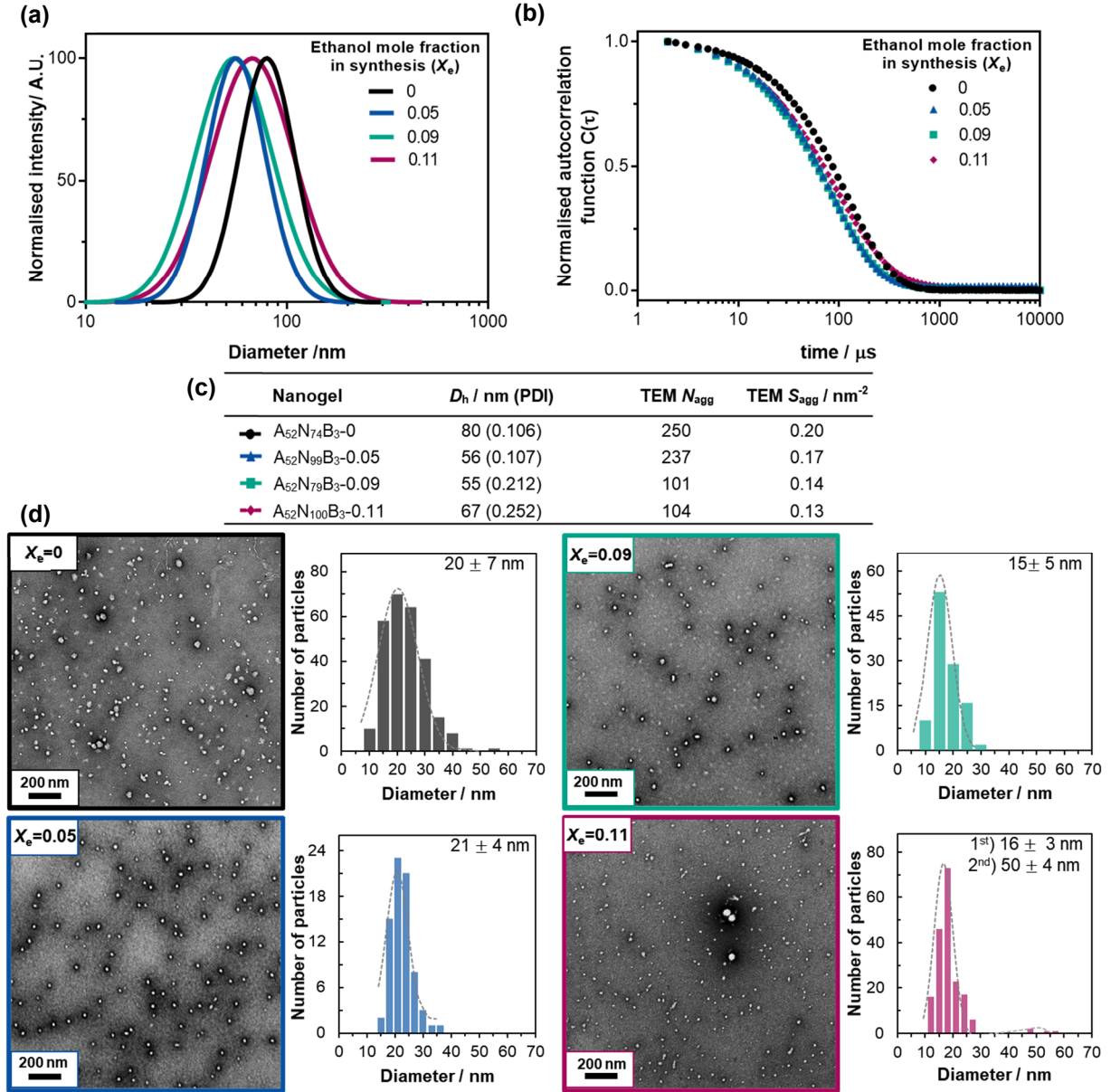


Figure 2.11: Size determination of the $A_{52}N_{100}B_3-X_e$. (a) Intensity average lognormal size distribution curves ($n=4$) and (b) their respective autocorrelation functions with time, (c) Summary of the D_h , mean aggregation numbers (N_{agg} , Equation 2.1) and average number of copolymer chains per unit surface area (S_{agg} , Equation 2.3), and (d) TEM images of the respective purified nanogel with their number particle size distributions. Data obtained from 0.1% w/w nanogel dispersions in DI water at neutral pH. Samples were stained with phosphotungstic acid (0.75% w/v, pH 7.2) for TEM.

N_{agg} estimated using $\bar{M}_{n,theo}$ data from Table 2.3.

Assuming that the D_{TEM} is the smallest size nanogels can assume (i.e. collapsed state) and that a nanogel is thus a hard sphere with a micellar shape (i.e. core-shell), the number of copolymer chains forming the nanogels (N_{agg}) can be estimated from the size as previously reported.^{4,80}

$$N_{agg} = \frac{M}{M_o} \quad \text{Equation 2.1}$$

Where M is the molar mass of a micelle and M_o is the molar mass of the polymer backbone.

Since the direct determination of the molar mass of one micelle can be difficult to determine, it can be estimated by relating it with its size, thus:

$$M = \frac{4 \pi N_A r^3}{3 v} \quad \text{Equation 2.2}$$

Where N_A is the Avogadro's number, r^3 is the average radius as determined by TEM, and v is the partial specific volume of the polymer ($v=1/\rho$; where ρ is the mass density; $\rho_{\text{PNIPAM}}=1.269 \text{ g cm}^{-3}$ from REF 81). Hence, the average number of copolymer chains per unit surface area (S_{agg}) can be also estimated as follows:

$$S_{\text{agg}} = \frac{N_{\text{agg}}}{4 \pi r^2} \quad \text{Equation 2.3}$$

In the insert table from Figure 2.11c it is observed that N_{agg} decrease when using higher ethanol mole fractions in the synthesis excluding the nanogel synthesised at $X_e=0.11$. For example, N_{agg} apparently decreases from 250 for $A_{52}N_{74}B_3-0$ to 101 for the $A_{52}N_{79}B_3-0.09$ nanogel. This suggests that the average number of PNIPAM chains present in a nanogel particle is lower for the nanogels synthesised in mixtures of cosolvents than those synthesised in only water. Moreover, the calculated S_{agg} values decreases from 0.20 nm^{-2} for $A_{52}N_{74}B_3-0$ to 0.14 nm^{-2} for the $A_{52}N_{79}B_3-0.09$ nanogel, which suggests a lower surface density of the PAA₅₂ stabiliser chains on the particles synthesised in cosolvents. Since the nanogels had roughly the same volume fraction of PNIPAM in the nanogel particles (i.e. similar PNIPAM DP) the reduction of the particle size with increasing ethanol mole fraction used in the synthesis indicates that a higher number of particles were produced. This was probably due to nucleation at a shorter critical DP caused by the loss of solvency of the growing PNIPAM chains in mixtures of water and ethanol.

By targeting a larger core-forming block, in this case a PNIPAM DP of 200, bigger particles were obtained than when targeting a DP of 100, as previously showed in Section 2.3.2.1. Figure 2.12a, and b demonstrates the effect of the synthesis in cosolvents on the hydrodynamic size of the purified nanogels. A more evident size decrease was observed at higher X_e used in the synthesis. For instance, the D_h decreased from 231 nm for $A_{52}N_{181}B_3-0$ to 90 nm for $A_{52}N_{184}B_3-0.12$. However, only near-monodisperse size distributions ($\text{PDI}<0.08$) were obtained for the nanogels synthesised in water and at a $X_e=0.05$. At $X_e \geq 0.09$, the size distribution dispersity increases but there was no evidence of the formation of bigger particles, as observed for the $A_{52}N_{100}B_3-0.11$ nanogel with a smaller PNIPAM volume fraction. From the correlogram, it is noted that the decay

of the correlation function is delayed for the bigger particles ($A_{52}N_{181}B_3-0$) since large particles move more slowly than smaller particles ($A_{52}N_{184}B_3-0.12$) (Figure 2.12b).

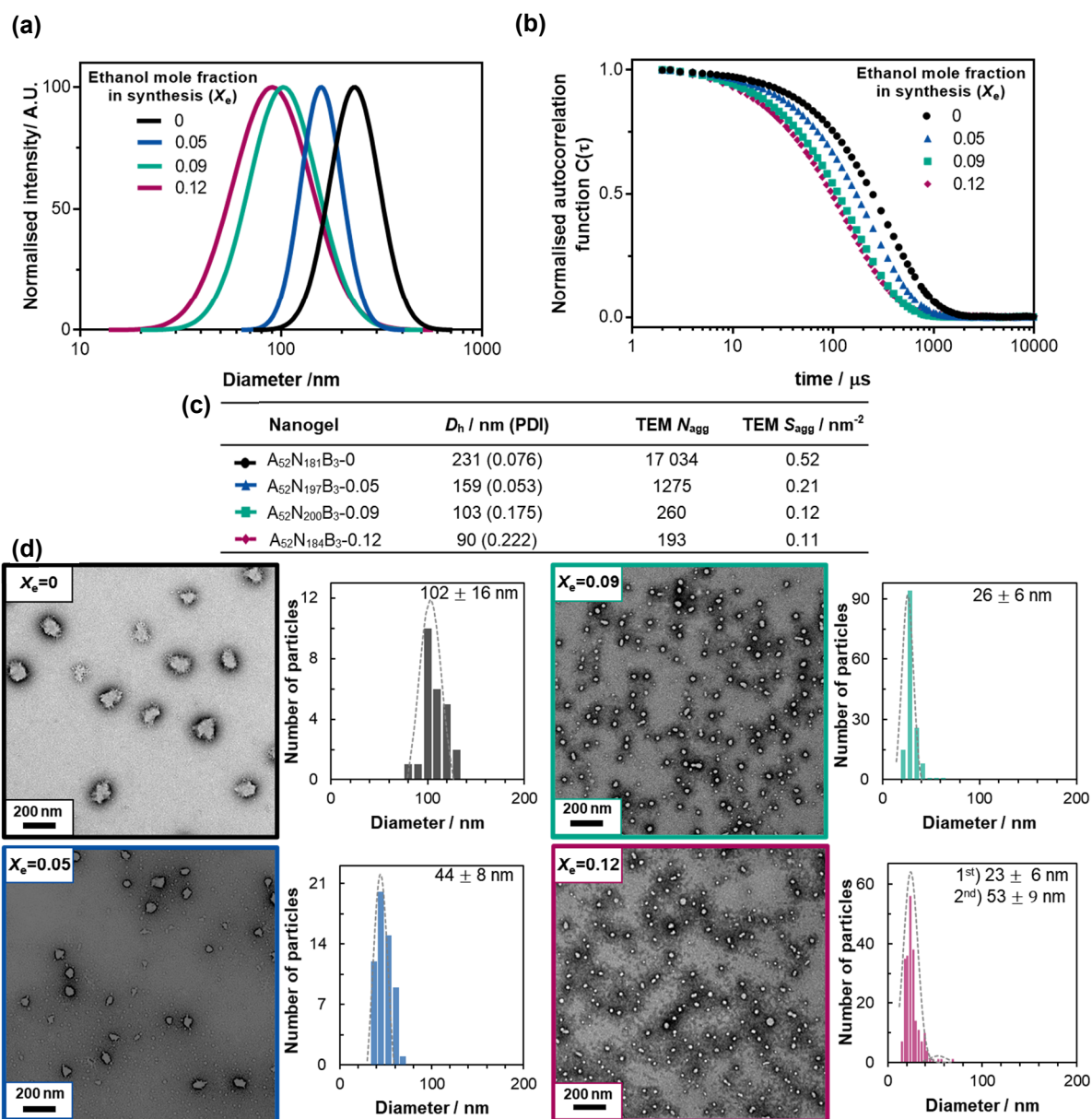


Figure 2.12: Size determination of the $A_{52}N_{200}B_3-X_e$. (a) Intensity average lognormal size distribution curves ($n=4$) and (b) their respective autocorrelation functions with time, (c) Summary of the D_h , mean aggregation numbers (N_{agg} , Equation 2.1) and average number of copolymer chains per unit surface area (S_{agg} , Equation 2.3), and (d) TEM images of the respective purified nanogel with their number particle size distributions. Data obtained from 0.1% w/w nanogel dispersions in DI water at neutral pH. Samples were stained with phosphotungstic acid (0.75% w/v, pH 7.2) for TEM.

N_{agg} estimated using $\bar{M}_{n,theo}$ data from Table 2.3.

In agreement with DLS, TEM analyses on the $A_{52}N_{200}B_3-X_e$ nanogels showed a decrease in size as more ethanol was used in the synthesis (Figure 2.12d). Considering the nanogel synthesised in water alone, it can be seen that the morphology tends to be semi-spherical, and as the ethanol composition increases the morphology tends to be evenly more-rounded in the edges.

As explained before, the semi-sphericity can be attributed to a constrained particle growth due to the presence of the crosslinker and/or to the fusion of growing particles during polymerisation. A faster reaction kinetics was observed for the RAFT dispersion polymerisation of NIPAM in water than in a mixture of water and ethanol targeting the same monomer composition (Figure 2A.13). This difference can be explained by the different polarity of both solvents, which could affect the monomer partitioning between the continuous phase (water-ethanol mixture rather than only water) and the growing particles. Hence, the nanogel particle size and its shape are a function of the monomer/copolymer solubility, monomer and crosslinker concentration, and solvents composition.

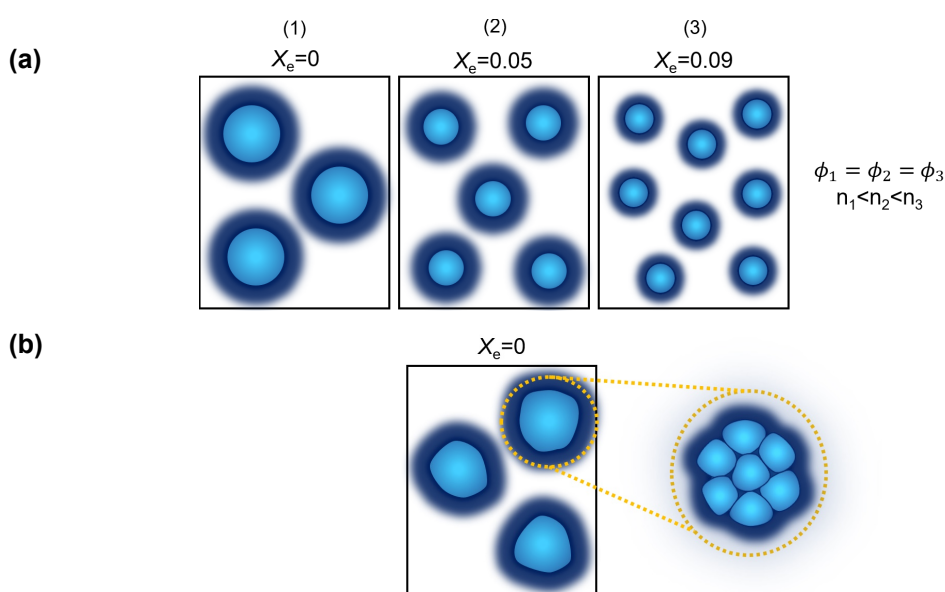


Figure 2.13: Cartoons showing (a) the effect of the ethanol mole fraction composition on the size of the nanogels and (b) the hypothesised fusion of nanogel particles.

A decrease of N_{agg} with increasing X_e was also noticed for the $A_{52}N_{200}B_3-X_e$ nanogels (Figure 2.12c). For example, N_{agg} decreased seemingly from 1275 for $A_{52}N_{197}B_3-0.05$ to 193 for $A_{52}N_{184}B_3-0.12$ (7-fold). As earlier explained, this reduction could be an indication of the production of a higher number of particles with increasing X_e used in synthesis. The apparent increased number of particles (n) is illustrated in Figure 2.13a, where nanogel particles with the same volume fraction (ϕ) have a decreased size with increasing synthesis cononsolvent composition (X_e). However, the significant increase of N_{agg} for nanogels synthesised in only water with a larger PNIPAM volume fraction (N_{agg} from 250 for $A_{52}N_{74}B_3-0$ to 17034 for $A_{52}N_{181}B_3-0$ 68-fold) suggests that a larger number of PNIPAM chains are confined in the $A_{52}N_{181}B_3-0$ nanogel. This could be related to the hypothesis that nascent nanogel particles fused together during polymerisation, though these remained in a semi-spherical shape due to the highly negatively

charged PAA_x. This is illustrated in Figure 2.13b, where a nanogel particle synthesised in water can be in reality the fusion of two or more nascent particles crosslinked together with some PAA potentially entrapped inside the structure.

In the case of the nanogels synthesised with a target PNIPAM DP of 300, the D_h decreased from 483 nm for A₅₂N₂₅₂B₃-0 to 202 nm for A₅₂N₂₅₉B₃-0.10 with apparent near-monodisperse size distributions (PDI ≤ 0.11) (Figure 2.14a and b). These results suggest that when a larger solvophobic block of PNIPAM is targeted, higher ethanol compositions can be used without detrimental consequences over the particle formation. However, a considerably larger N_{agg} was estimated for A₅₂N₂₅₂B₃-0, which was reduced to 1311 for the A₅₂N₂₅₉B₃-0.10 nanogel synthesised in consolvents (Figure 2.14c). It is evident from the TEM micrographs the interparticle-crosslinking for nanogels synthesised in $X_e=0$.

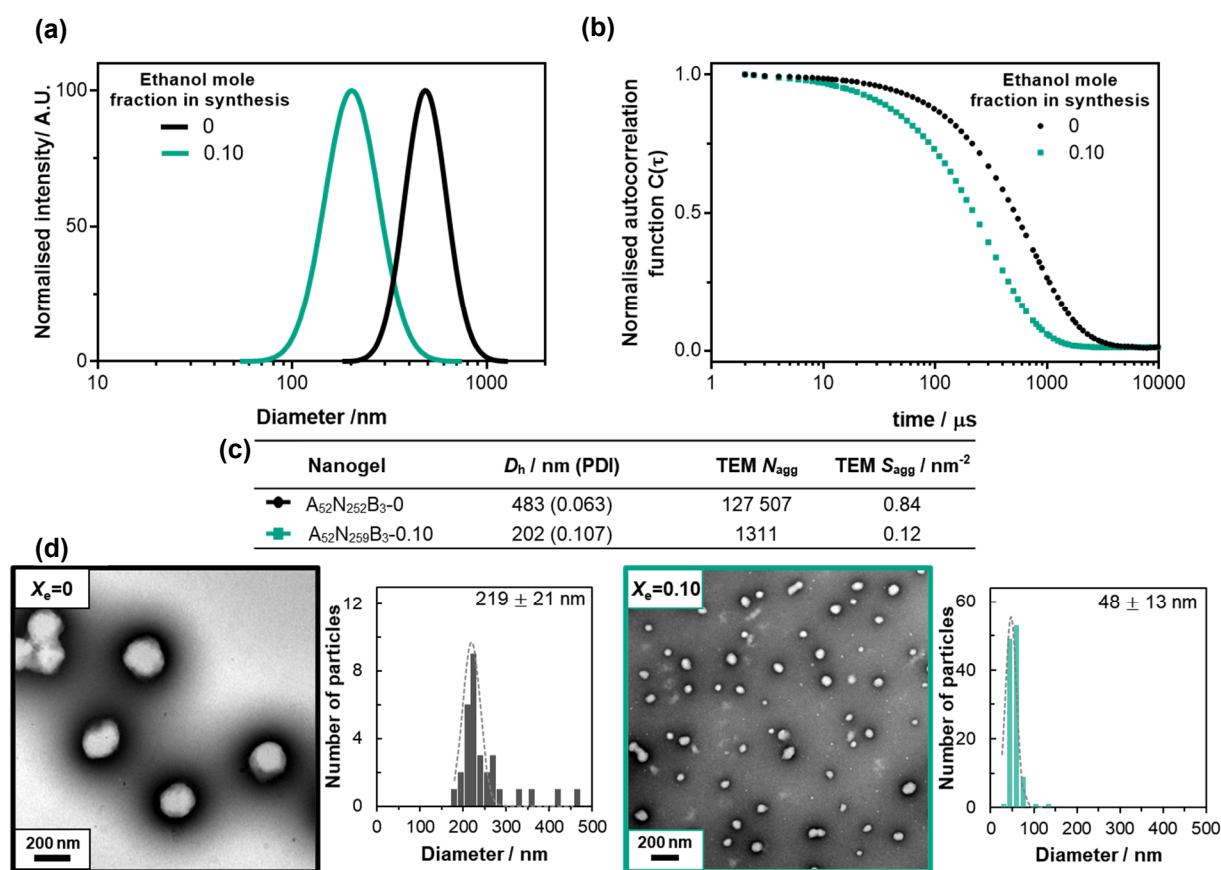


Figure 2.14: Size determination of the A₅₂N₃₀₀B₃- X_e nanogels. (a) Intensity average lognormal size distribution curves ($n=4$) and (b) their respective autocorrelation functions with time, (c) Summary of the D_h , mean aggregation numbers (N_{agg} , Equation 2.1) and average number of copolymer chains per unit surface area (S_{agg} , Equation 2.3), and (d) TEM images of the respective purified nanogel with their number particle size distributions. Data obtained from 0.1% w/w nanogel dispersions in DI water at neutral pH. Samples were stained with phosphotungstic acid (0.75% w/v, pH 7.2) for TEM.

N_{agg} estimated using $\bar{M}_{n,theo}$ data from Table 2.3.

The influence of the crosslinker on the morphology of the nanogels can be seen in the TEM micrographs in Figure 2.15. Considering the nanogels synthesised using either PAA₅₂ or PAA₈₄ with a target DP of 200 (shaded blue) in $X_e \sim 0.05$ as an example, it is evident the nanogels are less uniform in shape when using higher crosslinker compositions. This is more likely to be related to the constrained growth of the particles as more crosslinker is present during self-assembly, which in turn increases the propensity of the fusion of growing particles during polymerisation. Interestingly, when a larger volume fraction of PNIPAM is target (DP of 300 – shaded red) and more ethanol ($X_e \approx 0.1$) is used during the synthesis, nanogels with a more defined semi-sphericity are obtained when using either PAA₅₂ or PAA₈₄, even at high crosslinker densities. This could be attributed to a slower polymerisation rate when targeting a larger PNIPAM DP and a higher ethanol composition.

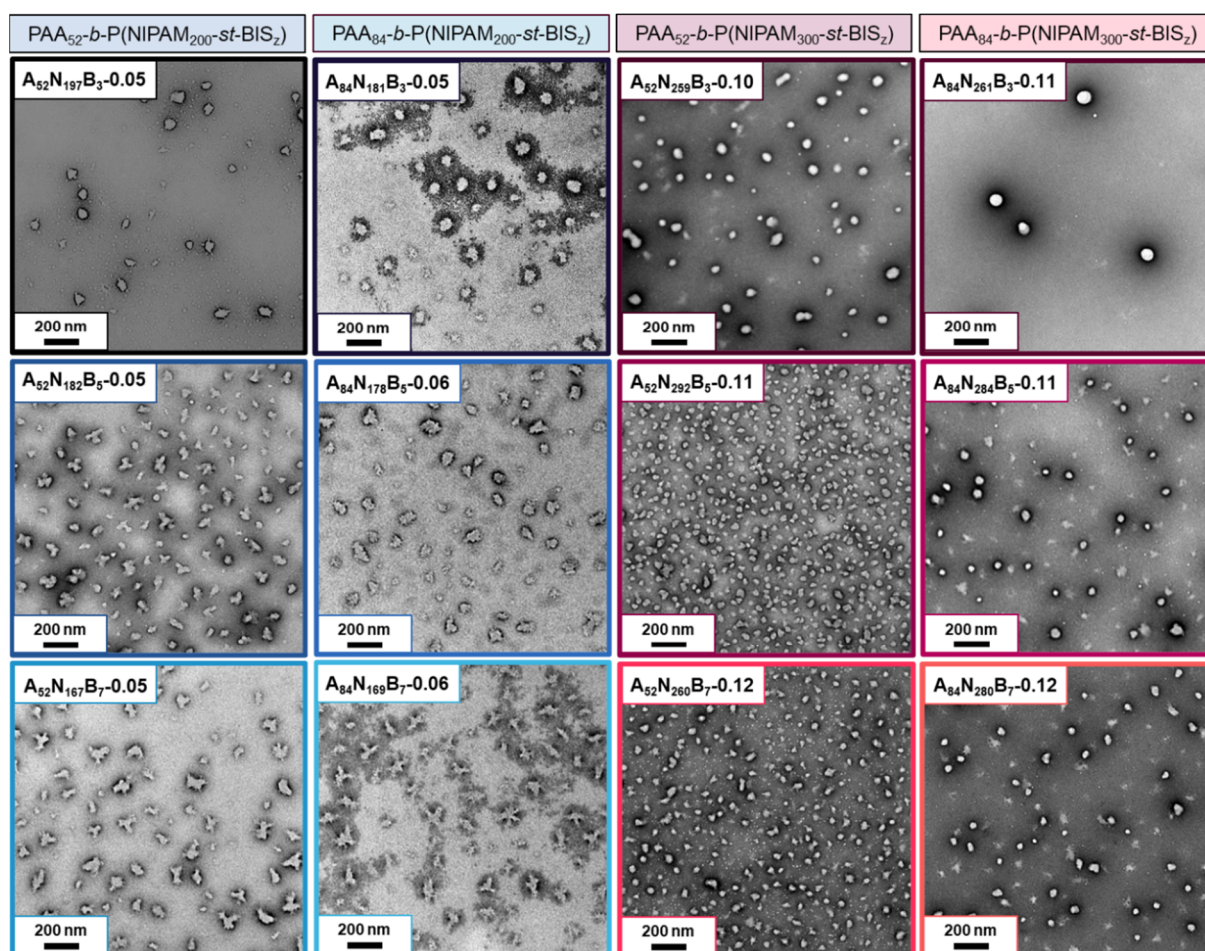


Figure 2.15: TEM micrographs of nanogels synthesised in mixtures of water and ethanol showing the effect of the crosslinker density and the DP of the stabiliser block on the morphology of nanogels. Nanogel samples (0.1% w/w) were stained with phosphotungstic acid (0.75% w/v, pH 7.2).

2.3.4. Insights into the internal structure of the anionic nanogels

(Note: AF4 experiments carried out by Edyta Niezabitowska at the University of Liverpool)

Information about the internal structure or polymer architecture of nanodispersions can be obtained by asymmetric-flow field-flow fractionation (AF4) with a combination of DLS and multi-angle light scattering (MALS) online detectors.⁸²⁻⁸⁵ AF4 separates particles based on their diffusion coefficient, where the larger the R_h the longer the elution time. The hydrodynamic radius (R_h) and the radius of gyration (R_g) can be determined during the size-fractionation of particles, where the dimensionless ratio between these two parameters provides information about the shape and internal structure of particles, i.e. the shape factor ($\rho=R_g/R_h$). Overall, a shape factor of 0.78 indicates a hard sphere, while a value closer to 1 suggests vesicles, and shape factors larger than 1 reveal elongated particles, e.g. rigid rods.⁸⁶⁻⁸⁸

Figure 2.16a shows the fractograms of three different nanogels, where each nanogel showed an increase in R_h and R_g with increasing elution time. If R_h and R_g increase at the same rate, it means that the population of nanogels have a consistent internal structure with particle size.⁸⁹ However, it was noted that the shape factor of nanogels (ρ) gradually increased with elution time for the three samples (Figure 2.16b). This is probably due to a different crosslinking density in the core, in which nanogel particles with greater size had an apparent more homogeneous crosslinking density than those with smaller size. For example, in the fractogram for the nanogel synthesised in water (A₅₂N₁₈₁B₃-0) there is shoulder at around 32 minutes on the MALS 90° signal, which corresponds to a secondary population of the nanogel particles. The main particle population (mean R_h 74 nm) had a shape factor from 0.5 to 0.55, which correlates to typical values for nanogels with a dense inner core and a less dense outer shell (Figure 2.17a).⁹⁰ This suggest that most of the particles have a core-shell structure. However, the second population (mean R_h 85 nm) showed a sharp increase in the shape factor up to 0.88, which suggest that the bigger nanogel particles have a different structure. An explanation can be found in the interparticle crosslinking during chain growth, thus forming nanogels with a higher crosslinking density than the shell. Another possible explanation can be related to the presence of some PAA₅₂ chains that could have been entrapped internally due to an early crosslinking resulting in a more uniform particle (Figure 2.17b).

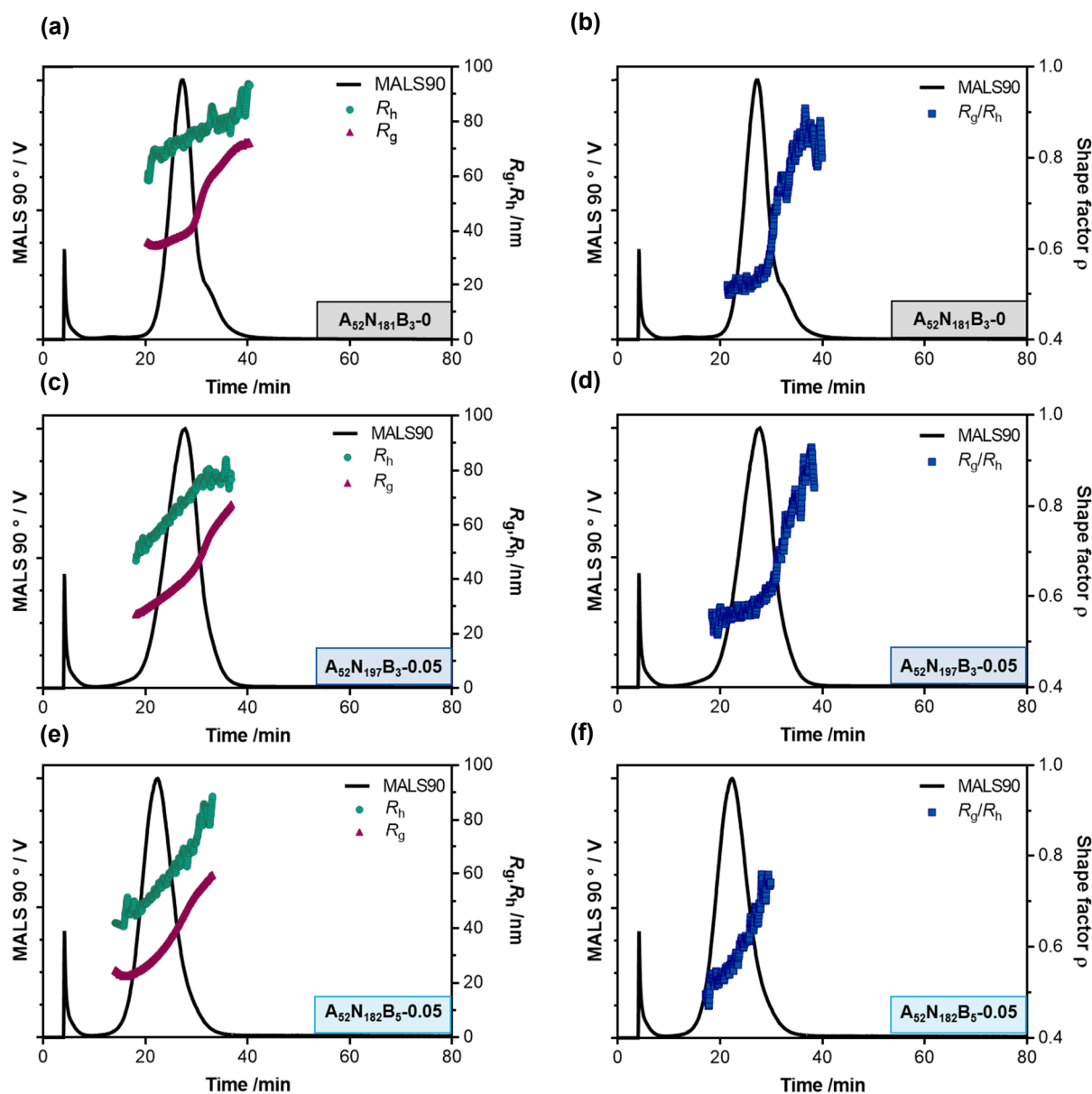


Figure 2.16: AF4-MALS-DLS analysis of $A_{52}N_yB_z-X_e$ nanogels. (—) Fractograms at 90° angle as function of elution time, (●) hydrodynamic radius R_h and (▲) radius of gyration R_g . (■) Shape factor of the corresponding nanogels. Fractograms obtained from nanogel sample dispersions (1% w/w, 20 μ L) using a mobile phase of 0.1 M NaNO_3 in Milli-Q H_2O at 28 $^\circ\text{C}$.

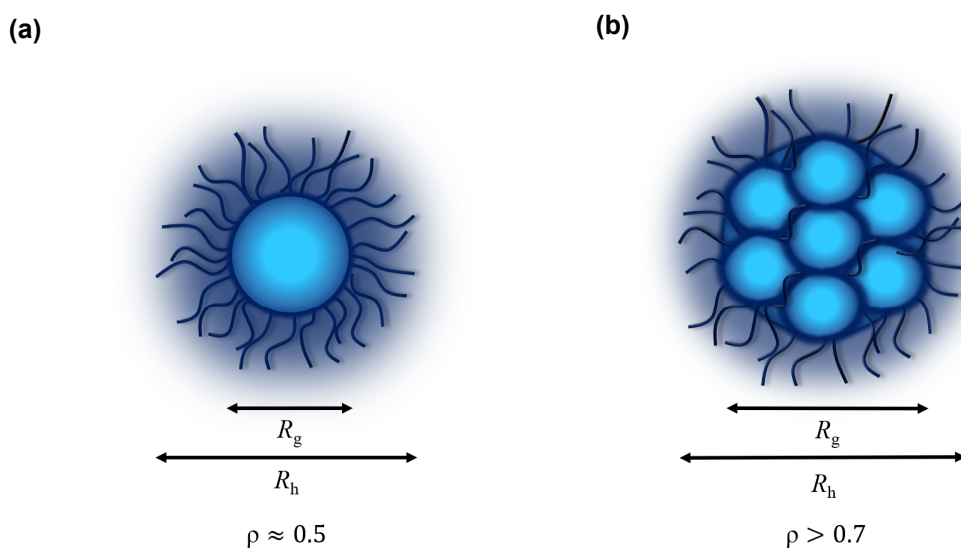


Figure 2.17: Cartoons showing (a) a nanogel with denser inner core compared to the outer shell (b) a nanogel with apparently more homogeneous internal crosslinking density.

In the case of the nanogel with similar composition but synthesised in cononsolvents ($A_{52}N_{197}B_3-0.05$), only one nanogel particle population was evident from the fractogram with a mean R_h of 69 nm and a shape factor ranging from 0.55 to 0.61 (Figure 2.16c and d). However, a similar abrupt increase in the shape factor up to 0.9 was observed for the bigger nanogel particles around 31 minutes, suggesting that these nanogel particles have a more homogeneous structure. In the case of the nanogel with a greater crosslinking density and synthesised in cononsolvents ($A_{52}N_{182}B_5-0.05$), it is noted that these eluted earlier than the nanogels with lower crosslinking density (Figure 2.16e). This is most likely to be related to the greater swelling of the nanogels with lower BIS concentration in the separation eluent. In contrast to the nanogels with lower crosslinking density, the $A_{52}N_{182}B_5-0.05$ nanogel showed a gradual increase in the shape factor ranging from 0.48 to 0.75 for the main nanogel particle population (Figure 2.16f). This could be an indication that the internal structure of the nanogel particles is apparently more homogeneous with increasing size as for the nanogels with lower crosslinking density. As previously observed in TEM micrographs (Figure 2.15), these nanogel particles have an irregular shape and it is more evident that the nanogel particles are the fusion of nascent particles due to the higher concentration of crosslinker during polymerisation resulting in an increased propensity for interparticle crosslinking.

Table 2.4 shows the summary of the mode values obtained from the fractograms. The discrepancy from the R_h values for the mode values and the R_h estimated by batch DLS is probably due to the presence of 0.1 M NaNO_3 in the mobile phase during fractionation, which can screen the carboxylate charges from the shell of the nanogels. Overall, it was noted that the three analysed nanogels mainly possessed a structure with a shell and more densely PNIPAM crosslinked core, where the addition of a small mole fraction of ethanol in the synthesis allows the formation of nanogel particles with a more even internal structure than those synthesised only in water.

Table 2.4: Summary of the mode values obtained from AF4-MALS-DLS. ^a

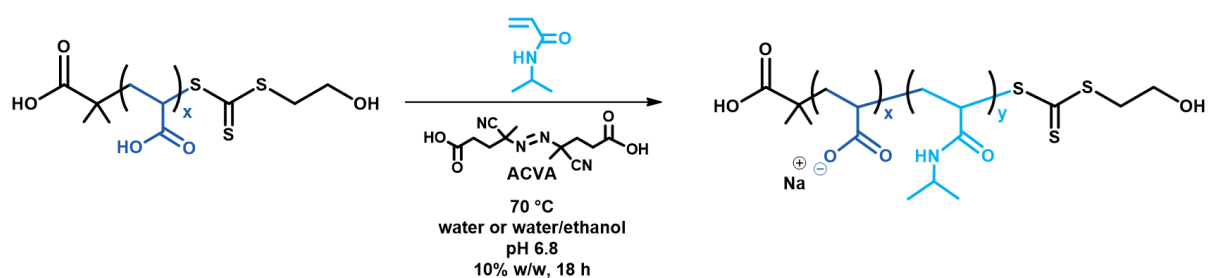
Nanogel	R_g / nm	R_h /nm	$R_{h,\text{batch}}$ /nm ^b	PDI ^b	ρ ^c
A ₅₂ N ₁₈₁ B ₃ -0	39 ± 0.50	74 ± 0.25	113 ± 1.7	0.080	0.53
A ₅₂ N ₁₉₇ B ₃ -0.05	40 ± 0.54	69 ± 0.25	78 ± 0.72	0.072	0.58
A ₅₂ N ₁₈₂ B ₅ -0.05	31 ± 0.50	55 ± 0.49	75 ± 0.43	0.070	0.56

^aData calculated for fractionation with an initial cross-flow of 1 mL min⁻¹ using a mobile phase of 0.1 M NaNO_3 in Milli-Q H₂O at 28 °C. ^bDetermined by batch DLS from 0.1% w/w nanogels dispersions in DI water at neutral pH at 27.5 °C. ^cObtained from $\rho=R_g/R_h$

2.3.5. Synthesis and characterisation of PAA_x-*b*-PNIPAM_y diblock copolymers

Despite the previous results have shown that the synthesis of nanogels in cononsolvents affects greatly the size, structure, and shape of the nanogels. A better understanding of the effect of adding ethanol to the aqueous dispersion polymerisation of PAA-*b*-PNIPAM nanogels on the physicochemical properties can be acquired for analogous soluble block copolymers. Thus, diblock copolymers without crosslinker were synthesised using the same RAFT-mediated PISA approach.

PAA₃₇ and PAA₈₄ macro-CTAs were used to prepare a series of PAA_x-*b*-PNIPAM_y diblock copolymers by RAFT dispersion polymerisation of NIPAM in either water or water/ethanol mixtures (Scheme 2.3). PNIPAM DPs similar to the ones used for the synthesis of nanogels were targeted. Overall, a change from a clear solution to a turbid dispersion was observed at around 8 minutes at 70 °C. After quenching of the reactions, the heterogeneous dispersions change to clear solutions at ambient temperature indicating the dissolution of the copolymer chains. ¹H NMR spectroscopy showed that almost full conversion of NIPAM (99%) was reached for the copolymers synthesised using PAA₃₇, whereas a lower NIPAM conversion (>93%) was reached when using PAA₈₄ as macro-CTA (Table 2.5). The full list of the conditions at which diblock copolymers were prepared, as well as the properties of these polymer can be found in Table 2.5. These results will be discussed in the accordingly sections.



Scheme 2.3: Synthesis of PAA_x-*b*-PNIPAM_y diblock copolymers using RAFT dispersion polymerisation. Note: Under the reaction conditions, PAA is seemingly ≈89% deprotonated.

A similar notation to the one used for the nanogels monomer composition is utilised henceforth (A_xN_y-X_e). Thus A, and N symbolises acrylic acid and *N*-isopropyl acrylamide, respectively, and X_e symbolises the ethanol mole fraction used in the synthesis. Hence, A_xN_y represents PAA_x-*b*-PNIPAM_y where x and y are the number-average DP of each monomer component as determined by ¹H NMR spectroscopy analyses.

Table 2.5: Summary of the synthesis and properties of $A_xN_y-X_e$ diblock copolymers.

Target composition [PAA _x]:[NIPAM] ^a		Ethanol mole fraction (X_e) ^b	Conversion ^c %	PNIPAM DP _{,theo} ^d	Cloud point (T_{cp}) ^e / °C	D_h / nm (PDI) ^f	
x=37	[1]:[100]	0	>99	100	42.6	ill-defined particles	
	[1]:[100]	0.06	99	99	43.1	139 (0.17)	
	[1]:[100]	0.11	99	99	44.5	178 (0.08)	
	[1]:[100]	0.14	>99	100	46.9	153 (0.13)	
	[1]:[199]	0	>99	199	34.2	49 (0.06)	
	[1]:[199]	0.06	>99	199	36.4	63 (0.04)	
	[1]:[199]	0.12	>99	199	38.6	93 (0.22)	
	[1]:[199]	0.15	99	197	39.4	140 (0.16)	
	[1]:[302]	0	>99	302	33.9	60 (0.04)	
	[1]:[302]	0.06	99	299	34.2	63 (0.09)	
	[1]:[302]	0.12	99	299	35.4	92 (0.15)	
	[1]:[302]	0.15	99	299	36.4	141 (0.16)	
	x=84	[1]:[202]	0.04	97	196	35.6	145 (0.14)
		[1]:[202]	0.09	96	194	37.5	202 (0.08)
[1]:[303]		0.05	97	294	34.6	132 (0.11)	
[1]:[303]		0.09	93	281	36.1	180 (0.06)	

^aGeneral reaction conditions: Target [HEMP]/[ACVA]=5, solids content 10% w/w, 70 °C for 18 h. ^bSolvent mixture used during the synthesis, H₂O-ethanol was used as the cononsolvent pair. ^cDetermined by ¹H NMR spectroscopy studies using the ratio of the sum of vinyl proton integrals and the polymer backbone. ^dEstimated using Equation 1.2 [NIPAM]/[PAA_x] \times conversion. ^eCloud points were estimated from the inflection point of the normalised absorbance curve of 1% w/w aqueous solutions at 550 nm on a heating rate of 0.12 °C min⁻¹. ^fThe hydrodynamic diameter of the aggregate structures at 50 °C was determined by DLS of 0.1% w/w aqueous solutions at pH 7.

After purification, the chemical structure of the diblock copolymers was confirmed by ¹H NMR spectroscopy. In all cases, the diblock copolymers had a similar structure regardless of the solvent mixture used in the synthesis, i.e. resonance of the proton peaks corresponding to the polymer backbone. The degree of polymerisation could not be estimated accurately since no end groups were observed in the collected spectra probably due to the high molar mass⁹¹ and also because of the overlap between the resonance peaks from the PAA chain backbone with those of PNIPAM. For simplicity, only the full spectroscopic characterisation of the A₃₇N₁₉₉-X_e diblock copolymers is shown here (Figure 2.18). However, the stacked spectra for A₃₇N₃₀₂-X_e, A₈₄N₂₀₂-X_e and A₈₄N₃₀₃-X_e can be found in the Appendix A (Figure 2A.14-16). By comparing each of the proton peaks, it is noted that these have a similar proton area, except from the proton peaks corresponding to the methylene group in the 1.3-1.8 ppm region. It is seen in the stacked ¹H NMR spectra that in this area the copolymers have a dissimilar intensity which can be related to a different tacticity, specifically the relative amounts of the meso (m) and racemic (r) diads. This referring to changes in the orientation of the amide pendant group with respect to the polymer backbone. The orientation of pendant groups can be quantified by the intensity of the

protons due to differences in the chemical environment that arise from the position of the pendant groups which can be located exclusively on the same side of the backbone (isotactic), lie on alternate sides (syndiotactic), or being located randomly on either side of the chain (atactic).⁹² A small increase of syndiotacticity was observed from 53% racemic content for A₃₇N₁₉₉-0 to 59% racemic content for A₃₇N₁₉₇-0.15. Hence, it is suggested that this small change in the tacticity of PNIPAM is caused by the use of cosolvents during PISA.

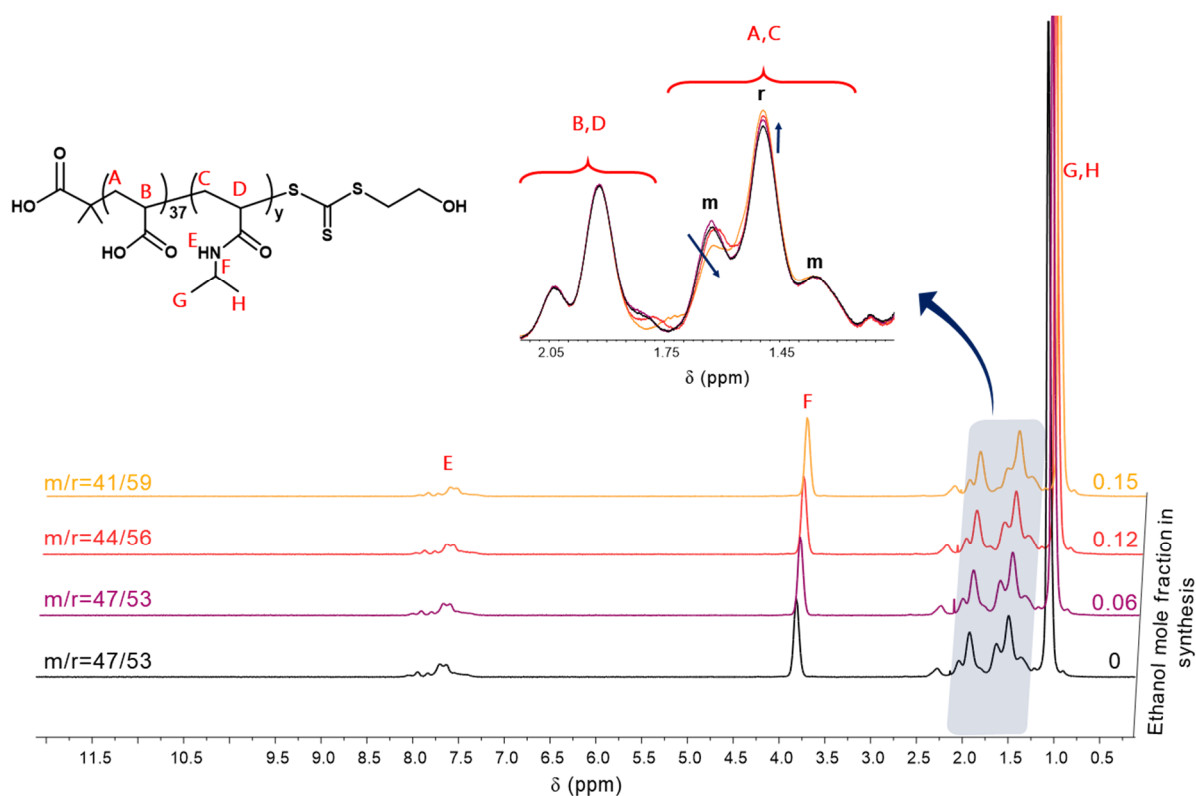


Figure 2.18: Stacked ¹H NMR spectra recorded in D₂O of purified A₃₇N₁₉₉-X_c diblock copolymers. The H₂O solvent peak was suppressed to gain better resolution of the spectra.

Previously, the changes in tacticity of PNIPAM synthesised in methanol-water mixtures by RAFT polymerisation in the presence of yttrium trifluoromethanesulfonate (Y(OTf)₃) as a Lewis acid has been investigated by Biswas *et al.*⁴⁸ They observed that the isotacticity of PNIPAM increases when using high mole fractions of methanol during the synthesis. For instance, the meso diad content increased from 55 to 86% with increasing methanol mole fraction composition from 0.31 to 1 when using Y(OTf)₃ at 0.1 M. In contrast to their observations, in this work the PAA-*b*-PNIPAM diblock copolymers synthesised in water are more meso-rich than those synthesised in higher ethanol compositions. This is probably because Biswas *et al.*⁴⁸ synthesised PNIPAM outside the consolvency region and in the ethanol-rich region, which are the conditions for solution polymerisation. Besides, by using a Lewis acid the tacticity of

homopolymers can change dramatically because they are able to form complexes with both monomers and propagating species.⁹³ Hence, it is suggested that the use of cononsolvents in the synthesis of PNIPAM could have an effect on the chain stereochemistry since a Lewis acid was not used here. In the literature, it is reported that the rate of polymerisation is influenced by the reaction medium, which can in some cases change the tacticity of polymers.⁹³ Additionally, this effect can be strengthened for reactions involving ionic species or monomers capable of forming hydrogen bonds, the latter being the case with NIPAM.

To prove if the use of cononsolvents affects the properties and tacticity of PNIPAM, a series of NIPAM polymers were synthesised in a range of water-ethanol mixtures at the same monomer and initiator concentrations *via* free radical precipitation polymerisation. PNIPAM- X_e homopolymers reached full conversion as judged by ^1H NMR spectroscopy. After purification, these were characterised by UV-vis spectroscopy, GPC and ^1H NMR spectroscopy. As determined by turbidimetry experiments, the cloud point temperature (T_{cp}) of all of the PNIPAM- X_e homopolymers was around 33 °C and no evident changes in T_{cp} were observed regardless of the X_e mole fraction composition (Appendix A, Figure 2A.17a). However, a gradual decrease in \bar{M}_n and \bar{M}_w/\bar{M}_n was observed from 2.8×10^5 Da ($\bar{M}_w/\bar{M}_n=5.4$) for PNIPAM synthesised in $X_e=0$ to 3.5×10^4 Da ($\bar{M}_w/\bar{M}_n=3.0$) for PNIPAM synthesised in $X_e=0.15$ (Appendix A, Figure 2A.17b). This difference in molar mass is related to the difference in solubility of the growing PNIPAM chains in water and in mixtures of water and ethanol during polymerisation as the lower LCST of PNIPAM in cononsolvents mean the chains will precipitate earlier in the polymerisation and thereby reducing \bar{M}_n . Figure 2.19 shows the stacked ^1H NMR spectra of the purified PNIPAM homopolymers synthesised in different X_e , where no changes in the tacticity were observed, i.e. the intensity in the methylene proton area was the same for all the polymers. Since no changes in tacticity were observed due to the use of cononsolvents by precipitation polymerisation, it is hypothesised that the relatively constrained chain growth of PNIPAM stabilised by PAA in a PISA process can restrict the NIPAM monomer addition during propagation steps influenced by cononsolvents, which ultimately results in a different stereosequence of the PNIPAM pendant groups. This in turn could have affected the chain folding and packing when synthesising nanogels.

In the work of Biswas *et al.*,⁴⁸ it was also noted that changes in the tacticity of PNIPAM alter the cloud point temperature accordingly to the composition of cononsolvents in which they were synthesised, which was also observed here. The full discussion of the effects of the cononsolvent composition on the thermal properties of the $A_xN_y-X_e$ diblock copolymers is

covered in Section 2.3.4.1 and the details of the properties are summarised in Table 2.5.

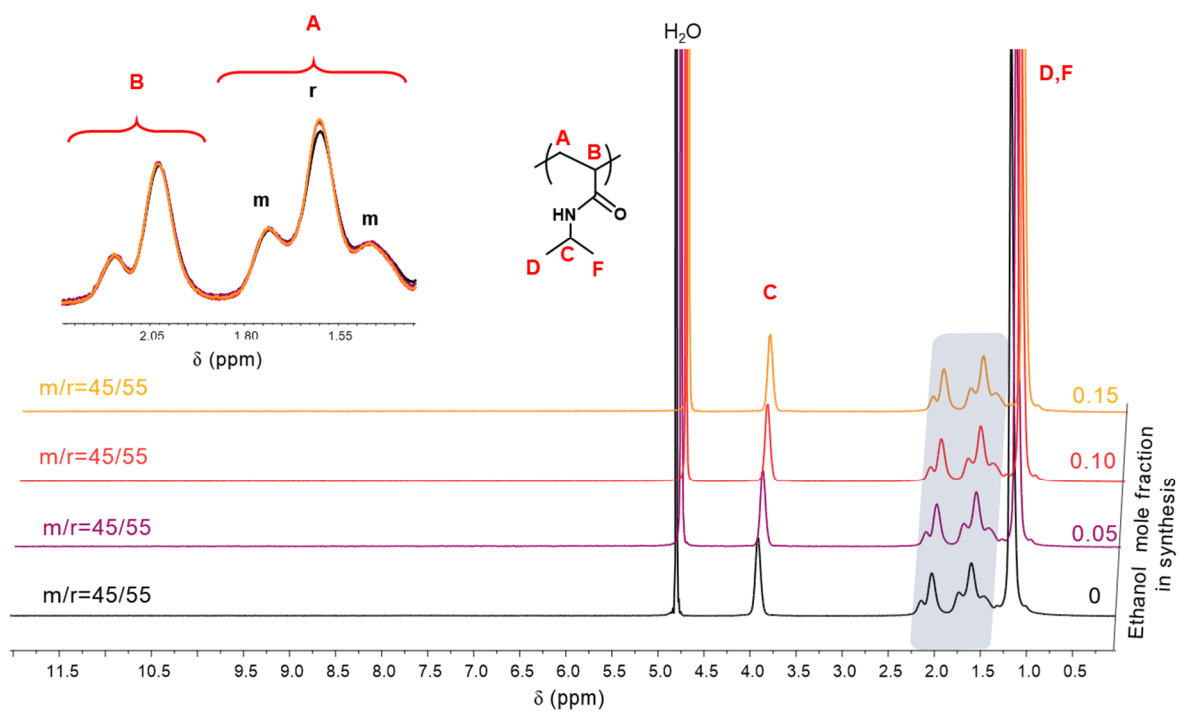


Figure 2.19: Stacked ^1H NMR spectra recorded in D_2O of purified PNIPAM- X_c homopolymers synthesised by free radical polymerisation. The H_2O solvent peak was suppressed to gain better resolution of the spectra.

2.3.4.1. The temperature behaviour of PAA-*b*-PNIPAM diblock copolymers

The synthesised diblock copolymers were thermosensitive since it was evident that the copolymers dissolved upon cooling. For example, the crude copolymer A₃₇N₁₉₉-0 was a turbid dispersion after polymerisation at the temperature reaction of 70 °C and a transparent solution after cooling down to 20 °C (Figure 2.20). Moreover, this transition was reversible since the solution became turbid when heated again.

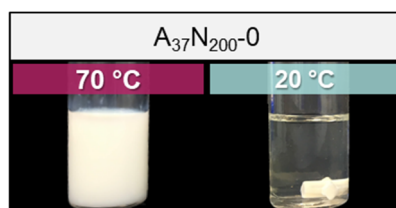


Figure 2.20: Digital photograph of the crude A₃₇N₁₉₉-0 copolymer at 70 and 20 °C.

As mentioned in Chapter 1, the temperature at which a phase solubility transition occurs is called critical solution temperature. In the case of PNIPAM homopolymer, this transition is an indication of the coil to globule transition of the polymer chains above the lower critical solution temperature (LCST), which can be observed macroscopically as a soluble-to-insoluble phase separation. In general, there are different factors that can affect the LCST of PNIPAM such as composition of PNIPAM-based copolymers, molar mass, solvent composition, and salt ion concentration.⁹⁴ For instance, it has been previously reported that PNIPAM with hydrophilic end-groups increased the LCST whilst hydrophobic end-groups decreased it; nonetheless, this effect is most significant for short polymers and diminishes for polymers with a molar mass above 10kDa.⁹⁵ Although this can be also observed in PNIPAM-based particles, other temperature transitions are seen according to the structure and the location of PNIPAM in the particle. Unlike the linear analogues, PNIPAM chains can either aggregate, collapse, or shrink depending on the structure, the degree of polymerisation and the composition of the temperature-sensitive particles.⁹⁶⁻⁹⁸ On one hand, when micellar particles with a hydrophobic core are coated with PNIPAM, the PNIPAM chains collapse onto the hydrophobic core as the temperature approaches the LCST.⁹⁷ Additionally, if the end-groups of PNIPAM, e.g. carboxylic acid⁹⁷ or carboxylic azo end-groups,⁹⁹ are ionised the phase separation can be suppressed in basic pH due to electrostatic repulsion which prevents demixing. On the other hand, copolymers comprising PNIPAM and a hydrophilic block, such as PAA, exhibit a different temperature response since the copolymer

aggregates in solution differently according to pH and temperature.^{100,101} Schilli *et al.*¹⁰⁰ observed that the behaviour of PNIPAM₅₀-*b*-PAA₁₁₀ copolymers in solution is influenced by hydrogen bonding, pH, and temperature. PNIPAM formed a core and PAA a corona at a pH>4 above the LCST but the opposite is observed at pH>4 below the LCST, i.e. PAA forms a core and PNIPAM a shell, and above the LCST larger aggregates were observed under the conditions of the latter case.¹⁰⁰ Khimani *et al.*¹⁰¹ observed a gradual shift in the cloud point temperature (T_{cp}) to lower temperatures for PNIPAM₁₄₉-*b*-PAA₄₆ copolymers with decreasing pH from 6.2 to 4.2 due to the protonation of PAA. However, at pH 10 and 12 the T_{cp} disappears due to the reduced phase separation caused by charged sites that increases solubility.¹⁰¹ Additionally, they stated that the observed T_{cp} of 38 °C at pH 6.2 was related to the shrinking of the chains *via* intramolecular collapse of unimers followed by the aggregation of collapsed chains into larger particles.¹⁰¹ The latter being observed by small angle neutron scattering (SANS) at 32 °C and a contraction of the PNIPAM segments was confirmed at 40 °C. Hence, it can be assumed that for copolymers of PAA and PNIPAM the cloud point temperature detected by turbidimetry is merely the thermal transition from unimers to aggregates triggered by changes in solubility of the PNIPAM block with increasing temperatures. However, detailed information about the structure of the copolymer aggregates can potentially be obtained by small angle scattering techniques and/or cryogenic transmission electronic microscopy.

Herein, the temperature behaviour of the $A_xN_y-X_e$ copolymers was investigated by UV-vis absorption spectroscopy and dynamic light scattering (DLS) at different temperatures only at neutral pH. DLS was used to assess the size of aggregates formed upon heating, and UV-vis spectroscopy at a wavelength of 550 nm was used to assess the sensitivity of the $A_xN_y-X_e$ copolymers to increasing temperature as indicated by changes in the light absorbance of the samples in aqueous solutions (i.e. the change from transparent solutions at room temperature to turbid dispersions upon heating). It is noteworthy that turbidimetry detects the outcome of the thermal transition (i.e. a macroscopic event) and not the actual cloud point;⁹⁶ however, in this work is termed as the cloud point (T_{cp}) since no other techniques were used as complementary techniques. Other techniques such as microcalorimetry, temperature-dependent ¹H NMR spectroscopy and scattering techniques are proposed to be used in future work.

To assess the effects of the consolvents composition used in synthesis on the thermal properties of $A_xN_y-X_e$ block copolymers, turbidimetry experiments of the $A_{37}N_y$ diblock copolymers synthesised in water is presented first as a reference. A transition from a transparent solution to a turbid dispersion was observed even though at around pH 7 PAA is highly

deprotonated ($\approx 89\%$) and the negative charge could have suppressed the T_{cp} . Figure 2.21 shows the effect of the mean DP of PNIPAM (y) on the temperature phase transition of aqueous solutions. It was noted a shift in the T_{cp} from 43 to 34 °C as the DP of PNIPAM increased from 99 to 199 and 299. It is suggested that the shorter PNIPAM block ($y=99$) had a greater T_{cp} due to a greater hydrophilicity contribution from the PAA₃₇ block at pH 7, effect that has been previously reported.¹⁰² However, this hydrophilicity contribution is reduced for larger PNIPAM blocks ($y>199$), and no variations on the T_{cp} were observed regardless of the different PNIPAM DPs.

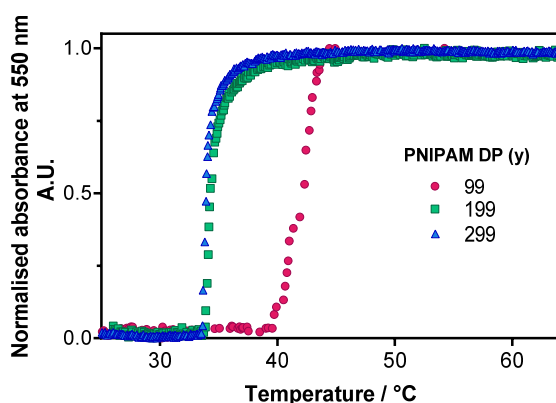


Figure 2.21: Turbidimetry experiments of $A_{37}N_y-0$ diblock copolymers in aqueous solution at pH 7. Cloud point curves of PNIPAM where $y = (\bullet)99$, $(\blacksquare)199$ and $(\blacktriangle)299$. The cloud points were determined from the inflection point of the normalised absorbance curve at 550 nm on a heating rate of 0.12 °C min^{-1} .

To investigate the effect of the PAA₃₇ block on the cloud point temperature of A_xN_y diblock copolymers, PNIPAM homopolymers were synthesised using RAFT solution polymerisation with HEMP CTA. The purified PNIPAM homopolymers had a number-average DP of 99 and 190 and a T_{cp} of 35 and 34 °C, respectively (Appendix A, Figure 2A.18a). These homopolymers had practically the same T_{cp} as determined for the diblock copolymers with a PNIPAM DP greater than 199. Hence, it is evident that the PAA₃₇ block has only a considerably effect on the T_{cp} for copolymers with short PNIPAM block (8 °C difference).

Interestingly, a shift in the T_{cp} of the aqueous solutions of diblock copolymers with the same monomer composition synthesised in different cononsolvents was observed. Considering the $A_{37}N_{199}-X_e$ diblock copolymers as an example, the turbidimetry experiments showed that the T_{cp} was increased from 34 °C for $A_{37}N_{199}-0$ to 39 °C for $A_{37}N_{197}-0.15$ (Figure 2.22). A similar increase in the T_{cp} with increasing X_e in the synthesis was observed for the $A_{37}N_y-X_e$ where $y=100$ and 302 (Figure 2A.19a and b) and for the $A_{84}N_y-X_e$ where $y=202$ and 303 (Figure 2A.20a and b). The shift in T_{cp} can be related to changes in tacticity of the polymers.¹⁰³ According to $^1\text{H NMR}$ studies (Figure 2.18.), copolymers synthesised in water are more meso-rich and hence slightly more

hydrophobic than those synthesised in mixes of cononsolvents, this matches with the observations in the turbidimetry experiments. For example, $A_{37}N_{199-0}$ (47% meso content) had a T_{cp} of 34 °C whilst $A_{37}N_{199-0.15}$ (41% meso) had a T_{cp} of 39 °C. The block copolymers with more meso-rich PNIPAM had a lower T_{cp} , due to the intermolecular interactions from a greater number of side groups on the same side of the chain, which can also affect the hydration between the neighbouring chain groups. In contrast, the block copolymers with more racemic PNIPAM (i.e. more side groups with alternate position) exhibit more intramolecular hydrogen bonding, which increases the interchain interactions between side chains, i.e. more heat energy is needed to break these interactions.^{103,104}

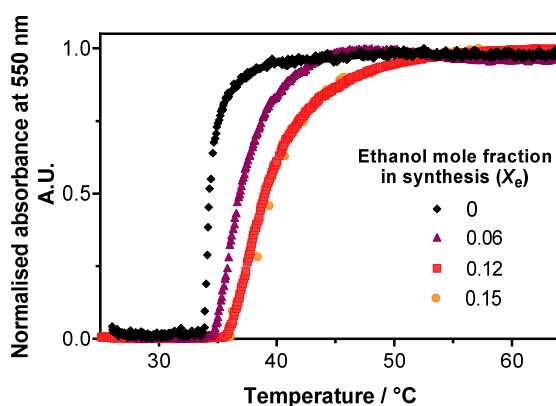


Figure 2.22: Turbidimetry experiments of $A_{37}N_{199-X_e}$ diblock copolymers in aqueous solution at pH 7. Water-ethanol mixtures used in the synthesis X_e of (\blacklozenge) 0, (\blacktriangle) 0.06, (\blacksquare) 0.12 and (\bullet) 0.15. The cloud points were determined from the inflection point of the normalised absorbance curve at 550 nm on a heating rate of 0.12 °C min⁻¹.

As earlier stated, PNIPAM homopolymers synthesised by precipitation polymerisation in cononsolvents have the same tacticity (45% meso) and the same T_{cp} of 33 °C regardless of the difference in molar mass. Hence, the use of cononsolvents has an effect on the stereochemistry of PNIPAM only for a PISA synthesis. It is hypothesised that the water-ethanol solvent composition affects the monomer partitioning and, more significantly the insertion of the monomer during chain growth in the nucleation and propagation steps.

It is well established that a small addition of ethanol into aqueous solutions of PNIPAM decreases the LCST.^{20,37–39} For example, PNIPAM₉₈ synthesised here by RAFT using HEMP CTA had a T_{cp} of 35 °C in only water, but a T_{cp} of 25 °C at $X_e=0.05$ and an even lower T_{cp} of 7 °C at $X_e=0.10$ (Appendix A, Figure 2A.18b). Although, several models have been developed to explain the shift in the cloud point behaviour of PNIPAM in cononsolvents, the actual dynamic mechanism of this phenomenon is still unclear.^{43,46,105–108} In the case of a RAFT-mediated PISA,

the addition on ethanol as a cosolvent pair with water for PNIPAM is thought to affect the solvency of the growing PNIPAM chains during polymerisation. Where the LCST of PNIPAM is shifted to lower temperatures with increasing water-ethanol compositions. Consequently, the ethanol mole fraction used in the synthesis should greatly affect the critical chain length at which the self-assembly of PAA-*b*-PNIPAM, occurs i.e. the nucleation step. To assess the magnitude at which the T_{cp} is shifted in the reaction medium, the purified block copolymers were dispersed in the same ethanol mole fraction used in their synthesis. Figure 2.23 shows the turbidimetry experiments of the diblock copolymers dissolved in the X_e composition these were synthesised. It is evident that the A₃₇N₁₉₉-0.15 copolymer had the greatest shift in the cloud point (from 39 °C in only water to 13 °C at $X_e=0.15$), whereas the A₃₇N₁₉₉-0.06 copolymer only showed a decreased in 11 °C (from 36 °C in only water to 25 °C $X_e=0.06$). Consequently, it is suggested that during the chain growth the onset of self-assembly is shifted to lower DP of PNIPAM for higher X_e , which eventually leads to an early constrained particle growth affecting the monomer addition on the radical centre (i.e. steric effects on the stereosequence).

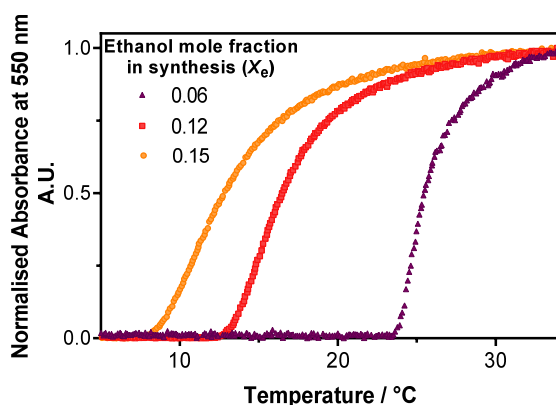


Figure 2.23: Turbidimetry experiments of A₃₇N₁₉₉- X_e diblock copolymers at pH 7 in the ethanol mole fraction these were synthesised. Cloud point curves of PNIPAM synthesised in X_e (▲) 0.06, (■) 0.12 and (●) 0.15. The cloud points were determined from the inflection point of the normalised absorbance curve at 550 nm on a heating rate of 0.12 °C min⁻¹.

To confirm that the addition of ethanol to the aqueous RAFT-mediated PISA was not detrimental to the control over the polymerisation of NIPAM, the molar mass of these diblocks should be determined. Unfortunately, the molar mass determination of PAA-*b*-PNIPAM diblock copolymers by GPC could not be determined due to inefficient esterification by methylation with TMS-diazomethane or by alkylation with benzyl bromide. Hence, 2-hydroxyethyl acrylamide (HEA) was used to prepare analogous PHEA-*b*-PNIPAM diblock copolymers using the same consolvency approach (properties of these copolymers can be found in the Appendix A; Table 2A.2). Figure 2.24a shows the turbidimetry experiments and the DMF GPC chromatograms

of the PHEA-*b*-PNIPAM diblock copolymers synthesised in either water or mixtures of water and ethanol as cosolvents. It is evident that changes in T_{cp} of the PHEA-*b*-PNIPAM copolymers was not as sharp and drastic as the one observed for the $A_xN_y-X_e$ copolymers, probably due to the absence of negative charges that help stabilise the aggregates. However, it is clear that the copolymer synthesised in water is slightly more hydrophobic than the ones synthesised in cosolvents. Moreover, the tacticity of the methylene group showed only 1% decrement in the meso content for the copolymers synthesised in cosolvents (Appendix A; Figure 2A.21). This suggests that the highly charged PAA macro-CTA at pH 7 influences more the T_{cp} and the stereosequence of the PNIPAM during PISA than a non-charged solvophilic macro-CTA. Furthermore, according to the GPC chromatograms unimodal distributions and high blocking efficiencies were observed for all the diblock copolymers (Figure 2.24b). The diblock copolymers synthesised in a higher ethanol composition tend to be broader and less symmetrical. On a lesser contribution this could also explain the decrease of T_{cp} of the $A_xN_y-X_e$ diblock copolymers at high ethanol mole fraction compositions used in the synthesis.

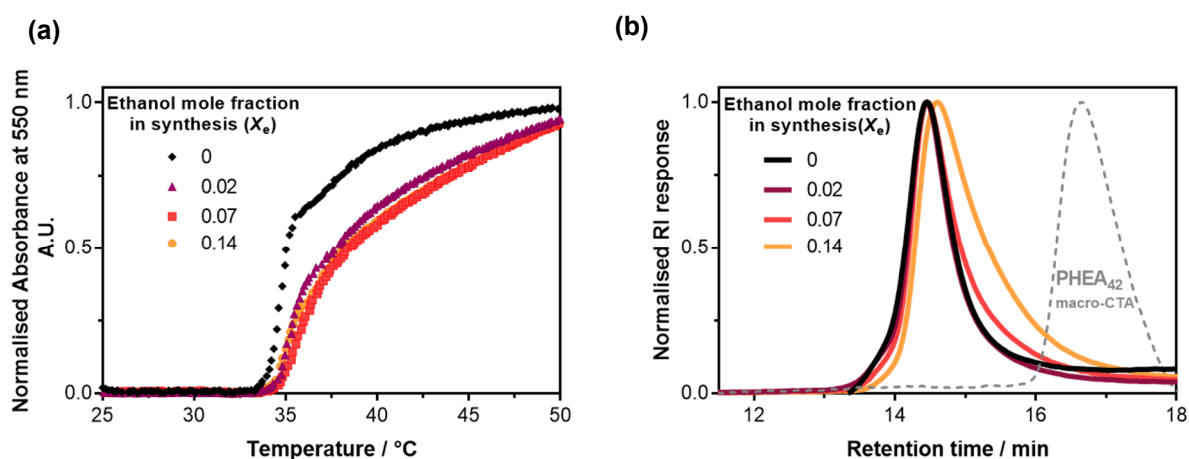


Figure 2.24: (a) Turbidimetry experiments and (b) DMF GPC chromatograms of PHEA₄₂-*b*-PNIPAM₂₀₀ diblock copolymers. Polymers were synthesised *via* RAFT dispersion polymerisation in either water or mixtures of cosolvents; target [NIPAM]:[PHEA₄₂]:[ACVA]=200:1:5, solids content 10% w/w, 70 °C for 6.5 h. Cloud point curves were determined from the inflection point of the normalised absorbance curves at 550 nm on a heating rate of 0.12 °C min⁻¹ of copolymer aqueous solutions. (GPC: DMF 0.1% LiBr eluent, vs PMMA standards).

2.3.4.2. The self-assembly of PAA-*b*-PNIPAM diblock copolymers

Considering that the $A_xN_y-X_e$ copolymers exhibited different T_{cp} and tacticity, these should reorganise and pack differently into aggregate structures upon heating. Hence, DLS was used to assess the size changes of these copolymers with temperature at neutral pH. First, the ability of detecting aggregates from soluble polymers was evaluated with temperature. Figure 2.25 shows the temperature dependent self-assembly of the $A_{37}N_{199}$ -0.06 copolymer, selected as an example. At 25 °C, the diblock copolymers are soluble chains or unimers that can be observed at around 4 nm, with the formation of some ill-defined structures at around 20 to 80 nm. The small peaks perceived below 1 nm in Figure 2.25a, cannot correspond to the size of free soluble chains. According to Kirichenko *et al.*,¹⁰⁹ these are artefact peaks that can be attributed to the time of particle entrance-exit from the scattering volume and the experiment duration time, i.e. longer than 120 s per experiment. Moreover, it is observed one single decay of the correlation function at 25 °C, even though ill-defined structures of different sizes were seen with average sizes of 20 to 80 nm (Figure 2.25b). Previously, Schilli *et al.*¹⁰⁰ reported that hydrogen bonding between the acrylamide and acrylic acid groups leads to the formation of some aggregates at room temperature. Hence, the ill-defined structures seen could be due to the formation of interpolymer hydrogen bonding.

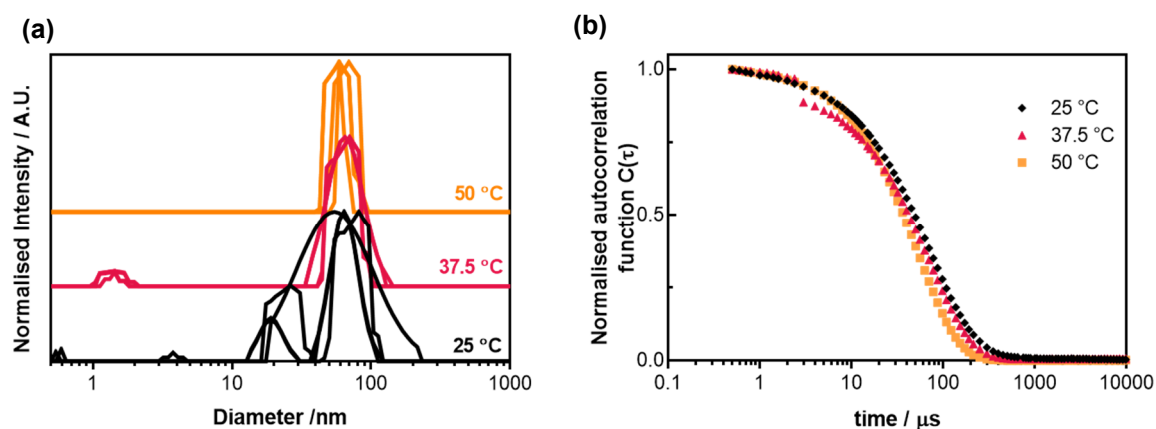


Figure 2.25: Size determination studies for the self-assembly of the $A_{37}N_{199}$ -0.06 with temperature. (a) Intensity average size distribution curves ($n=4$) and (b) their respective autocorrelation function with time. DLS data obtained from 0.1% w/w diblock solutions in DI water at neutral pH.

Above the cloud point temperature (37.5 °C), some unimers are still observed with the formation of more defined structures, this observed as monomodal size distributions. However, it is noted in Figure 2.25b that the correlation function breaks up, this could be an indication of the aggregation of polymer chains into presumably self-assembled structures. At a temperature of

50 °C, a monomodal and narrow size distribution is observed with a D_h of 63 nm. Moreover, the correlation function shows a single decay of the correlation function with a linear baseline. This indicating the formation of stable aggregates at 50 °C and neutral pH. It was also noted that the distributions got narrower at a higher temperature, probably due to the increasing hydrophobic character of the PNIPAM chains above the T_{cp} . Based on the diameter and dispersity values of the aggregated chains (PDI <0.04), it is suggested that at high temperatures the structures are likely to be forming micellar spheres, however another technique such as small-angle X-ray scattering (SAXS) would provide more information regarding the morphology of these nano-objects with different temperatures.

The ζ -potential of the $A_{37}N_{199}-X_e$ copolymers aqueous solutions was determined at the temperature of 25, 37.5 and 50 °C (Table 2.6). It was observed that the ζ -potential was more negative with increasing temperatures. For instance, the $A_{37}N_{199}-0.06$ copolymer had a ζ -potential of -24 mV at 25 °C, -42 mV at 37.5 °C and -44 mV at 50 °C. The more negative ζ -potentials may be due an increase in the surface charge density caused by the shrinking of the aggregates as observed by DLS. Moreover, it was observed that the $A_{37}N_{199}-0$ block copolymer had the less negative value of the ζ -potentials at 25 °C in comparison to the $A_{37}N_{199}-X_e$ copolymers synthesised with small quantities of ethanol, e.g. -5 mV for $A_{37}N_{199}-0$ and -27 mV for $A_{37}N_{199}-0.12$. This could suggest a different interaction of the copolymer chains synthesised with mixtures of water and ethanol at a temperature below the T_{cp} than for copolymers synthesised in only water. The copolymers synthesised with ethanol could be forming some aggregates, and the $A_{37}N_{199}-0$ copolymer could be present only as soluble chains at 25°C. However, other complementary techniques such as small-angle scattering or cryogenic transmission electronic microscopy could provide insights into the structure of these ill-defined aggregates at 25 °C.

Table 2.6: Summary of the ζ -potential values of the $A_{37}N_{199}-X_e$ copolymers at different temperatures.^a

Diblock copolymer	ζ -Potential at 25 °C / mV	ζ -Potential at 37.5 °C / mV	ζ -Potential at 50 °C / mV
$A_{37}N_{199}-0$	-4.8 ± 0.5	-38.1 ± 2.3	-40.2 ± 0.6
$A_{37}N_{199}-0.06$	-24.4 ± 3.5	-41.9 ± 2.4	-43.9 ± 2.0
$A_{37}N_{199}-0.12$	-27.4 ± 1.3	-44.9 ± 4.0	-46.7 ± 1.6
$A_{37}N_{197}-0.15$	-26.5 ± 2.2	-45.4 ± 5.1	-48.4 ± 1.6

^a ζ -potential measurements (n=5) for 0.1% w/w diblock copolymer solutions in DI water with a 1 mM KCl background electrolyte at pH 7.

A temperature of 50 °C was chosen to compare the size of the diblock copolymer aggregates in aqueous solutions since at a temperature above the T_{cp} it is ensured that the $A_xN_y-X_e$ copolymer chains are forming stable aggregates in solution. Considering the $A_{37}N_{199}-X_e$ diblock copolymers

as an example, a size increase is observed for copolymers synthesised with more ethanol (Figure 2.26). A similar increase in size with increasing X_e in the synthesis was observed for all the aqueous dispersion solutions of the purified diblock copolymers with a similar monomer composition. These DLS experiments can be found in the Appendix A ($A_{37}N_y-X_e$, where $y=100$ and 302 are shown in Figure 2A.22a and b, respectively, and the $A_{84}N_y-X_e$, where $y=202$ and 303 are presented in Figure 2A.23a and b, respectively).

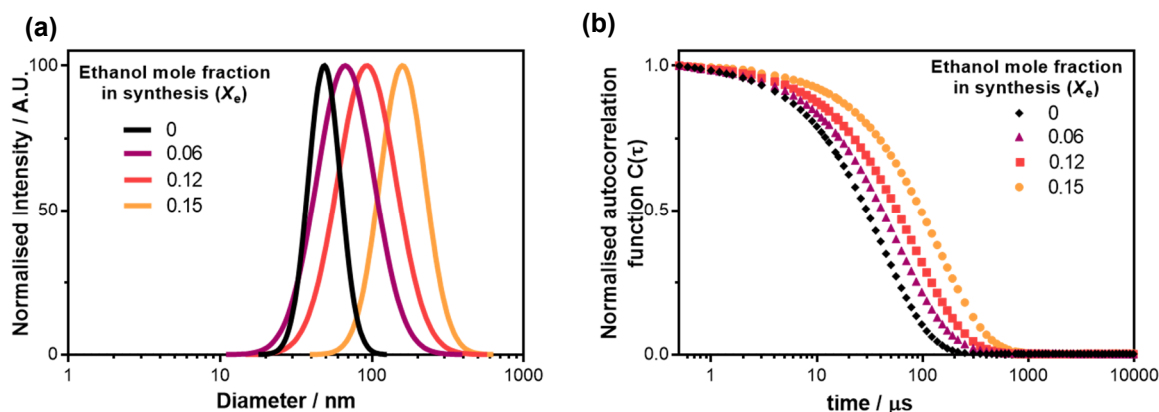


Figure 2.26: Size determination of the aggregate structures of $A_{37}N_{199}-X_e$ copolymers. (a) The log-normal size distributions of the self-assembled structures at 50 °C and (b) their respective autocorrelation function with time ($n=4$). DLS data obtained from 0.1% w/w diblock solutions in DI water at pH 7.

It is suggested that the change in size can be related to the different tacticity of the copolymers. A previous work has shown that above the LCST of PNIPAM, the stereochemistry has no influence on the shrinking behaviour but the interchain and intrachain interactions.¹¹⁰ For example, the $A_{37}N_{199}-0$ copolymer, which is the less hydrophilic of the $A_{37}N_{199}-X_e$ copolymers with a 47% meso content and a T_{cp} of 34 °C, self-assembled into aggregates with a D_h of 49 nm (PDI=0.06). Whilst the $A_{37}N_{199}-0.15$, that is more hydrophilic with a 41% meso content and a T_{cp} of 39 °C, had a greater D_h of 140 nm (PDI=0.16). These results suggest that PNIPAM chains of the $A_{37}N_{199}-0$ copolymer (more isotactic PNIPAM block), can pack more closely than a less isotactic PNIPAM copolymer, probably due to more intermolecular interactions between the side groups of the $A_{37}N_{199}-0$ copolymer. Another possible explanation can be found in a different hydration of the PNIPAM chains due to the different stereosequence of the PNIPAM side groups. Although some hydration of PNIPAM is lost during the coil-to-globule transition, previous experiments have shown the presence of H-bonding interactions between water and the PNIPAM side groups above the LCST.¹¹¹ Hence, if the $A_{37}N_{199}-0.15$ is more hydrophilic, above the T_{cp} the PNIPAM core would be more swollen than the $A_{37}N_{199}-0$.

2.4. Conclusions

This chapter aimed to show the effects of the synthesis cononsolvent composition on the size and morphology of PAA-*b*-P(NIPAM-*st*-BIS) nanogels prepared using RAFT dispersion polymerisation. Prior to investigating the effect of the water-ethanol composition as cononsolvent pair of PNIPAM, a series of nanogels were synthesised in only water to show that the size and morphology of the nanogels can be altered by varying the DP of the core-forming block and the shell-stabiliser block. The addition of small quantities of ethanol to the aqueous dispersion polymerisation of NIPAM proved to affect the size of the nanogels. Overall, nanogels synthesised with the same target monomer composition revealed a gradual decrease in size with increasing ethanol content used for their synthesis. These results suggest that the addition of ethanol affects the nucleation step and thus the organisation and the aggregation number of PNIPAM growing chains during polymerisation due to the cononsolvency effects. TEM analyses revealed that nanogels with a semi-spherical shape were produced due to the use of a highly charged stabiliser block and the constrained chain growth owed to an early crosslinking. However, nanogels synthesised in mixtures of cononsolvents had a more uniform spherical shape probably due to a different monomer partitioning and kinetics of polymerisation than for the nanogels synthesised in only water. The synthesis of nanogels in cononsolvents allowed the incorporation of higher crosslinker composition. However, a high crosslinker density appeared to be detrimental for the control of the morphology of the nanogels when using PAA₅₂ as macro-CTA, whilst a larger shell-stabiliser block allowed the synthesis of nanogel particles with more uniform sphericity at higher volume fractions of PNIPAM. Hence, it is concluded that the final size and morphology of the nanogels is dependent on the close relationship between the cononsolvent composition and the chain lengths of both of the blocks. AF4-MALS-DLS analyses revealed for two nanogel samples that the vast majority of the nanogel particles possessed a core-shell structure regardless of the mixture composition these were synthesised in ($X_c=0$ or $X_c=0.05$).

In order to determine the effects of the cononsolvent composition on the RAFT dispersion polymerisation of NIPAM, a series of PAA-*b*-PNIPAM diblock copolymers were prepared in the absence of crosslinker. NMR spectroscopy studies suggested a slight change in the stereochemistry of the copolymers synthesised in different cononsolvents compositions, where the copolymers synthesised only in water resulted meso-richer than those synthesised in higher ethanol content. Changes in the T_{cp} and particle size of the aggregate copolymer chains according to ethanol compositions support the changes observed in the tacticity of the PNIPAM block.

A different stereosequence suggest a different intramolecular interaction between the neighbouring groups and hydration, which can result in different chain packing. Although more analyses would provide a better insight into the structure of the diblock copolymers, a deeper understanding of the use of cononsolvents on the RAFT dispersion polymerisation of NIPAM has been presented, where the addition of small quantities of a cononsolvent allows good control over the dispersion polymerisation.

2.5. Experimental

2.5.1. Materials

2-mercaptoethanol ($\geq 99\%$), carbon disulfide ($\geq 99\%$), (trimethylsilyl)diazomethane (2 M solution in diethyl ether), 4,4'-azobis(4-cyanopentanoic acid) (ACVA, 98%), butylhydroxytoluene (BHT) and lithium bromide (LiBr, $\geq 99\%$) were purchased from Sigma-Aldrich and used as received. Potassium phosphate tribasic (Alfa aesar, 97%) and 2-bromoisobutyric acid (Acros Organics, 98%) were used without further purification. Acrylic acid (AA) (Merck, $\geq 99\%$) was passed through a column of basic Al_2O_3 prior to use. 2,2'-Azobis(2-methylpropionitrile) (AIBN) (Sigma-Aldrich) and *N*-isopropyl acrylamide (NIPAM) (Fluorochem) were recrystallised from *n*-hexane and dried before use. *N,N'*-methylene bisacrylamide (BIS) (Sigma-Aldrich) was recrystallised from hot methanol and dried before use. SnakeSkin™ dialysis tubing (ThermoFisher scientific) of 3.5 kDa molecular weight cut-off (MWCO) was used to purify the macro-CTAs and nanogel dispersions. For nuclear magnetic resonance (NMR) experiments, samples were prepared in either D_2O or CDCl_3 (Sigma Aldrich).

2.5.2. Synthesis of 2-(hydroxyethylthiocarbonothioylthio)-2-methylpropanoic acid (HEMP)

2-mercaptoethanol (6.1 mL, 87.54 mmol) and potassium phosphate tribasic (19.16 g, 87.54 mmol) were added to acetone (150 mL). Carbon disulfide (11 mL, 0.17 mol) was added to the mixture after 30 min, followed by the addition of 2-bromoisobutyric acid (14.92 g, 87.54 mmol). The mixture was left to stir for 16 h followed by N_2 purging for extra 2 h. Afterwards, the mixture was filtered to remove solids and volatiles were removed under reduced pressure. The product was acidified by addition of hydrochloric acid (1 M, 2×100 mL) and the organic phase was extracted with DCM (2×100 mL). The organic phase was then washed with a saline solution (100 mL). All the organic phases were collected and dried over Na_2SO_4 and the volatiles removed under reduced pressure. Finally, the crude product was recrystallised from a mixture of hot hexane and ethyl acetate (7:3 v/v ratio) to give a bright yellow solid product (17.2 g, 86 %); m.p. 62-64 °C; δH (400 MHz; CDCl_3 , 25 °C) (ppm): 3.86 (2H, m, CH_2OH), 3.53 (2H, t, CH_2SC), 1.72 (6H, s, $\text{SC}(\text{CH}_3)_2$); δC (100 MHz; CDCl_3 , 25 °C): 25.5 ($\text{C}(\text{S})\text{SC}(\text{CH}_3)_2$), 39.0 ($\text{CH}_2\text{SC}(\text{S})\text{S}$), 60.8 (CH_2OH), 177.9 ($\text{C}(\text{O})\text{OH}$), 220.8 ($\text{SC}(\text{S})\text{S}$); $\bar{\nu}_{\text{max}}$ (ATR) cm^{-1} : 3420 (m, R-OH), 1692 (vs, C=O), 1254 (s, S- CH_2 -R), 1380 (s, $\text{C}(\text{CH}_3)_2$), 1160 (s, C=S), 1053 (vs, R- CH_2 -OH), 809 (s, S-C-S); $\text{C}_7\text{H}_{13}\text{O}_3\text{S}_3$ (240.4); TOF MS: m/z calcd. for $\text{C}_7\text{H}_{13}\text{O}_3\text{S}_3^+ [\text{M}+\text{H}]^+$ 241.4; found 241.1.

2.5.3. Synthesis of poly(acrylic acid) macro-CTA *via* ethanolic RAFT solution polymerisation.

The macro-CTAs with different DPs were synthesised similarly but targeting different molar ratios of [AA]:[HEMP]. Using the PAA₅₂ synthesis as an example: A mixture of HEMP (0.56 g, 2.31 mmol), AA (10 g, 138.78 mmol), AIBN (0.076 g, 0.46 mmol) and ethanol (to give a 25% w/w solids solution) was purged thoroughly with N₂ for 30 minutes. The flask was then placed onto a DrySyn® heating block preheated to 70 °C and left to react for 130 minutes. The reaction was quenched by removing the flask from the heat source and opened to air. AA conversion (78%) was calculated by ¹H NMR spectroscopy. The product was recovered by precipitation from diethyl ether (400 mL). Further product purification was performed by dialysis against water and freeze-drying to give a pale yellow solid. $\bar{M}_{n,theory}=3,987 \text{ g mol}^{-1}$; δH (400 MHz; D₂O, 25 °C) (ppm): 3.83 (2H, t, CH₂OH), 3.60 (2H, t, -CH₂SC-), 2.39 (1H, br. s, -CH-), 1.93-1.60 (2H, br. t, -CH₂-); δC (100 MHz; D₂O, 25 °C): 34.3 (-CH₂-), 41.5 (-CH-), 178.9 (C(O)); $\bar{\nu}_{max}$ (ATR) cm⁻¹: 2935 (br. s, R-COOH), 1701 (vs, C=O), 1449 (w, -CH₂-), 1411 (w, R-CH₂-S), 1214 (m, -COOH), 1162 (s, C=S), 794 (m, -C-(CH₃)₂). Molar mass determination of PAA by gel permeation chromatography was determined after esterification of the carboxylic groups. PAA samples were dissolved in THF/methanol mixes followed by the dropwise addition of trimethylsilyldiazomethane. Addition of the methylation agent ended when the production of N₂ stopped, and the yellow colour remain unchanged. The solutions were left to stir allowing the solvents to evaporate overnight. The polymeric film was then dissolved in THF for GPC determination. $\bar{M}_n=4.7 \text{ kDa}$, $\bar{M}_w/\bar{M}_n=1.19$.

2.5.4. Synthesis of poly(acrylic acid)-*b*-poly(*N*-isopropylacrylamide-*st*-*N,N'*-methylene bisacrylamide) nanogels *via* RAFT dispersion polymerisation

The molar ratio of [NIPAM]:[PAA_x] was adjusted between 100 to 300 to give a range of nanogels with different sizes. RAFT dispersion polymerisation of NIPAM and BIS was performed in either water or different compositions of water-ethanol (H₂O:EtOH) mole fractions at 10% w/w solids content. An example of nanogel synthesis targeting a PAA₅₂-*b*-(PNIPAM₂₀₀-*st*-BIS₃) at a $X_e=0.05$ ethanol mole fraction was as follows: PAA₅₂ (0.0352 g, 0.009 mmol), NIPAM (0.2003 g, 1.770 mmol), BIS (0.0041 g, 0.027 mmol), were dissolved in a mixture of H₂O:EtOH (1.8724 g of H₂O and 0.2112 g of ethanol). The pH of the solution was adjusted to pH 6.68 using an aqueous solution of NaOH (0.07 mL, 0.35 mmol). The mixture was purged with N₂ for 30 minutes, followed by the addition of the degassed ACVA solution in ethanol (0.124 mL, 14.27 mM) *via*

microsyringe. All the quantities of solids and volume of solutions added were calculated in advance to give a final concentration of 10% w/w solids before reaction. The mixture was then placed into an oil bath previously set at 70 °C and left to react for 18 h. Total monomer conversion (98 %) was estimated by moisture analysis. The product solution was then purified by dialysis against DI water to exchange the solvents to water. $\bar{\nu}_{\max}$ (ATR) cm^{-1} : 3290 (br. m, -CONH), 2973 (m, R-COOH), 2934 and 2873 (m, -CH₂), 1640 and 1539 (s, -CONR₂), 1457 (m, -CH₂-), 1409 (w, -COOH), 1386 and 1367 (m, -C(CH₃)₂), 1172 (m, C=S), 1130 (m, -C(CH₃)₂), 879 (w, S=C(S)S).

2.5.5. Synthesis of poly(acrylic acid)-*b*-poly(*N*-isopropylacrylamide) copolymers *via* RAFT dispersion polymerisation

PAA₃₇ and PAA₈₄ macro-CTAs were chain extended by NIPAM at a different monomer-to-macro-CTA molar ratios in either water or water-ethanol (H₂O:EtOH) cononsolvents mixtures at 10% w/w solids content. An example of a diblock copolymer synthesis targeting a molar ratio of [NIPAM]:[PAA₃₇] of 200 in a 0.06 ethanol mole fraction was as follows: the PAA₃₇ macro-CTA (0.0258 g, 0.0089 mmol), and NIPAM monomer (0.2001 g, 1.77 mmol) were dissolved in a mixture of H₂O:EtOH (1.7542 g of H₂O and 0.1983 g of ethanol). The pH of the solution was then adjusted to pH 6.7 using a NaOH solution (0.05 mL, 0.25 mmol). All the quantities of solids and volume of solutions added were calculated in advance to give a final concentration of 10% w/w solids before reaction. The solution was then degassed under nitrogen for 30 min, followed by the addition of ACVA in ethanol (0.14 mL, 3.15 mg mL⁻¹). The solution was immersed into an oil bath preheated to 70 °C and left to react for 18 hours. NIPAM monomer conversion (99 %) was estimated by ¹H NMR spectroscopy. The crude product was dialysed against DI water to exchange ethanol to water. For further characterisation the copolymer was freeze-dried to give a white solid. $\bar{M}_{n,\text{theory}} = 28,644 \text{ g mol}^{-1}$; δH (400 MHz, D₂O, 25 °C): 3.85 (br. d, H, -NCH), 2.25-1.96 (br. d, 1H, -CH-), 1.53 (br. t, 2H, -CH₂-), 1.09 (br. s, 6H, -CH(CH₃)₂); δC (100 MHz; D₂O, 25 °C): 21.5 (-CH₂-), 41.7 (-CH-), 175.2 (C(O)); $\bar{\nu}_{\max}$ (ATR) cm^{-1} : 3283 (br. m, -CONH), 2973 (m, R-COOH), 2929 and 2876 (w, -CH₂-), 1634 and 1538 (s, -CON-R₂), 1459 (m, -CH₂-), 1387 and 1367 (m, -C(CH₃)₂), 1172 (w, C=S).

2.5.6. Synthesis of poly(*N*-isopropylacrylamide) *via* ethanolic RAFT solution polymerisation.

Two different molar ratios of [NIPAM]:[HEMP] of 100:1 and 200:1 were targeted. Using the PNIPAM₁₀₀ synthesis as an example: A mixture of NIPAM (3.01 g, 26.59 mmol), HEMP (0.06 g, 0.27 mmol), AIBN (0.008 g, 0.08 mmol) and ethanol (to give a 25% w/w solids solution) was purged thoroughly with N₂ for 30 minutes. The flask was then placed onto a DrySyn® heating block preheated to 70 °C and left to react for 240 minutes. The reaction was quenched by removing the flask from the heat source and opened to air. NIPAM conversion (98%) was calculated by ¹H NMR spectroscopy. The product was recovered by precipitation into hexane (400 mL). The product was then dissolved in water and purified by dialysis against water and freeze-drying to give a pale-yellow solid. PNIPAM₉₈ $\bar{M}_n = 9.0$ kDa, $\bar{M}_w/\bar{M}_n = 1.31$. PNIPAM₁₉₀: conversion (95%) $\bar{M}_n = 19.6$ kDa, $\bar{M}_w/\bar{M}_n = 1.35$; δ H (400 MHz; CDCl₃, 25 °C) (ppm): 3.42 (br. s, H, -NCH), 2.67 (s, 2H, -CH₂SC), 2.48-1.95 (br. d, 1H, -CH-), 1.95-1.46 (br. t, 2H, -CH₂-), 1.11 (br. s, 6H, -CH(CH₃)₂).

2.5.7. Synthesis of poly(*N*-isopropylacrylamide) *via* free radical precipitation polymerisation.

NIPAM (0.5 g, 4.4 mmol) was dissolved in the corresponding water-ethanol cononsolvent mixture and degassed with N₂ for 30 minutes. Ammonium persulfate (0.32 mL, 69.3 mM) in water previously degassed was added *via* syringe into each of the NIPAM solutions to give a 10% w/w solids solution. The target mole fractions of ethanol and water were $X_e=0$, $X_e=0.5$, $X_e=0.10$ and $X_e=0.15$. Solutions were immersed into an oil bath preheated to 70 °C and left to react overnight. NIPAM monomer conversion (100 %) was estimated by ¹H NMR spectroscopy. The crude product was dialysed against DI water to exchange ethanol to water. For further characterisation, the polymers were freeze-dried to give white solids. δ H (400 MHz, D₂O, 25 °C): 3.81 (br. d, H, -NCH), 2.30-1.79 (br. d, 1H, -CH-), 1.79-1.27 (br. t, 2H, -CH₂-), 1.27-0.24 (br. s, 6H, -CH(CH₃)₂)

2.6. Characterisation

2.6.1. NMR Spectroscopy

Nuclear Magnetic Resonance (NMR) experiments were performed at 25 °C on a 400 MHz Bruker Avance III HD spectrometer. Each collected spectrum was calibrated using the residual solvent peak as reference. ^1H NMR spectra were collected over 64 scans averaged per spectrum. NMR data was analysed with MNova software from Mestrelab Research.

2.6.2. Gravimetric analyses

The monomer conversion for the synthesis of nanogels was estimated gravimetrically using a KERN DAB 100-3 electronic moisture analyser. Samples were weighed and heated up to 190 °C to determine their solid content.

2.6.3. Gel permeation chromatography (GPC)

Molar masses and polydispersities of PAA by GPC were determined after esterification of the carboxylic groups. The PAA kinetic samples were analysed using an Agilent 1260 Infinity LC GPC/SEC system fitted with 2 × PLgel Mixed-C 5 μm (300 × 7.5 mm) columns. DMF (HPLC, 0.1 mg mL⁻¹ LiBr) was used as eluent at a flow rate of 1 mL min⁻¹ at 50 °C. The equipment was calibrated with near-monodisperse poly(methyl methacrylate) standards (molar mass range between 5.45 × 10² – 2.00 × 10⁶ g mol⁻¹). Analyte samples were prepared at a concentration of 2 mg mL⁻¹ in DMF (HPLC, 0.1 mg mL⁻¹ LiBr) using 0.1% v/v toluene as flow rate marker and filtered through a 0.45 μm polytetrafluoroethylene (PTFE) filter before injection (100 μL). The molar mass of the PAA_x macro-CTAs and the PNIPAM homopolymers were recorded on Agilent PL-GPC 50 system fitted with 2 × PLgel Mixed-C 5 μm (300 × 7.5 mm) columns. For the PAA_x macro-CTAs THF (HPLC, 4% v/v acetic acid, 0.025% w/v BHT) was used as eluent at a flow rate of 1 mL min⁻¹ at 25 °C. In the case of PNIPAM and PHEA polymers, DMF (HPLC, 0.1 mg mL⁻¹ LiBr) was used as eluent. In both cases, the equipment was calibrated with near-monodisperse poly(methyl methacrylate) (PMAA) standards (molar mass range between 5.45 × 10² – 2.00 × 10⁶ g mol⁻¹). Analyte samples were prepared at a 2 mg mL⁻¹ concentration in their corresponding solvent and 150 μL of each sample was the volume injected. Molar masses and dispersities were calculated with Agilent GPC Software.

2.6.4. Fourier transform infrared spectroscopy (ATR-FTIR)

ATR-FTIR was used to assess the chemical composition of materials. IR spectra were recorded on a PerkinElmer SpectrumTM 100 FT-IR spectrometer using a universal diamond ATR (UATR) accessory. Data was collected over 5 scans in the 450 to 4000 cm^{-1} region. The IR data was recorded on a Bruker software and further processed in Excel.

2.6.5. Dynamic light scattering (DLS)

Determination of the hydrodynamic particle diameter of the purified nanogels (0.1% w/w) was obtained using a NanoBrook Omni particle analyser using a 35 mW diode laser with a nominal 640 nm wavelength. Data was obtained at a scattering angle of 173° . Each DLS measurement consisted of 4 or 5 runs of 3 minutes at count rates between 440-550 kcps. Temperature dependent DLS experiments were performed from low to high temperatures with increments of 12.5°C with 8 minutes in-between intervals to allow thermal stabilisation. The method of the constrained regularization method for inverting data (CONTIN) was used to obtain the size distribution from the autocorrelation function.

2.6.6. UV-vis spectrophotometry

The absorbance of the copolymer aqueous solutions (1% w/w) at 550 nm as a function of temperature was recorded on a Cary 300 Bio UV-vis spectrophotometer fitted with a Peltier temperature controlled multi-cell block. The temperature was increased from 10 to 60°C at a heating rate of $0.12^\circ\text{C min}^{-1}$. The cloud points were calculated from the inflection point of each absorbance curve.

2.6.7. Aqueous electrophoresis

ζ -potential measurements for the aqueous nanogel dispersions (0.1% w/w) and diblock copolymers (0.1% w/w) containing KCl (1 mM) as background electrolyte were determined on a Malvern Zetasizer Nano-ZS instrument. The smoluchowski relationship was used to determine the ζ -potential from the electrophoretic mobility. For temperature-dependent measurements, a time of 8 minutes before the measurement was set to allow thermal stabilisation.

2.6.8. Transmission electron microscopy (TEM)

TEM images were collected using a Phillips CM100 microscope operating at 100 kV and adapted with a Gatan CCD camera. Nanogel dispersions (0.1% w/w, 10 μL) were placed onto freshly glow discharge-treated carbon-coated grids for 60 seconds and then blotted with filter paper. Phosphotungstic acid (0.75% w/w, 5 μL) staining solution was then placed onto the sample and left for 20 seconds to finally blot it again with filter paper to remove excess staining solution. The grid was then dried with an adapted vacuum hose. Image J software was used to estimate the mean diameter of each nanogel.

2.6.9. Asymmetric-flow field-flow fractionation (AF4)

AF4 experiments were performed on an MT2000 with RI and UV-Vis detectors. The AF4 instrument was coupled online with a multi-angle light scattering detector (MALS) with a detector with 21 angles (from 7° to 164°) operating at 532 nm power wavelength. Both instruments were provided by Postnova Analytics, Landsberg/Germany. The hydrodynamic radius R_h of the nanogels was estimated by DLS measurements using a Malvern Zetasizer Nano ZS (running Malvern Zetasizer software V7.12) with a 633 nm He-Ne laser at scattering angle of 173° . A ZEN0023 flow cell was used for DLS measurements at a flow rate of 0.5 mL min^{-1} at 28°C , which was coupled online to the MT2000. A 350 μm spacer and 10 kDa regenerative cellulose (RC) membrane were fitted in the separation channel. The conditions used for the separations were based on previously reported methodologies.^{112,113} A mobile phase of 0.1 M NaNO_3 in Milli-Q H_2O was used for the experiments. Type I DI water was obtained from a water purification system with a resistivity of $>18 \text{ M}\Omega \text{ cm}^{-1}$ (PURELAB option R, Veolia). The solutions were filtered using Corning bottle top vacuum filter system with cellulose acetate membrane with a pore size of 0.22 μm . Each nanogel sample was injected (20 μL , 1% w/w) by the autosampler. Three runs were performed for each nanogel to ensure reproducibility. A blank run was measured between injections to ensure that the system had no impurities. The UV-Vis detector was set to 280 nm wavelength. The conditions used for the separations was as follows: The injection/focusing time was 3 minutes using a cross flow from 2 to 0.5 mL min^{-1} . The selected cross flow rate (initial values of 2 mL min^{-1} to 0.5 mL min^{-1}) was kept constant for the first 0.2 minutes (t_0 - $t_{0.2}$). Afterwards, the cross flow was reduced in a power manner (exponent 0.2) from its initial value to 0.1 over a period of 40 minutes. Following the complete reduction in cross flow, the tip-flow 0.1 mL min^{-1} continued for other 40 minutes. The cross-flow profile over time for fractionation

conditions of the nanogels is shown in Figure 2.27.

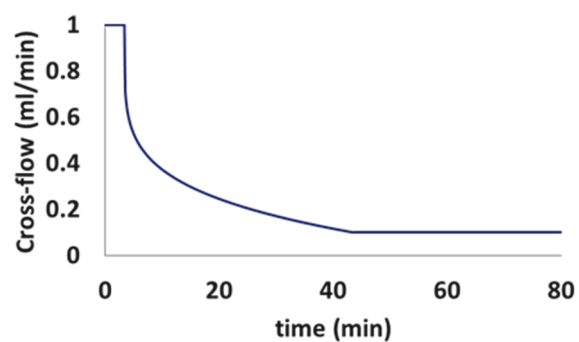


Figure 2.27: The cross-flow profile over time chosen for the separation of the nanogel particles.

2.7. References

1. Sanson, N. & Rieger, J. Synthesis of nanogels/microgels by conventional and controlled radical crosslinking copolymerization. *Polym. Chem.* **1**, 965–977 (2010).
2. An, Z. *et al.* Facile RAFT precipitation polymerization for the microwave-assisted synthesis of well-defined, double hydrophilic block copolymers and nanostructured hydrogels. *J. Am. Chem. Soc.* **129**, 14493–14499 (2007).
3. Rieger, J., Grazon, C., Charleux, B., Alaimo, D. & Jérôme, C. Pegylated thermally responsive block copolymer micelles and nanogels *via in situ* RAFT aqueous dispersion polymerization. *J. Polym. Sci. Part A Polym. Chem.* **47**, 2373–2390 (2009).
4. Grazon, C., Rieger, J., Sanson, N. & Charleux, B. Study of poly(*N,N*-diethylacrylamide) nanogel formation by aqueous dispersion polymerization of *N,N*-diethylacrylamide in the presence of poly(ethylene oxide)-*b*-poly(*N,N*-dimethylacrylamide) amphiphilic macromolecular RAFT agents. *Soft Matter* **7**, 3482–3490 (2011).
5. Shen, W. *et al.* Biocompatible, antifouling, and thermosensitive core-shell nanogels synthesized by RAFT aqueous dispersion polymerization. *Macromolecules* **44**, 2524–2530 (2011).
6. Liu, G., Qiu, Q. & An, Z. Development of thermosensitive copolymers of poly(2-methoxyethyl acrylate-co-poly(ethylene glycol) methyl ether acrylate) and their nanogels synthesized by RAFT dispersion polymerization in water. *Polym. Chem.* **3**, 504–513 (2012).
7. Picos-Corrales, L. A. *et al.* Core-shell nanogels by RAFT crosslinking polymerization: Synthesis and characterization. *J. Polym. Sci. Part A Polym. Chem.* **50**, 4277–4287 (2012).
8. Liu, X. B., Zhou, J. F. & Ye, X. D. Phase transition of poly(acrylic acid-co-*N*-isopropylacrylamide) core-shell nanogels. *Chinese J. Chem. Phys.* **25**, 463–468 (2012).
9. Hou, L., Ma, K., An, Z. & Wu, P. Exploring the volume phase transition behavior of POEGA- and PNIPAM-based core-shell nanogels from infrared-spectral insights. *Macromolecules* **47**, 1144–1154 (2014).
10. Rajan, R. & Matsumura, K. Tunable dual-thermoreponsive core – shell nanogels exhibiting UCST and LCST behavior. *Macromol. Rapid Commun.* **38**, 1700478 (2017).
11. Liu, G., Qiu, Q., Shen, W. & An, Z. Aqueous dispersion polymerization of 2-methoxyethyl acrylate for the synthesis of biocompatible nanoparticles using a hydrophilic RAFT polymer and a redox initiator. *Macromolecules* **44**, 5237–5245 (2011).
12. Yan, L. & Tao, W. One-step synthesis of pegylated cationic nanogels of poly(*N,N'*-dimethylaminoethyl methacrylate) in aqueous solution *via* self-stabilizing micelles using an amphiphilic macroRAFT agent. *Polymer (Guildf)*. **51**, 2161–2167 (2010).
13. An, Z., Qiu, Q. & Liu, G. Synthesis of architecturally well-defined nanogels *via* RAFT polymerization for potential bioapplications. *Chem. Commun.* **47**, 12424–12440 (2011).
14. Sanson, N. & Rieger, J. Synthesis of nanogels/microgels by conventional and controlled radical crosslinking copolymerization. *Polym. Chem.* **1**, 965–977 (2010).
15. Ahmed, M. & Narain, R. Intracellular delivery of DNA and enzyme in active form using degradable carbohydrate-based nanogels. *Mol. Pharm.* **9**, 3160–3170 (2012).
16. Bhuchar, N., Sunasee, R., Ishihara, K., Thundat, T. & Narain, R. Degradable thermoresponsive nanogels for protein encapsulation and controlled release. *Bioconjug. Chem.* **23**, 75–83 (2012).

17. Kotsuchibashi, Y. & Narain, R. Dual-temperature and pH responsive (ethylene glycol)-based nanogels *via* structural design. *Polym. Chem.* **5**, 3061–3070 (2014).
18. Narain, R., Wang, Y., Ahmed, M., Lai, B. F. L. & Kizhakkedathu, J. N. Blood components interactions to ionic and nonionic glyconanogels. *Biomacromolecules* **16**, 2990–2997 (2015).
19. Fu, W. *et al.* UCST-Type Thermosensitive hairy nanogels synthesized by RAFT Polymerization-Induced Self-Assembly. *ACS Macro Lett.* **6**, 127–133 (2017).
20. Xu, Y., Li, Y., Cao, X., Chen, Q. & An, Z. Versatile RAFT dispersion polymerization in cononsolvents for the synthesis of thermoresponsive nanogels with controlled composition, functionality and architecture. *Polym. Chem.* **5**, 6244–6255 (2014).
21. Li, Y. *et al.* Formation of Multidomain Hydrogels *via* thermally induced assembly of PISA-generated triblock terpolymer nanogels. *Macromolecules* **49**, 3038–3048 (2016).
22. Ma, K., Xu, Y. & An, Z. Templateless synthesis of polyacrylamide-based nanogels *via* RAFT dispersion polymerization. *Macromol. Rapid Commun.* **36**, 566–570 (2015).
23. Singhsa, P., Manuspiya, H. & Narain, R. Study of the RAFT homopolymerization and copolymerization of N-[3-(dimethylamino)propyl]methacrylamide hydrochloride and evaluation of the cytotoxicity of the resulting homo- and copolymers. *Polym. Chem.* **8**, 4140–4151 (2017).
24. Wang, X., Shen, L. & An, Z. Dispersion polymerization in environmentally benign solvents *via* reversible deactivation radical polymerization. *Prog. Polym. Sci.* **83**, 1–27 (2018).
25. Crowther, H. M. & Vincent, B. Swelling behavior of poly(*N*-isopropylacrylamide) microgel particles in alcoholic solutions. *Colloid Polym. Sci.* **276**, 46–51 (1998).
26. Winnik, F. M., Ringsdorf, H. & Venzmer, J. Methanol-water as a co-nonsolvent system for poly(*N*-isopropylacrylamide). *Macromolecules* **23**, 2415–2416 (1990).
27. Winnik, F. M., Ottaviani, M. F., Bossmann, S. H., Garcia-Garibay, M. & Turro, N. J. Consolvency of poly(*N*-isopropylacrylamide) in mixed water-methanol solutions: a look at spin-labeled polymers. *Macromolecules* **25**, 6007–6017 (1992).
28. Heskins, M. & Guillet, J. E. Solution properties of poly(*N*-isopropylacrylamide). *J. Macromol. Sci. Part A - Chem.* **2**, 1441–1455 (1968).
29. Schild, H. G. & Tirrell, D. A. Microcalorimetric detection of lower critical solution temperatures in aqueous polymer solutions. *J. Phys. Chem.* **94**, 4352–4356 (1990).
30. Nayak, S., Bhattacharjee, S. & Chaudhary, Y. S. *In situ* encapsulation and release kinetics of pH and temperature responsive nanogels. *J. Phys. Chem. C* **116**, 30–36 (2012).
31. Liu, X., Guo, H. & Zha, L. Study of pH/temperature dual stimuli-responsive nanogels with interpenetrating polymer network structure. *Polym. Int.* **61**, 1144–1150 (2012).
32. Xing, Z. *et al.* Dual stimuli responsive hollow nanogels with IPN structure for temperature controlling drug loading and pH triggering drug release. *Soft Matter* **7**, 7992 (2011).
33. Biswas, C. S. *et al.* Synthesis, characterization, and drug release properties of poly(*N*-isopropylacrylamide) gels prepared in methanol-water cononsolvent medium. *J. Appl. Polym. Sci.* **125**, 2000–2009 (2012).
34. Xia, Y. *et al.* Controllable stabilization of poly(*N*-isopropylacrylamide)-based microgel films through biomimetic mineralization of calcium carbonate. *Biomacromolecules* **13**, 2299–2308 (2012).

-
35. Town, A. R. *et al.* Dual-stimuli responsive injectable microgel/solid drug nanoparticle nanocomposites for release of poorly soluble drugs. *Nanoscale* **9**, 6302–6314 (2017).
 36. Town, A. R. *et al.* Tuning HIV drug release from a nanogel-based *in situ* forming implant by changing nanogel size. *J. Mater. Chem. B* (2019) doi:10.1039/C8TB01597J.
 37. Schild, H. G., Muthukumar, M. & Tirrell, D. A. Cononsolvency in mixed aqueous solutions of poly(*N*-isopropylacrylamide). *Macromolecules* **24**, 948–952 (1991).
 38. Hore, M. J. A., Hammouda, B., Li, Y. & Cheng, H. Cononsolvency of poly(*N*-isopropylacrylamide) in deuterated water/ethanol mixtures. *Macromolecules* **46**, 7894–7901 (2013).
 39. López-León, T., Bastos-González, D., Ortega-Vinuesa, J. L. & Elaïssari, A. Salt effects in the cononsolvency of poly(*N*-isopropylacrylamide) microgels. *ChemPhysChem* **11**, 188–194 (2010).
 40. Tao, C. Te & Young, T. H. Phase behavior of poly(*N*-isopropylacrylamide) in water-methanol cononsolvent mixtures and its relevance to membrane formation. *Polymer (Guildf)*. **46**, 10077-10084 (2005).
 41. Scherzinger, C., Lindner, P., Keerl, M. & Richtering, W. Cononsolvency of poly(*N,N*-diethylacrylamide) (PDEAAM) and poly(*N*-isopropylacrylamide) (PNIPAM) based microgels in water/methanol mixtures: Copolymer vs core-shell microgel. *Macromolecules* **43**, 6829–6833 (2010).
 42. Biswas, C. S., Wang, Q., Du, B. & Stadler, F. J. Testing of the effect of parameters on the cononsolvency of random copolymer gels of *N*-isopropylacrylamide and *N*-ethylacrylamide in methanol-water mixed solvents by simple gravimetric method. *Polym. Test.* **62**, 177–188 (2017).
 43. Hao, J., Cheng, H., Butler, P., Zhang, L. & Han, C. C. Origin of cononsolvency, based on the structure of tetrahydrofuran-water mixture. *J. Chem. Phys.* **132**, (2010).
 44. Yamauchi, H. & Maeda, Y. LCST and UCST behavior of poly(*N*-isopropylacrylamide) in DMSO/water mixed solvents studied by IR and micro-Raman spectroscopy. *J. Phys. Chem. B* **111**, 12964–12968 (2007).
 45. Osaka, N. & Shibayama, M. Pressure effects on cononsolvency behavior of poly(*N*-isopropylacrylamide) in water/DMSO mixed solvents. *Macromolecules* **45**, 2171–2174 (2012).
 46. Wang, J. *et al.* Preferential adsorption of the additive is not a prerequisite for cononsolvency in water-rich mixtures. *Phys. Chem. Chem. Phys.* **19**, 30097–30106 (2017).
 47. Pérez-Ramírez, H. A. *et al.* PNIPAM in water-acetone mixtures: Experiments and simulations. *Phys. Chem. Chem. Phys.* **21**, 5106–5116 (2019).
 48. Biswas, C. S., Mitra, K., Singh, S. & Ray, B. Synthesis of low polydisperse isotactic poly(*N*-isopropylacrylamide)s in environment-friendly and less toxic methanol-water mixtures by RAFT polymerization. *J. Chem. Sci.* **128**, 415–420 (2016).
 49. Wang, Q. *et al.* Random copolymer gels of *N*-isopropylacrylamide and *N*-ethylacrylamide: effect of synthesis solvent compositions on their properties. *RSC Adv.* **7**, 9381–9392 (2017).
 50. Chiang, W. H. *et al.* Dual stimuli-responsive polymeric hollow nanogels designed as carriers for intracellular triggered drug release. *Langmuir* **28**, 15056–15064 (2012).
 51. Pruettiphap, M., Rempel, G. L., Pan, Q. & Kiatkamjornwong, S. Morphology and drug release behavior of *N*-isopropylacrylamide/acrylic acid copolymer as stimuli-responsive nanogels. *Iran. Polym. J.* **26**, 957–969 (2017).
-

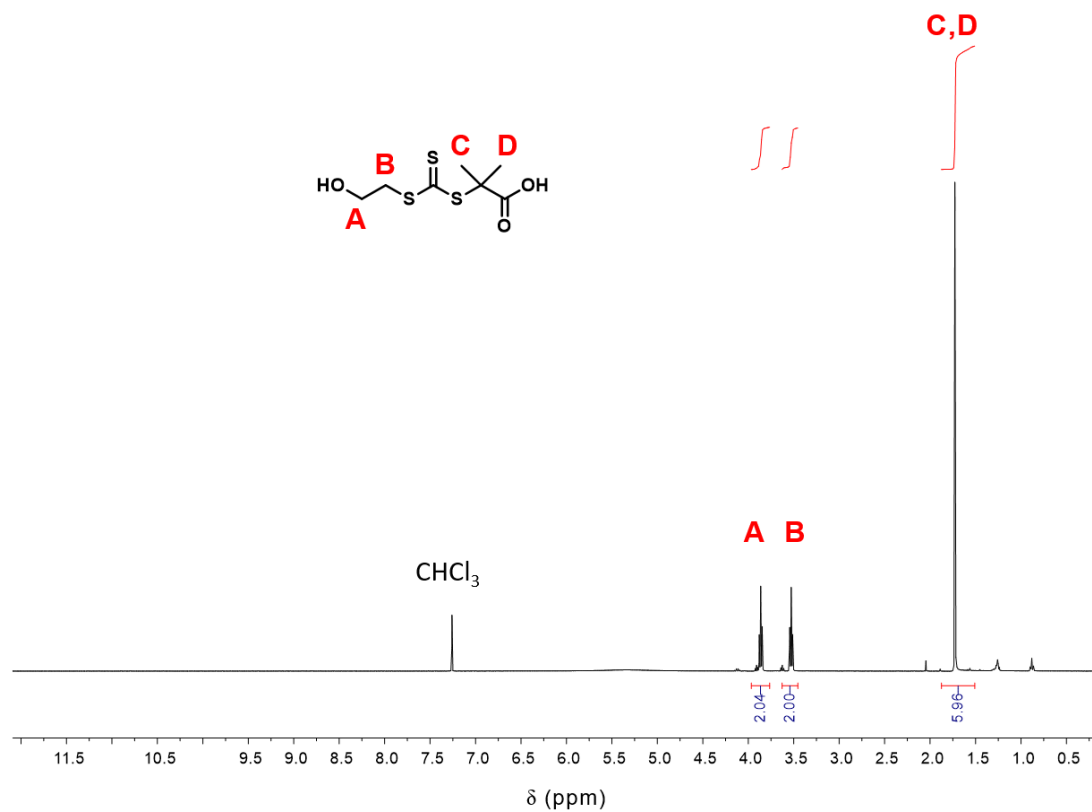
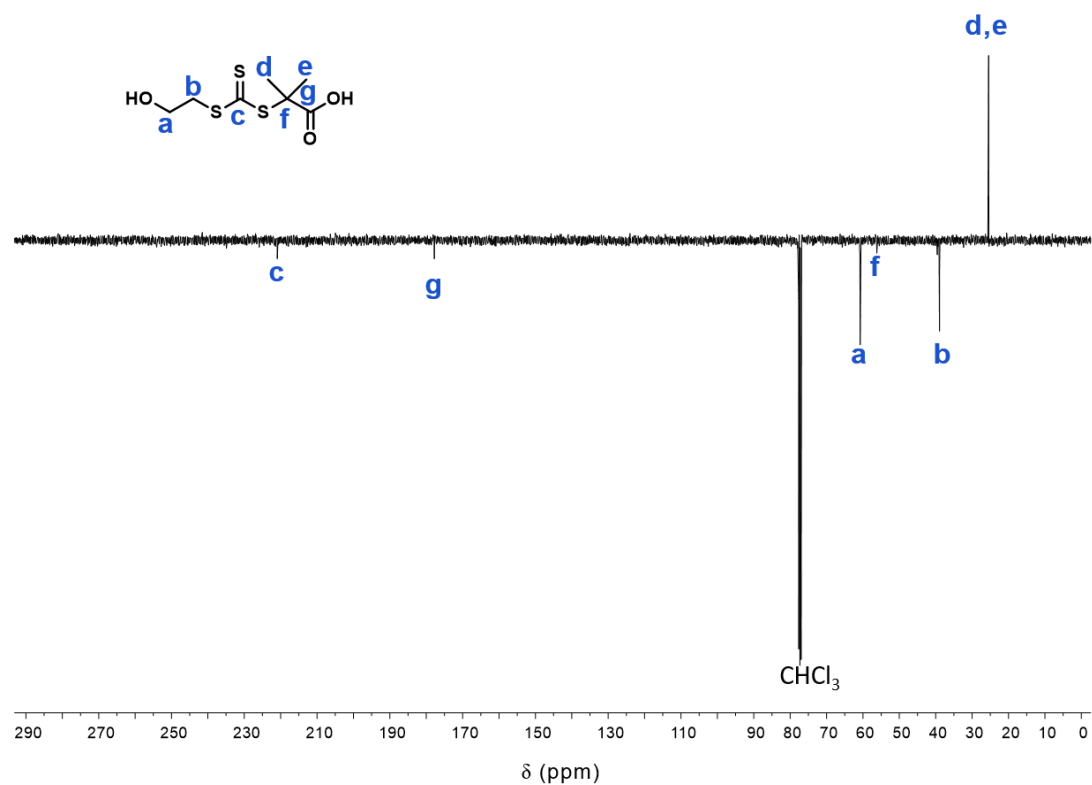
-
52. Xia, L. W., Ju, X. J., Liu, J. J., Xie, R. & Chu, L. Y. Responsive hydrogels with poly(*N*-isopropylacrylamide-co-acrylic acid) colloidal spheres as building blocks. *J. Colloid Interface Sci.* **349**, 106–113 (2010).
 53. Cong, H. & Zheng, S. Poly(*N*-isopropylacrylamide)-block-poly(acrylic acid) hydrogels: synthesis and rapid thermoresponsive properties. *Colloid Polym. Sci.* **292**, 2633–2645 (2014).
 54. Farooqi, Z. H., Ullah, H., Mujtaba, S. & Siddiq, M. Stability of poly(*N*-isopropylacrylamide-co-acrylic acid) polymer microgels under various conditions of temperature, pH and salt concentration. *Arab. J. Chem.* **10**, 329–335 (2017).
 55. Chiefari, J. *et al.* Living free-radical polymerization by reversible addition–fragmentation chain transfer: The RAFT process. *Macromolecules* **31**, 5559–5562 (1998).
 56. Ji, J., Jia, L., Yan, L. & Bangal, P. R. Efficient synthesis of poly(acrylic acid) in aqueous solution via a RAFT process. *J. Macromol. Sci. Part A Pure Appl. Chem.* **47**, 445–451 (2010).
 57. Loiseau, J. *et al.* Synthesis and characterization of poly(acrylic acid) produced by RAFT polymerization. Application as a very efficient dispersant of CaCO₃, Kaolin, and TiO₂. *Macromolecules* **36**, 3066–3077 (2003).
 58. Chaduc, I. *et al.* Effect of the pH on the raft polymerization of acrylic acid in water. Application to the synthesis of poly(acrylic acid)-stabilized polystyrene particles by RAFT emulsion polymerization. *Macromolecules* **46**, 6013–6023 (2013).
 59. Swift, T., Swanson, L., Geoghegan, M. & Rimmer, S. The pH-responsive behaviour of poly(acrylic acid) in aqueous solution is dependent on molar mass. *Soft Matter* **12**, 2542–2549 (2016).
 60. Thomas, D. B., Convertine, A. J., Hester, R. D., Lowe, A. B. & McCormick, C. L. Hydrolytic Susceptibility of Dithioester Chain Transfer Agents and Implications in Aqueous RAFT Polymerizations †. *Macromolecules* **37**, 1735–1741 (2004).
 61. Ferguson, C. J. *et al.* Ab Initio Emulsion Polymerization by RAFT-Controlled Self-Assembly. *Macromolecules* **38**, 2191–2204 (2005).
 62. Hülya, A. Chapter 13: Block and graft copolymerization by controlled/living radical polymerization methods. in *Polymerization* 284–285 (IntechOpen, 2012).
 63. Lacík, I. *et al.* SEC analysis of poly(acrylic acid) and poly(methacrylic acid). *Macromol. Chem. Phys.* **216**, 23–37 (2015).
 64. López-Pérez, L. *et al.* Methylation of poly(acrylic acid), prepared using RAFT polymerization, with trimethylsilyldiazomethane: A metamorphosis of the thiocarbonyl group to a thiol-end group. *Polymer (Guildf)*. **168**, 116–125 (2019).
 65. Perrier, S. 50th Anniversary Perspective: RAFT Polymerization - A User Guide. *Macromolecules* **50**, 7433–7447 (2017).
 66. Canning, S. L., Smith, G. N. & Armes, S. P. A Critical appraisal of RAFT-mediated polymerization-induced self-assembly. *Macromolecules* **49**, 1985–2001 (2016).
 67. Blanz, A., Armes, S. P. & Ryan, A. J. Self-assembled block copolymer aggregates: from micelles to vesicles and their biological applications. *Macromol. Rapid Commun.* **30**, 267–277 (2009).
 68. Figg, C. A. *et al.* Polymerization-induced thermal self-assembly (PITSA). *Chem. Sci.* **6**, 1230–1236 (2015).
 69. Lansalot, M. & Rieger, J. Polymerization-Induced Self-Assembly. *Macromol. Rapid Commun.* **40**, 1800885 (2019).
-

-
70. McCormick, C. L. & Lowe, A. B. Aqueous RAFT polymerization: Recent developments in synthesis of functional water-soluble (co)polymers with controlled structures. *Acc. Chem. Res.* **37**, 312–325 (2004)
 71. Lee, H., Mok, H., Lee, S., Oh, Y. K. & Park, T. G. Target-specific intracellular delivery of siRNA using degradable hyaluronic acid nanogels. *J. Control. Release* **119**, 245–252 (2007).
 72. Oh, J. K., Drumright, R., Siegwart, D. J. & Matyjaszewski, K. The development of microgels/nanogels for drug delivery applications. *Prog. Polym. Sci.* **33**, 448–477 (2008).
 73. Barnett, C. E. Some applications of wave-length turbidimetry in the infrared. *J. Phys. Chem.* **46**, 69–75 (1942).
 74. Todica, M., Stefan, R., Pop, C. V. & Olar, L. IR and raman investigation of some poly(acrylic) acid gels in aqueous and neutralized state. *Acta Phys. Pol. A* **128**, 128–135 (2015).
 75. Lovett, J. R., Warren, N. J., Ratcliffe, L. P. D., Kocik, M. K. & Armes, S. P. pH-responsive non-ionic diblock copolymers: ionization of carboxylic acid end-groups induces an order-order morphological transition. *Angew. Chemie Int. Ed.* **54**, 1279–1283 (2015).
 76. Jones, E. R., Semsarilar, M., Wyman, P., Boerakker, M. & Armes, S. P. Addition of water to an alcoholic RAFT PISA formulation leads to faster kinetics but limits the evolution of copolymer morphology. *Polym. Chem.* **7**, 851–859 (2016).
 77. Liu, Y., Li, J., Cheng, X., Ren, X. & Huang, T. S. Self-assembled antibacterial coating by *N*-halamine polyelectrolytes on a cellulose substrate. *J. Mater. Chem. B* **3**, 1446–1454 (2015).
 78. Wen, S.-P., Saunders, J. G. & Fielding, L. A. Investigating the influence of solvent quality on RAFT-mediated PISA of sulfonate-functional diblock copolymer nanoparticles. *Polym. Chem.* **11**, 3416–3426 (2020).
 79. Åkerlöf, G. Dielectric constants of some organic solvent-water mixtures at various temperatures. *J. Am. Chem. Soc.* **54**, 4125–4139 (1932).
 80. Owen, S. C., Chan, D. P. Y. & Shoichet, M. S. Polymeric micelle stability. *Nano Today* **7**, 53–65 (2012).
 81. Zhang, L., Daniels, E. S., Dimonie, V. L. & Klein, A. Synthesis and characterization of PNIPAM/PS core/shell particles. *J. Appl. Polym. Sci.* **118**, 2502–2511 (2010).
 82. Boye, S. *et al.* From 1D Rods to 3D networks: a biohybrid topological diversity investigated by asymmetrical flow field-flow fractionation. *Macromolecules* **48**, 4607–4619 (2015).
 83. Wagner, M., Holzschuh, S., Traeger, A., Fahr, A. & Schubert, U. S. Asymmetric flow field-flow fractionation in the field of nanomedicine. *Anal. Chem.* **86**, 5201–5210 (2014).
 84. Vežočník, V. *et al.* Size fractionation and size characterization of nanoemulsions of lipid droplets and large unilamellar lipid vesicles by asymmetric-flow field-flow fractionation/multi-angle light scattering and dynamic light scattering. *J. Chromatogr. A* **1418**, 185–191 (2015).
 85. Fuentes, C., Castillo, J., Vila, J. & Nilsson, L. Application of asymmetric flow field-flow fractionation (AF4) and multiangle light scattering (MALS) for the evaluation of changes in the product molar mass during PVP-*b*-PAMPS synthesis. *Anal. Bioanal. Chem.* **410**, 3757–3767 (2018).
 86. Brewer, A. K. & Striegel, A. M. Particle size characterization by quadruple-detector hydrodynamic chromatography. *Anal. Bioanal. Chem.* **393**, 295–302 (2009).
 87. Brewer, A. K. & Striegel, A. M. Characterizing the size, shape, and compactness of a polydisperse prolate ellipsoidal particle *via* quadruple-detector hydrodynamic chromatography. *Analyst* **136**, 515–519 (2011).
-

-
88. Iavicoli, P. *et al.* Application of Asymmetric Flow Field-Flow Fractionation hyphenations for liposome–antimicrobial peptide interaction. *J. Chromatogr. A* **1422**, 260–269 (2015).
 89. Niezabitowska, E. *et al.* Insights into the internal structures of nanogels using a versatile asymmetric-flow field-flow fractionation method. *Nanoscale Adv.* **2**, 4713–4721 (2020).
 90. Deen, G. R. & Pedersen, J. S. Investigation on the structure of temperature-responsive *N*-isopropylacrylamide microgels containing a new hydrophobic crosslinker. *Cogent Chem.* **1**, 1012658 (2015).
 91. Izunobi, J. U. & Higginbotham, C. L. Polymer molecular weight analysis by ¹H NMR spectroscopy. *J. Chem. Educ.* **88**, 1098–1104 (2011).
 92. Cowie, J. M. G. & Arrighi, V. *Polymers: Chemistry and Physics of Modern Materials*. CRC Press (2008).
 93. Moad, G. & Solomon, D. H. *The Chemistry of Radical Polymerization. The Chemistry of Radical Polymerization* (2006).
 94. Halperin, A., Kröger, M. & Winnik, F. M. Poly(*N*-isopropylacrylamide) Phase diagrams: Fifty years of research. *Angew. Chemie Int. Ed.* **54**, 15342–15367 (2015).
 95. Xia, Y., Burke, N. A. D. & Stöver, H. D. H. End group effect on the thermal response of narrow-disperse poly(*N*-isopropylacrylamide) prepared by atom transfer radical polymerization. *Macromolecules* **39**, 2275–2283 (2006).
 96. Gibson, M. I. & O’Reilly, R. K. To aggregate, or not to aggregate? Considerations in the design and application of polymeric thermally-responsive nanoparticles. *Chem. Soc. Rev.* **42**, 7204–7213 (2013).
 97. Fitzgerald, P. A., Gupta, S., Wood, K., Perrier, S. & Warr, G. G. Temperature- and pH-responsive micelles with collapsible poly(*N*-isopropylacrylamide) headgroups. *Langmuir* **30**, 7986–7992 (2014).
 94. Blackman, L. D., Wright, D. B., Robin, M. P., Gibson, M. I. & O’Reilly, R. K. Effect of micellization on the thermoresponsive behavior of polymeric assemblies. *ACS Macro Lett.* **4**, 1210–1214 (2015).
 99. Ren, H. *et al.* Charged end-group terminated poly(*N*-isopropylacrylamide)-*b*-poly(carboxylic azo) with unusual thermoresponsive behaviors. *Macromolecules* **51**, 3290–3298 (2018).
 100. Schilli, C. M. *et al.* A New double-responsive block copolymer synthesized via RAFT polymerization: poly(*N*-isopropylacrylamide)-*block*-poly(acrylic acid). *Macromolecules* **37**, 7861–7866 (2004).
 101. Khimani, M., Yusa, S., Aswal, V. K. & Bahadur, P. Aggregation behavior of double hydrophilic block copolymers in aqueous media. *J. Mol. Liq.* **276**, 47–56 (2019).
 102. Gao, X. *et al.* PH- and thermo-responsive poly(*N*-isopropylacrylamide-co-acrylic acid derivative) copolymers and hydrogels with LCST dependent on pH and alkyl side groups. *J. Mater. Chem. B* **1**, 5578–5587 (2013).
 103. Katsumoto, Y. & Kubosaki, N. Tacticity effects on the phase diagram for poly(*N*-isopropylacrylamide) in water. *Macromolecules* **41**, 5955–5956 (2008).
 104. Autieri, E., Chiessi, E., Lonardi, A., Paradossi, G. & Sega, M. Conformation and dynamics of poly(*N*-isopropylacrylamide) trimers in water: A molecular dynamics and metadynamics simulation study. *J. Phys. Chem. B* **115**, 5827–5839 (2011).
-

-
105. Mukherji, D., Marques, C. M. & Kremer, K. Polymer collapse in miscible good solvents is a generic phenomenon driven by preferential adsorption. *Nat. Commun.* **5**, 1–6 (2014).
 106. Scherzinger, C., Schwarz, A., Bardow, A., Leonhard, K. & Richtering, W. Cononsolvency of poly(*N*-isopropyl acrylamide) (PNIPAM): Microgels versus linear chains and macrogels. *Curr. Opin. Colloid Interface Sci.* **19**, 84–94 (2014).
 107. Pica, A. & Graziano, G. An alternative explanation of the cononsolvency of poly(*N*-isopropylacrylamide) in water-methanol solutions. *Phys. Chem. Chem. Phys.* **18**, 25601–25608 (2016).
 108. Kyriakos, K. *et al.* Solvent dynamics in solutions of PNIPAM in water/methanol mixtures—a quasi-elastic neutron scattering study. *J. Phys. Chem. B* **120**, 4679–4688 (2016).
 109. Kirichenko, M. N., Sanoeva, A. T. & Chaikov, L. L. Appearance of an artifact peak in the particle size distribution measured by DLS at low concentrations. *Bull. Lebedev Phys. Inst.* **43**, 256–260 (2016).
 110. Paradossi, G. & Chiessi, E. Tacticity-dependent interchain interactions of poly(*N*-isopropylacrylamide) in water: toward the molecular dynamics simulation of a thermoresponsive microgel. *Gels* **3**, 13 (2017).
 111. Tavagnacco, L., Zaccarelli, E. & Chiessi, E. On the molecular origin of the cooperative coil-to-globule transition of poly(*N*-isopropylacrylamide) in water. *Phys. Chem. Chem. Phys.* **20**, 9997–10010 (2018).
 112. Rebolj, K., Pahovnik, D. & Žagar, E. Characterization of a protein conjugate using an asymmetrical-flow field-flow fractionation and a size-exclusion chromatography with multi-detection system. *Anal. Chem.* **84**, 7374–7383 (2012).
 13. Gaulding, J. C., Smith, M. H., Hyatt, J. S., Fernandez-Nieves, A. & Lyon, L. A. Reversible inter- and intra-microgel cross-linking using disulfides. *Macromolecules* **45**, 39–45 (2012).

Appendix A

Figure 2A.1: ^1H NMR spectrum of recrystallised HEMP CTA.Figure 2A.2: ^{13}C NMR spectrum of recrystallized HEMP CTA.

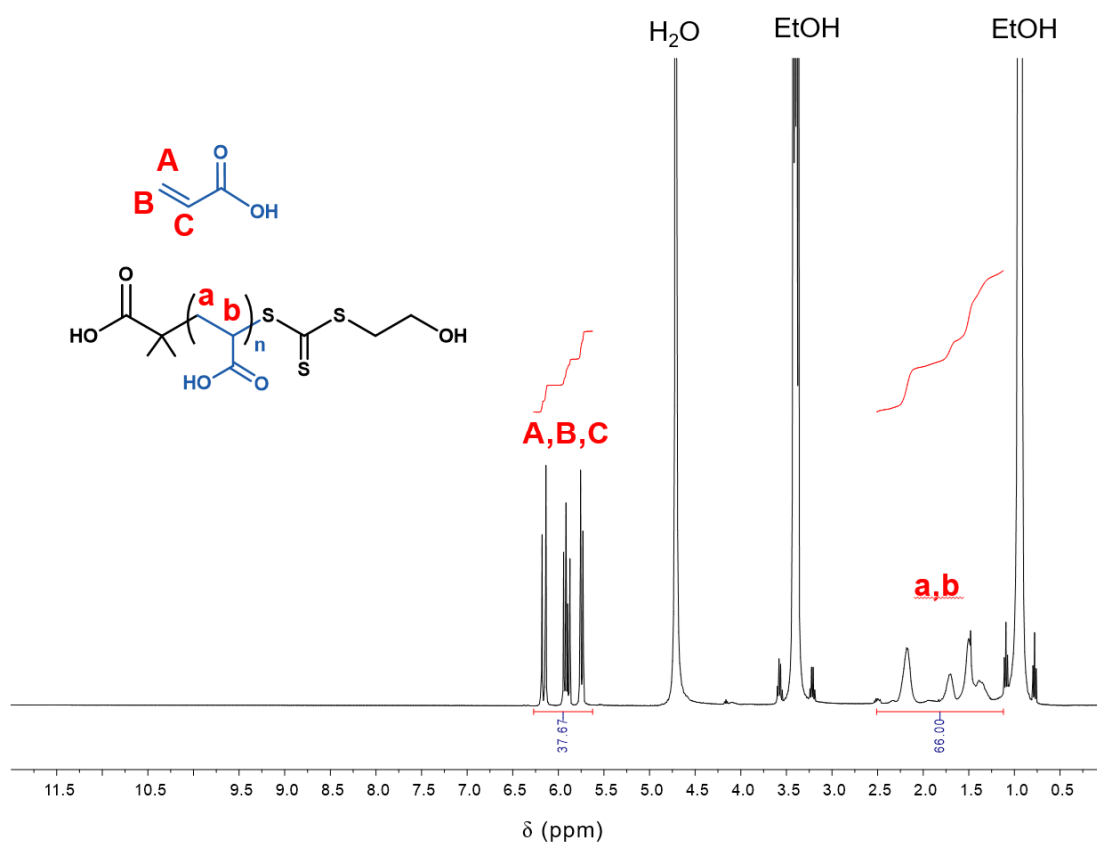


Figure 2A.3: ¹H NMR spectrum of PAA₃₇ macro-CTA before purification for polymer conversion determination.

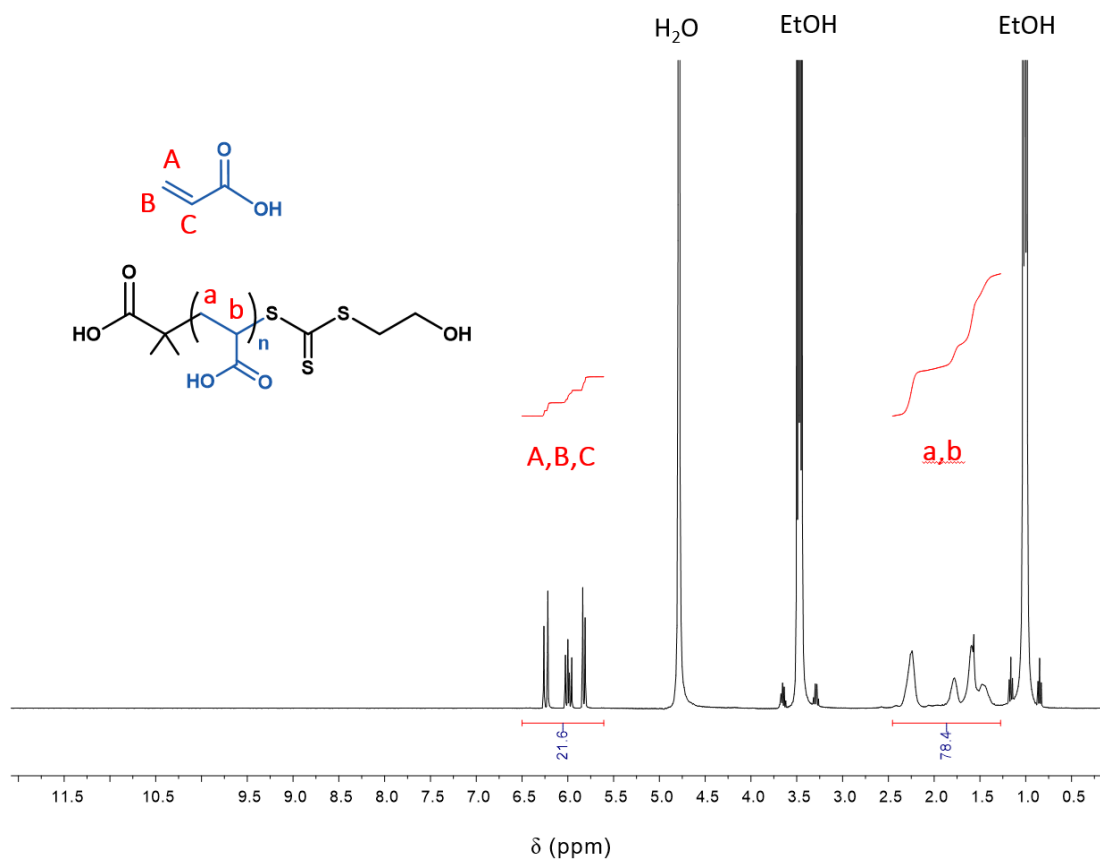


Figure 2A.4: ¹H NMR spectrum of PAA₅₂ macro-CTA before purification for polymer conversion determination.

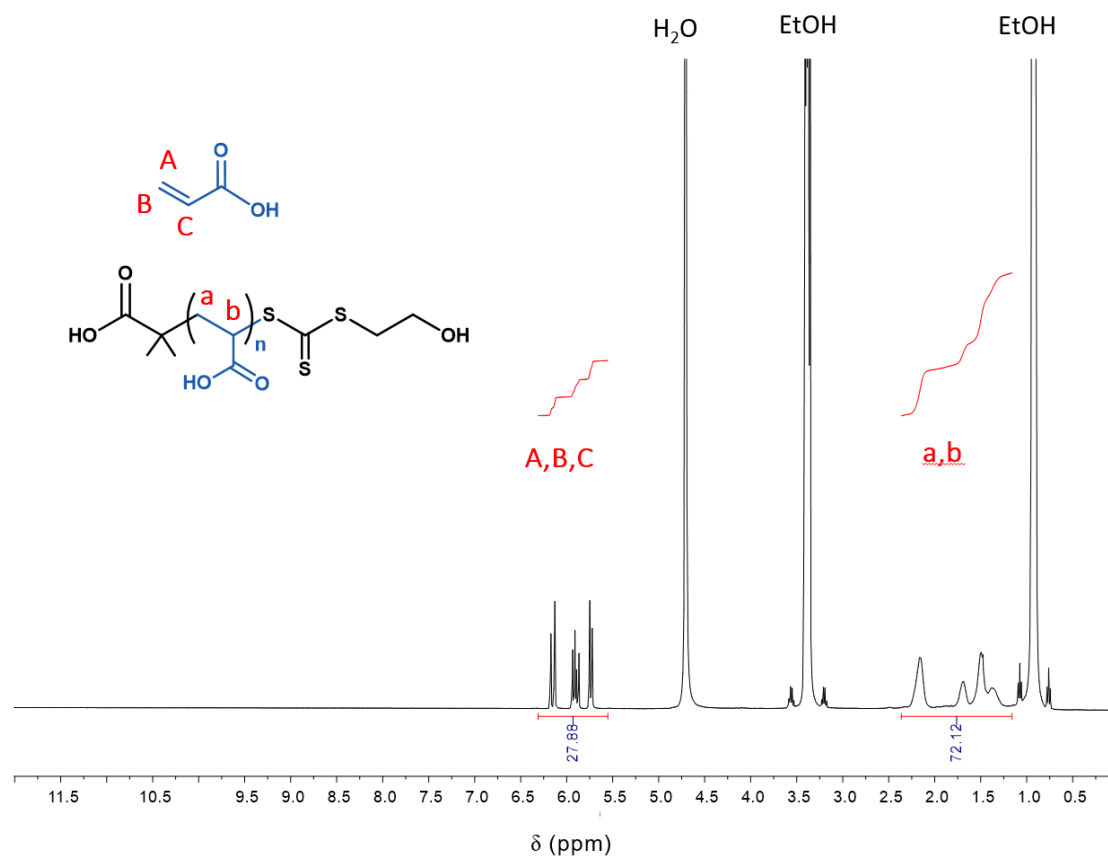


Figure 2A.5: ^1H NMR spectrum of PAA₈₄ macro-CTA before purification for polymer conversion determination.

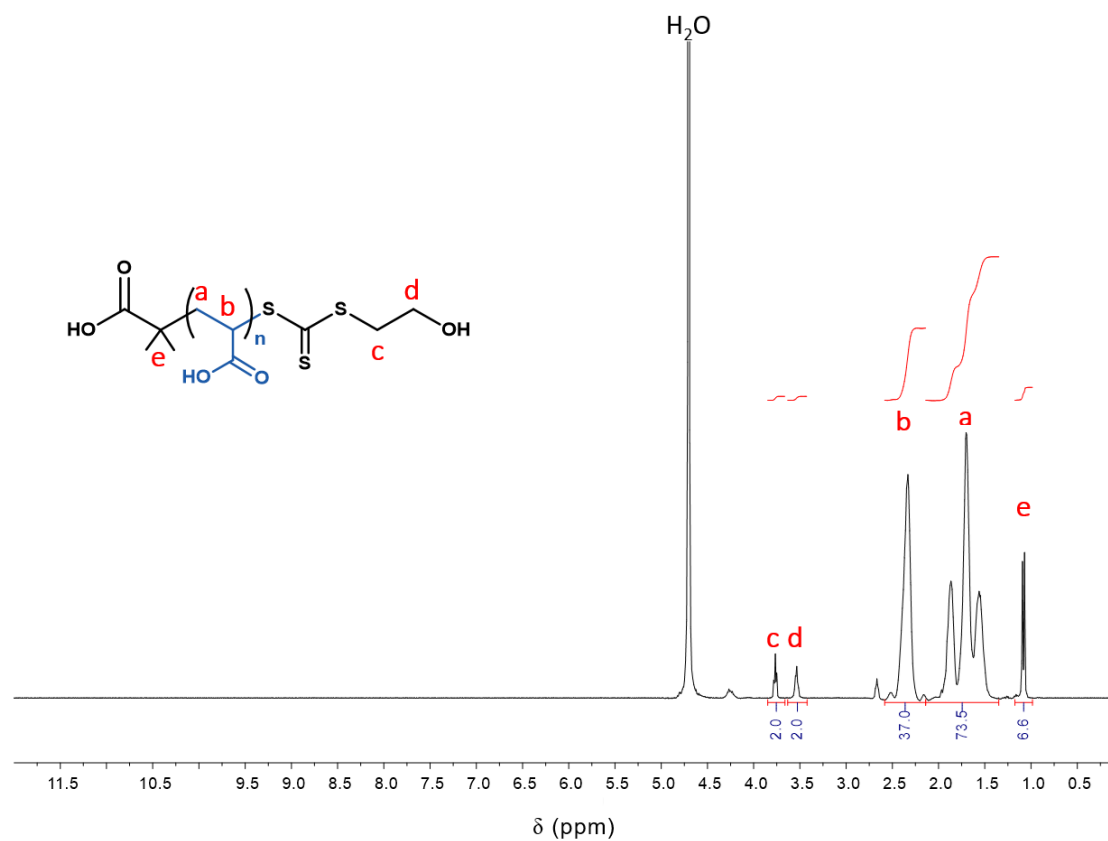


Figure 2A.6: ^1H NMR spectrum of PAA₃₇ macro-CTA after purification for DP determination.

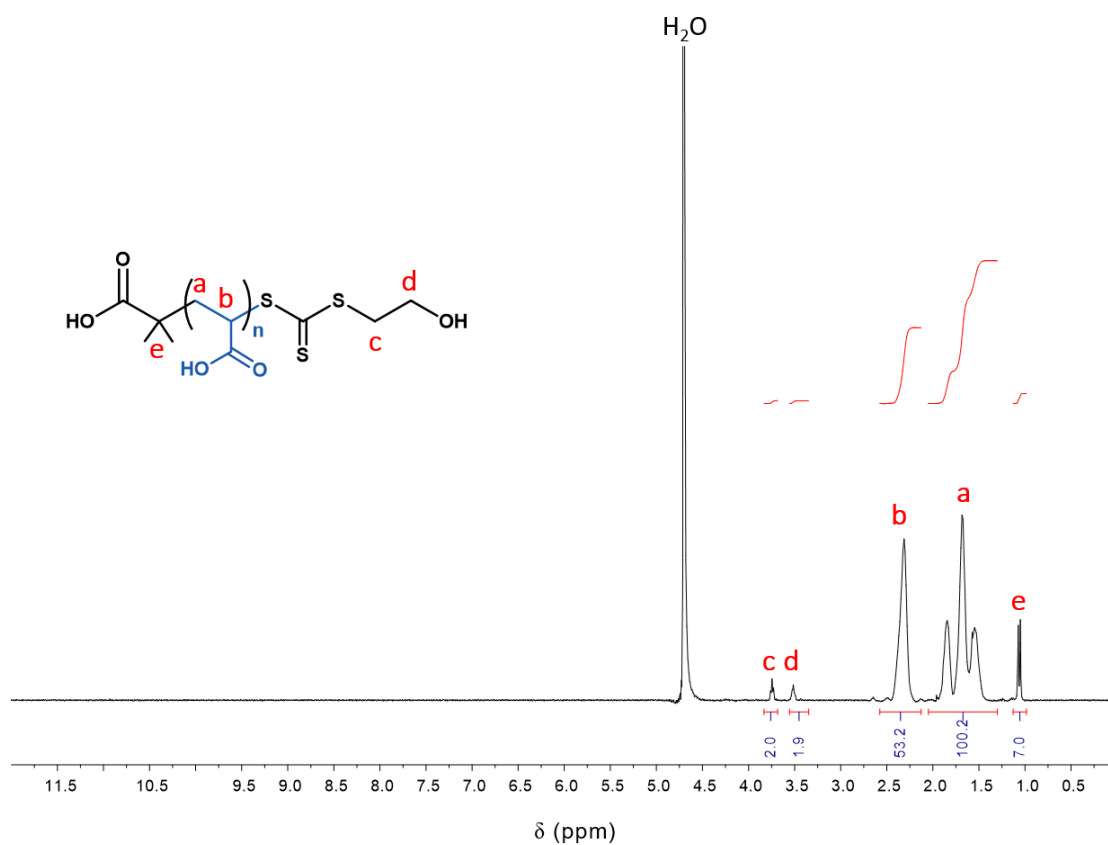


Figure 2A.7: ¹H NMR spectrum of PAA₅₂ macro-CTA after purification for DP determination.

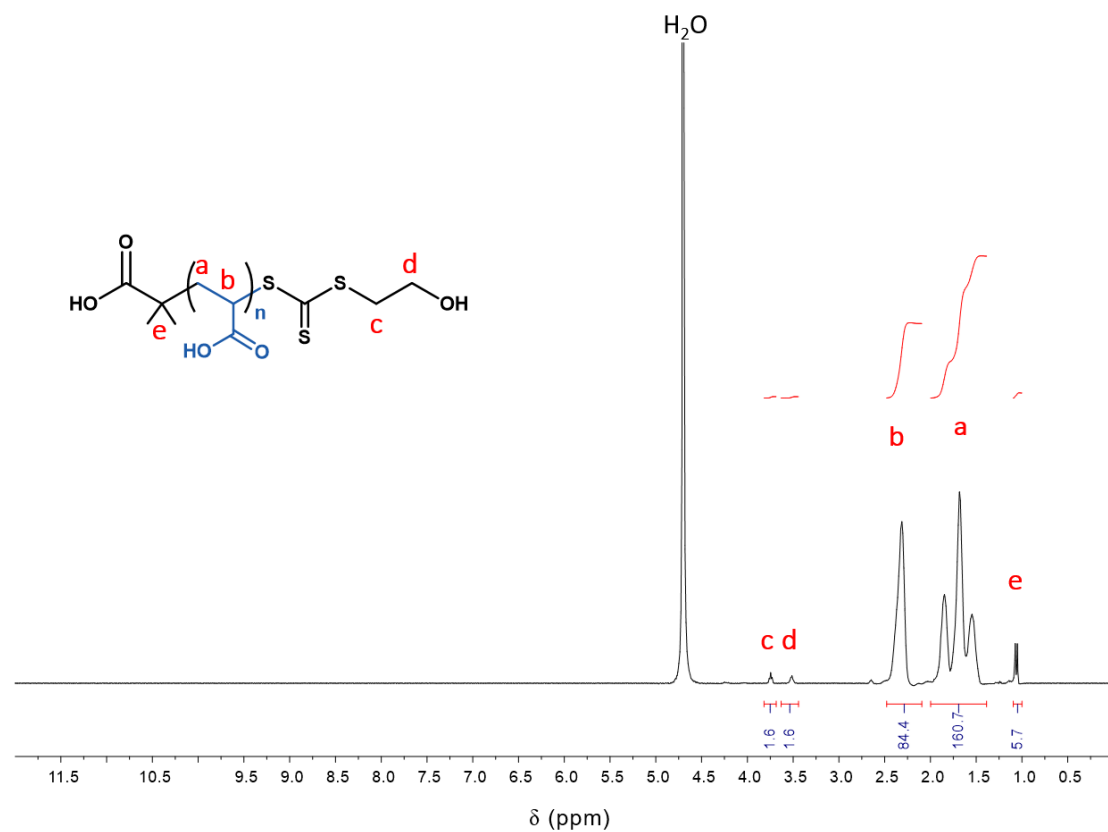


Figure 2A.8: ¹H NMR spectrum of PAA₈₄ macro-CTA after purification for DP determination.

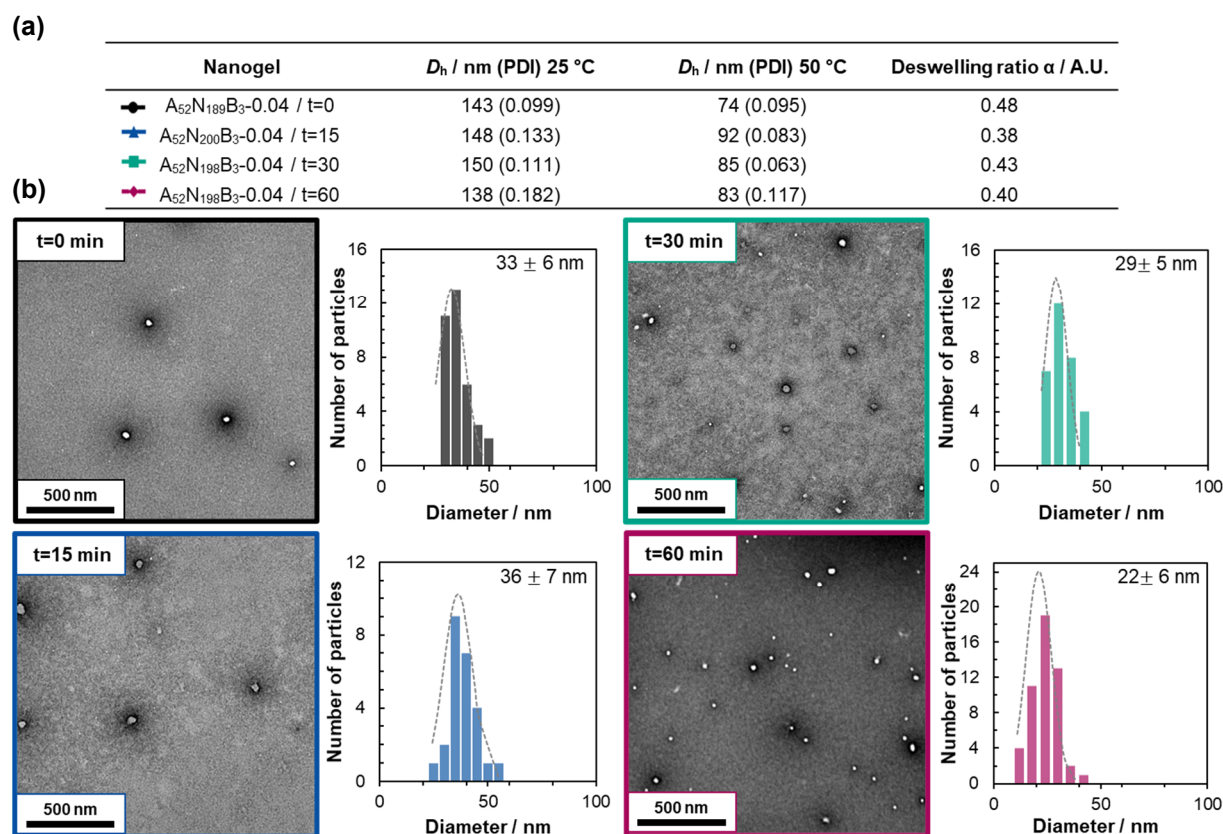


Figure 2A.9: The effect of adding the crosslinker at different times (t) during the polymerisation on the properties of $A_{52}N_{200}B_3-0.04$ nanogels. (a) Summary of the size determination by DLS at 25 and 50 °C and the deswelling ratio at 50 °C determined with Equation 3.2, and (b) TEM images of the respective purified nanogel with their number particle size distributions. Data obtained from 0.1% w/w nanogels dispersions in DI water at neutral pH. Samples were stained with phosphotungstic acid (0.75% w/v, pH 7.2) for TEM.

Table 2A.1: Summary of the optimisation parameters for the synthesis of $A_xN_yB_z$ nanogels synthesised by RAFT dispersion polymerisation.

Target composition [PAA _x]:[NIPAM]:[BIS]		Initiator ^a	Solvent ^b	Solids content %	pH	Conversion ^c %	Note
x=48	[1]:[100]:[3]	VA-044	Water	10%	2.7	/	Precipitate
	[1]:[200]:[6]	VA-044	Water	10%	2.7	/	Precipitate
	[1]:[300]:[9]	VA-044	Water	10%	2.7	/	Precipitate
	[1]:[100]:[3]	VA-044	Water	5%	4.3	/	Slushy aggregates
	[1]:[200]:[6]	VA-044	Water	5%	4.3	/	Slushy aggregates
	[1]:[300]:[9]	VA-044	Water	5%	4.4	/	Slushy aggregates
	[1]:[100]:[3]	ACVA	Water	10%	4.3	/	Aggregates
	[1]:[100]:[3]	ACVA	$X_e=0.05$	9%	7.0	95%	107 nm (0.15) ^d
	[1]:[100]:[3]	VA-044	$X_e=0.07$	11%	6.9	62%	56 nm (0.25) ^d
	[1]:[100]:[3]	ACVA	Water	10%	6.9	98%	129 nm (0.096) ^d
	[1]:[100]:[3]	ACVA	$X_e=0.03$	10%	7.2	91%	120 nm (0.068) ^d
	[1]:[100]:[3]	ACVA	$X_e=0.07$	10%	6.7	82%	106 nm (0.112) ^d
	[1]:[100]:[3]	ACVA	$X_e=0.09$	10%	7.0	99%	87 nm (0.140) ^d
	[1]:[100]:[3]	ACVA	$X_e=0.11$	12%	6.9	99%	81 nm (0.124) ^d
	[1]:[100]:[3]	ACVA	$X_e=0.13$	10%	7.0	87%	80 nm (0.155) ^d
[1]:[300]:[9]	ACVA	$X_e=0.11$	10%	7.0	94%	148 nm (0.048) ^d	
x=94	[1]:[100]:[3]	VA-044	Water	10%	3.9	/	Slushy aggregates
	[1]:[200]:[6]	VA-044	Water	10%	4.3	/	Slushy aggregates
	[1]:[300]:[9]	VA-044	Water	10%	4.4	/	Slushy aggregates
	[1]:[100]:[3]	ACVA	$X_e=0.11$	10%	7.0	95%	140 nm (0.146) ^d
	[1]:[200]:[6]	ACVA	$X_e=0.11$	10%	7.0	92%	314 nm (0.044) ^d
[1]:[300]:[9]	ACVA	$X_e=0.11$	10%	6.9	85%	548 nm (0.152) ^d	
x=52	[1]:[300]:[3]	ACVA	$X_e=0.05$	10%	5.3	88%	Bimodal size distribution
	[1]:[300]:[5]	ACVA	$X_e=0.02$	10%	5.5	81%	Bimodal size distribution

^a(1,2-Bis(2-(4,5-dihydro-1H-imidazol-2-yl)propan-2-yl)diazene dihydrochloride) (VA-044) or 4,4'-azobis(4-cyanopentanoic acid) (ACVA) used as initiators as indicated, targeting $[PAA_x]/[I]=5/1$ where I is the initiator at a reaction temperature of 50 °C for VA-044 or 70 °C for ACVA. ^bEthanol mole fraction (X_e) Water-ethanol pair. ^cGravimetric determination by moisture analysis of solids content against predicted solids content. ^dSize determination of 0.1% w/w nanogels dispersions in DI water at pH 7 and 25 °C by dynamic light scattering (DLS).

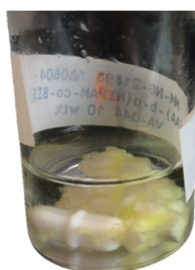


Figure 2A.10: Digital photograph of the crude mixture when the polymerisation was attempted without any pH adjustment. At $pH \approx 2.7$, using VA-044 as initiator and target composition of $[PAA_{48}]:[NIPAM]:[BIS]$ of 1:100:1 at 10% w/w and 50 °C.

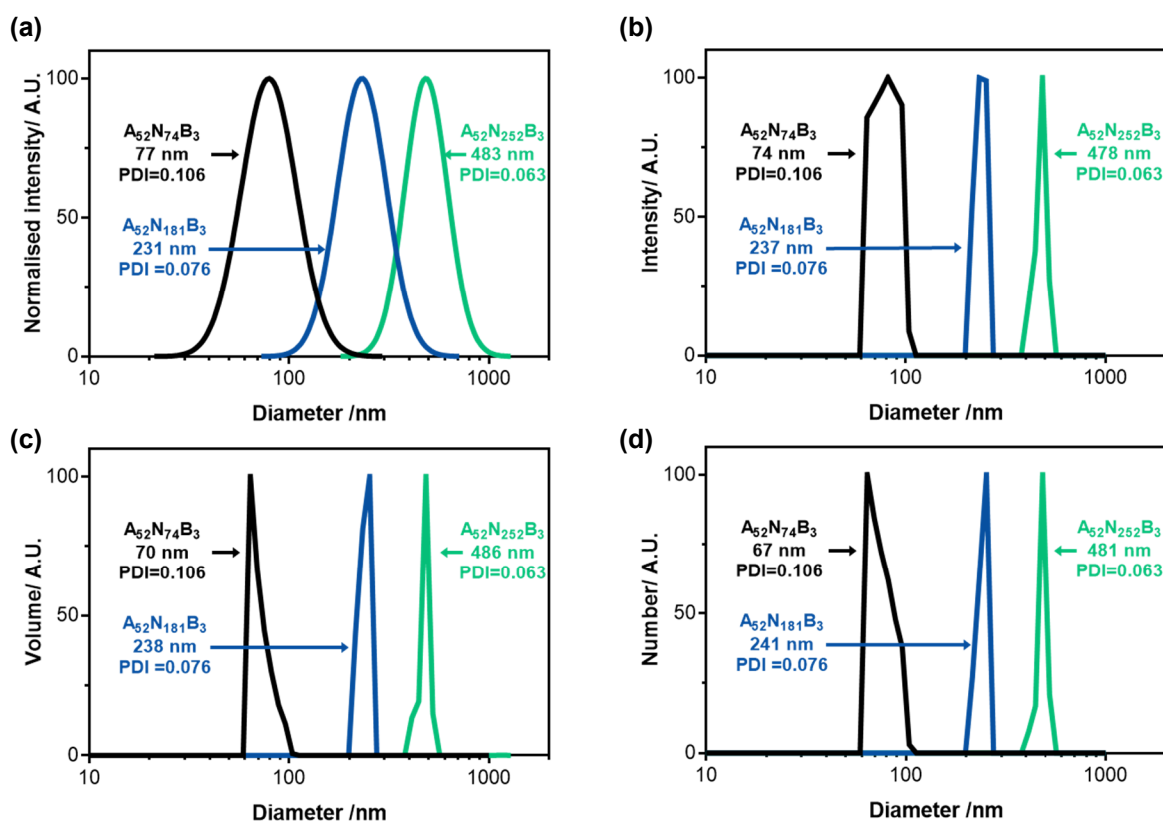


Figure 2A.11: Size distributions obtained from DLS of the $A_{52}N_yB_3$ nanogels synthesised in water. (a) Intensity average log-normal size distribution, (b) intensity size distribution curves, (c) volume size distribution, and (d) number size distribution. Data obtained from 0.1% w/w nanogels dispersions in DI water at neutral pH at 25 °C.

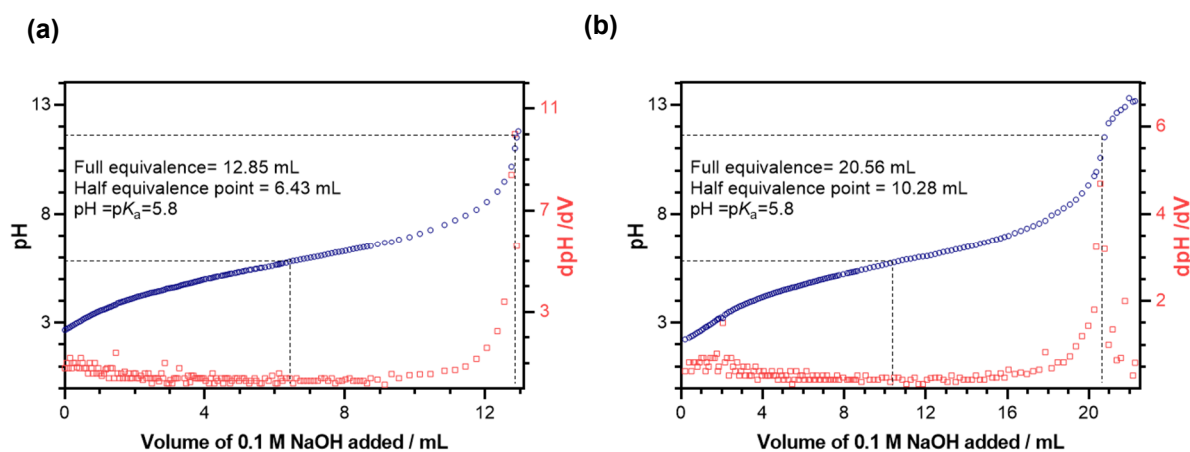


Figure 2A.12: Acid titration curves of (a) PAA_{52} and (b) PAA_{84} at 10 mg mL^{-1} aqueous solution.

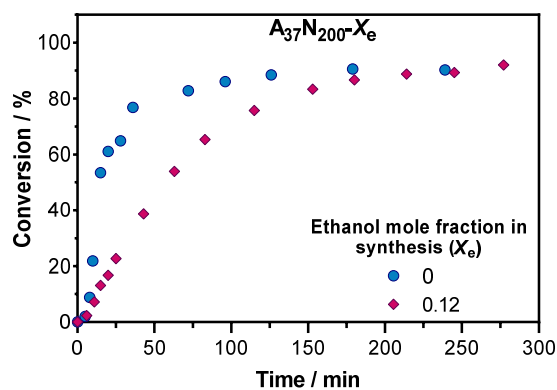


Figure 2A.13: Kinetic study of the RAFT dispersion polymerisation of NIPAM by chain extension of PAA₃₇ as macro-CTA. NIPAM conversion vs time curve for consolvent synthesis composition of $X_e=0$ (●) and $X_e=0.12$ (◆). Synthesis of a PAA₃₇-*b*-PNIPAM₂₀₀ at 70 °C and 10% w/w.

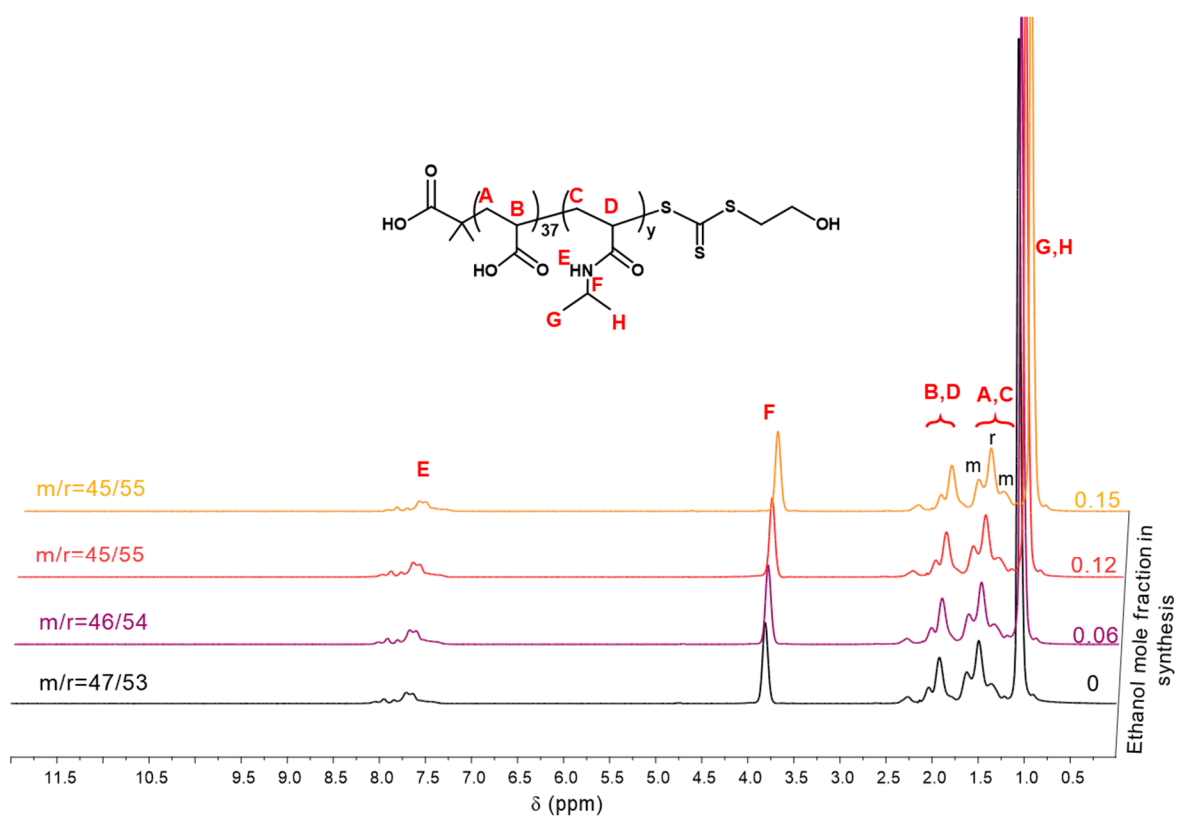


Figure 2A.14: Stacked ¹H NMR spectra recorded in D₂O of purified A₃₇N₃₀₂- X_e diblock copolymers. The H₂O solvent peak was suppressed to gain better resolution of the spectra.

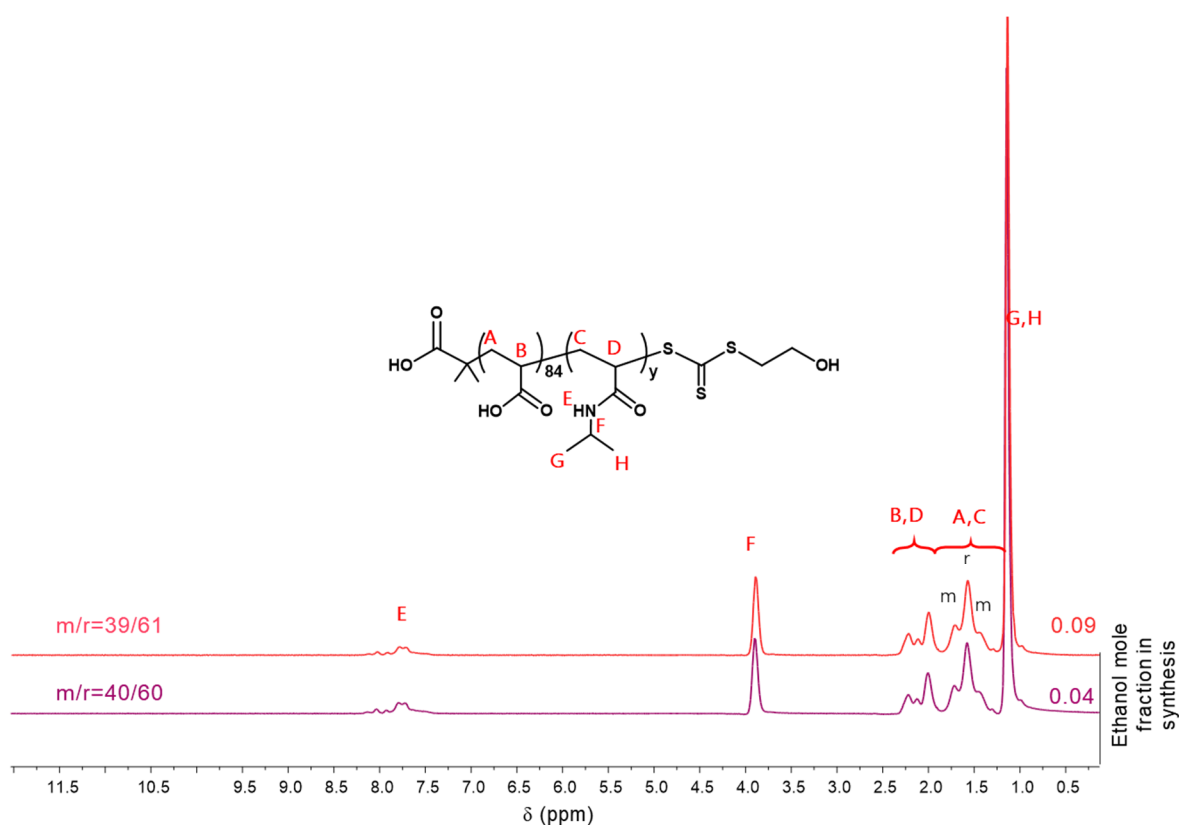


Figure 2A.15: Stacked ^1H NMR spectra recorded in D_2O of purified $A_{84}N_{202}-X_c$ diblock copolymers. The H_2O solvent peak was suppressed to gain better resolution of the spectra.

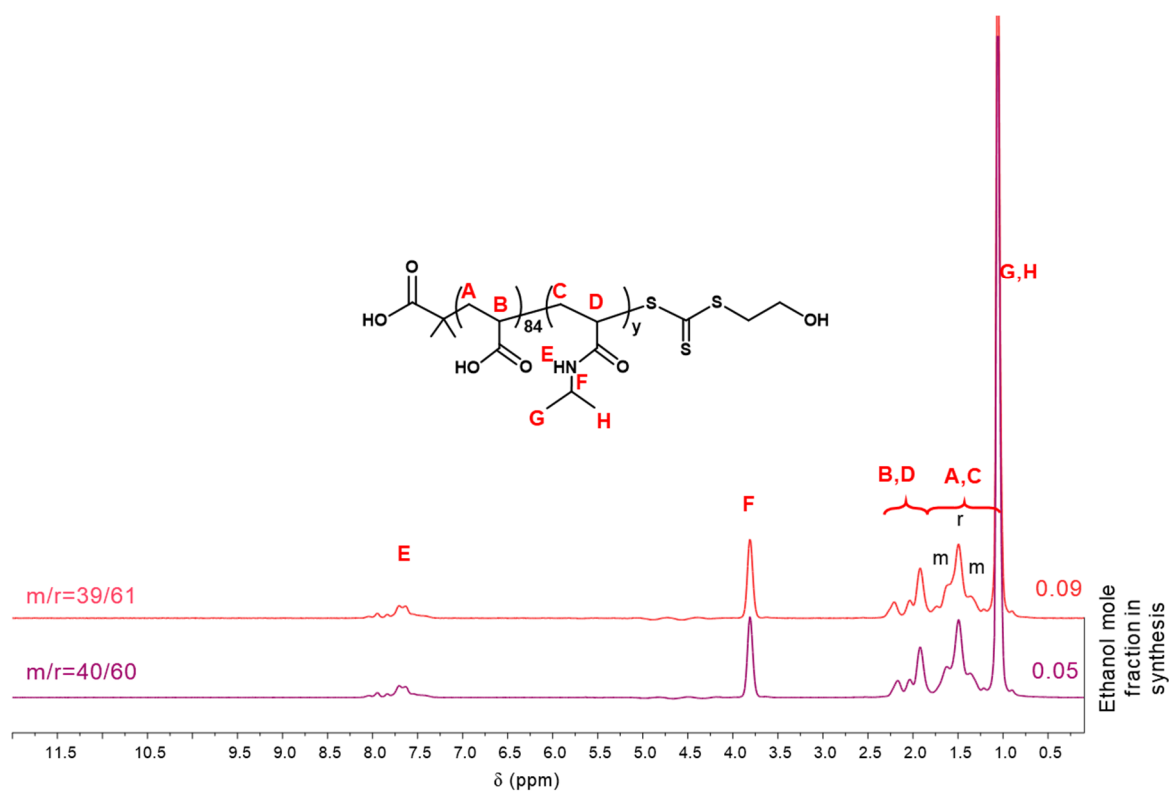


Figure 2A.16: Stacked ^1H NMR spectra recorded in D_2O of purified $A_{84}N_{303}-X_c$ diblock copolymers. The H_2O solvent peak was suppressed to gain better resolution of the spectra.

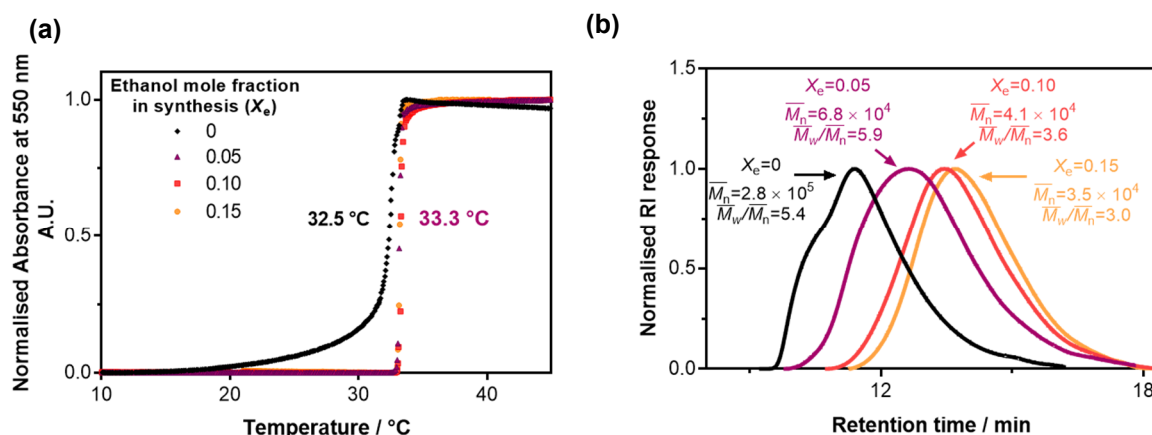


Figure 2A.17: Characterisation of PNIPAM- X_e , synthesised by free radical polymerisation. (a) Cloud point curves and (b) DMF GPC chromatograms of PNIPAM- X_e . The cloud points were determined from the inflection point of the normalised absorbance curve at 550 nm on a heating rate of 0.12 °C min^{-1} . (GPC: DMF 0.1% LiBr eluent, calibrated with near-monodisperse PMMA standards)

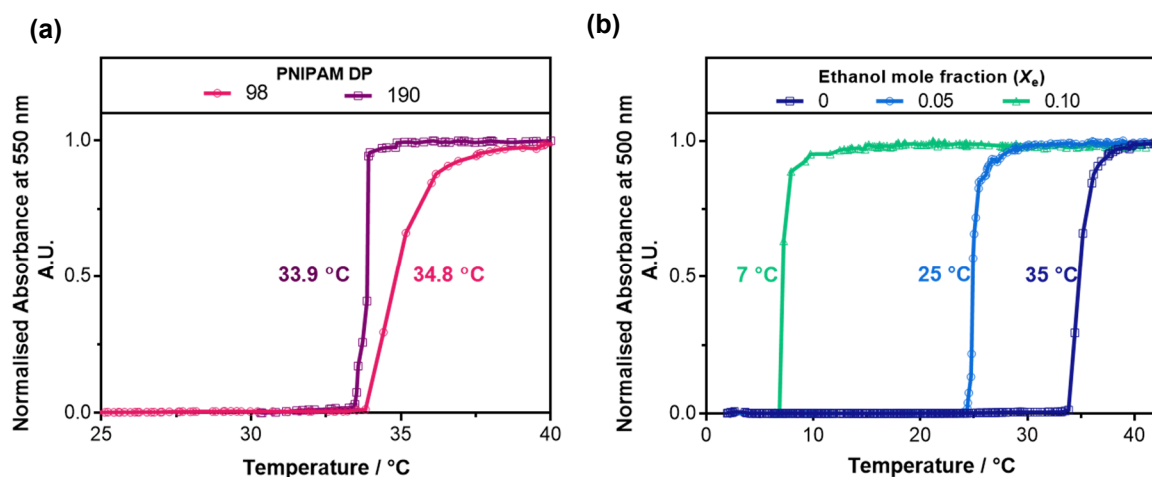


Figure 2A.18: Turbidimetry experiments of PNIPAM-HEMP homopolymers in aqueous solution. Cloud point curves of PNIPAM with different DP and (b) cloud point curves of PNIPAM₉₈ in different X_e fractions. Polymers were synthesised *via* RAFT ethanolic polymerisation. The cloud points were determined from the inflection point of the normalised absorbance curve at 550 nm on a heating rate of 0.12 °C min^{-1} .

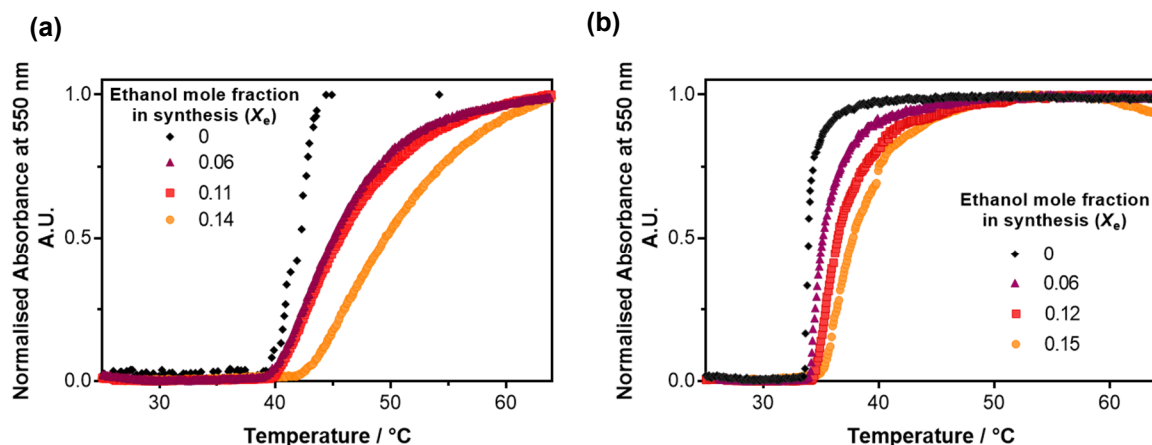


Figure 2A.19: Turbidimetry experiments of $A_{37}N_y-X_e$ diblock copolymers in aqueous solution at pH 7. Cloud point curves of PNIPAM targeting DP of (a) 100, (b) 302. Polymers were synthesised *via* RAFT dispersion polymerisation in either water or water/ethanol mixtures. The cloud points were determined from the inflection point of the normalised absorbance curve at 550 nm on a heating rate of 0.12 °C min^{-1} .

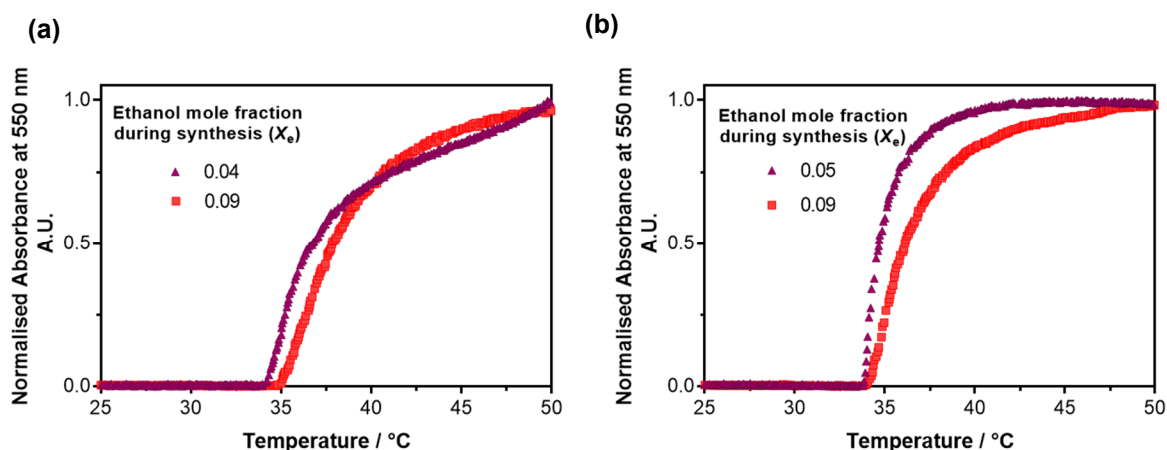


Figure 2A.20: Turbidimetry experiments of $A_{84}N_y-X_c$ diblock copolymers in aqueous solution at pH 7. Polymers were synthesised *via* RAFT dispersion polymerisation in water/ethanol mixtures (X_e). Cloud point curves of PNIPAM targeting DP of (a) 202 and (b) 303. The cloud points were determined from the inflection point of the normalised absorbance curve at 550 nm on a heating rate of $0.12\text{ }^\circ\text{C min}^{-1}$.

Table 2A.2: Summary of the synthesis and properties of $PHEA_{42}-b\text{-}PNIPAM_y$ copolymers synthesised by RAFT dispersion polymerisation in either water or water/ethanol mixtures.^a

Ethanol mole fraction (X_e) ^b	Conversion ^c %	Actual PNIPAM DP ^d	Cloud point ^e $^\circ\text{C}$	$\bar{M}_{n,\text{theo}}$ ^f kDa	$\bar{M}_{n,\text{SEC}}$ ^f kDa	\bar{M}_w/\bar{M}_n ^f
0	100	200	35.6	25.2	40.2	1.3
0.06	98	196	37.5	24.7	35.0	1.4
0.11	98	196	34.6	24.7	29.8	1.5
0.14	95	190	36.1	24.0	21.8	1.7

^aGeneral reaction conditions: Targeted $[\text{HEMP}]/[\text{ACVA}]=5$, solids content 10% w/w, $70\text{ }^\circ\text{C}$ for 6.5 h. $PHEA_{42}$ $\bar{M}_{n,\text{GPC}}=5.8\text{ kDa}$, $\bar{M}_w/\bar{M}_n=1.13$ ^bSolvent mixture used during the synthesis, H_2O -ethanol was used as the cosolvent pair. ^cDetermined by ^1H NMR spectroscopy studies using the ratio of the sum of vinyl proton integrals and the polymer backbone. ^dEstimated for $[\text{NIPAM}]/[\text{PHEA}_{42}]\times\text{conversion}$. ^eCloud points were estimated from the inflection point of the normalised absorbance curve of 1% w/w solutions in water at 550 nm on a heating rate of $0.12\text{ }^\circ\text{C min}^{-1}$. ^fGPC: GPC: DMF 0.1% LiBr eluent, vs PMMA standards.

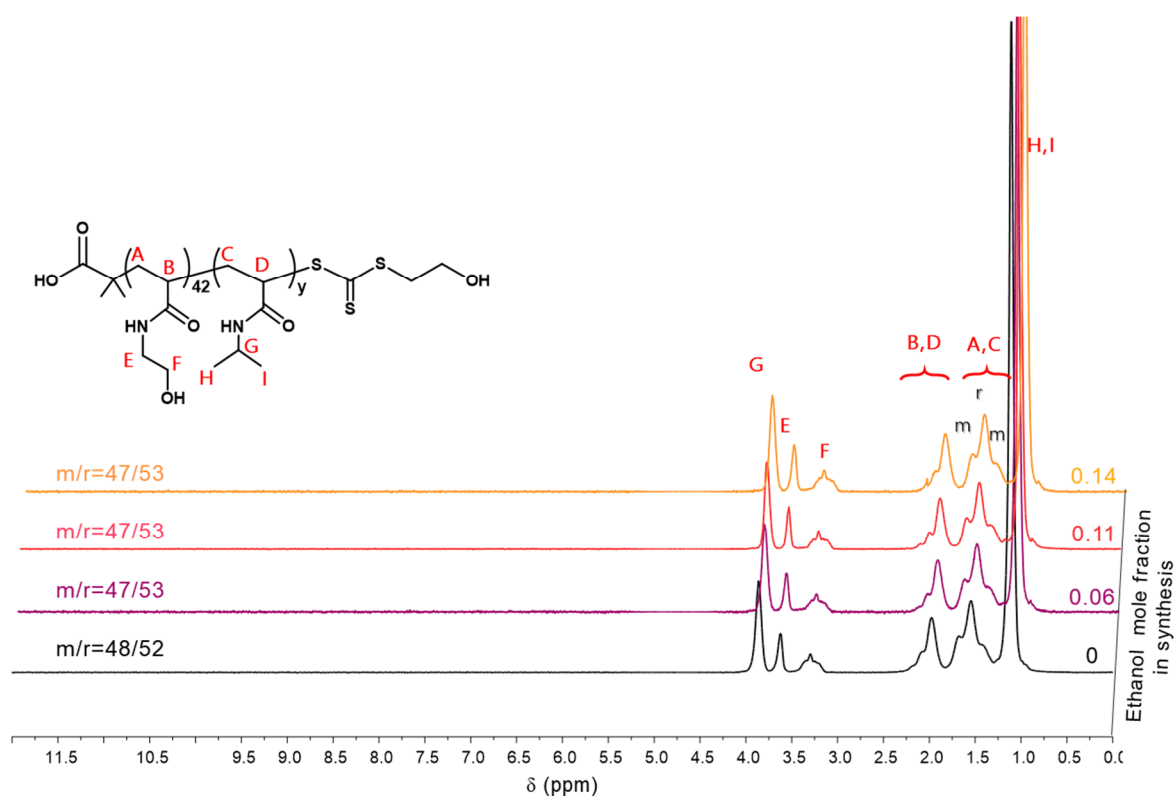


Figure 2A.21: Stacked ^1H NMR spectra recorded in D_2O of $\text{PHEA}_{42}\text{-}b\text{-PNIPAM}_y$ synthesised in either water or water-ethanol mixtures. The H_2O solvent peak was suppressed to gain better resolution of the spectra.

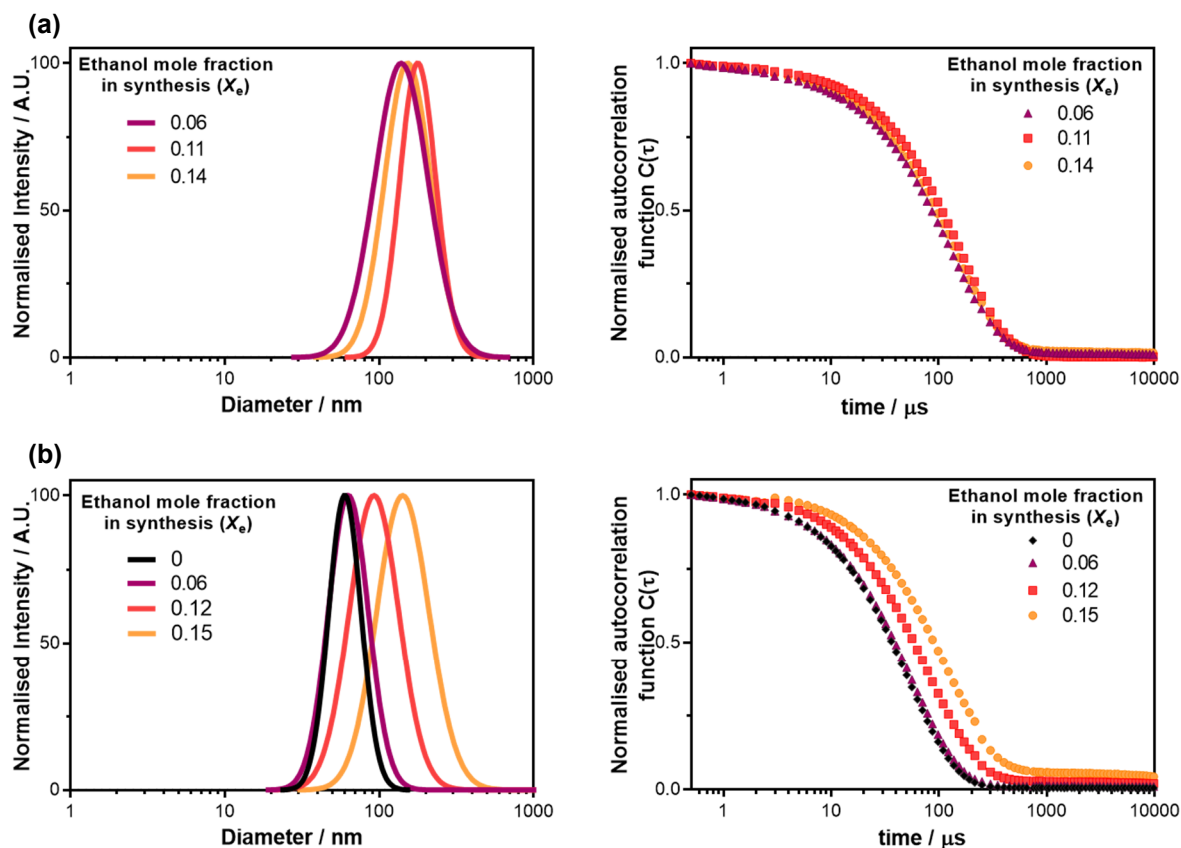


Figure 2A.22: Size determination studies of the self-assembly of $\text{A}_{37}\text{N}_y\text{-X}_c$ copolymers where $y =$ (a) 100, and (b) 302. DLS data obtained from 0.1% w/w nanogel dispersions in water at pH 7 and 50°C .

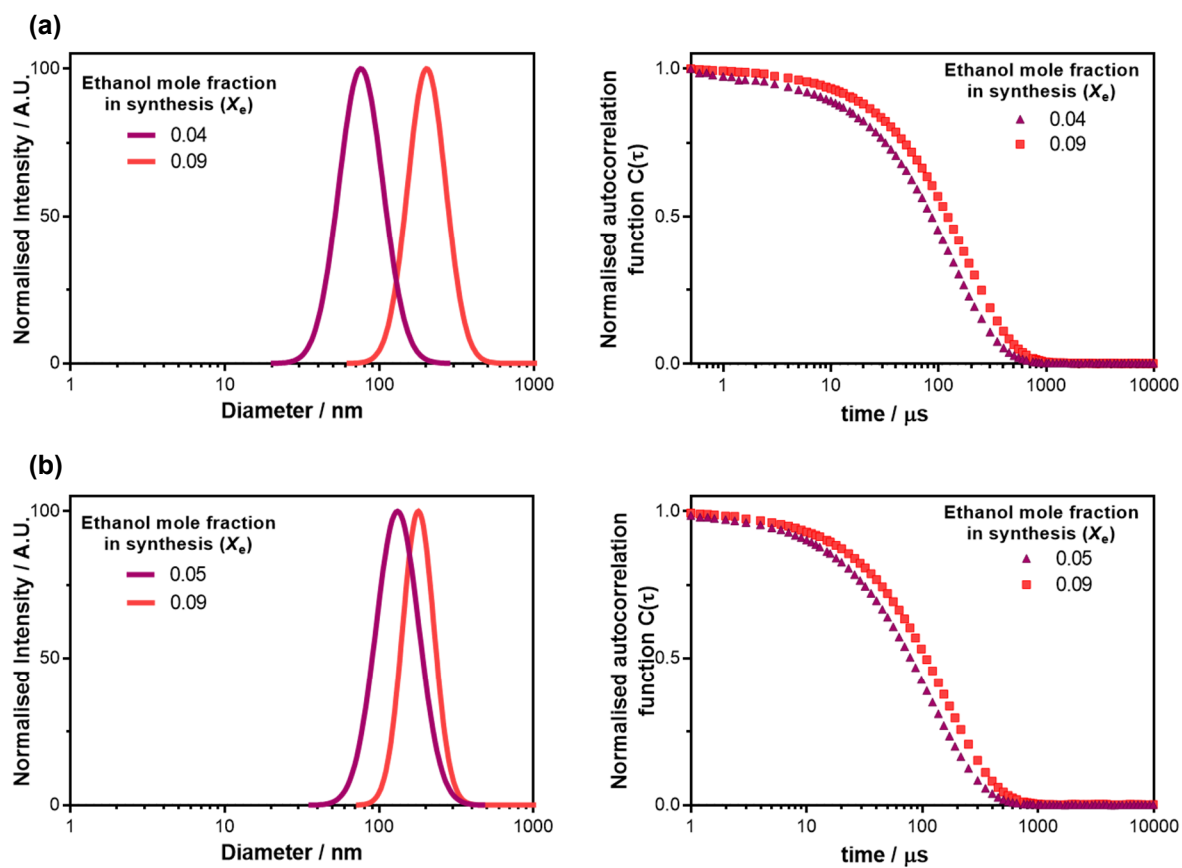


Figure 2A.23: Size determination studies of the self-assembly of $A_{84}N_y-X_c$ copolymers where $y =$ (a) 202, and (b) 303. DLS data obtained from 0.1% w/w nanogels dispersions in DI water at pH 7 and 50 °C.

CHAPTER 3

Anionic nanogels:

Effects of synthesis variables on
their stimuli-responsive behaviour

3.1. Chapter outlook

This chapter expands upon the work shown in Chapter 2, particularly on the effect of the synthesis variables on the stimuli-responsive behaviour of the PAA-*b*-P(NIPAM-*st*-BIS) ($A_xN_yB_z$) nanogels. Especially, the effect of the synthesis cosolvent composition on the properties of these nanogels was studied. An investigation of the volume phase transition temperature (VPTT) of nanogels is presented with variations in temperature, pH, and ionic strength. The volume change of nanogels in aqueous solution is analysed by temperature-dependent DLS studies. Additionally, the effect of the pH on the net charge of nanogels is investigated by ζ -potential measurements. Finally, an investigation on the rheological response of the nanogel dispersions is shown with different temperatures and concentrations of CaCl_2 since macroscopic gelation of nanogel particles is observed above the VPTT of the nanogels upon Ca^{2+} coordination with the carboxylate groups.

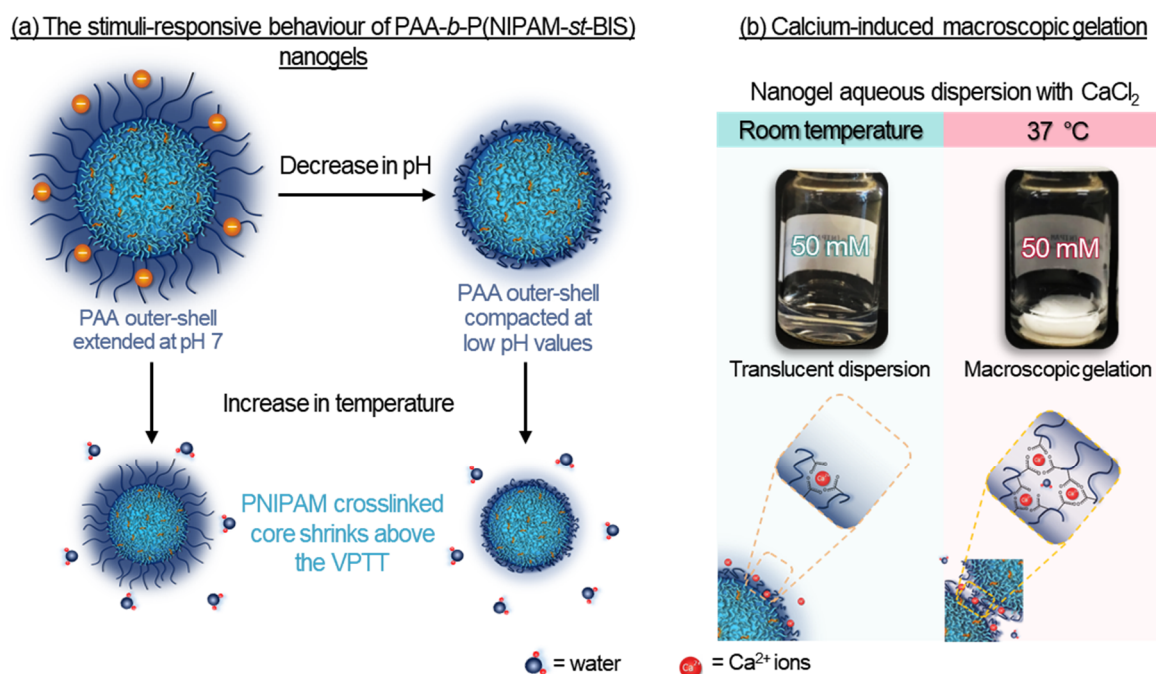


Figure 3.1: A schematic of the stimuli-responsive behaviour of $A_xN_yB_z$ anionic nanogels. (a) A cartoon representation of the effect of pH and temperature on the volume of the nanogels. (b) The photographs of the macroscopic gel formation at 37°C by calcium ionic crosslinking with the carboxylate groups of PAA as depicted in the cartoon.

3.2. Introduction

Stimuli-responsive nanogels are nanomaterials of particular interest for several biomedical applications comprising gene¹ and drug delivery,² biosensors,^{3,4} imaging⁵ and tissue engineering.⁶ Their unique ability to respond to stimuli by exhibiting changes in their physicochemical properties has positioned them as one of the increasingly investigated platforms for medicine-related applications. By using polymers that undergo structural changes in response to variations in stimulus, “smart” nanogels can be prepared to display sensitivity to environmental stimuli found within the body such as temperature, pH, or ionic strength.⁷ One of the most studied polymers to design nanogels is PNIPAM due to its ability to exhibit a sharp phase transition at around 31-35 °C in aqueous media,^{8,9} which is near physiological conditions. Unlike linear polymers, PNIPAM thermoresponsive crosslinked materials can absorb and retain large quantities of water without dissolving, hence these can swell and deswell with temperature (Figure 3.2a).¹⁰ The point at which this occurs is known as volume phase transition temperature (VPTT).¹¹ Below the VPTT, PNIPAM assumes a swollen conformation, in which its networks, specifically the amide groups, interact with water molecules through hydrogen bonding (Figure 3.2b). Upon heating, the hydrogen bonding is disrupted leading to increased dehydration of the chains followed by a sharp reduction in size due to the chains collapse.

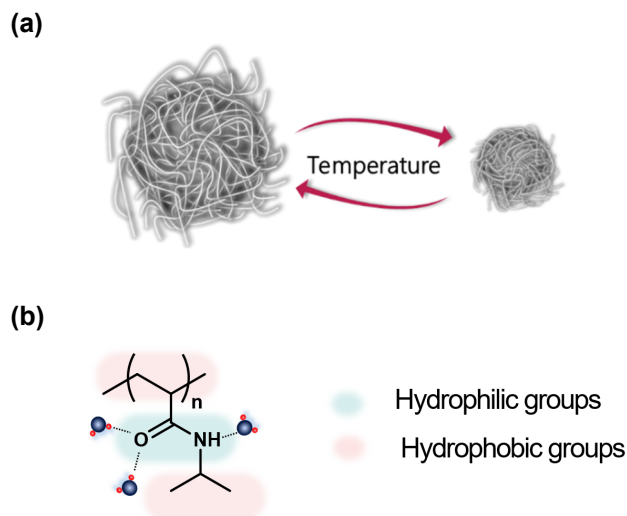


Figure 3.2: (a) Cartoon showing the temperature-dependent deswelling behaviour of PNIPAM and (b) the chemical structure of PNIPAM showing the hydrogen bonding with water. Below the VPTT, PNIPAM chains are hydrated and the amide groups are hydrogen bonding with water (shaded in green) and above VPTT, the hydrogen bonding is weakened and the hydrophobic character of PNIPAM predominates the conformation (shaded in red).

The modification of the VPTT of PNIPAM by copolymerisation with other monomers is well-established, where hydrophilic or hydrophobic monomers shift the phase transition temperature to higher or lower values, respectively.¹² Particularly, the use of pH-sensitive

monomers for the copolymerisation of NIPAM has been of interest, as a dual stimuli-responsive behaviour is introduced into the system. Some examples of unsaturated monocarboxylic acids used as comonomers of NIPAM are acrylic acid,^{13–21} methacrylic acid,^{13,17,22–24} vinylacetic acid,²⁵ and allylacetic acid.^{26–28} Most of these studies have shown the influence of the concentration of the organic acid and the pH on the swelling/deswelling behaviour of these carboxylic containing PNIPAM materials. Generally, the deprotonation of the carboxylic acid groups leads to interchain electrostatic repulsion and an increase in osmotic pressure due to increased hydrophilicity. Considering the particular case of P(AA-*co*-NIPAM) microgels as an example, Mohsen *et al.*²⁹ have shown the effect of the pH on the conformational changes of these microgels. At a pH below the pK_a of acrylic acid, the microgels are collapsed due to the protonation of the carboxylic groups, and as the pH increases so does the hydrodynamic radius of the microgels, as they rearrange into a swollen configuration.²⁹ Additionally, Morris *et al.*³⁰ compared the pH response between P(AA-*co*-NIPAM) and PNIPAM microgels. Their experimental results showed that PNIPAM microgels do not exhibit changes in their volume according to pH variations in contrast to the carboxylic acid containing PNIPAM microgels.³⁰ Moreover, other publications have shown that the colloidal stability of this type of microgel is highly dependent on concentration, temperature, pH and, ionic strength,^{31,32} where flocculation or aggregation of the microgels can occur with increasing temperature and ionic strength, and at a pH below the pK_a of AA. At this point, it is important to highlight that the synthetic methodologies used for the preparation of P(AA-*co*-NIPAM) microgels can affect their structure and thus their properties. For instance, by using one-step polymerisation the carboxyl groups are distributed within the microgel network, whereas in a two-step polymerisation core-shell nanogels can be produced. In the former case, Farooqi *et al.*³² have shown the temperature sensitivity can be lost at a pH above the pK_a under their synthetic conditions. In the latter case, the temperature phase transition is preserved when the P(NIPAM-*co*-AA) shell is highly charged.¹⁸

As described in Chapter 2, the use of RAFT-mediated dispersion polymerisation is thought to prepare anionic nanogels with a densely crosslinked core and a hairy stabiliser shell. Hence, in agreement with the literature, it is expected that a dual response is exhibited within a range of temperature and pH conditions for the synthesised core crosslinked nanogels, especially under physiological conditions. Additionally, since the stimuli-responsive behaviour of networks of NIPAM and AA depends on a balance between the hydrophilic and hydrophobic content, which is also influenced by pH, it is expected that changes on the PNIPAM-core size and the PAA shell thickness affect the VPTT of nanogels. As previously shown, the cononsolvent composition used in the synthesis affects the properties of the synthesised nanogels. Hence, the VPTT of the

nanogels should have also been altered in agreement with the shift in the cloud points temperatures for the uncrosslinked PAA-*b*-PNIPAM diblock copolymers with increasing ethanol mole fraction used in the synthesis.

This Chapter aims to expand upon the work presented in Chapter 2, specifically on the stimuli-responsive behaviour of the PAA-*b*-P(NIPAM-*st*-BIS) ($A_xN_yB_z$) anionic nanogels. First, an investigation of the effect of the DP of the core-forming block and the shell-stabiliser block on the VPTT was conducted on the nanogels synthesised in water. Next, to test the effect of the synthesis cononsolvent composition on the phase transition, temperature-dependent DLS studies were performed on the nanogels synthesised with the same target monomer composition but different ethanol mole fraction compositions. Then, the effect of pH and ionic strength on the VPTT of aqueous dispersion of nanogels was evaluated by DLS experiments. Finally, an investigation on the ionic response of the nanogels is shown with different temperatures and concentrations of different salts.

3.3. Results and discussion

3.3.1. The temperature dependent deswelling behavior of the anionic nanogels

As shown in Chapter 2, it is suggested that the synthesised nanogels possess a temperature-sensitive and densely crosslinked core with a pH-responsive hairy shell. Figure 3.3 shows a cartoon of the predicted shrinking of the crosslinked core with increasing temperature at neutral pH. Below the VPTT, the core and the shell are predominantly hydrophilic, thus the nanogel is swollen and the shell is highly negatively charged. As the temperature increases above the VPTT, water becomes a poor solvent for the PNIPAM core and it is gradually expelled due to the disruption of hydrogen bonding between the amide groups and water molecules, i.e. the hydrophobic character of PNIPAM predominates. Nonetheless, the negatively charged shell presumably remains in an extended configuration at these conditions due to its relatively high hydrophilicity.

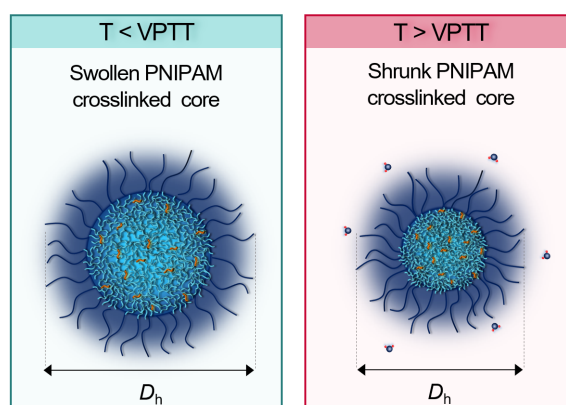


Figure 3.3: Cartoon showing the effect of temperature on the hydrodynamic size of the $A_xN_yB_z$ nanogels below and above the volume phase temperature transition (VPTT).

To assess the size changes of nanogels with temperature and thus their VPTT, DLS was used to determine the hydrodynamic diameter (D_h) of the PAA-*b*-P(NIPAM-*st*-BIS) ($A_xN_yB_z$) nanogels over a temperature range as it will be shown below. The experimental D_h data was fitted with a Boltzmann sigmoidal model using a least squares regression to assist in the determination of the VPTT of all of the aqueous nanogel dispersions. The fit using sigmoidal models have previously been reported to determine the VPTT indicating a good approximation to experimental data.^{33,34} Herein, Equation 3.1 relates the hydrodynamic size (D_h) at a specific temperature (T), where D_t

and D_b are respectively the swollen (“top” temperature at 12.5 °C) and shrunken (“bottom” temperature 60 °C) hydrodynamic diameters, ω is the halfway point between the swollen and shrunken state (i.e. VPTT) and σ is the steepness of the curve (i.e. the sharpness around the phase transition).

$$D_h = D_t + \frac{D_t - D_b}{1 + e^{\left(\frac{\omega - T}{\sigma}\right)}} \quad \text{Equation 3.1}$$

The notation utilised to describe the nanogels monomer composition and the synthesis consolvent composition is in accordance with the notation used in Chapter 2. Thus A, N, B symbolise acrylic acid (AA), *N*-isopropylacrylamide (NIPAM) and *N,N'*-bismethylacrylamide (BIS), respectively. Thus $A_xN_yB_zX_e$ indicates $PAA_x-b-P(NIPAM-st-BIS)_{y,z}$, where x,y and z represents the number-average DP of each monomer component and X_e represents the mole fraction of ethanol used in the synthesis of each nanogel.

As determined by DLS, the nanogels displayed a reversible swelling-deswelling behaviour with minimal hysteresis between heating and cooling. Considering the $A_{52}N_{181}B_3-0$ nanogel as an example, it is noted that this nanogel re-swells during cooling and displayed the same VPTT of ~ 37 °C between heating and cooling (Figure 3.4a). However, the initial swollen size was not fully recovered during cooling probably due to the formation of intramolecular interactions between the amide groups of the NIPAM/BIS core during heating.³⁵

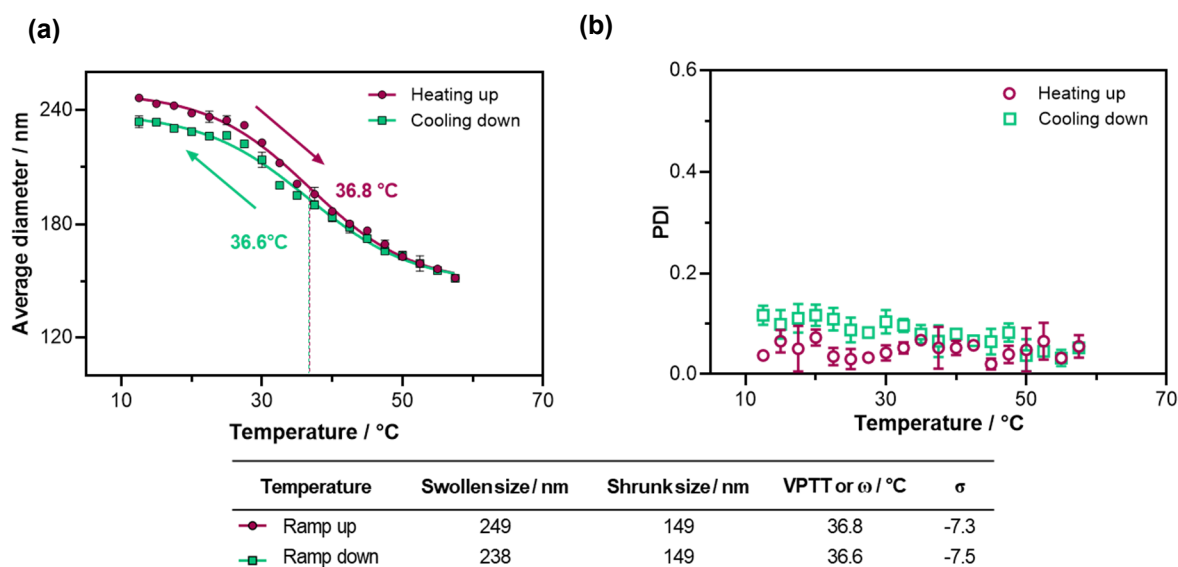


Figure 3.4: DLS analysis on the hysteresis of the $A_{52}N_{181}B_3-0$ nanogel. (a) The hydrodynamic diameter as a function of temperature, and (b) their corresponding PDI values versus temperature ($n=3$). Data obtained from 0.1% w/w nanogel dispersions in DI water at neutral pH. Data fitted using Equation 3.1.

3.3.1.1. The effect of the DP of the core-forming block on the VPTT of nanogels synthesised in water

Prior to investigating the effect of the synthesis consolvent composition on the stimuli-responsive behaviour of the anionic nanogels, the VPTT of nanogels synthesised in water with varying DP of PNIPAM was determined as a reference for those synthesised in consolvents. Figure 3.5a shows the dependence of the VPTT of the nanogels according to the DP of PNIPAM at a fixed mole ratio of crosslinker to PAA₅₂ macro-CTA of 3:1. A gradual decrease in the VPTT from around 41 °C to 34 °C was observed when the DP of PNIPAM was increased from 74 to 252, respectively. As outlined in Chapter 2, this behaviour can be attributed to a higher hydrophobic character with increasing PNIPAM content with respect to PAA. As expected, the phase transition temperature of the nanogels is relatively close to the cloud point temperature (T_{cp}) of the uncrosslinked PAA-*b*-PNIPAM diblock copolymers previously reported in Table 2.5. For example, the A₃₇N₁₀₀-0 diblock copolymer had a T_{cp} of ~43°C as determined by UV-vis spectrophotometry and the analogous nanogel (A₅₂-N₇₄B₃-0) had a VPTT of ~41°C as estimated from DLS experiments. It is also noted in Figure 3.5b that the PDI values remained near monodisperse with a slight tendency to lower values as the nanogel particles shrunk, which indicates that these nanogels are stable and do not agglomerate from 10 to 60 °C and at neutral pH.

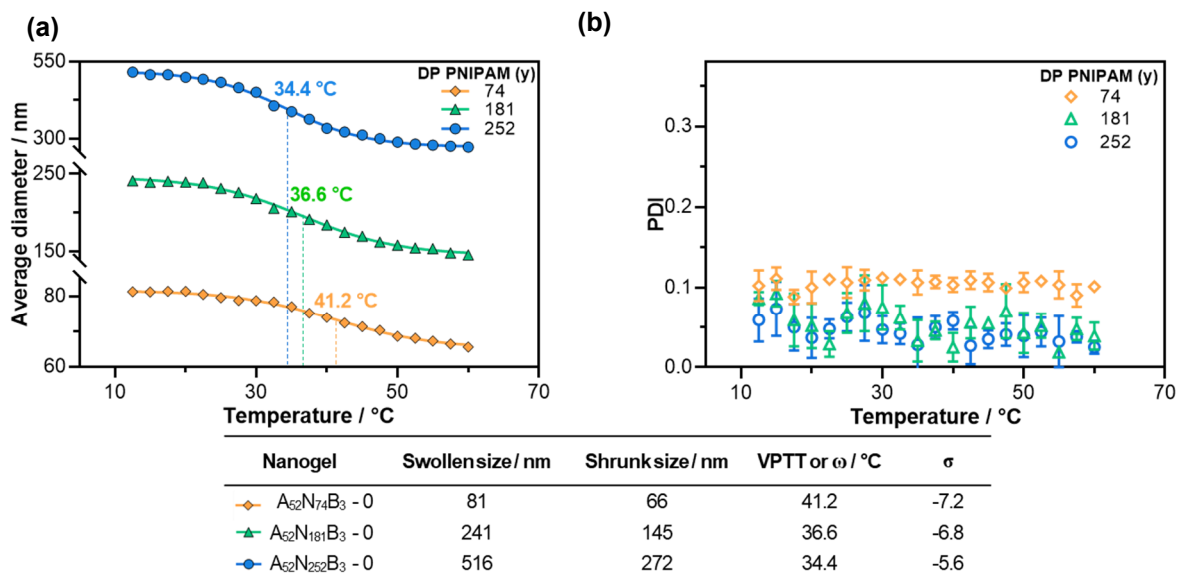


Figure 3.5: DLS analysis of the A₅₂N_yB₃-0 nanogels, where y=74 (◇), 181 (▲) and 252 (●). (a) The hydrodynamic diameter as a function of temperature, (b) their corresponding PDI values versus temperature (n=3). Data obtained from 0.1% w/w nanogel dispersions in DI water at pH 7. Data fitted using Equation 3.1.

Moreover, it was also observed that the larger the PNIPAM DP the sharper the shrinking

transition (i.e. smaller σ values) and the lower the temperature at which shrinking starts. For instance, the $A_{52}N_{252}B_3-0$ nanogel starts shrinking at 21 °C whereas in the $A_{52}N_{74}B_3-0$ nanogel starts at 24 °C. This trend that can be more clearly seen in Figure 3.6a in terms of the deswelling ratio.

The extent of nanogel deswelling with temperature can be expressed in terms of the deswelling ratio (α) and it is estimated from the swollen hydrodynamic diameter (D_t) and the hydrodynamic diameter at a given temperature (D) as follows:³⁶

$$\alpha = \frac{D}{D_t} \quad \text{Equation 3.2}$$

Moreover, to enable comparison between the deswelling behaviour of the nanogels, the hydrodynamic size can be standardised by the normalisation of the D_h at a given temperature (D) from the swollen hydrodynamic diameter at 12.5 °C (D_t) and the shrunk hydrodynamic diameter at 60 °C (D_b) using the following equation:

$$D_{h,\text{norm}} = \frac{D - D_b}{D_t - D_b} \quad \text{Equation 3.3}$$

It is noted from Figure 3.6a that the $A_{52}N_{252}B_3-0$ nanogel reduced in size by more than 50%, whereas the $A_{52}N_{74}B_3-0$ nanogel had a considerably lower extent of size reduction of 20% at 60 °C. This is related to the larger volume fraction of PNIPAM for increasing PNIPAM DPs with respect to PAA and to a lower crosslink density. Figure 3.6b shows the normalisation of the change in the hydrodynamic diameter of the nanogels as a function of temperature. It is evident the effect of PNIPAM DP on the VPTT, where the VPTT was shifted to lower temperatures from 41 °C for $A_{52}N_{74}B_3-0$ to 37 °C for $A_{52}N_{181}B_3-0$ and to 34 °C for $A_{52}N_{252}B_3-0$.

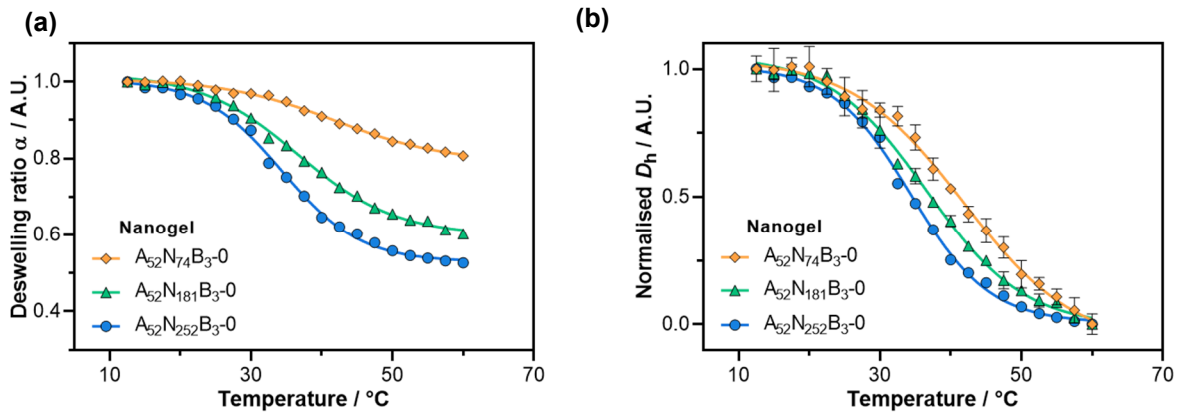


Figure 3.6: Deswelling behaviour of the $A_{52}N_yB_3-0$ nanogels, $y=74$ (\diamond), 181 (\triangle) and 252 (\bullet). (a) Deswelling ratio α and (b) normalised deswelling.

3.3.1.2. The effect of the DP of the shell-stabiliser block on the VPTT of nanogels synthesised in water

As presented in Chapter 2, nanogels synthesised from PAA₈₄ had seemingly greater sizes than those nanogels synthesised from PAA₅₂ when targeting a similar PNIPAM DP, presumably due to a greater shell thickness. Figure 3.7a shows the effect of varying the DP of the PAA on the VPTT of nanogels synthesised in only water with the same target PNIPAM DP of 200. It is noted that the VPTT was apparently shifted from ~ 37 °C for A₅₂N₁₈₁B₃-0 nanogel to 38 °C for A₈₄N₁₆₅B₃-0 nanogel due to possible increase hydrophilicity. Since the A₅₂N₁₈₁B₃-0 nanogel started shrinking at a lower temperature than the A₈₄N₁₆₅B₃-0 nanogel (21 versus 24 °C), it can be hypothesised that the hydrophilicity of the PAA shell also influences the onset of shrinking, this can be better observed in Figure 3.8a. Moreover, as judged by the PDI values both of these nanogels were near monodisperse and were stable over the temperature range tested (Figure 3.7b).

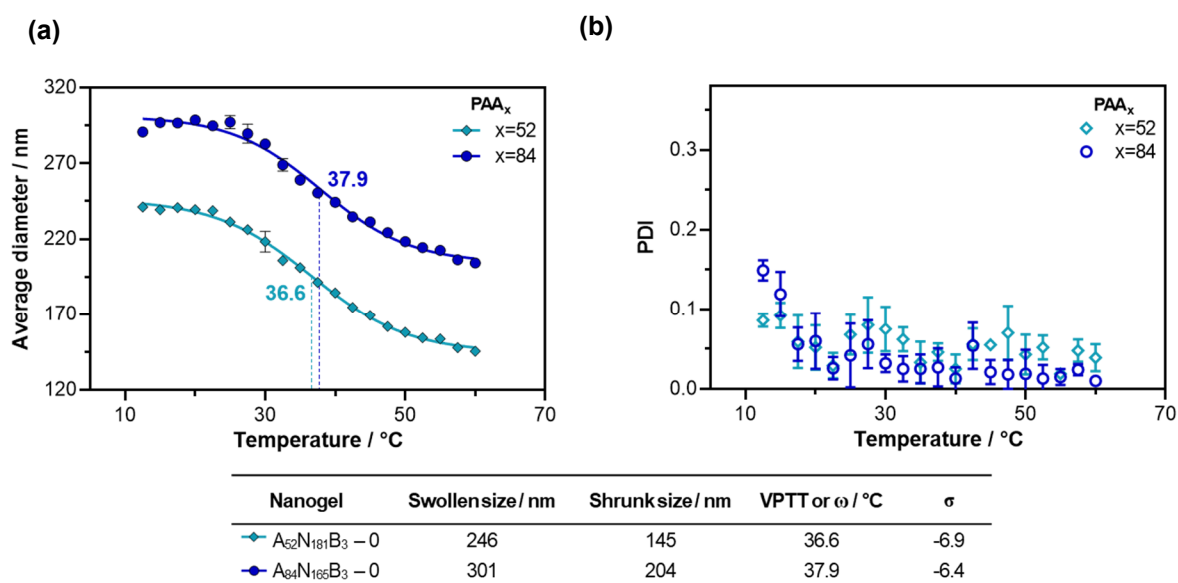


Figure 3.7: DLS analysis of the (◆) A₅₂N₁₈₁B₃-0 and (●) A₈₄N₁₆₅B₃-0 nanogels. (a) The hydrodynamic diameter as a function of temperature, (b) their corresponding PDI values versus temperature (n=3). Data obtained from 0.1% w/w nanogel dispersions in DI water at neutral pH. Data fitted using Equation 3.1.

By comparing the change in diameter of the two nanogels and the slope of phase transition (σ) shown in Figure 3.7 these are apparently similar, suggesting that the number-average DP of the PAA does not affect greatly the temperature behaviour of the nanogels. However, in terms of the deswelling ratio (Figure 3.8a), the A₅₂N₁₈₁B₃-0 nanogel was able to shrink up to 40% in size in comparison to 30% deswelling for the A₈₄N₁₆₅B₃-0 nanogel due to the higher volume fraction of PNIPAM to PAA of the A₅₂N₁₈₁B₃-0 nanogel. It is also noted from Figure 3.8b that by

standardising the diameter changes of the two nanogels the difference in their estimated VPTT is minimal in contrast to results shown in Figure 3.7.

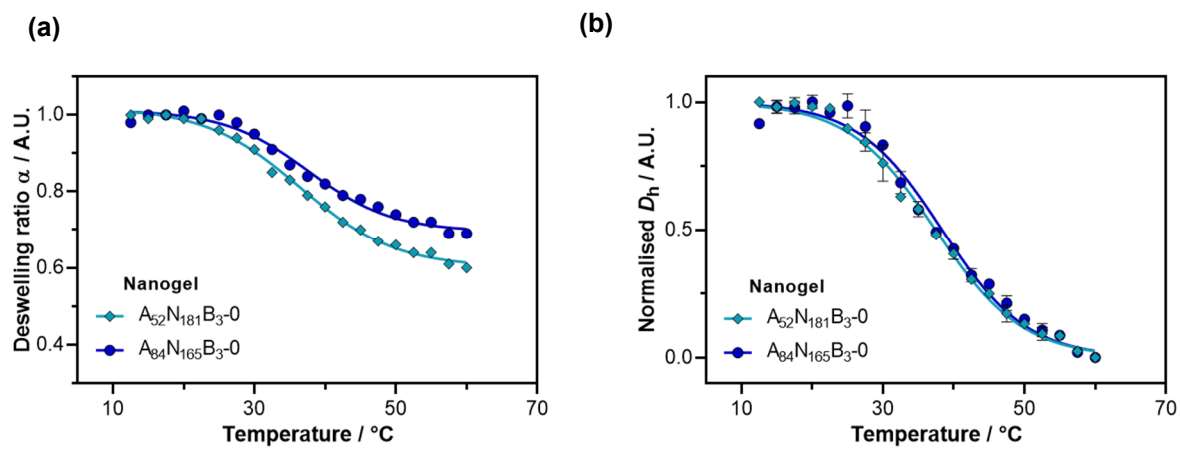


Figure 3.8: Deswelling behaviour of the (\diamond) $A_{52}N_{181}B_3-0$ and (\bullet) $A_{84}N_{165}B_3-0$ nanogels. (a) Deswelling ratio α and (b) normalised deswelling.

3.3.1.3. The effect of the synthesis cononsolvent composition on the VPTT of the nanogels

As outlined in Chapter 2, the use of water-ethanol mixtures as cononsolvent pair for the RAFT-mediated dispersion polymerisation of NIPAM affected the final size of the nanogels when targeting the same monomer composition. Generally, the addition of ethanol as cononsolvent produced nanogels with smaller sizes than those produced only in water. As shown for the PAA-*b*-PNIPAM diblock copolymers, this was attributed to changes in the solubility of the PNIPAM growing chains in cononsolvents which affected the critical DP for the self-assembly, and as suggested by ¹H NMR spectroscopy experiments changed the tacticity, which could result in different chain packing during particle formation. The effect of synthesis cononsolvent composition on the thermoresponsive behavior of nanogel aqueous dispersions was investigated by temperature-dependent DLS experiments. For brevity, only the DLS studies of the A₅₂N₂₀₀B₃-X_e nanogels are shown here. However, DLS studies for A₅₂N₁₀₀B₃-X_e and A₅₂N₃₀₀B₃-X_e nanogels, which showed roughly similar results, can be found in the appendix B (Figure 3B.1-2).

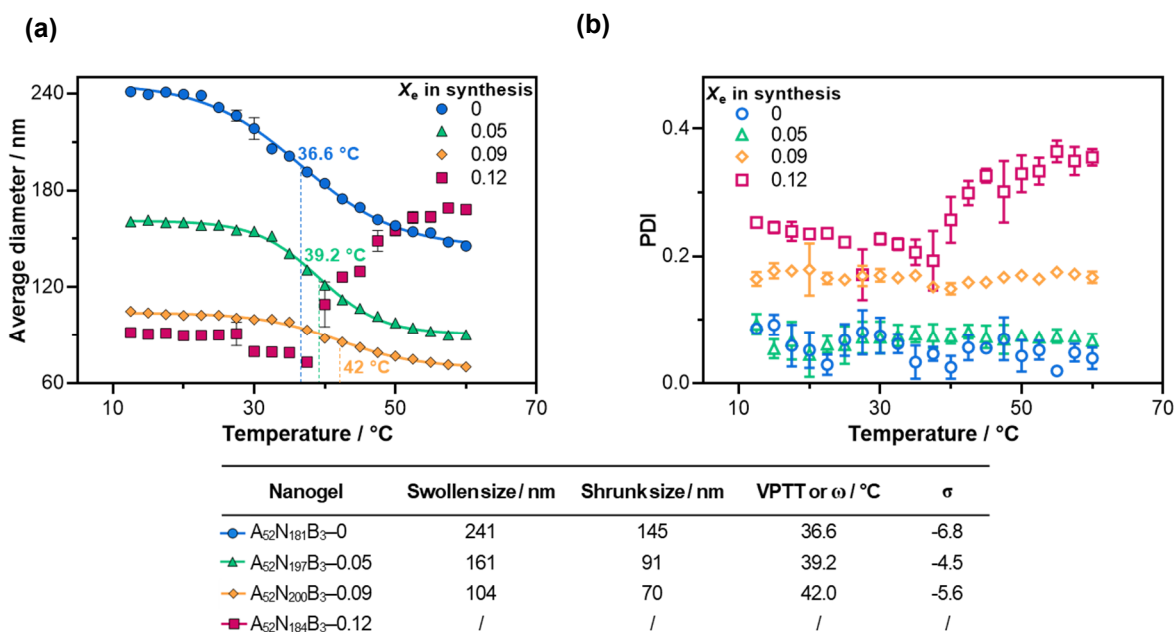


Figure 3.9: DLS analysis of the A₅₂N₂₀₀B₃-X_e nanogels synthesised in cononsolvents.

(a) The hydrodynamic diameter as a function of temperature, (b) their corresponding PDI values versus temperature (n=3). Data obtained from 0.1% w/w nanogel dispersions in DI water at pH 7. Data fitted using Equation 3.1.

It is noted from Figure 3.9 that all the nanogels shrank as the temperature increased, excluding the A₅₂N₁₈₄B₃-0.12 nanogel. An explanation for this discrepancy will be discussed further below. Overall, the results showed that the VPTT was shifted to greater temperatures for nanogels

synthesised with increasing ethanol mole fractions up to $X_e=0.09$. For example, the VPTT increased from 37 °C for $A_{52}N_{181}B_3-0$, to 39 °C for $A_{52}N_{197}B_3-0.05$ and to 42 °C for $A_{52}N_{200}B_3-0.09$. The VPTT shift is more clearly observed in the normalised D_h change with temperature shown in Figure 3.10b. As previously shown, a shift in the T_{cp} to higher temperatures was observed for the diblock copolymers synthesised in increasing ethanol mole fraction composition up to $X_e=0.15$, which agrees with the observation that the VPTT is shifted to higher temperatures for nanogels synthesised in consolvents. The shift in the T_{cp} was previously attributed to the different content of meso diads, where diblock copolymers synthesised in water were more meso-rich (i.e. less hydrophilic) than those synthesised in consolvents, hence this have a lower T_{cp} . An increase in racemic diads generates an alternating chirality where geometrical constraints make the formation of local hydrogen bonding between amide groups difficult and hence water molecules interact more strongly with the polymer, thus explaining the enhanced hydrophilicity and higher T_{cp} .³⁷ Another explanation for the shift of the VPTT of nanogels synthesised in consolvents can be found in the relatively lower concentration of the PNIPAM chains in the nanogel particles due to the prompt chain collapse during the polymerisation caused by consolvency, which ultimately leads to the formation of more nanogel particles in solution (i.e. more particles are nucleated). This difference can subtly affect the hydrophilic-hydrophobic balance between the core and the shell, thus also affecting the VPTT in a probably minor contribution than the change in tacticity of the PNIPAM chains.

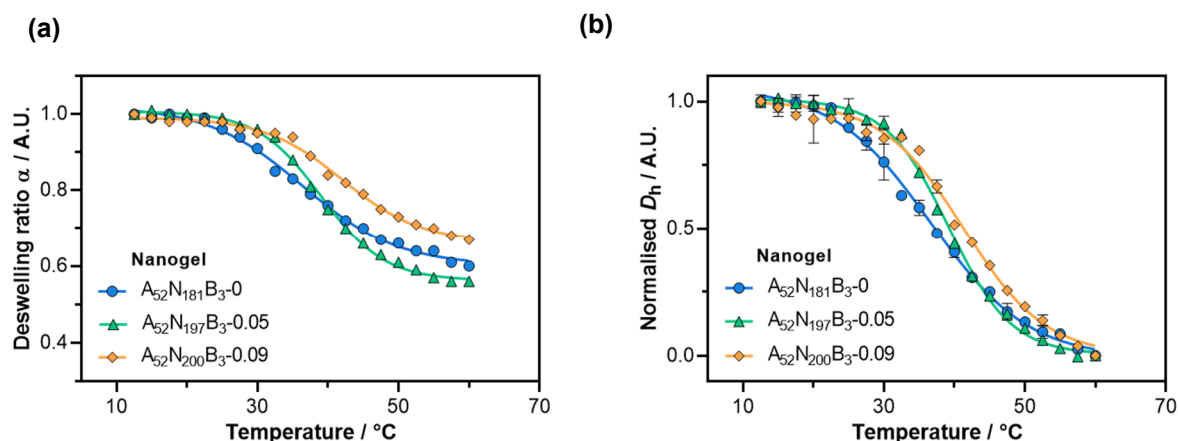


Figure 3.10: Deswelling behaviour of the $A_{52}N_{200}B_3-X_e$ nanogels. (a) Deswelling ratio α and (b) normalised deswelling.

On closer investigation, the deswelling ratio of nanogels also changed according to the synthetic reaction solvent media. It is noted from Figure 3.10a that the $A_{52}N_{181}B_3-0$ nanogel had larger deswelling ratio of 40%, whereas the $A_{52}N_{200}B_3-0.09$ nanogel only decreased in size up to 33% at 60 °C. This can be explained by the relatively higher hydrophilicity of the $A_{52}N_{200}B_3-0.09$

nanogel in which the amide groups formed stronger hydrogen bonds with water molecules than with other neighbouring amide groups due to their higher racemic diad content. In contrast, the $A_{52}N_{181}B_3-0$ nanogel, which is more likely to form hydrogen bonds between the neighbouring amide groups than with water, can release more water molecules upon heating than the $A_{52}N_{200}B_3-0.09$ nanogel. In the case of the $A_{52}N_{197}B_3-0.05$ nanogel, this seems to deswell more than the $A_{52}N_{181}B_3-0$ nanogel (44 % versus 40% at 60 °C). This slight difference can be attributed to the higher content of PNIPAM with respect to PAA and to crosslinker for $A_{52}N_{197}B_3-0.05$ than for $A_{52}N_{181}B_3-0$ nanogel. Besides, as shown in Chapter 2, these two nanogels displayed a change in their internal structure as determined by AF4 experiments (Section 2.3.4), in which the $A_{52}N_{181}B_3-0$ nanogel clearly showed a second population with a more uniform structure ($\rho=0.88$) than the main particle population (core-shell structure $\rho=0.5$ to 0.55) suggesting interparticle crosslinking and/or the presence of PAA chains trapped internally. In contrast, the $A_{52}N_{197}B_3-0.05$ nanogel only showed one main particle population by AF4 (core-shell structure $\rho=0.55$ to 0.61) with an increasing shape factor for bigger nanogel particles of $\rho=0.9$. This change in shape factor could also explain the different deswelling between these two nanogels, in which the interparticle crosslinking and/or PAA trapped internally decreased the deswelling ratio of the $A_{52}N_{181}B_3-0$ nanogel in comparison to $A_{52}N_{197}B_3-0.05$ nanogel. Lastly, it was also noted that the nanogels synthesised in water alone started shrinking at lower temperatures than those synthesised in cononsolvents (Figure 3.10a). For example, the onset of shrinking for the $A_{52}N_{181}B_3-0$ nanogel was 21 °C, whereas the ones synthesised in ethanol mole fractions of 0.05 and 0.09 was at 29 °C and 34 °C, respectively. The same pattern was observed for the $A_{52}N_{259}B_3-0.10$ nanogel (Appendix B, Figure 3B.2) which started shrinking at 28 °C followed by a sharp transition ($\sigma=-3.5$) with a VPTT of 36 °C.

Referring back to the $A_{52}N_{184}B_3-0.12$ nanogel, this nanogel showed a temperature response that deviated from the nanogels synthesised in lower ethanol compositions (Figure 3.9a). The $A_{52}N_{184}B_3-0.12$ nanogel showed a gradual decrease in size with temperature up to 37.5 °C where after this temperature its size apparently increased reaching a plateau at 53 °C as judged by the intensity average size data. This can be an indication of particles agglomerating; however, since the Rayleigh scattering of light depends on the sixth power of the diameter of the particles ($I \propto D^6$) agglomerates might be present in small amounts as these scatter light much more strongly than smaller particles.³⁸ Figure 3.11a shows the MSD intensity size distributions at different temperatures, where at 45 and 60 °C two size distributions were observed in comparison to those size distributions at lower temperatures. To assess the influence of each intensity-weighted

distribution, the intensity data was automatically transformed into a number-weighted size distribution using the Particle Solutions Software, where much smaller average sizes were determined (Figure 3.11b). No peak was observed at around 400 nm, which could suggest that the agglomeration observed is minimal. Hence, the area of the curve (~2.7%) at smaller sizes corresponded to the actual size of the nanogels than the distribution of the possible agglomerates (~97.3%), which strongly skewed the average size intensity data to greater values as observed in Figure 3.9a. Alternatively, the slight increase in size above the VPTT observed on the autocorrelation function and the number-weight size distribution could be attributed to the loss of control over the polymerisation. The higher the ethanol mole fraction the lower the dielectric constant,³⁹ hence the electrostatic repulsion between the charged shells is weakened leading to poor nanogel stabilisation during polymerisation. In this scenario, it can be hypothesised that this nanogel might not truly possess a defined core-shell structure in contrast to the other nanogels, where more of the PAA chains were trapped within the core and/or nanogel particles were crosslinked together due to a higher ethanol mole composition used in the synthesis. As consequence, above the VPTT of PNIPAM A₅₂N₁₈₄B₃-0.12 nanogel would be able to swell due to the hydrophilicity of PAA and the electrostatic repulsion of the carboxylate groups.

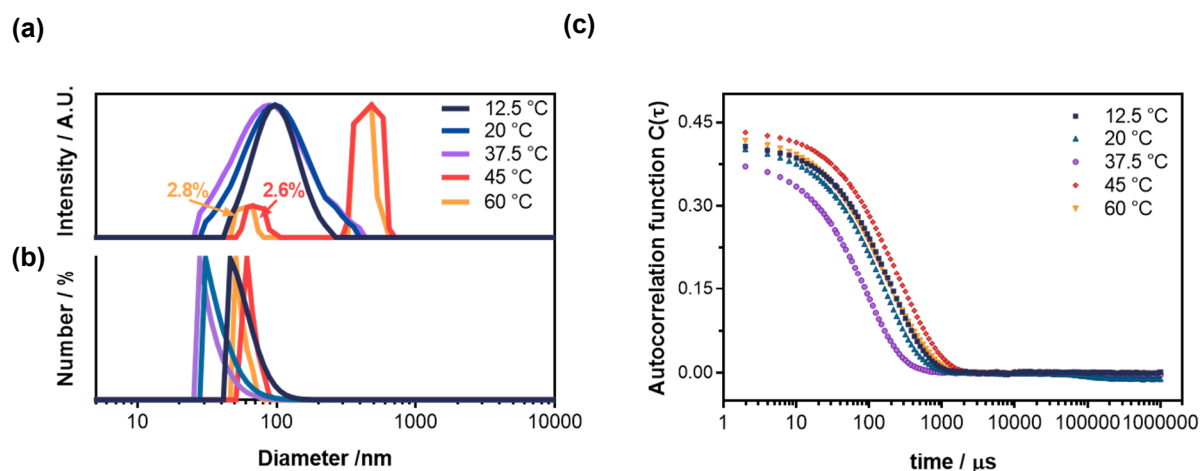


Figure 3.11: DLS analysis of the A₅₂N₁₈₄B₃-0.12 nanogel at different temperatures. (a) MSD intensity-weighted size distributions, (b) number-weighted size distributions, and (c) their corresponding autocorrelation functions.

3.3.1.4. The effect of the crosslink density on the VPTT of nanogels synthesised in cononsolvents

The properties of nanogels are influenced by their degree of crosslinking, hence tailoring of this property is of relevance for biomedical applications.⁴⁰ Considering the $X_c=0.05$ composition for the synthesis of nanogels, the effect of the crosslinking density on the VPTT was investigated by varying the molar ratio of PAA₅₂ to BIS from 1:3 to 1:7 targeting the same PNIPAM DP of 200. Vogel *et al.*⁴¹ have shown that the crosslinking density of PNIPAM microgels affects the shrinking extent, where the swelling ratio of microgels increased with decreasing crosslinker concentration. However, they reported no changes in the VPTT of 32 °C with variations on the crosslinking density. Here, the VPTT of >37 °C was higher due to the increased hydrophilicity given from PAA. Figure 3.12 shows the deswelling with temperature of nanogels with different crosslink densities. As shown in Chapter 2, nanogels synthesised with lower crosslinker concentrations had bigger sizes when swollen than nanogels with higher crosslink densities due to a more loosely crosslinked core. For instance, the swollen size decreased from 161 nm for A₅₂N₁₉₇B₃-0.05 to 145 nm for A₅₂N₁₆₇B₇-0.05 nanogel. However, upon heating, the A₅₂N₁₉₇B₃-0.05 shrank more than nanogels with a higher crosslink density (Figure 3.13a).

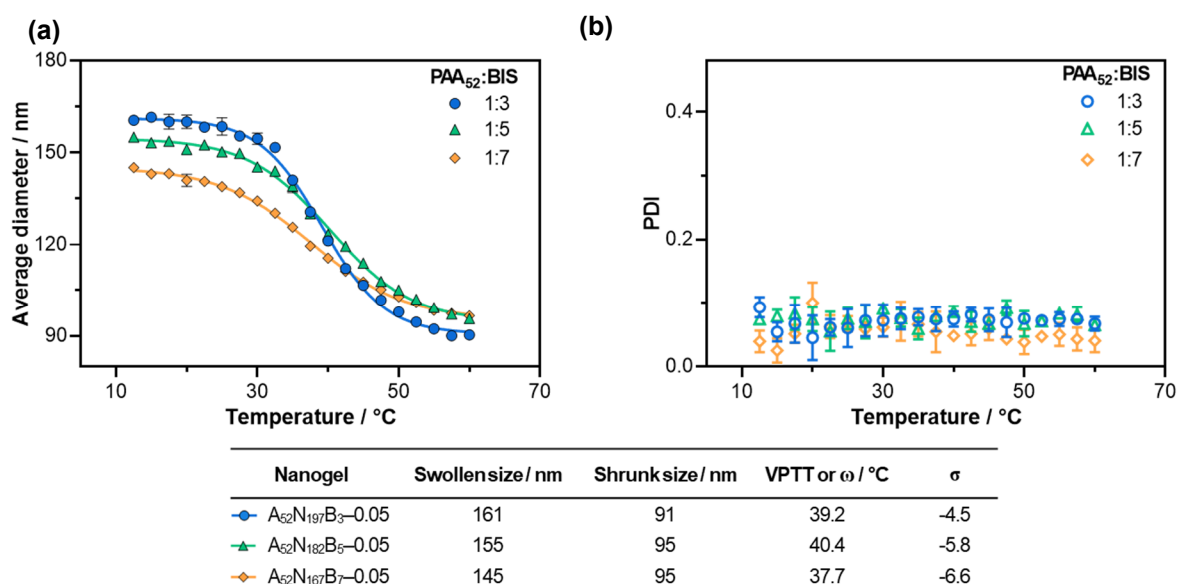


Figure 3.12: DLS analysis of the A₅₂N₂₀₀B_z-0.05 nanogels, where z=3 (●), 5 (▲) and 7 (◆). (a) The hydrodynamic diameter as a function of temperature, (b) their corresponding PDI values versus temperature (n=3). Data obtained from 0.1% w/w nanogel dispersions in DI water at neutral pH. Data fitted using Equation 3.1.

As expected, the deswelling ratio decreased with increasing crosslink density from 44% for A₅₂N₁₉₇B₃-0.05 to 38% for A₅₂N₁₈₂B₅-0.05 to 33% for A₅₂N₁₆₇B₇-0.05. Moreover, it is observed

that the phase transition apparently changed with the crosslink density (Figure 3.13b). However, DLS size measurements could be misleading since the hydrodynamic radius is related to the size of a hypothetical hard sphere,⁴² and nanogels with greater crosslinker concentration looked less uniform in shape as judged by TEM micrographs (see Appendix B, Figure 3B.3). Besides, as shown by AF4 experiments, the $A_{52}N_{182}B_5-0.05$ had a gradual increase in shape factor from $\rho=0.48$ to 0.75 suggesting an apparent more uniform structure for nanogel particles with increasing sizes. Hence, suggesting interparticle crosslinking, which can affect the phase transition by modifying the hydrophilic-hydrophobic contribution between the shell and the core.

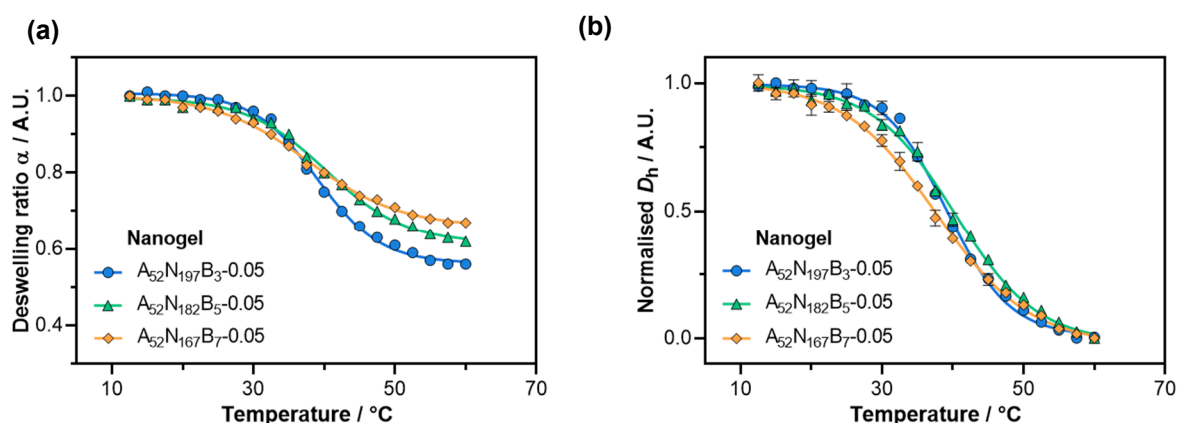


Figure 3.13: Deswelling behaviour of the $A_{52}N_{200}B_z-0.05$ nanogels, where $z=3$ (\bullet), 5 (\blacktriangle) and 7 (\blacklozenge). (a) Deswelling ratio α and (b) normalised deswelling.

3.3.1.5. The effect of the DP of the shell-stabiliser block on the VPTT of nanogels synthesised in consolvents

As discussed earlier, nanogels synthesised in only water from PAA with different DP but with the same target PNIPAM DP had roughly the same VPTT, suggesting a minor contribution from the DP of PAA on the temperature behaviour of the nanogels. However, diblock copolymers synthesised in consolvents differed in the meso diad content. For instance, the meso diads decreased for uncrosslinked copolymers from 47% for $A_{37}N_{199}-0.06$ (Figure 2.18) to 40% for $A_{84}N_{196}-0.04$ (Figure 2A.15). Figure 3.14a and d shows the shift in the VPTT from ~ 39 °C for $A_{52}N_{197}B_3-0.05$ to ~ 42 °C for $A_{84}N_{181}B_3-0.05$ nanogels. This agrees with previous observations, where PNIPAM gels with higher meso content had lower T_{cp} in water.⁴³ Herein, nanogels with a likely higher meso content had a lower VPTT since these tend to be less hydrophilic.

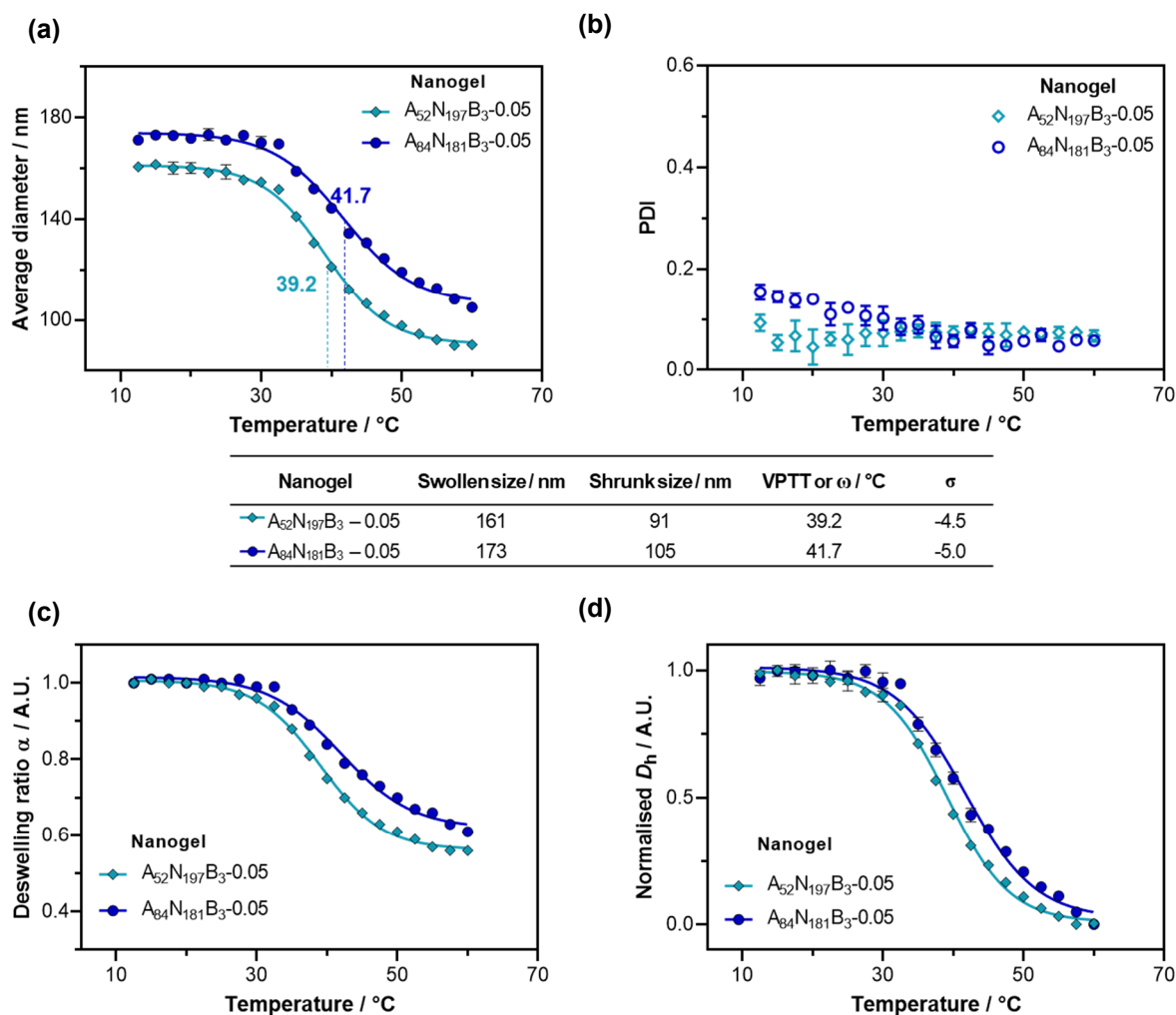


Figure 3.14: DLS analysis of the (\blacklozenge) $A_{52}N_{197}B_3-0.05$ and (\bullet) $A_{84}N_{181}B_3-0.05$ nanogels. (a) The hydrodynamic diameter as a function of temperature, (b) their corresponding PDI values versus temperature ($n=3$), (c) deswelling ratio α and (d) normalised deswelling.

It is also noted from Figure 3.14c that the $A_{52}N_{197}B_3-0.05$ deswells up to 44% in size at 60 °C, whereas the $A_{84}N_{181}B_3-0.05$ only decreased in size 41% at 60 °C. In this case, the difference can be attributed to the interplay of the change in the tacticity of the PNIPAM core and the higher volume fraction of PNIPAM for $A_{52}N_{197}B_3-0.05$ than for $A_{84}N_{181}B_3-0.05$ nanogel.

3.3.2. The pH-responsive behavior of the anionic nanogels

The effect of pH on the VPTT of P(NIPAM-*co*-AA) hydrogels and microgels has been reported extensively.^{16,18,20,21} These studies demonstrated that the swelling/deswelling behavior of these dual responsive materials depends on the balance between the hydrophilic-hydrophobic interactions of NIPAM and the electrostatic interactions of the carboxylate groups of the acrylic acid influenced by pH. Considering that the nanogels presented here have a predominantly PNIPAM crosslinked inner-core that is only sensitive to temperature and not to pH, changes in size below the VPTT of nanogels are attributed mainly to conformational changes in the PAA outer-shell with pH variations. Figure 3.15 shows a cartoon of the predicted contraction of the outer-shell of the nanogels in a swollen state as the pH is decreased to mildly acidic pH values in a salt-free solution. The protonation of the carboxylate groups reduces the electrostatic repulsion between the carboxylate groups, which ultimately decreases the thickness of shell. Nonetheless, the variation of temperature makes this process more complex since adjustment of pH by addition of HCl or NaOH increases the ionic strength of solution and alters the Debye screening, which contributes to the hydrophobic character of PNIPAM upon heating.^{16,44}

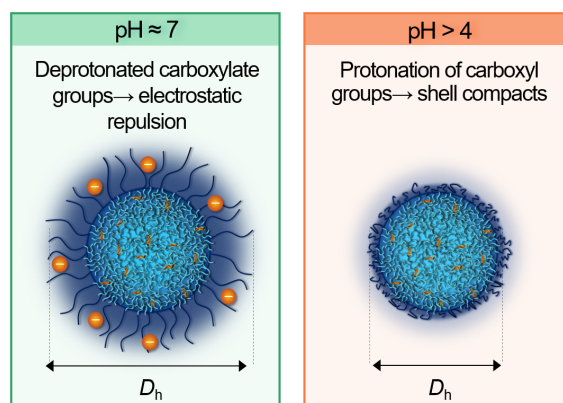


Figure 3.15: Cartoon showing the effect of pH value on the hydrodynamic size of the $A_xN_yB_z$ nanogels at neutral and at mildly acidic pH.

To evaluate if the consolvency affected the pH-responsive behaviour of the nanogels, the $A_{52}N_{181}B_3-0$ and the $A_{52}N_{197}B_3-0.05$ were studied by DLS and electrophoresis experiments. The effect of the pH and temperature on the deswelling behaviour of both nanogels is shown in Figure 3.16, where two major effects were observed. Firstly, that the D_h in the swollen state is reduced with decreasing the solution pH as expected, due to the protonation of the carboxylate groups which reduces the shell thickness (~6% protonation of PAA₅₂ at pH 7 to ~39% at pH 6 to

86% at pH 5). Secondly, upon heating a deswelling transition was observed in all cases up to pH ~ 4 . At pH 4, the shell still had some charge ($\sim 2\%$ deprotonation of PAA₅₂ with pK_a of 5.8) that was sufficient to stabilise the nanogel particles at high temperature. Furthermore, the phase transition was sharper in more acidic pH (i.e. smaller σ values) in both nanogels, due probably to a greater hydrophobic character upon heating.

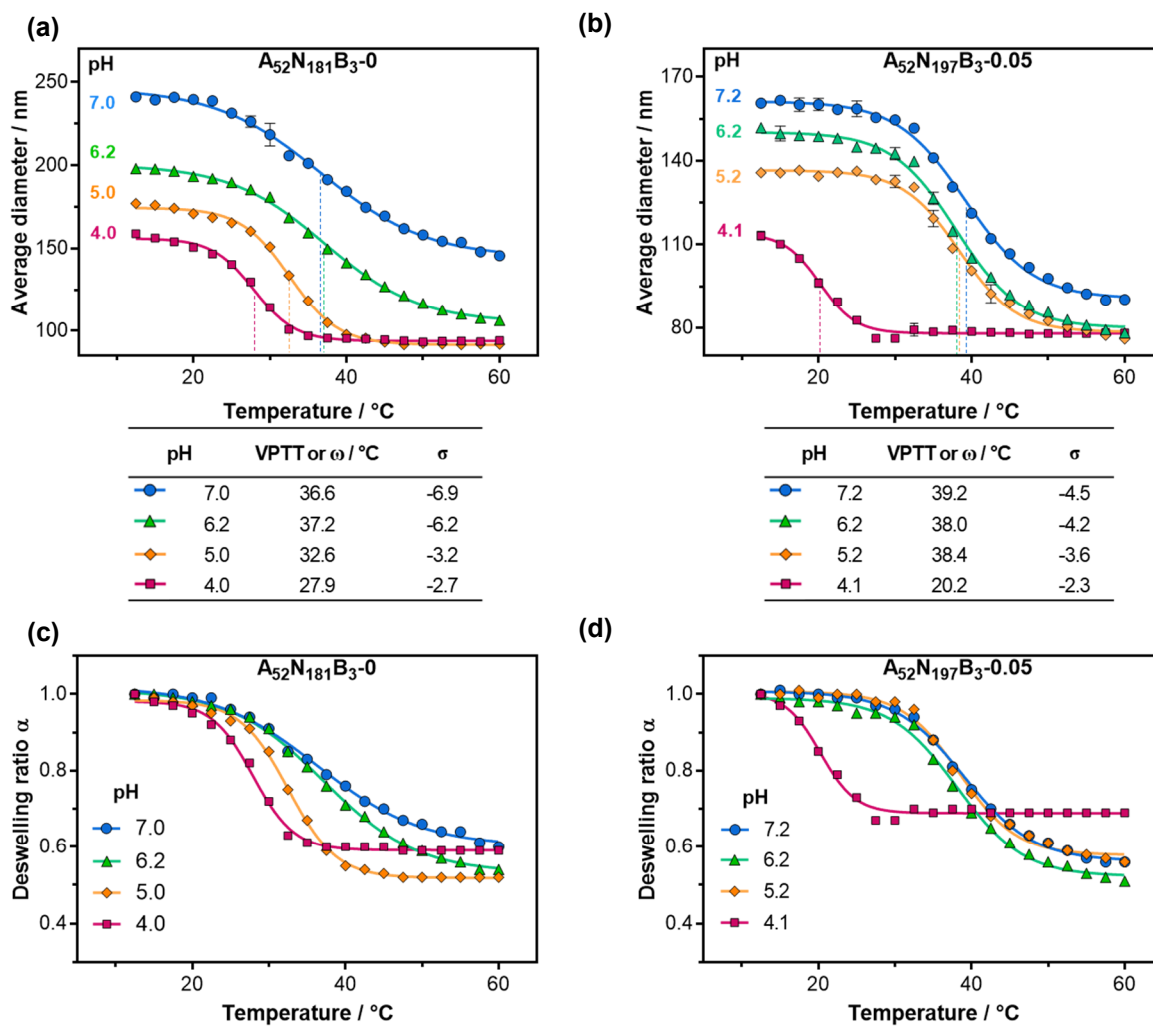


Figure 3.16: Effect of the pH on the deswelling behaviour of the (a) $A_{52}N_{181}B_3-0$ and (b) $A_{52}N_{197}B_3-0.05$ nanogels and the deswelling ratio of (c) $A_{52}N_{181}B_3-0$ and (d) $A_{52}N_{197}B_3-0.05$ nanogels.

Despite these similarities, some differences were observed that can be attributed to the synthesis in cosolvents. Primarily, the nanogel synthesised in $X_c=0.05$ and above pH 5 started shrinking at a considerably high temperature, in all cases around 29 °C regardless of the pH, followed by a sharp deswelling upon heating (Figure 3.16). In the case of the nanogel synthesised in only water, the onset of shrinking was shifted to lower temperatures as the pH was gradually decreased from 7 to 4, and a more gradual deswelling was observed with increasing temperature. This could be related to the PNIPAM core that is more syndiotactic and hence more hydrophilic

for $A_{52}N_{197}B_3-0.05$ than for $A_{52}N_{181}B_3-0$ which is more prone to release water molecules upon heating due to its tacticity. However, in terms of the deswelling ratio, the adjustment of the pH seems to have a greater effect on the increasing deswelling ratio with decreasing pH for the nanogel $A_{52}N_{181}B_3-0$ nanogel. An increase in the deswelling ratio is expected due to the lowered osmotic pressure of the shell with decreasing pH. However, at pH 4 both nanogels showed a reduction in the swelling ratio probably due to the build-up of the solution ionic strength with increasing addition of HCl. The supposition of the increased ionic strength by the adjustment of the pH with HCl and NaOH can be proved by comparing the VPTT of the nanogels, which was $28\text{ }^\circ\text{C}$ for $A_{52}N_{181}B_3-0$ and $20\text{ }^\circ\text{C}$ for $A_{52}N_{197}B_3-0.05$, with the reported VPTT of around $32\text{ }^\circ\text{C}$ for neutral PNIPAM microgels.^{44,45} It is well-established that a reduction of the critical solution temperature for linear PNIPAM is observed in the presence of ions in solution.^{47,48}

Considering the nanogels synthesised from the PAA_{84} macro-CTA in either $X_c=0$ or $X_c=0.05$, consistent deswelling trends were observed with pH variations (Figure 3.17).

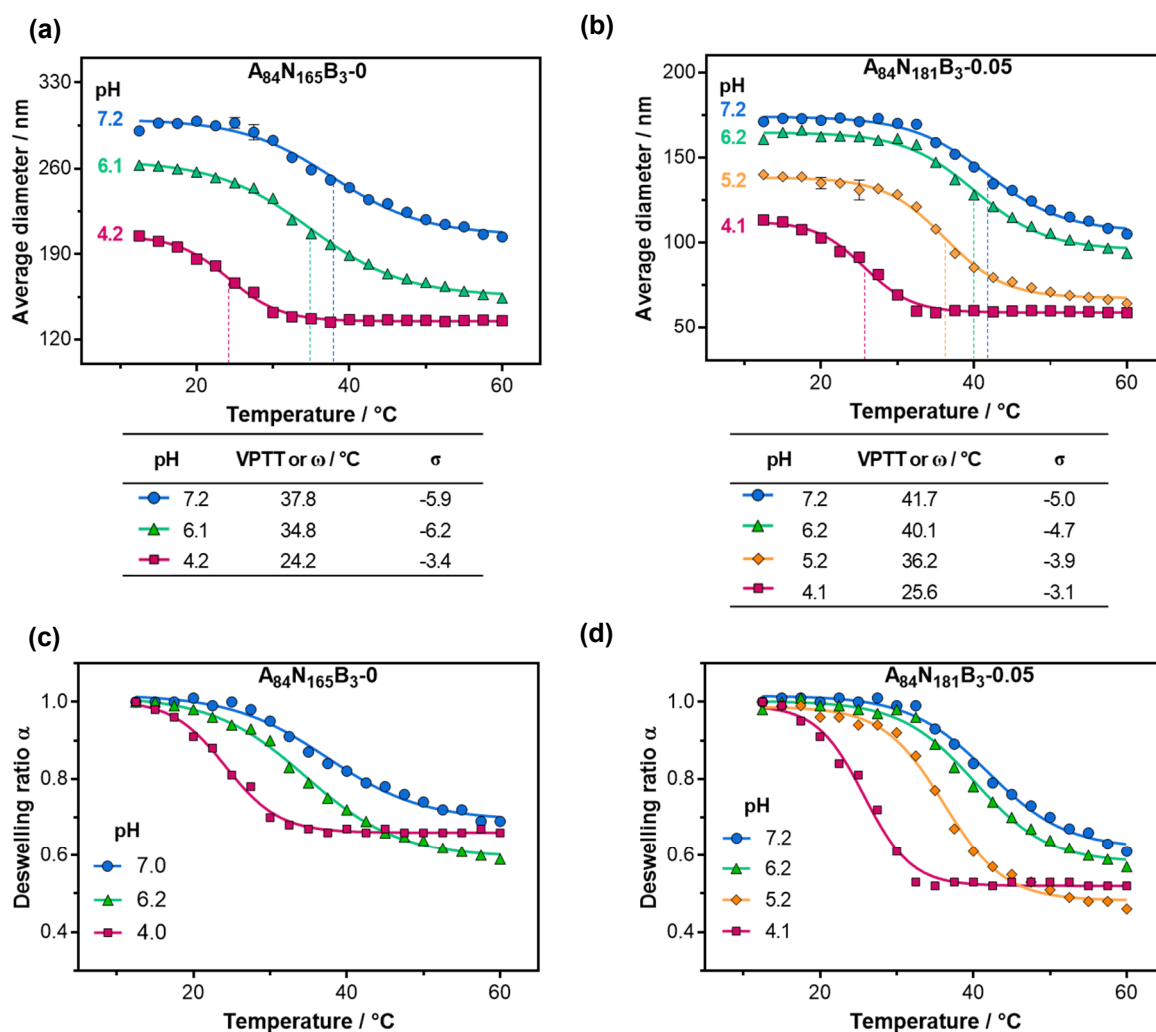


Figure 3.17: Effect of the pH on the deswelling behaviour of the (a) $A_{84}N_{165}B_3-0$ and (b) $A_{84}N_{181}B_3-0.05$ nanogels and the deswelling ratio of (c) $A_{84}N_{165}B_3-0$ and (d) $A_{84}N_{181}B_3-0.05$ nanogels.

The pH-dependent electrophoretic mobility of the nanogels at 25 °C using 1 mM KCl as a background electrolyte was reported as the ζ -potential using the Smoluchowski approximation, where the double layer is assumed to be very thin compare to the particle size.⁴⁹ Although, it is known that ζ -potential measurements do not provide accurate surface charge density values (accuracy of ± 2 mV), they are able to provide qualitative information about ζ -potential changes with pH.⁵⁰ Hence, a comparison of the influence of pH on the ζ -potential of A₅₂N₁₈₁B₃-0 and A₅₂N₁₉₇B₃-0.05 nanogels is shown in Figure 3.18a and b, respectively. It can be observed that the pH strongly affects the measured charge of the nanogel particles. In both cases, ζ -potentials were negative across the pH range tested and no charge conversion from negative to positive was observed at acidic pH. Below the pK_a of the PAA₅₂ macro-CTA (pK_a~5.8), ζ -potentials became less negative at more acidic pH, reaching a constant value of around -2 mV (A₅₂N₁₈₁B₃-0) and -6 mV (A₅₂N₁₉₇B₃-0.05) below pH 3.5. The negative charge at low pH can be also attributed to the ionisable carboxylic acid end-group of the HEMP RAFT agent, which can affect the net charge of the particles.^{51,52} Above the pK_a of the PAA₅₂ macro-CTA, ζ -potentials increased accordingly to the solution pH due to the dissociation of the carboxylic acid groups of PAA. From the range of pH 8 to 10, ζ -potentials reached a constant value of approximately -35 mV for A₅₂N₁₈₁B₃-0 and -30 mV for A₅₂N₁₉₇B₃-0.05. Even though, the difference between the apparent surface charge of these nanogels was relatively small, a possible explanation to this variation could be accounted for the slightly dissimilar morphology of these nanogels. As shown in AF4 experiments (Chapter 2, Section 2.3.4), the A₅₂N₁₈₁B₃-0 nanogel presented a small population of bigger nanogel particles suggesting interparticle crosslinking and/or the presence of PAA chains trapped internally. Hence, affecting the shell thickness and as a consequence the apparent charge density. Besides, the curvature of A₅₂N₁₈₁B₃-0 nanogel is likely to be more deviated from that of a sphere which is supposed when using the Smoluchowski approximation.

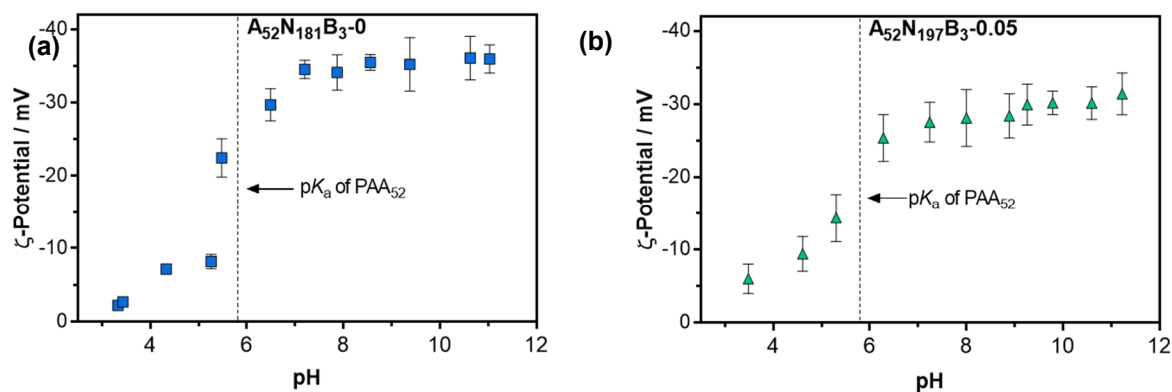


Figure 3.18: Effect of the pH on the ζ -potential of (a) A₅₂N₁₈₁B₃-0 and (b) A₅₂N₁₉₇B₃-0.05 nanogels. Data obtained from 0.1% w/w nanogel dispersions in DI water with 1 mM KCl as a background electrolyte at 25 °C. pK_a of PAA₅₂ as determined in Appendix A, Figure 2A.12.

The influence of pH on the ζ -potential of a nanogel with a greater crosslink density ($A_{52}N_{182}B_5-0.05$) than the $A_{52}N_{197}B_3-0.05$ nanogel but similar PNIPAM DP is shown in Figure 3.19a. The $A_{52}N_{182}B_5-0.05$ nanogel was chosen as it was evident by AF4 and TEM results that some nanogel particles were intercrosslinked during synthesis (See Chapter 2, Figure 2.15 and 2.16). From the range of pH 8 to 10, ζ -potentials reached a constant value of approximately -34 mV which is larger than the ζ -potential of -30 mV reached for $A_{52}N_{197}B_3-0.05$ as shown above in Figure 3.18b. However, a nanogel with the same crosslink density but higher volume fraction of PNIPAM ($A_{52}N_{292}B_5-0.05$) seems to have a greater effect on the measured ζ -potential as it reached a lower ζ -potential of -29 mV in the basic pH range.

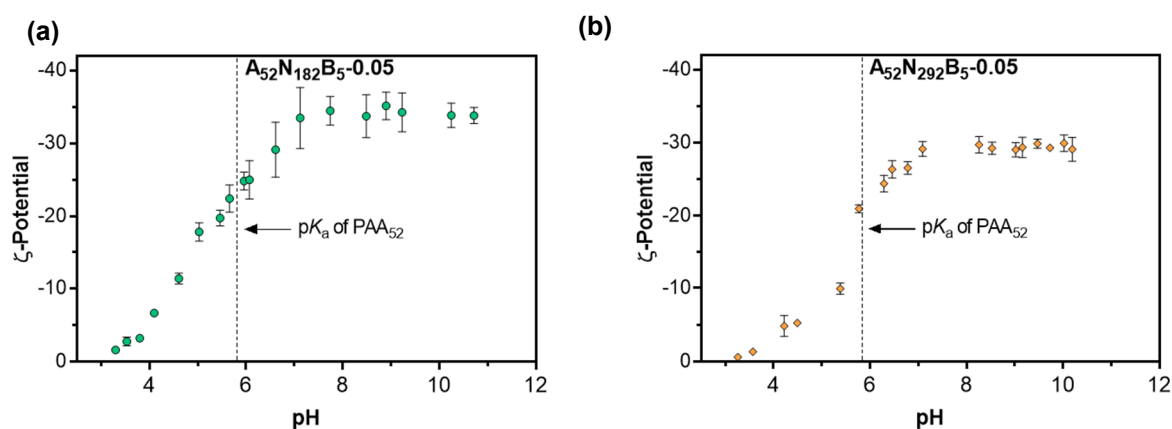


Figure 3.19: Effect of the pH on the ζ -potential of (a) $A_{52}N_{182}B_5-0.05$ and (b) $A_{52}N_{292}B_5-0.05$ nanogels. Data obtained from 0.1% w/w nanogel dispersions in DI water with 1 mM KCl as a background electrolyte at 25 °C. pK_a of PAA₅₂ as determined in Appendix A, Figure 2A.12.

Larger ζ -potentials were obtained for nanogels synthesised using the PAA₈₄ as macro-CTA, due likely to the higher charge density of a thicker shell (Figure 3.20). The $A_{84}N_{181}B_3-0.05$ had a ζ -potential of -35 mV in the basic pH region whereas the analogous nanogel synthesised from PAA₅₂ ($A_{52}N_{197}B_3-0.05$) reached a plateau of -30 mV.

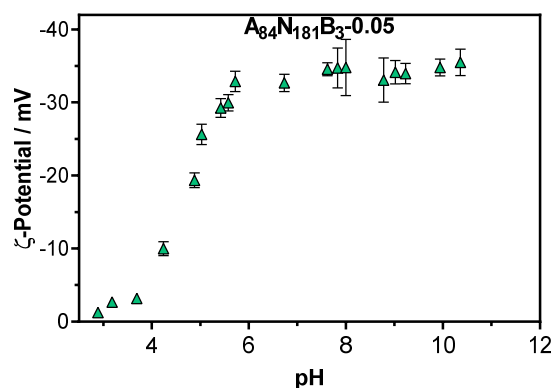


Figure 3.20: Effect of the pH on the ζ -potential of the $A_{84}N_{181}B_3-0.05$ nanogel. Data obtained from 0.1% w/w nanogel dispersion in DI water with 1 mM KCl as a background electrolyte at 25 °C.

3.3.3. The response of nanogels to metal-ions

Due to the presence of charges in the shell of the nanogels at dispersion pH of 7, these are sensitive to changes in the ionic strength, where the addition of a salt would reduce the thickness of the shell as a result of charge screening. It is reported that the deswelling behaviour of acrylic acid-containing PNIPAM microgels is also affected by the ionic strength.¹⁶ Overall, the Debye length is reduced as the ionic strength is increased, thus diminishing the electrostatic repulsion between the carboxylate groups. In this work, the sensitivity of the nanogels to metal-ions of different valency, Na^+ and Ca^{2+} , was assessed by DLS. Figure 3.21 shows the deswelling effect when adding NaCl and CaCl_2 at the same solution ionic strength ($\mu=45$ mM) on two nanogels with a similar monomer composition but synthesised in either $X_e=0$ or $X_e=0.05$. The pH of the nanogel dispersion was around 7 before any salt addition.

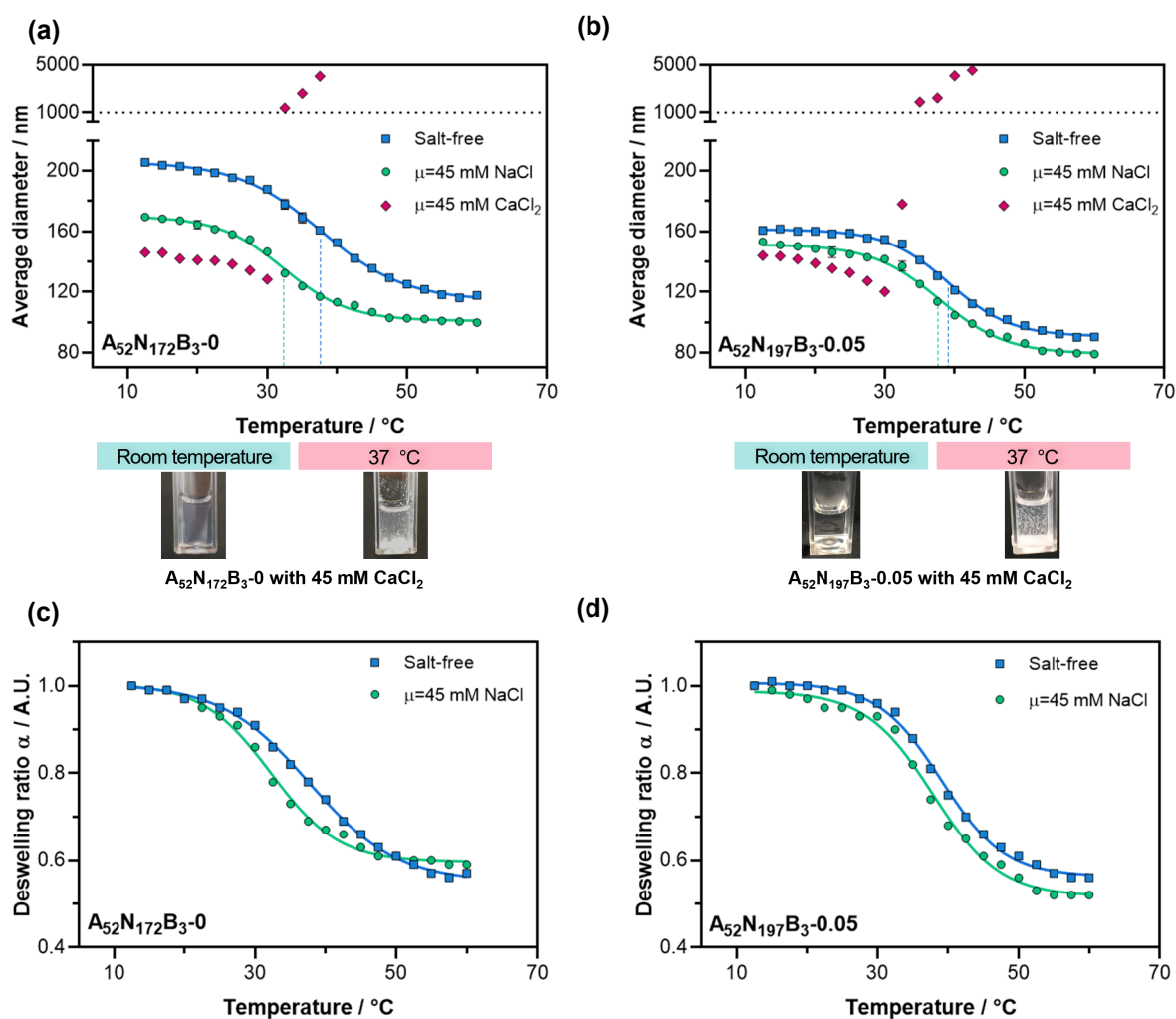


Figure 3.21: DLS studies on the addition of NaCl and CaCl_2 to (a) $\text{A}_{52}\text{N}_{181}\text{B}_3-0$ and (b) $\text{A}_{52}\text{N}_{197}\text{B}_3-0.05$ nanogels and their corresponding deswelling ratio (c) $\text{A}_{52}\text{N}_{172}\text{B}_3-0$ and (d) $\text{A}_{52}\text{N}_{197}\text{B}_3-0.05$. Data obtained from 0.1% w/w nanogels dispersions in DI water at pH around 7.

In both cases, it was observed that in the swollen state ($T < VPTT$) the addition of a salt decreased the D_h , due to a reduction in the electrostatic repulsion and increase in the diffusion coefficient (Figure 3.21a and b). Notably, in a Ca^{2+} containing solution the D_h decreased more than in the presence of Na^+ . These cannot be related to the size of the ions, since their ionic radii are similar ($Na^+ = 102$ pm and $Ca^{2+} = 100$ pm).⁵³ For that reason, the decrease of the D_h is merely due to the divalent character of Ca^{2+} . Contrary to monovalent cations such as Na^+ , studies have shown that divalent cations coordinate to polyacrylates in an entropy-driven process.^{54,55} Buló *et al.*⁵⁶ have shown that for short polyacrylates, in dilute solutions, the polymer chains coil and many Ca^{2+} locally cluster sharing carboxylate groups. Their modelling also suggested that the binding of Na^+ to a single carboxylate group involves an indirect coordination with a water molecule, whereas Ca^{2+} directly coordinates to the carboxylate favouring dehydration. The difference in the ionic binding between monovalent and divalent cations to the carboxylate groups explains the difference in decreased size observed by DLS. In the presence of $CaCl_2$, aggregation was observed when temperature was increased. This aggregation started at around 32.5 °C in both nanogels and the macroscopic nanogel aggregation at 37 °C can be observed in the insert images for each of the two nanogels. In the case of the $NaCl$ -containing solutions, these do not aggregate upon heating. However, the deswelling ratio was apparently affected (Figure 3.21c and d). While the deswelling ratio of the $A_{52}N_{197}B_3-0.05$ nanogel increased 4% in the presence of $NaCl$, the deswelling ratio of the $A_{52}N_{171}B_3-0$ nanogel decreased 2% at 60 °C. This agrees with previous results in which the $A_{52}N_{181}B_3-0$ synthesised in only water had probably some PAA trapped internally due to interparticle crosslinking.

3.3.3.1. Ion-induced macroscopic gelation

Given that the nanogels were able to form macroscopic aggregates upon Ca^{2+} coordination with the carboxylate groups from the outer shell of the nanogels, the nanogel aggregation at $37\text{ }^{\circ}\text{C}$ was assessed under a range of CaCl_2 salt concentrations. Figure 3.22a shows the effect of injecting a nanogel dispersion (9.7% w/w) into a Dulbecco's phosphate-buffered saline solution (DPBS) ($\mu\sim 0.15\text{ M}$, pH 7.4) at $37\text{ }^{\circ}\text{C}$ to give a 1% w/w nanogel dispersion in the absence and presence of CaCl_2 . No aggregation was observed in the absence of CaCl_2 . However, the presence of Ca^{2+} ions led to the macroscopic aggregation of nanogel particles at $37\text{ }^{\circ}\text{C}$, as previously observed by DLS experiments, to form dense macroscopic gels. Upon cooling, the macroscopic gels rehydrated becoming more transparent and less dense. Surprisingly, these did not fully re-dissolve, with aggregates still observed after 12 days (Figure 3.22b). At very low CaCl_2 concentrations, more syneresis was observed than at larger CaCl_2 concentrations. This behaviour suggests that the increase in the ionic strength, specifically of counterions, might be preventing the ionic inter-crosslinking of adjacent particles in solution.

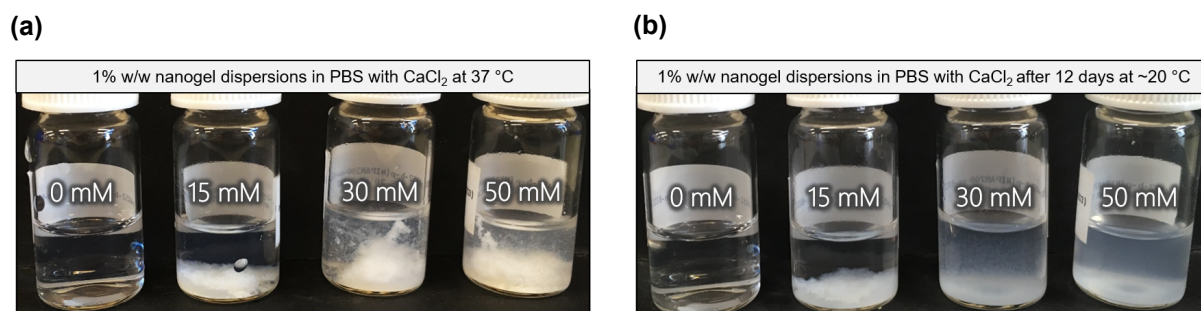


Figure 3.22: Images showing the macroscopic gelation of $\text{A}_{52}\text{N}_{181}\text{B}_3\text{-0.11}$ nanogel (1% w/w) injected into PBS (pH 7.4) with CaCl_2 . (a) Mixtures kept at $37\text{ }^{\circ}\text{C}$. (b) Mixtures after 12 days kept at room temperature ($\sim 20\text{ }^{\circ}\text{C}$). Photographs shown in (a) were taken after addition of the nanogel dispersion into PBS *via* syringe.

To assess the effect of only CaCl_2 on the macroscopic gelation, the salt was added into nanogel dispersions in DI water (9.7% w/w and neutral pH) followed by incubation at $37\text{ }^{\circ}\text{C}$. Figure 3.23a shows the transparent dispersions at room temperature with different CaCl_2 concentrations. At $37\text{ }^{\circ}\text{C}$, a white dense gel appeared in the Ca^{2+} -containing dispersions (Figure 3.23b). Contrary to above, at a higher Ca^{2+} concentration apparently more syneresis was observed, which suggests a greater ionic crosslinking between neighbouring nanogel particles. Moreover, upon cooling the macroscopic gels gradually rehydrated after 2 minutes at ambient temperature (Figure 3.23c) and finally re-disperse as nanogel dispersions became transparent after 7 minutes at ambient

temperature (Figure 3.23d). This suggests that nanogel particles re-disperse possibly due to the low ionic strength and chains rehydration.

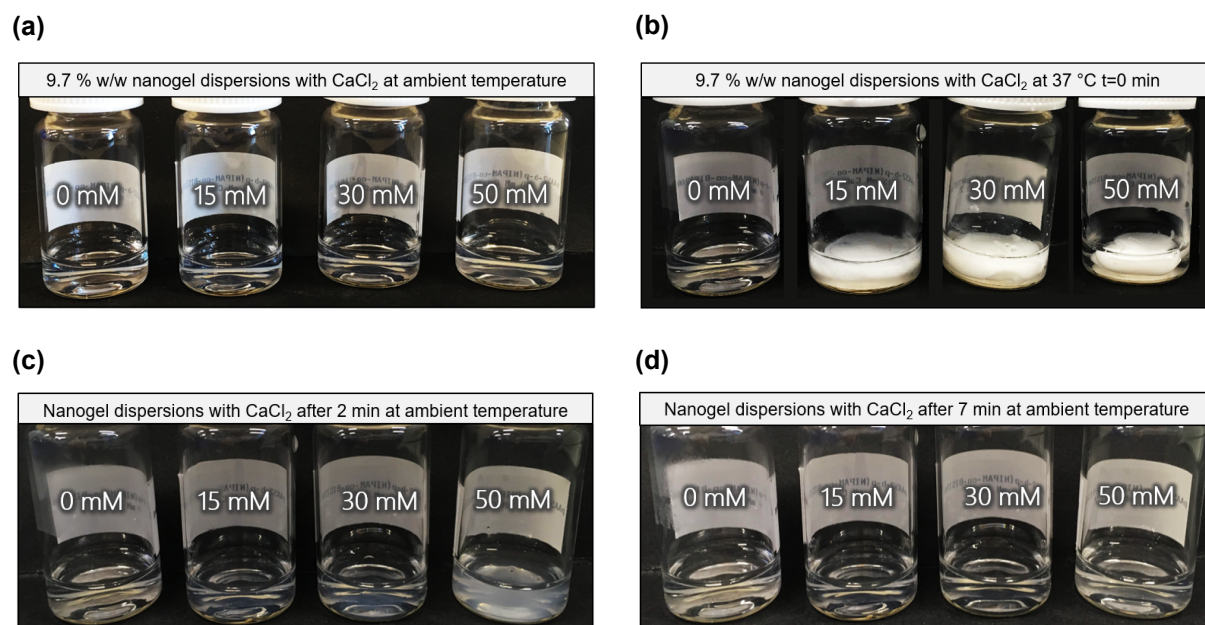


Figure 3.23: Images showing the macroscopic gelation of $A_{52}N_{181}B_3-0.11$ nanogel (9.7% w/w, \sim pH 7) with varying $CaCl_2$ concentrations. (a) Nanogel dispersions at 20 °C before incubation. (b) Nanogel dispersions kept at 37 °C for 5 min (c) Nanogel dispersions after 2 min in ambient temperature (d) Nanogel dispersions after 7 min in ambient temperature.

Interestingly, the presence of Ca^{2+} at low concentrations did not induce macroscopic gelation of nanogel particles in solution at pH 7 and below the critical phase transition temperature, instead this process requires that water molecules to be expelled from the core of the particles to induced colloidal instability. Figure 3.24 shows a cartoon depicting the effect of adding $CaCl_2$ into a salt-free nanogel dispersion, where the salt dissociates and the Ca^{2+} ions coordinate predominantly with the neighbouring carboxylate groups from the PAA chains in the nanogel surface. This complex coordination is believed to be accompanied by the liberation of water from the hydration shell.⁵⁶ Upon heating, the PNIPAM core shrinks and water bound to the PNIPAM chains is also expelled, thus increasing hydrophobicity and van der Waals interaction, which also promotes a higher ionic interaction between neighbouring nanogel particles.

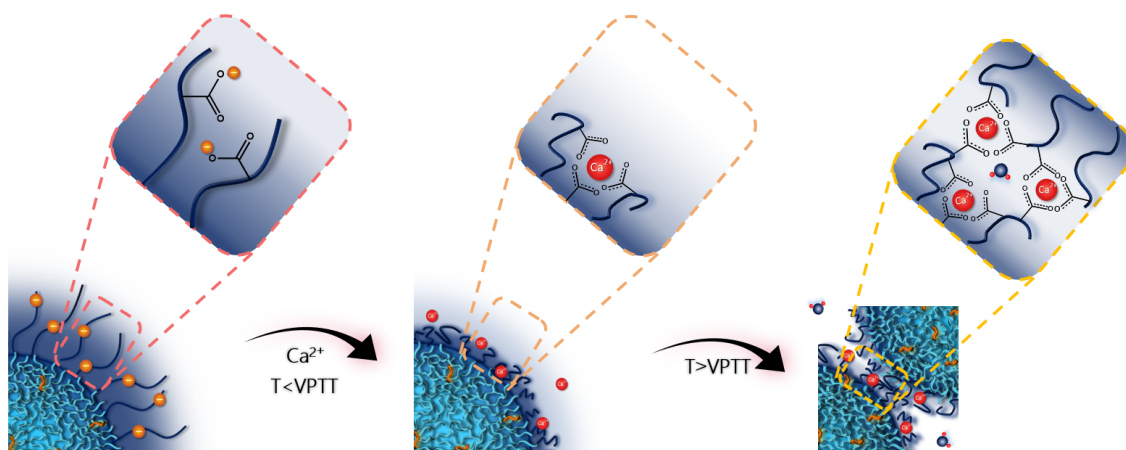


Figure 3.24: Cartoon showing the coordination of Ca^{2+} with carboxylate groups at high pH from the shell of the nanogels.

3.3.3.2. Rheological analysis of the calcium-nanogel aggregates

To monitor the *in situ* formation of Ca^{2+} -nanogel aggregates at pH 7, the temperature-dependent mechanical properties were assessed by oscillatory rheology using temperature sweep experiments from 15 to 60 °C at a heating ramp of 1 °C min⁻¹. A nanogel synthesised in a scale-up reaction was used for the rheological analysis ($A_{52}N_{195}B_3-0.04$ with a D_h of 138 nm and PDI of 0.08). First, the effect of the nanogel concentration on the storage (G') and loss (G'') moduli at a fixed CaCl_2 concentration of 50 mM ($\mu=0.15$ M) was investigated under 1% strain and a constant frequency of 1 Hz (Figure 3.25). Colloidal gelation is normally associated with a change from the viscous behaviour ($G'' > G'$) to the elastic behaviour ($G' > G''$) with a considerable rise in the magnitude of G' .⁵⁸ At low temperatures, both the 5.0% and 9.8% w/w dispersions behaved as viscous liquids ($G'' > G'$) and around the VPTT, both moduli increased abruptly. This rheological change agrees with previous observations of PNIPAM-derived micro- and nanogels.^{59,60} The macroscopic gelation temperature (T_{gel}) was determined as the crossover point of the storage (G') and loss (G'') moduli and found to be 33 °C and 35 °C for the 9.8% and 5.0% w/w dispersions respectively. Above the VPTT, $G' > G''$ which suggested the formation of a 3D network, where Ca^{2+} ionically crosslinks neighbouring shrunken nanogel particles. The more concentrated sample formed a stiffer gel at T_{gel} since it had a greater G' (3.4 Pa vs 0.3 Pa). However, at even higher temperatures a decrease in both moduli was observed, suggesting the formation of a dense aggregate, that is more noticeable at a 9.8% w/w nanogel concentration. In the absence of salt, the 9.8% w/w nanogel dispersion behaved as a viscous liquid ($G'' > G'$) and G' and G'' remained unchanged over the temperature range, which again shows the high colloidal stability of these nanogels due to electrostatic repulsion given by the carboxylate groups at pH 7.

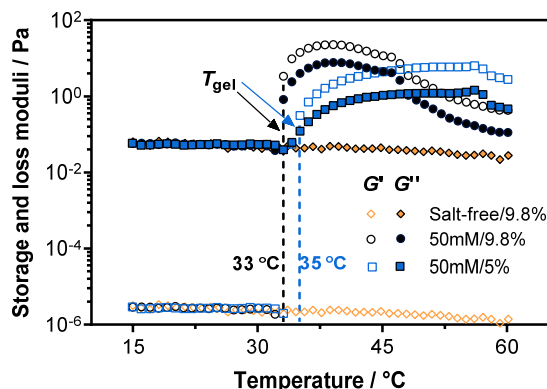


Figure 3.25: Temperature-dependence of G' and G'' for nanogel dispersions with and without CaCl_2 at different nanogel concentrations. Salt-free nanogel dispersion at nanogel concentration of (\diamond) 9.8% w/w and 50 mM CaCl_2 nanogel dispersions at a nanogel concentration of (\bullet) 9.8% and (\blacksquare) 5% w/w. Empty symbols correspond to G' and filled symbols to G'' . Measurements were performed on $\text{A}_{52}\text{N}_{195}\text{B}_3\text{-0.04}$ nanogels at a constant strain of 1% and a frequency of 1 Hz.

Considering that the addition of CaCl_2 salt is essential for the aggregation of the nanogels, the concentration of CaCl_2 added to the dispersions was studied further. Figure 3.26 shows the effect of salt concentration on the G' and G'' at a fixed 5% w/w nanogel concentration. In all cases, it was observed that below the T_{gel} the dispersions behaved as a liquid ($G'' > G'$) and above the T_{gel} these had a solid-like behaviour ($G' > G''$) as previously assessed. However, the T_{gel} is considerably affected by the salt concentration, where at higher CaCl_2 concentrations (100 mM) the lower the T_{gel} (33 vs 39 °C). This difference can be attributed to two factors: (i) a higher charge screening and (ii) the reduced solubility of PNIPAM core in water due to a higher ionic strength. Interestingly, the calcium-nanogel aggregates reached a similar G' and G'' magnitude around 56 °C, which might suggest that the concentration of Ca^{2+} mainly affects the gelation point, whereas the nanogel concentration had a greater effect on the stiffness of the calcium aggregates.

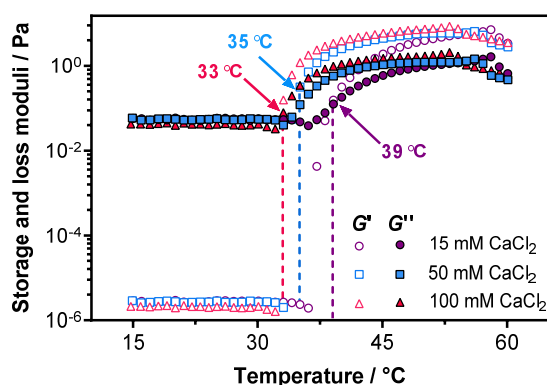


Figure 3.26: Temperature-dependence of G' and G'' for nanogel dispersions at 5% w/w with different CaCl_2 concentrations. CaCl_2 concentration of (\bullet) 15, (\blacksquare) 50, (\blacktriangle) 100 mM CaCl_2 . Empty symbols correspond to G' and filled symbols to G'' . Measurements were performed on $\text{A}_{52}\text{N}_{195}\text{B}_3\text{-0.04}$ nanogels at a constant strain of 1% and a frequency of 1 Hz.

3.4. Conclusions

This chapter has demonstrated the ability of PAA-*b*-P(NIPAM-*st*-BIS) anionic nanogels to exhibit conformational changes as a response to variations in temperature, pH and ionic strength. The effect of the synthesis variables on the VPTT of anionic nanogels such as the target DP of the core-forming block and the shell-stabiliser block was investigated for nanogels synthesised in either water or water-ethanol mixtures as a cosolvent pair of PNIPAM. For nanogels synthesised in only water, the VPTT mainly depended on the volume fraction of PNIPAM, where the VPTT gradually decreased with increasing volume fraction of PNIPAM. Additionally, a minimal contribution on the VPTT related to the DP of PAA used to prepare nanogels was noticed, even though these had different hydrodynamic diameters.

In the case of the nanogels synthesised in mixtures of cosolvents, a detrimental effect on the VPTT of nanogels was noted for nanogels synthesised in the higher ethanol mole fraction of $X_e=0.12$ when targeting a PNIPAM DP of 200. However, at lower ethanol mole fractions ($X_e \leq 0.09$) the nanogels shrank with increasing temperature and were colloidally stable as expected. It was found that the VPTT of nanogels with a similar target DP of PNIPAM increased to higher temperatures with increasing X_e used in the nanogel synthesis, as also noticed for diblock copolymers with the same monomer composition as shown in Chapter 2. The shift in the VPTT could be attributed to the different meso diads content of the $A_xN_yB_z-X_e$ anionic nanogels, which was probably caused by the constrained chain growth during nanogel preparation in cosolvents. An increase in racemic diads could generate an alternating configuration where geometric constraints make the formation of local hydrogen bonding difficult between amide groups from PNIPAM and hence water molecules interact stronger with the polymer, which ultimately affects the VPTT. In contrast to nanogels synthesised in only water, the number-average DP of PAA seems to alter the VPTT of nanogels synthesised in $X_e=0.05$, where nanogels synthesised from PAA₈₄ had a greater VPTT in agreement with the increased racemic diads content determined for the corresponding diblock copolymer.

The pH-sensitivity of nanogels was evaluated by DLS, where the size of the nanogels was reduced with decreasing the pH of the nanogel dispersions due to the protonation of the carboxylate groups which reduces the shell thickness. Furthermore, the VPTT transition from a swollen to shrunken state was observed up to pH 4. The effect of the synthesis cosolvent composition on the pH and temperature transition was also presented, where the difference in deswelling behaviour could also be attributed to changes in the tacticity of the PNIPAM core. In

which, the nanogel synthesised in $X_e=0$ was more hydrophobic and probably tended to release water molecules more easily than the nanogel synthesised in $X_e=0.05$. Electrophoresis experiments showed the variation of the ζ -potential with pH, where nanogels synthesised in water showed a higher ζ -potential due to interparticle crosslinking and/or the presence of PAA chains trapped internally which ultimately affects the shell thickness. Lastly, the ability of these nanogels to macroscopically aggregate in the presence of Ca^{2+} cation under a range of nanogel and CaCl_2 concentrations was observed temperatures close to body temperature.

3.5. Materials and methods

3.5.1. Materials

The properties of the nanogels used in this chapter were previously presented in the Chapter 2.

3.5.2. Dynamic light scattering (DLS)

Determination of the hydrodynamic particle diameter of the purified nanogels (0.1% w/w) was obtained using a NanoBrook Omni particle analyser using a 35 mW diode laser with a nominal 640 nm wavelength. Data was obtained at a scattering angle of 173°. Each DLS measurement consisted of 4 runs of 3 minutes at count rates between 440-550 kcps. Temperature dependent DLS experiments were performed from low to high temperatures with increments of 2.5 °C with 8 minutes in-between intervals to allow thermal stabilisation. The pH of the solutions was manually adjusted by addition of NaOH or HCl solutions using a Hach H160 ISFET probe. The method of the constrained regularization method for inverting data (CONTIN) was used to obtain the size distribution from the autocorrelation function.

3.5.3. Aqueous electrophoresis

ζ -potential measurements for the aqueous nanogel dispersions (0.1 %w/w) containing KCl (1 mM) as a background electrolyte were determined on a Malvern Zetasizer Nano-ZS instrument at 25 °C. The smoluchowski relationship was used to determine the ζ -potential from the electrophoretic mobility. The pH of the solutions was manually adjusted by addition of NaOH or HCl solutions using a Hach H160 ISFET probe.

3.5.4. Rheological measurements

Measurements were performed in an MCR 502 rheometer (Anton Paar) equipped with a Peltier temperature controller and a solvent trap to minimise water evaporation. A parallel plate geometry was employed using a 50 mm polyphenylene sulphide (PPS) with a 0.5 mm gap between plates. The *in situ* formation of macroscopic Ca²⁺-nanogel aggregates was investigated using a temperature sweep from 15 to 60 °C at a heating ramp of 1 °C min⁻¹ at a 1% strain under a frequency of 1 Hz.

3.6. References

1. Kandil, R. & Merkel, O. M. Recent progress of polymeric nanogels for gene delivery. *Curr. Opin. Colloid Interface Sci.* **39**, 11–23 (2019).
2. Chacko, R. T., Ventura, J., Zhuang, J. & Thayumanavan, S. Polymer nanogels: A versatile nanoscopic drug delivery platform. *Adv. Drug Deliv. Rev.* **64**, 836–851 (2012).
3. Riedinger, A. *et al.* ‘Nanohybrids’ based on pH-responsive hydrogels and inorganic nanoparticles for drug delivery and sensor applications. *Nano Lett.* **11**, 3136–3141 (2011).
4. Zhou, S. *et al.* Facile fabrication of dextran-based fluorescent nanogels as potential glucose sensors. *Chem. Commun.* **49**, 9473–9475 (2013).
5. Maya, S. *et al.* Smart stimuli sensitive nanogels in cancer drug delivery and imaging: A Review. *Curr. Pharm. Des.* **19**, 7203–7218 (2013).
6. Sivashanmugam, A., Arun Kumar, R., Vishnu Priya, M., Nair, S. V. & Jayakumar, R. An overview of injectable polymeric hydrogels for tissue engineering. *Eur. Polym. J.* **72**, 543–565 (2015).
7. Soni, K. S., Desale, S. S. & Bronich, T. K. Nanogels: An overview of properties, biomedical applications and obstacles to clinical translation. *J. Control. Release* **240**, 109–126 (2016).
8. Heskins, M. & Guillet, J. E. Solution Properties of Poly(*N*-isopropylacrylamide). *J. Macromol. Sci. Part A - Chem.* **2**, 1441–1455 (1968).
9. Schild, H. G. & Tirrell, D. A. Microcalorimetric detection of lower critical solution temperatures in aqueous polymer solutions. *J. Phys. Chem.* **94**, 4352–4356 (1990).
10. Constantin, M., Cristea, M., Ascenzi, P. & Fundueanu, G. Lower critical solution temperature versus volume phase transition temperature in thermoresponsive drug delivery systems. *Express Polym. Lett.* **5**, 839–848 (2011).
11. Brijitta, J., Tata, B. V. R. & Kaliyappan, T. Phase behavior of poly(*N*-isopropylacrylamide) nanogel dispersions: Temperature dependent particle size and interactions. *J. Nanosci. Nanotechnol.* **9**, 5323–5328 (2009).
12. Rzaev, Z. M. O., Dinçer, S. & Pişkin, E. Functional copolymers of *N*-isopropylacrylamide for bioengineering applications. *Prog. Polym. Sci.* **32**, 534–595 (2007).
13. Huglin, M. B., Liu, Y. & Velada, J. Thermoreversible swelling behaviour of hydrogels based on *N*-isopropylacrylamide with acidic comonomers. *Polymer (Guildf)*. **38**, 5785–5791 (1997).
14. Velada, J. L., Liu, Y. & Huglin, M. B. Effect of pH on the swelling behaviour of hydrogels based on *N*-isopropylacrylamide with acidic comonomers. *Macromol. Chem. Phys.* **199**, 1127–1134 (1998).
15. Bulmus, V., Ding, Z., Long, C. J., Stayton, P. S. & Hoffman, A. S. Site-specific Polymer–Streptavidin bioconjugate for pH-controlled binding and triggered release of Biotin. *Bioconjug. Chem.* **11**, 78–83 (2000).
16. Kratz, K., Hellweg, T. & Eimer, W. Influence of charge density on the swelling of colloidal poly(*N*-isopropylacrylamide-*co*-acrylic acid) microgels. *Colloids Surfaces A Physicochem. Eng. Asp.* **170**, 137–149 (2000).
17. Hoare, T. & Pelton, R. Functional group distributions in carboxylic acid containing poly(*N*-isopropylacrylamide) Microgels. *Langmuir* **20**, 2123–2133 (2004).

18. Jones, C. D. & Lyon, L. A. Synthesis and characterization of multiresponsive core-shell microgels. *Macromolecules* **33**, 8301–8306 (2000).
19. Serpe, M. J., Jones, C. D. & Lyon, L. A. Layer-by-layer deposition of thermoresponsive microgel thin films. *Langmuir* **19**, 8759–8764 (2003).
20. Pei, Y. *et al.* The effect of pH on the LCST of poly(*N*-isopropylacrylamide) and poly(*N*-isopropylacrylamide-*co*-acrylic acid). *J. Biomater. Sci. Polym. Ed.* **15**, 585–594 (2004).
21. Begum, R., Farooqi, Z. H. & Khan, S. R. Poly(*N*-isopropylacrylamide-acrylic acid) copolymer microgels for various applications: A review. *Int. J. Polym. Mater. Polym. Biomater.* **65**, 841–852 (2016).
22. Brazel, C. S. & Peppas, N. A. Synthesis and characterization of thermo- and chemomechanically responsive poly(*N*-isopropylacrylamide-*co*-methacrylic acid) hydrogels. *Macromolecules* **28**, 8016–8020 (1995).
23. Zhou, S. & Chu, B. Synthesis and volume phase transition of poly(methacrylic acid-*co*-*N*-isopropylacrylamide) microgel particles in water. *J. Phys. Chem. B* **102**, 1364–1371 (1998).
24. Khan, S. R., Farooqi, Z. H., Ajmal, M., Siddiq, M. & Khan, A. Synthesis, characterization, and silver nanoparticles fabrication in *N*-isopropylacrylamide-based polymer microgels for rapid degradation of p-nitrophenol. *J. Dispers. Sci. Technol.* **34**, 1324–1333 (2013).
25. Hoare, T. & Pelton, R. Highly pH and temperature responsive microgels functionalized with vinylacetic acid. *Macromolecules* **37**, 2544–2550 (2004).
26. Chen, G. & Hoffman, A. S. A new temperature- and pH-responsive copolymer for possible use in protein conjugation. *Macromol. Chem. Phys.* **196**, 1251–1259 (1995).
27. Karg, M. *et al.* Temperature, pH, and ionic strength induced changes of the swelling behavior of PNIPAM-poly(allylactic acid) copolymer microgels. *Langmuir* **24**, 6300–6306 (2008).
28. Khan, J., Siddiq, M., Akram, B. & Ashraf, M. A. *In-situ* synthesis of CuO nanoparticles in P(NIPAM-*co*-AAA) microgel, structural characterization, catalytic and biological applications. *Arab. J. Chem.* **11**, 897–909 (2018).
29. Mohsen, R., Vine, G. J., Majcen, N., Alexander, B. D. & Snowden, M. J. Characterization of thermo and pH responsive NIPAM based microgels and their membrane blocking potential. *Colloids Surfaces A Physicochem. Eng. Asp.* **428**, 53–59 (2013).
30. Morris, G. E., Vincent, B. & Snowden, M. J. Adsorption of lead ions onto *N*-isopropylacrylamide and acrylic acid copolymer microgels. *J. Colloid Interface Sci.* **190**, 198–205 (1997).
31. Xiong, W., Gao, X., Zhao, Y., Xu, H. & Yang, X. The dual temperature/pH-sensitive multiphase behavior of poly(*N*-isopropylacrylamide-*co*-acrylic acid) microgels for potential application in *in situ* gelling system. *Colloids Surfaces B Biointerfaces* **84**, 103–110 (2011).
32. Farooqi, Z. H., Khan, H. U., Shah, S. M. & Siddiq, M. Stability of poly(*N*-isopropylacrylamide-*co*-acrylic acid) polymer microgels under various conditions of temperature, pH and salt concentration. *Arab. J. Chem.* **10**, 329–335 (2017).
33. Navarro-Verdugo, A. L., Goycoolea, F. M., Romero-Meléndez, G., Higuera-Ciajara, I. & Argüelles-Monal, W. A modified Boltzmann sigmoidal model for the phase transition of smart gels. *Soft Matter* **7**, 5847–5853 (2011).
34. Bandyopadhyay, S., Sharma, A., Ashfaq Alvi, M. A., Raju, R. & Glomm, W. R. A robust method to calculate the volume phase transition temperature (VPTT) for hydrogels and hybrids. *RSC Adv.* **7**, 53192–53202 (2017).

-
35. Futscher, M. H., Philipp, M., Müller-Buschbaum, P. & Schulte, A. The Role of backbone hydration of poly(*N*-isopropyl acrylamide) across the volume phase transition compared to its monomer. *Sci. Rep.* **7**, 17012 (2017).
 36. Igor, G. & Mattiasson, B. Chapter 5: Microgels from smart polymers. in *Smart Polymers: Applications in Biotechnology and Biomedicine* 148 (CRC Press, 2007).
 37. De Oliveira, T. E., Mukherji, D., Kremer, K. & Netz, P. A. Effects of stereochemistry and copolymerization on the LCST of PNIPAm. *J. Chem. Phys.* **146**, 034904 (2017).
 38. Barnett, C. E. Some applications of wave-length turbidimetry in the infrared. *J. Phys. Chem.* **46**, 69–75 (1942).
 39. Åkerlöf, G. Dielectric constants of some organic solvent-water mixtures at various temperatures. *J. Am. Chem. Soc.* **54**, 4125–4139 (1932).
 40. Chai, Q., Jiao, Y. & Yu, X. Hydrogels for Biomedical Applications: Their Characteristics and the Mechanisms behind Them. *Gels* **3**, 6 (2017).
 41. Rey, M., Hou, X., Tang, J. S. J. & Vogel, N. Interfacial arrangement and phase transitions of PNIPAM microgels with different crosslinking densities. *Soft Matter* **13**, 8717–8727 (2017).
 42. Bhattacharjee, S. DLS and zeta potential - What they are and what they are not? *J. Control. Release* **235**, 337–351 (2016).
 43. Biswas, C. S. *et al.* Synthesis and study of the properties of stereocontrolled Poly(*N*-isopropylacrylamide) gel and its linear homopolymer prepared in the presence of a Y(OTf)₃ Lewis acid: Effect of the composition of methanol–water mixtures as synthesis media. *Langmuir* **28**, 7014–7022 (2012).
 44. Schroeder, R. *et al.* Electrostatic interactions and osmotic pressure of counterions control the pH-dependent swelling and collapse of polyampholyte microgels with random distribution of ionizable groups. *Macromolecules* **48**, 5914–5927 (2015).
 45. Wu, C. & Zhou, S. Light scattering study of spherical poly(*N*-isopropylacrylamide) microgels. *J. Macromol. Sci. - Phys.* **36**, 345–355 (1997).
 46. Wu, C. A comparison between the ‘coil-to-globule’ transition of linear chains and the “volume phase transition” of spherical microgels. *Polymer (Guildf)*. **39**, 4609–4619 (1998).
 47. Zhang, Y., Furyk, S., Bergbreiter, D. E. & Cremer, P. S. Specific ion effects on the water solubility of macromolecules: PNIPAM and the Hofmeister series. *J. Am. Chem. Soc.* **127**, 14505–14510 (2005).
 48. Humphreys, B. A., Wanless, E. J. & Webber, G. B. Effect of ionic strength and salt identity on poly(*N*-isopropylacrylamide) brush modified colloidal silica particles. *J. Colloid Interface Sci.* **516**, 153–161 (2018).
 49. Delgado, A. V., González-Caballero, F., Hunter, R. J., Koopal, L. K. & Lyklema, J. Measurement and interpretation of electrokinetic phenomena. *Pure Appl. Chem.* **77**, 1753–1805 (2005).
 50. Lowry, G. V. *et al.* Guidance to improve the scientific value of zeta-potential measurements in nanoEHS. *Environ. Sci. Nano* **3**, 953–965 (2016).
 51. Yildirim, T. *et al.* Dual pH and ultrasound responsive nanoparticles with pH triggered surface charge-conversional properties. *Polym. Chem.* **8**, 1328–1340 (2017).
 52. Gibson, R. R., Armes, S. P., Musa, O. M. & Fernyhough, A. End-group ionisation enables the use of poly(*N*-(2-methacryloyloxy)ethyl pyrrolidone) as an electrosteric stabiliser block for polymerisation-induced self-assembly in aqueous media. *Polym. Chem.* **10**, 1312–1323 (2019).
-

-
53. Shannon, R. D. Revised effective ionic radii and systematic studies of interatomic distances in halides and chalcogenides. *Acta Crystallogr. Sect. A* **A32**, 751–767 (1976).
 54. Tribello, G. A., Liew, C. C. & Parrinello, M. Binding of calcium and carbonate to polyacrylates. *J. Phys. Chem. B* **113**, 7081–7085 (2009).
 55. Sinn, C. G., Dimova, R. & Antonietti, M. Isothermal titration calorimetry of the polyelectrolyte/water interaction and binding of Ca^{2+} : Effects determining the quality of polymeric scale inhibitors. *Macromolecules* **37**, 3444–3450 (2004).
 56. Buló, R. E. *et al.* ‘Site binding’ of Ca^{2+} ions to polyacrylates in water: A molecular dynamics study of coiling and aggregation. *Macromolecules* **40**, 3437–3442 (2007).
 57. Satoh, M., Hayashi, M., Komiyama, J. & Iijima, T. Competitive counterion binding and hydration change of Na poly(acrylate) MgCl_2 , CaCl_2 in aqueous solution. *Polymer (Guildf)*. **31**, 501–505 (1990).
 58. Minami, S., Suzuki, D. & Urayama, K. Rheological aspects of colloidal gels in thermoresponsive microgel suspensions: formation, structure, and linear and nonlinear viscoelasticity. *Curr. Opin. Colloid Interface Sci.* **43**, 113–124 (2019).
 59. Liao, W., Zhang, Y., Guan, Y. & Zhu, X. X. Fractal structures of the hydrogels formed *in situ* from poly(*N*-isopropylacrylamide) microgel dispersions. *Langmuir* **28**, 10873–10880 (2012).
 60. Town, A. *et al.* Understanding the phase and morphological behavior of dispersions of synergistic dual-stimuli-responsive poly(*N*-isopropylacrylamide) nanogels. *J. Phys. Chem. B* **123**, 6303–6313 (2019).

Appendix B

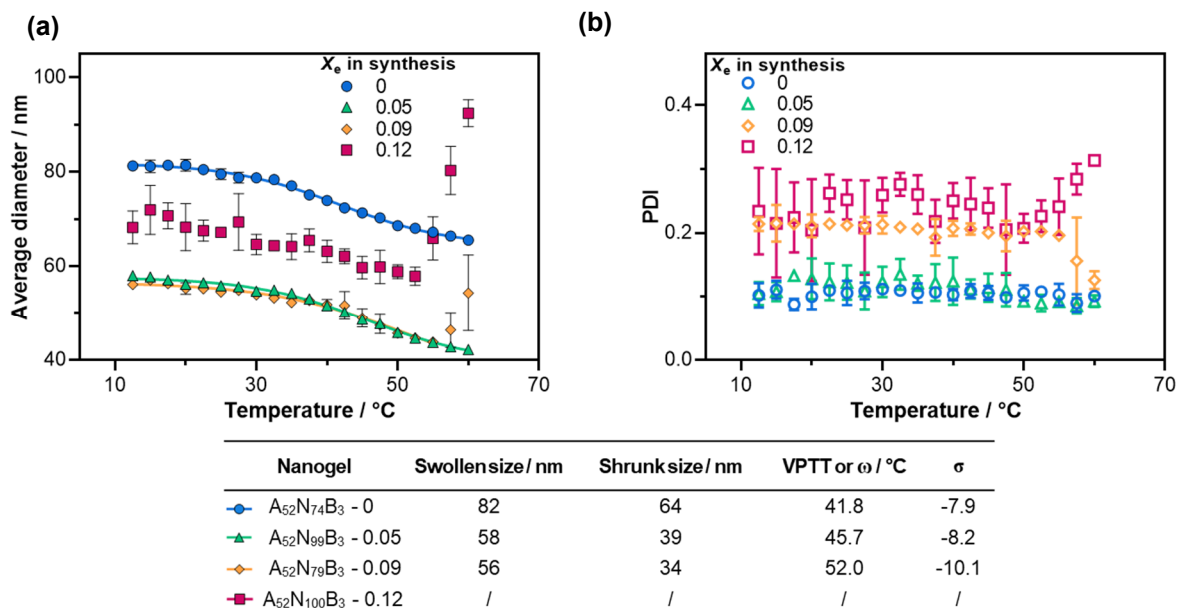


Figure 3B.1: DLS analysis of the $A_{52}N_{100}B_3-X_e$ nanogels synthesised in consolvents. (a) The hydrodynamic diameter as a function of temperature, (b) their corresponding PDI values versus temperature ($n=3$). Data obtained from 0.1% w/w nanogel dispersions in DI water at pH 7. Data fitted using Equation 3.1.

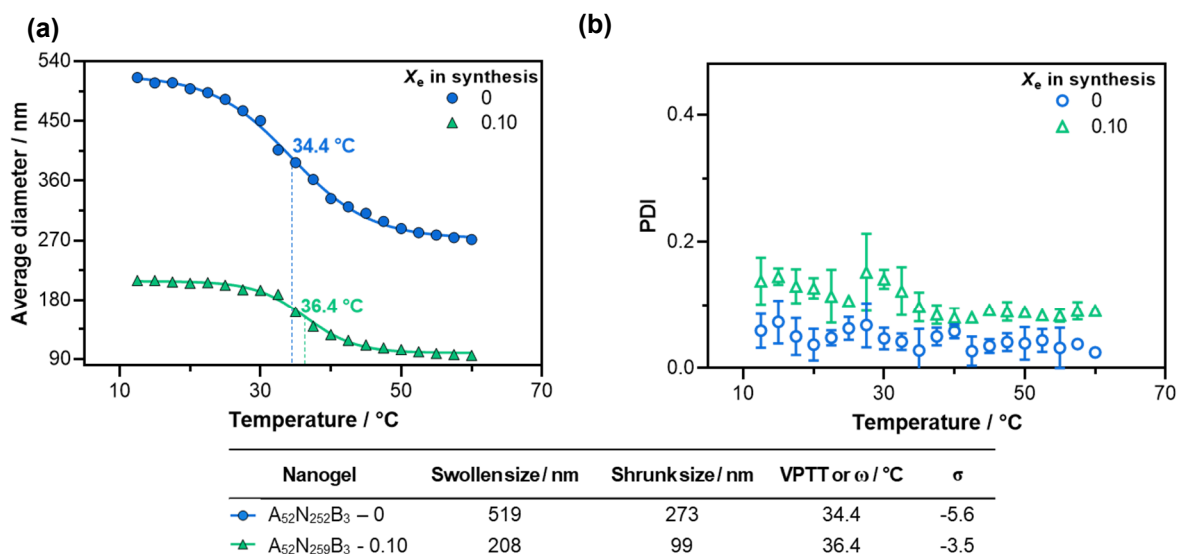


Figure 3B.2: DLS analysis of the $A_{52}N_{300}B_3-X_e$ nanogels synthesised in consolvents. (a) The hydrodynamic diameter as a function of temperature, (b) their corresponding PDI values versus temperature ($n=3$). Data obtained from 0.1% w/w nanogel dispersions in DI water at pH 7. Data fitted using Equation 3.1.

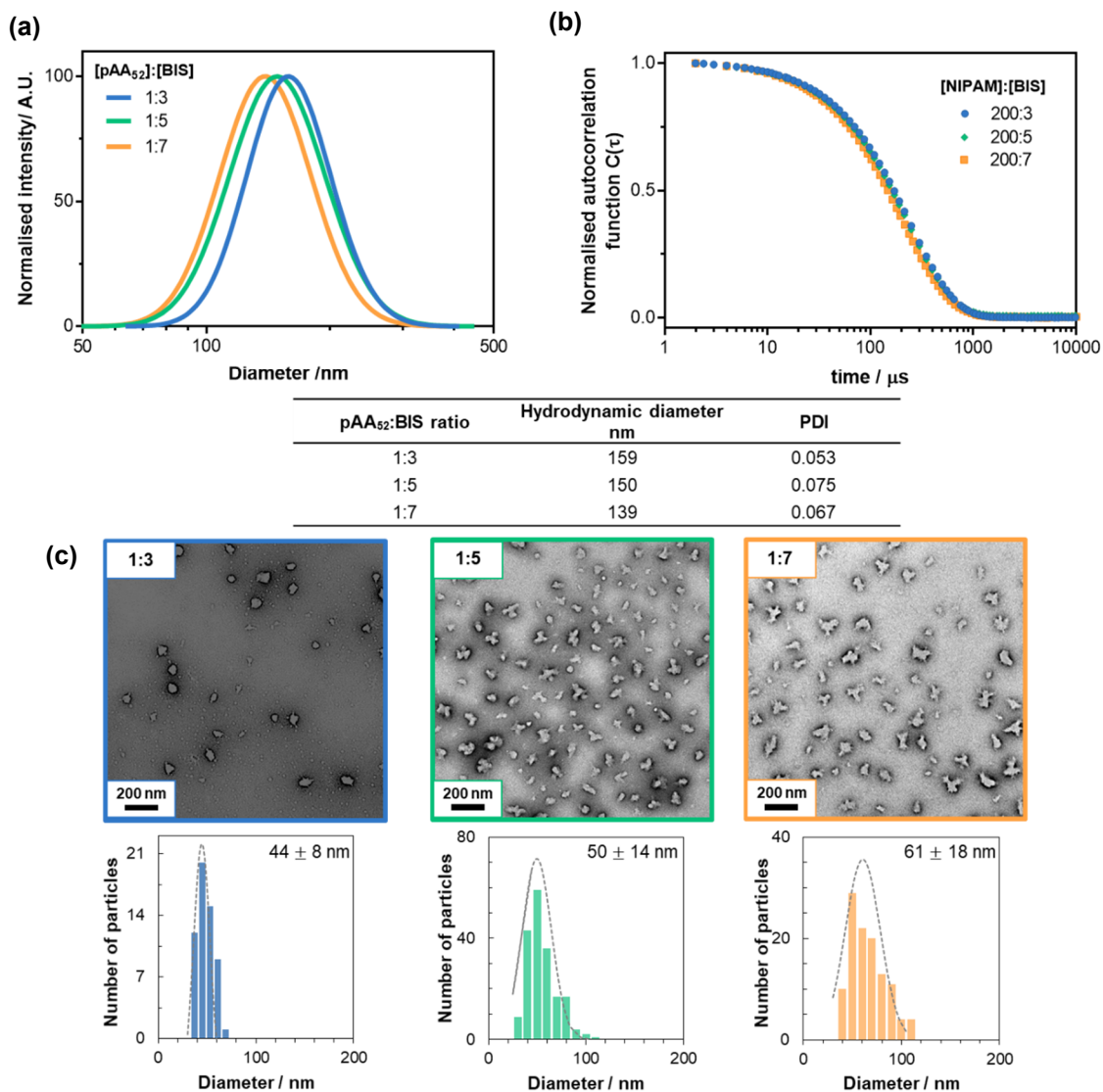


Figure 3B.3: Size determination of the $A_{52}N_{200}B_z-0.05$ nanogels, where $z=3,5$, and 7 . (a) Intensity average lognormal size distribution curves ($n=4$) and (b) their respective autocorrelation function with time, and (c) TEM images of the respective purified nanogel with their number particle size distributions. DLS and TEM data obtained from 0.1% w/w nanogel dispersions in DI water at pH 7 and 25 °C. Phosphotungstic acid (0.75 w/w%, pH 7) was used as the TEM stain.

CHAPTER 4

Cationic nanogels: Synthesis and properties

4.1. Chapter outlook

To expand the versatility of RAFT aqueous dispersion polymerisation to produce multi-responsive nanogels, this chapter aimed to explore the synthesis of cationic nanogels made from a poly(2-(dimethylamino)ethyl methacrylate) (PDMAEMA) based macro-CTA and NIPAM. Similar to the work presented in previous chapters, an investigation of the effect of the shell-stabiliser block and the core-forming block on the properties of uncrosslinked copolymers and nanogels was conducted. The temperature-responsive behaviour of the nanogels was confirmed by determining the changes in size with the temperature at a neutral pH. Additionally, an investigation of the pH-sensitivity of the nanogels was conducted by DLS and aqueous electrophoresis. Finally, the effects of the addition of salt on the colloidal stability of the nanogels was investigated.

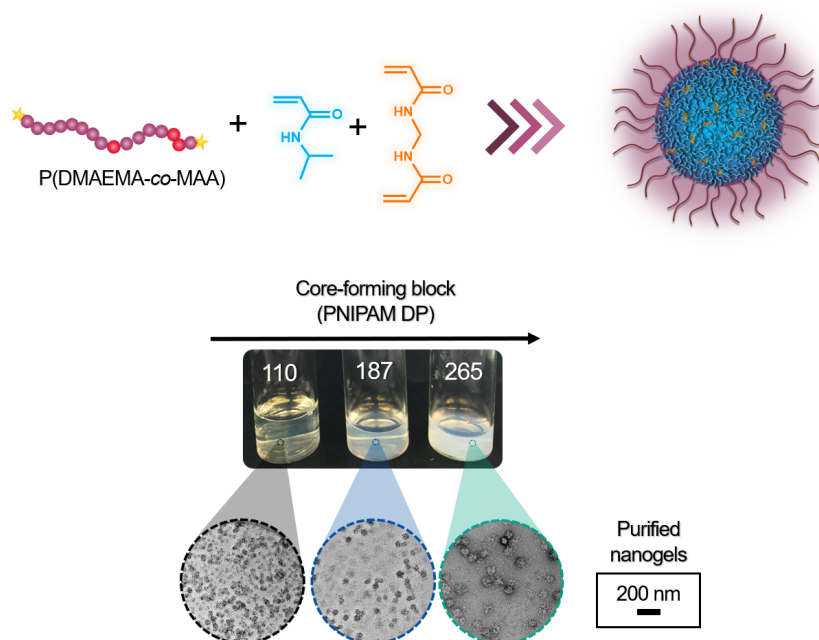


Figure 4.1: A schematic illustration of the preparation of PDMAEMA-based nanogels *via* RAFT dispersion polymerisation.

4.2. Introduction

In contrast to studies on anionic PNIPAM-based nanogels, their cationic analogues have received scant attention. In particular, the use of poly(2-(dimethylamino)ethyl methacrylate) (PDMAEMA), a polymer that is responsive to pH, temperature and ionic strength,¹ seems to be less explored to form crosslinked PNIPAM micro- and nanogels. A few examples of PDMAEMA/PNIPAM crosslinked systems include their potential use as drug²⁻⁴ or gene⁵ delivery nanocarriers, and as building blocks for 3D stem cell culture and recovery.⁶ PDMAEMA homopolymer itself has shown to possess antimicrobial properties depending on the bacteria type,⁷ and which cytotoxicity is influenced by the concentration and molar mass of PDMAEMA,⁸ if it is copolymerised with other monomers^{9,10} or if it has been quaternised by using an alkylating agent.¹¹⁻¹³ Hence, PDMAEMA could be considered as a good candidate for the preparation of cationic nanogels *via* RAFT dispersion polymerisation since it is suitable for use in a wide range of biomedical applications. Previously, Yan and Tao¹⁴ have reported the synthesis of PDMAEMA nanogels *via* a RAFT aqueous dispersion polymerisation by using an amphiphilic PEG macro-CTA. However, PDMAEMA was presumably located in the crosslinked core due to the synthetic conditions. It is well-established that aqueous solutions of PDMAEMA exhibit a cloud point temperature that varies according to molar mass, pH, degree of quaternisation or comonomer composition.¹⁵⁻¹⁹ Generally, the cloud point can be increased to higher temperatures upon ionisation of the amino groups²⁰ or can be eliminated at low degrees of quaternisation.²¹ Hence, PDMAEMA could be used as the solvophilic stabilising block for the aqueous RAFT dispersion polymerisation of NIPAM in acidic pH.

Previous investigations have shown that the free radical copolymerisation of NIPAM and DMAEMA results in hydrogels that respond to temperature and pH stimuli.²² In the case of uncrosslinked materials, aqueous dispersions of PNIPAM-*b*-PDMAEMA diblock copolymers were able to self-assemble into presumably micellar objects with increasing temperature.²³ However, the phase transition was determined by the solution pH, in which the cloud point decreased from 41 °C at pH 6 to 28 °C at pH 9 due to decreased solubility of PDMAEMA in water since DMAEMA chains are deprotonated at high pH values.²³ Moreover, Huang *et al.*²⁴ have demonstrated that neutral and alkaline solutions of an ABC triblock copolymer of PMMA-*b*-PDMAEMA-*b*-PNIPAM can exhibit a two-stage thermally-induced collapse, the first corresponding to the LCST of PNIPAM and the second to the PDMAEMA block above pH 7. In contrast, the same triblock copolymer displayed only a one-stage transition in an acidic solution

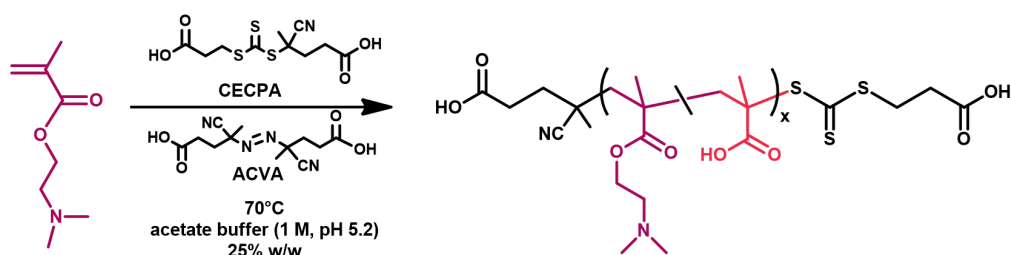
attributed to the hydrophobic NIPAM and highly hydrophilic PDMAEMA block.²⁴ Li *et al.*²⁵ have also demonstrated the doubly thermo-responsive behaviour of copolymers with PNIPAM and PDMAEMA blocks but containing a polystyrene (PS) core synthesised *via* PISA dispersion polymerisation. Hence, it is expected that nanogels containing PNIPAM and PDMAEMA nanogel may exhibit a complex phase behaviour, hence only water was proposed as the polymerisation solvent and the use of cononsolvents was not evaluated here.

Since minimal effort has been made to prepare nanogels under dispersion conditions containing PDMAEMA and PNIPAM, this chapter aims to expand upon the versatility of RAFT aqueous dispersion polymerisation to produce multi-responsive nanogels. PDMAEMA, a pH- and temperature-responsive cationic polyelectrolyte, is assessed here to produce PNIPAM-containing nanogels. Similar to the work presented in previous chapters, an investigation of the effect of parameters such as the DP of the macro-CTA, and the molar ratios of monomer to macro-CTA on the properties of uncrosslinked copolymers and nanogels was performed. Analogously, temperature-dependent DLS studies were performed on the synthesised nanogels to determine the volume phase transition temperature (VPTT). Followed by the effect of pH and ionic strength on the VPTT of aqueous dispersions of nanogels.

4.3. Results and discussion

4.3.1. Synthesis and characterisation of PDMAEMA-based macro-CTAs

For the RAFT solution polymerisation of 2-(dimethylamino)ethyl methacrylate (DMAEMA), 4-(((2-carboxyethyl)thio)carbonothioyl)thio)-4-cyanopentanoic acid (CECPA), a commercially available chain-transfer agent (CTA), was chosen for its suitability to control the polymerisation of methacrylic monomers. The reaction was carried out at 70 °C using ACVA as the water-soluble initiator at a molar ratio of CTA to initiator of 10 to 1 (Scheme 4.1). The reaction was conducted in an acetic acid/sodium acetate buffer solution (1 M, pH 5.2), which influenced the charge and stability of the monomer. Previous studies have shown that cationic 2-(dimethylamino)ethyl (DMAE) esters are susceptible to hydrolysis in the presence of water under acidic or basic conditions.^{26–28} However, their corresponding polymers have a substantial hydrolytic stability in aqueous solutions, which varies accordingly to the presence of terminal alkyl groups on the amino group or by the presence of a methyl adjacent to the ester group.²⁶ Zheng and co-workers²⁸ extensively monitored the hydrolysis of DMAE monomers in water, focusing on polymerisation conditions such as pH and temperature. In the case of DMAEMA, their ¹H NMR spectroscopy studies showed that this monomer is quite stable in acidic medium (pH <5.7) at 25 °C for 20 h, i.e. no detectable variation was observed. However, the decomposition rate of DMAEMA is increased with rising temperature at the inherent pH of 10.1 of DMAEMA in water, e.g. 16% decomposition at 25 °C vs 90% at 60 °C within 2 h.²⁸ In the case of the polymerisation of DMAEMA in water, Carlsson *et al.*²⁹ have investigated its aqueous RAFT polymerisation at pH 7 to form a cationic macro-CTA. They observed that a small fraction of methacrylic acid (7%) was formed during polymerisation thus resulting in the formation of a P(DMAEMA-*co*-MAA) copolymer with an overall positive charge. Hence, it was hypothesised that DMAEMA would be relatively stable during polymerisation using an acetic acid/acetate buffer solution (1 M, pH 5.2). Besides previous studies have reported similar reaction conditions used in this work.³⁰ However, their studies lack NMR analyses from the crude reaction that could indicate the hydrolysis of DMAEMA.



Scheme 4.1: The synthesis of $\text{P(DMAEMA-co-MAA)}_x$ macro-CTA by RAFT aqueous solution polymerisation using CECPA as RAFT agent. Note: Under the reaction conditions, the amino groups are mainly protonated, and the carboxylic groups are minorly deprotonated.

Herein, the kinetics of the reaction of DMAEMA in an acetate buffer solution at 70 °C for a target molar ratio of DMAEMA to CECPA of 62 to 1 was studied using ^1H NMR spectroscopy in D_2O over 4 hours (Figure 4.2). Under the reaction conditions, DMAEMA was converted into polymer and hydrolysed into methacrylic acid (MAA) and dimethylethanolamine (DMEA) (Figure 4.2a and b). The hydrolysis products of DMAEMA can be observed in the stacked ^1H NMR spectra at specified time intervals (Figure 4.2c). The appearance of two vinylic protons ($\text{R}=\text{CH}_2$) located at $\delta=5.58$ and $\delta=5.27$ ppm indicated the formation of MAA, and the oxymethylene (O-CH_2 -) and the aminomethylene ($-\text{CH}_2\text{-N}$) protons centred at $\delta=3.79$ and $\delta=3.10$ ppm indicated the presence of DMEA. The appearance of the protons corresponding to the oxymethylene (O-CH_2 -) at $\delta=4.18$ ppm from the polymer pendent groups suggested the formation of PDMAEMA. However, the kinetic studies also showed that the MAA was gradually consumed during the polymerisation thus leading to the formation of P(DMAEMA-co-MAA) copolymer (Figure 4.2b and Figure 4.3). It is also noted that the formation of DMEA reached a maximum value of around 45% within 120 min and remained almost invariable after this time (Figure 4.2b). Hence, it is suggested that PDMAEMA is indeed hydrolytically more stable than its monomer counterpart²⁶ since no more DMEA was formed after the depletion of DMAEMA.

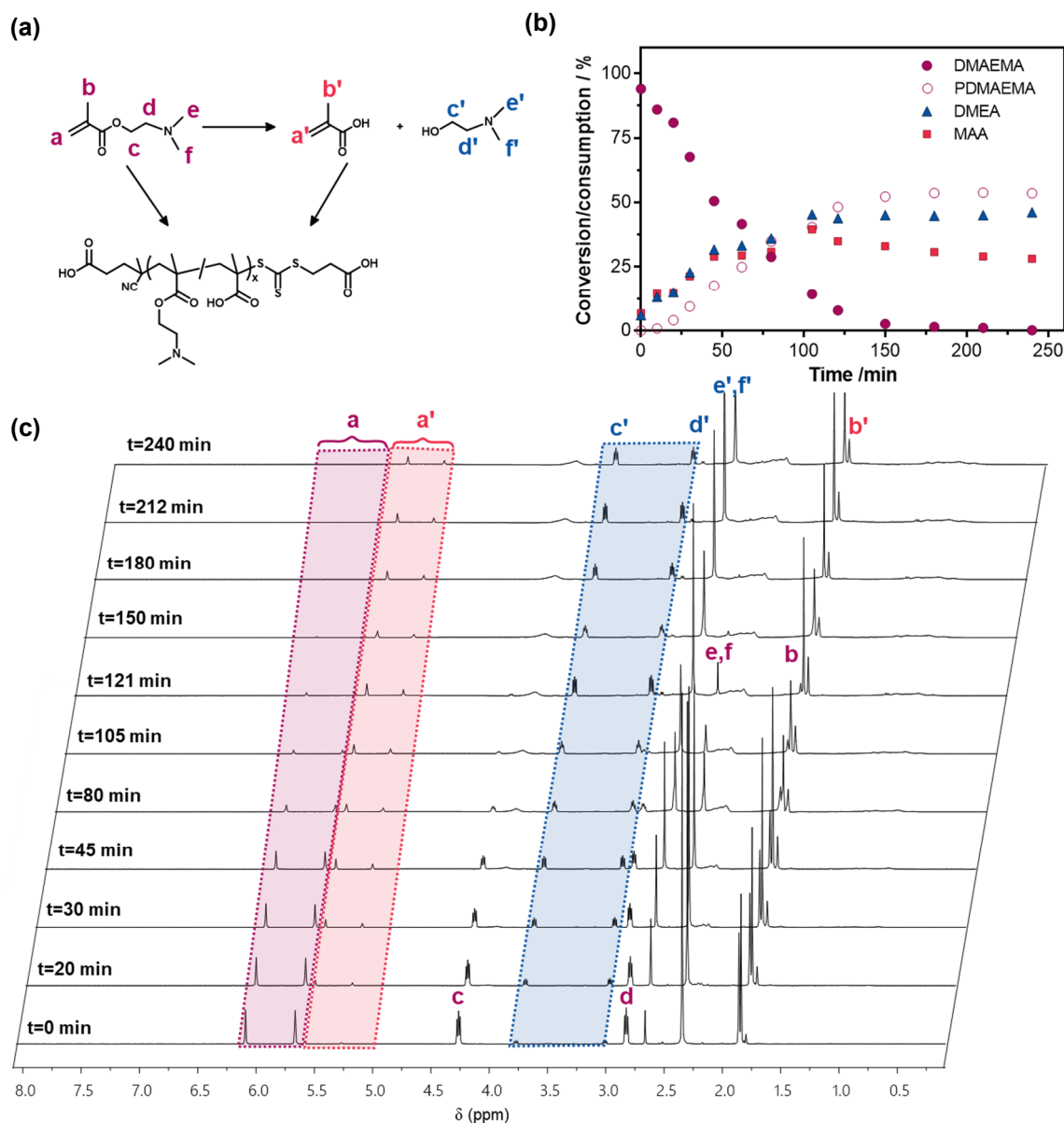


Figure 4.2: The conversion of DMAEMA with time for a targeted DP of 62 (a) Reaction scheme of the polymerisation and hydrolysis of DMAEMA, (b) Conversion of (●) DMAEMA into (○) PDMAEMA (▲) DMEA and (■) MAA vs time curves and (c) stacked ¹H NMR spectra recorded in D₂O of the reactions of DMAEMA. Target composition of [DMAEMA]:[CECPA]:[ACVA] of 62:1:0.1 at 25% w/w and 70 °C in an acetate buffer solution (1 M, pH 5.2). The H₂O residual solvent signal was suppressed to improve the resolution of the spectra.

Figure 4.3a shows the polymerisation of DMAEMA and MAA, where a maximum conversion of DMAEMA into PDMAEMA of 54% was achieved within 180 min with 14% of MAA incorporated into the copolymer. After DMAEMA was depleted, MAA continued to react and it reached a total incorporation into polymer of 18% at 240 min, time at which the reaction was stopped. When the reaction was stopped, 28% of MAA was left unreacted. The corresponding semi-logarithmic kinetic plot of the polymerisation of each monomer is shown in Figure 4.3b.

It was observed that both monomers seemingly followed a pseudo-first-order kinetics. The apparent kinetic constants of DMAEMA and MAA ($K_{appD}=9.8\times 10^{-5} \text{ s}^{-1}$ and $K_{appM}=1.5\times 10^{-5} \text{ s}^{-1}$, respectively) were calculated from the slopes of the linear kinetic curves. These kinetic results show that the DMAEMA was more reactive than MAA, and it was incorporated into polymer chains faster than MAA. An average number of each monomer incorporated into the copolymer chains can be estimated from the initial feed ratio of DMAEMA and the conversion of each monomer into polymer (Figure 4.3c). It is suggested that an asymmetric gradient-like copolymer was formed due to the gradual copolymerisation of MAA.

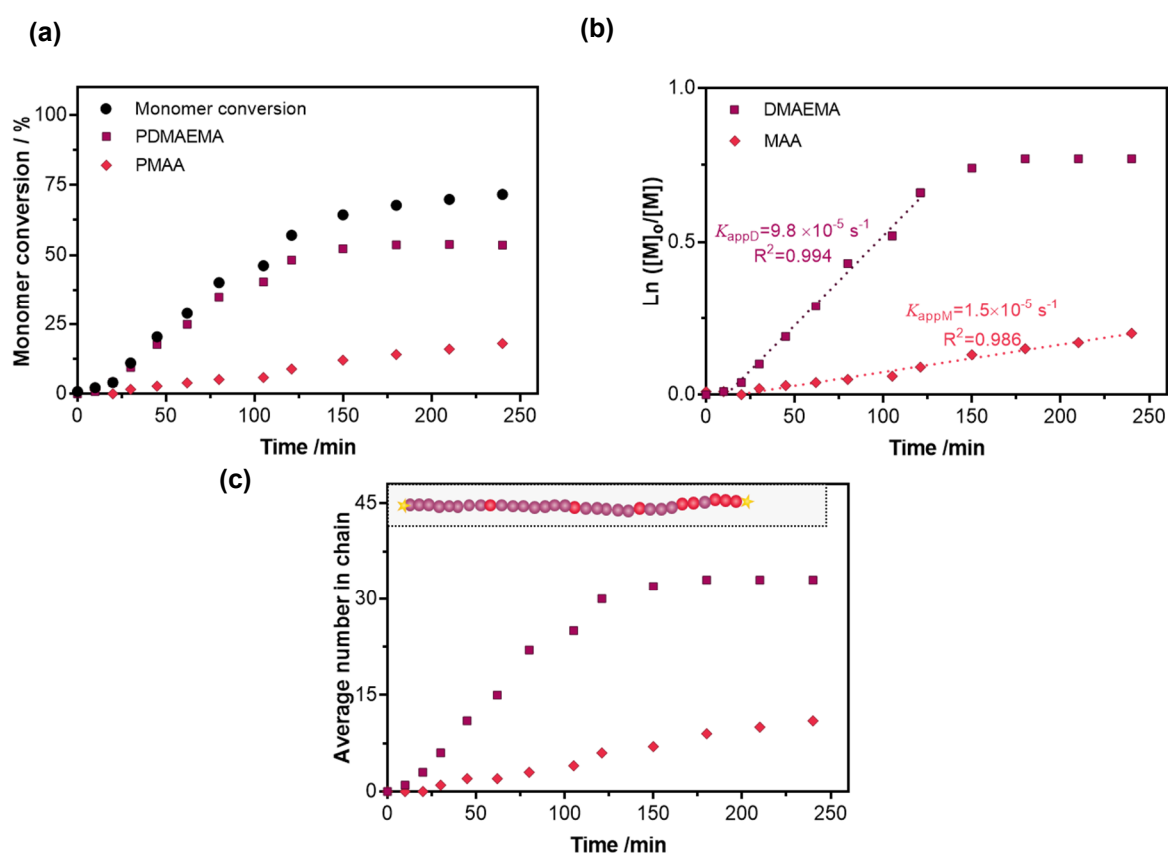


Figure 4.3: Kinetic studies of the RAFT polymerisation of DMAEMA and MAA as determined by ^1H NMR spectroscopy. (a) DMAEMA (■), MAA (◆) and the total monomer (●) conversion vs time curves. (b) the semi-logarithmic plot of the RAFT polymerisation of each monomer, and (c) the average number of each monomer in the copolymer with time and the insert cartoon showing the composition. Target composition of [DMAEMA]:[CECPA]:[ACVA] of 62:1:0.1.

The study of the polymerisation and hydrolysis of DMAEMA targeting a composition of [DMAEMA]:[CECPA]:[ACVA] of 126:1:0.1 can be found in the Appendix C, Figure 4C.3-4. Overall, a slower polymerisation rate was observed ($K_{appD}=8.9 \times 10^{-5} \text{ s}^{-1}$ and $K_{appM}=1.1 \times 10^{-5} \text{ s}^{-1}$) and more DMAEMA was hydrolysed into DMEA and MAA than when a lower DP was targeted. For instance, the formation of DMEA reached a maximum value of around 52% within 180 min, and at this time a DMAEMA conversion of 46% was achieved with 11% conversion of MAA into

polymer. A reduced polymerisation rate could be due to a different ACVA initiator concentration used in the reactions at the same DMAEMA concentration of 2.2 M, i.e. 1×10^{-2} M ACVA for a target DP of 62 and 5×10^{-3} M for a target DP of 126. Additionally, it is suggested that a greater concentration of hydrolysis products was obtained since this parallel reaction was unaffected by the lower concentration of the initiator as in the case of polymerisation rate. The evolution of the molar mass during the polymerisation determined by GPC was attempted for both kinetic studies using an acidic aqueous buffer as eluent (aqueous solution at pH 2 containing 0.5 M acetic acid, 0.3 M NaH_2PO_4); however, no conclusive results could be obtained. This could be attributed to the presence of PMAA which could have interacted with the column media.

Two P(DMAEMA-*co*-MAA) macro-CTAs with different DP were prepared using similar reaction conditions to those used for the kinetic studies. Table 4.1 shows the details of the properties of these two macro-CTAs. For the sake of brevity, the P(DMAEMA-*co*-MAA)_x macro-CTAs will be referred to as DM_x, where x represents the number-average DP of the macro-CTA as determined by ¹H NMR spectroscopy of the purified copolymer. As expected, the amount of DMEA produced during the synthesis of the macro-CTAs, as well as the amount of MAA converted into polymer agreed with those values determined by the kinetic studies. For example, in the case of the DM₅₇ macro-CTA, when the reaction was quenched after 115 min a total amount of 42% of DMEA was formed and 6% MAA was incorporated into polymer. However, after purification approximately 21% of the macro-CTA was estimated to be PMAA by ¹H NMR spectroscopy (Appendix C, Figure 4C.7) suggesting some additional hydrolysis during purification. Nonetheless, the DM_x macro-CTAs carry an overall positive charge (>79%).

Table 4.1: Summary of the synthesis and properties of DM_x macro-CTAs.^a

[DMAEMA]/[CECPA]	[CECPA]/[ACVA]	Total Conversion ^b %	macro-CTA DP ^c	PDMAEMA DP ^d	$\bar{M}_{n,theo}$ ^e kDa	$\bar{M}_{n,GPC}$ ^f kDa	\bar{M}_w/\bar{M}_n ^f
62/1	10/1	56	57	45	8.4	14.3	1.27
124/1	10/1	50	87	64	12.3	21.5	1.20

^aGeneral reaction conditions: solids content 25% w/w in sodium acetate buffer (1 M, pH 5.2) at 70 °C.

^bThe sum of the conversion of DMAEMA and MAA to polymer as determined by ¹H NMR spectroscopy. (Appendix C, Figure 4C.5-6). ^cCalculated from the end group analysis *via* ¹H NMR spectroscopy by comparison of the two methylene protons peak area at $\delta=2.61$ ppm from CECPA end groups to the total area of the methyl group attached to the α C of the copolymer backbone located in the range of $\delta=1.44$ to 0.65 ppm (Appendix C, Figure 4C.7-8). ^dCalculated by comparison of the methylene protons from CECPA end groups to the oxymethylene protons total area at $\delta=4.38$ ppm; using the following equation $DP = \text{Area per proton of backbone}/\text{area per proton of end-groups}$. ^eCalculated using the equation $\bar{M}_n = M_e + (\phi)M_1 + (x-\phi)M_2$, where M_e is the molecular mass of the end groups from CECPA CTA, ϕ the DP of PDMAEMA, x the macro-CTA DP, and M_1 and M_2 are the molar masses of DMAEMA and MAA, respectively. ^fDetermined by aqueous GPC of the purified P(DMAEMA-*co*-MAA)_x macro-CTAs. (GPC: acidic aqueous buffer (pH 2) containing 0.5 M acetic acid, 0.3 M NaH_2PO_4 , calibrated with near-monodisperse PEG/PEO standards).

GPC studies in an acidic aqueous buffer showed unimodal molar mass distributions with relatively low dispersities ($\bar{M}_w/\bar{M}_n < 1.27$) (Figure 4.4). Nevertheless, the number average molar mass ($\bar{M}_{n, \text{GPC}}$) as determined from GPC does not match with the theoretical molar mass ($\bar{M}_{n, \text{theo}}$) values. This may be associated to the PEG/PEO standards used for the determination of the molar mass, which do not match with the hydrodynamic volume of the DM_x macro-CTAs. Previous studies showed a better match between theoretical and GPC molar masses of the quaternised version of PDMAEMA using the same eluent conditions and PEG/PEO standards.³¹ Hence, the discrepancy found in this work can be attributed to the presence of MAA units distributed along the macro-CTA polymer backbone.

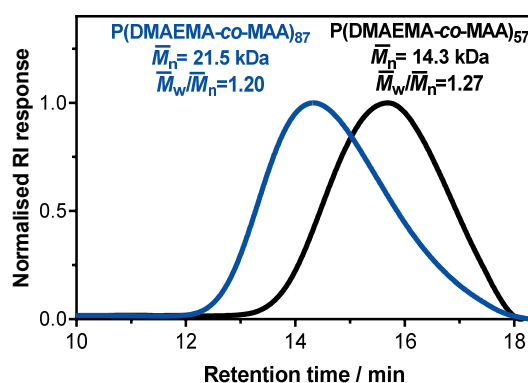


Figure 4.4: Aqueous GPC chromatograms of the series of DM_x macro-CTAs. (GPC: acidic aqueous buffer at pH 2 containing 0.5 M acetic acid, 0.3 M NaH_2PO_4 , calibrated with near-monodisperse PEG/PEO standards).

The presence of both acidic and basic groups in the DM_{57} polyampholyte was confirmed by potentiometric titration, where two $\text{p}K_a$ values were observed (Figure 4.5). Between pH 3 and pH 11, two regions with slightly distinct slopes were observed. The first $\text{p}K_{a1}$ at pH 4.5 corresponds to the half deprotonation of the methacrylic acid units, while the second and most prominent $\text{p}K_{a2}$ at pH 8.2 is due to the half deprotonation of the tertiary amine group of DMAEMA monomer units. These values agree well with the values previously reported in the literature.^{26,32}

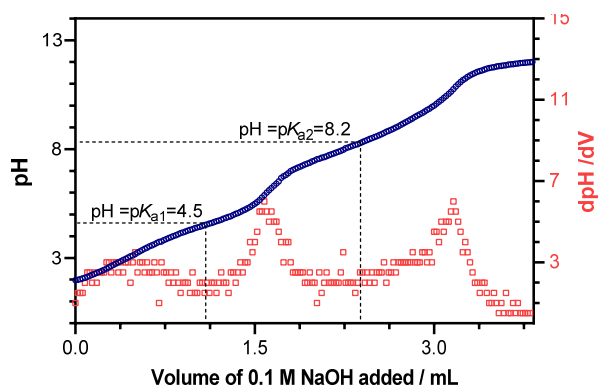


Figure 4.5: Acid titration curve of the DM_{57} macro-CTA.

PDMAEMA exhibits a temperature response in aqueous solutions that varies according to molar mass and pH.^{16,17} Consequently, the temperature response with pH of the DM_x macro-CTAs was determined by UV-vis spectroscopy experiments at 550 nm (Figure 4.6). In the case of the DM₅₇ macro-CTA, a solubility change with temperature was only observed above the p*K*_{a2} of 8.2 within the temperature range from 10 to 70 °C (Figure 4.6a). For instance, a *T*_{cp} of 64 °C was observed at pH 8.5, temperature that was decreased to 53 °C at pH 9.5. The shift in the cloud point was not surprising since the deprotonation of the dimethylamino groups decreases the hydrophilic character of the polymer.^{17,33} For example, at pH 8.5 the DMAEMA units are 33% protonated and at pH 9.5 the protonation of the DMAEMA units is reduced to 4.8%, which increases the hydrophobic character of PDMAEMA. Moreover, the deprotonated carboxylate units from PMAA at basic pH (deprotonation of 99.9% at pH 8.5) did not affect the expected changes in solubility of PDMAEMA with temperature considerably. For instance, literature cloud points of a PDMAEMA homopolymer with an average DP of 108 were 56.5 °C at pH 8 and 46.9 °C at pH 9.²⁰ Hence, the thermoresponsive behaviour of DM₅₇ at highly basic pH also suggests that most of the copolymer is comprised of PDMAEMA, as judged by UV-vis spectroscopy experiments. A similar temperature responsive behaviour in basic pH was observed for the DM₈₇ macro-CTA (Figure 4.6b).

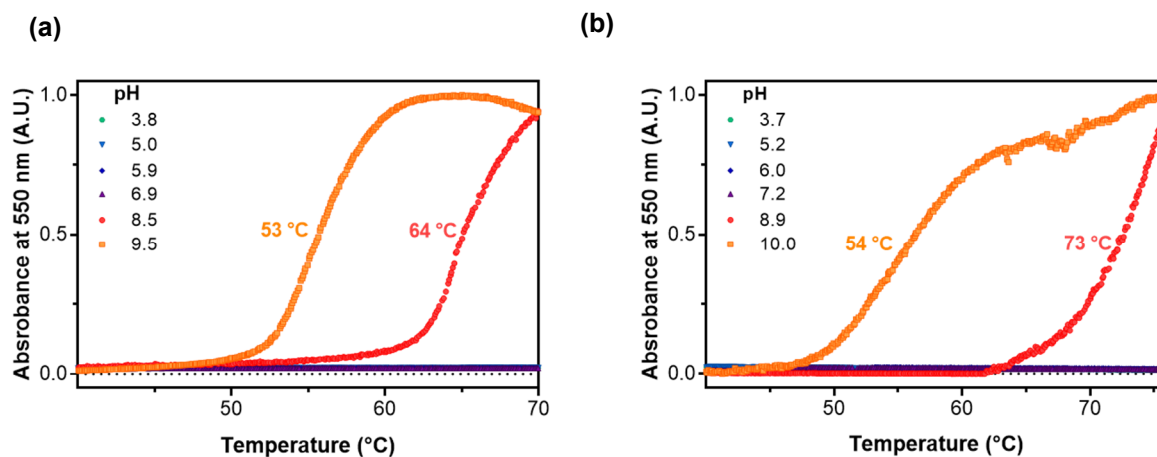


Figure 4.6: Turbidimetry experiments at different pH of the (a) DM₅₇ and (b) DM₈₇ macro-CTAs in aqueous solution. The cloud points were determined from the inflection point of the normalised absorbance curve at 550 nm on a heating rate of 0.12 °C min⁻¹.

4.3.2. Synthesis and properties of P(DMAEMA-*co*-MAA)-*b*-PNIPAM copolymers

The chain extension of the DM_x macro-CTA was first assessed with NIPAM in the absence of BIS *via* RAFT dispersion polymerisation (Figure 4.7a). The reaction was conducted in an acetic acid/acetate buffer solution (1 M, pH 5.2) so that the macro-CTA was highly charged and hydrophilic. High monomer conversion (99%) was achieved as determined by ¹H NMR spectroscopy and no hydrolysis products (i.e. DMEA) were observed at the set conditions (Figure 4.7b).

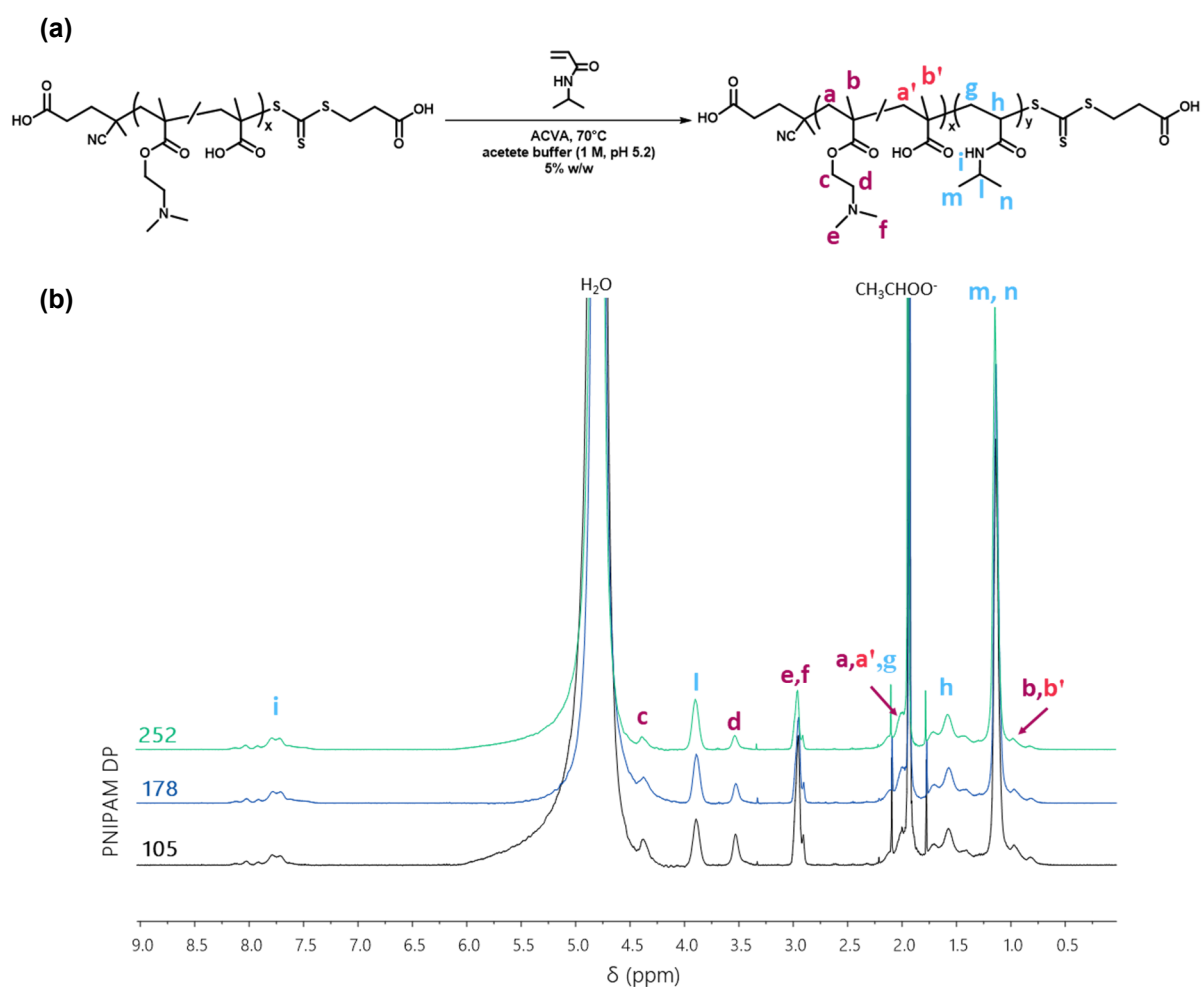


Figure 4.7: The synthesis and characterisation of DM₅₇N_y copolymers. (a) Reaction scheme of the polymerisation of NIPAM using DM₅₇ as macro-CTA and (b) stacked ¹H NMR spectra recorded in D₂O of the crude reaction mixture for the DM₅₇ chain extension with NIPAM. Note: Under the reaction conditions, the amino groups are mainly protonated, and the carboxylic groups are minorly deprotonated.

A notation is utilised hereafter to represent the copolymer composition (DM_xN_y). Thus DM_x , and N_y symbolises the P(DMAEMA-co-MAA) macro-CTA and NIPAM, respectively, where x and y are the number-average DP of each monomer component as determined by 1H NMR spectroscopy analyses.

After purification, the temperature behaviour of the DM_xN_y copolymers was investigated by UV-vis absorption spectroscopy and dynamic light scattering (DLS) at different temperatures. As in Chapter 2, DLS was used to assess the size of aggregates formed upon heating but at the acetate buffer conditions in which these copolymers were synthesised in, and also in water at pH 7. UV-vis spectroscopy at a wavelength of 550 nm was used to assess the sensitivity of the $A_xN_y-X_e$ copolymers to increasing temperature, as indicated by changes in the light absorbance of the samples in either acetate buffer solutions or aqueous solutions at neutral pH. As pointed out in Chapter 2 (Section 2.3.4.1), turbidimetry detects the outcome of the thermal transition (i.e. a macroscopic event) and not the actual cloud point;³⁴ however, in this work is termed as the cloud point (T_{cp}) since no other techniques were used as complementary techniques. Other techniques such as microcalorimetry, temperature-dependent 1H NMR spectroscopy and scattering techniques are recommended to be used in future work.

The full properties of the synthesised terpolymers can be found in Table 4.2.

Table 4.2: Summary of the results of the synthesis and properties of DM_xN_y copolymer.

Target composition [DM_x]:[NIPAM] ^a		Conversion ^b %	DP _{theo} ^c	$\bar{M}_{n,theo}$ ^d kDa	$D_{h,buffer}/nm$ (PDI) ^e	$D_{h,water}/nm$ (PDI) ^f	$T_{cp,buffer}$ ^g °C	$T_{cp,water}$ ^h °C
x=57	[1]:[115]	99	114	21.3	59 (0.04)	ill-defined	16.6	38.1
	[1]:[191]	99	190	29.9	82 (0.03)	145 (0.18)	16.3	37.3
	[1]:[287]	99	285	40.7	79 (0.4)	154 (0.15)	15.0	36.7
x=87	[1]:[159]	99	158	30.2	92 (0.05)	37 (0.14)	17.3	39.7
	[1]:[239]	99	238	39.3	106 (0.05)	57 (0.10)	16.1	37.1

a General reaction conditions: $[DM_x]/[ACVA]=5$, solids content 5% w/w in acetate buffer at 70 °C for 18 h. b Determined by 1H NMR spectroscopy. c Estimated from $DP=[NIPAM]/[DM_x]\times conversion$. e Calculated with $\bar{M}_n=M_{CTA}+(\phi)M_1+(x-\phi)M_2+yM_3$, where M_{CTA} is the molar mass of the CTA end groups, ϕ the DP of PDMAEMA, x the P(DMAEMA-co-MAA) macro-CTA DP and y is the DP of NIPAM, and M_1 , M_2 , and M_3 are the molar masses of the corresponding monomer unit. e D_h of the self-assembled structures at 50 °C as determined by DLS of 0.1% w/w solutions in acetate buffer (1 M, pH 5.2). f D_h of the self-assembled structures at 62.5 °C in water at pH 7. g Cloud points of 1% w/w copolymer solutions in acetate buffer (1 M, pH 5.2) at 550 nm on a heating rate of 0.12 °C min⁻¹. h Cloud points of 1% w/w copolymer solutions in water.

4.3.2.1. The temperature response of P(DMAEMA-*co*-MAA)-*b*-PNIPAM copolymers

Turbidimetry experiments conducted in acetate buffer (1 M, pH 5.2) at 550 nm showed that the DM_xN_y copolymers exhibit a phase transition with temperature (Figure 4.8). Considering that both DM_x macro-CTAs do not exhibit a temperature response in acidic pH within the temperature range tested (Figure 4.6), the T_{cp} is due to the phase change of the PNIPAM block in aqueous solutions. In agreement with the observations previously described in Chapter 2, two trends were observed for the DM_xN_y copolymers. On one hand, the T_{cp} tended to slightly lower temperatures with larger PNIPAM DPs due to a higher hydrophobic contribution of the PNIPAM block upon heating. On the other hand, the T_{cp} was shifted to relatively higher temperatures when using DM_{87} in comparison to the DM_{54} macro-CTA due to a relatively greater hydrophilic contribution from the DM_{87} block (Figure 4.8 and Table 4.2).

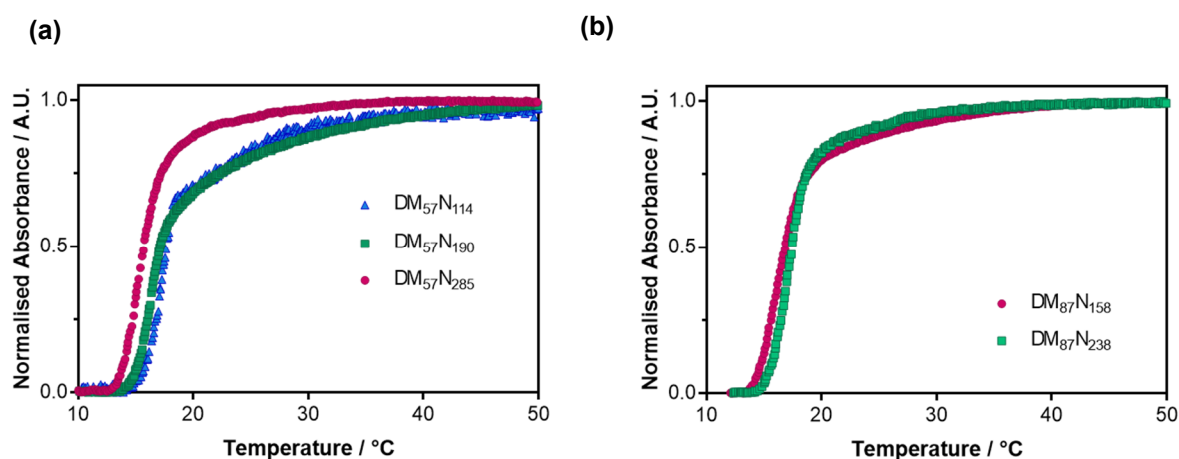


Figure 4.8: Turbidimetry experiments of purified DM_xN_y diblock copolymers in acetate buffer (1 M, pH 5.2). Copolymers synthesised from (a) DM_{57} and (b) DM_{87} , where y corresponds to the DP of the PNIPAM block. The cloud points were determined from the inflection point of the normalised absorbance curve at 550 nm on a heating rate of $0.12\text{ }^\circ\text{C min}^{-1}$.

It was also noted that the cloud points determined in acetate buffer were considerably lower than those determined in water (Table 4.2 and Figure 4.9). For example, the $DM_{57}N_{190}$ exhibited a T_{cp} in acetate buffer at $16\text{ }^\circ\text{C}$ and a T_{cp} at $37\text{ }^\circ\text{C}$ in water (salt-free solution at pH 7). Since PNIPAM is not pH-sensitive, this difference may be explained by the “salting-out” effect caused by acetate ions (i.e. 1 M).³⁵ It has been previously reported that the LCST of PNIPAM decreases roughly linearly as a function of the acetate anion concentration, thus behaving as a kosmotropic anion.^{36–38} This “salting-out” effect on the LCST behaviour of PNIPAM is thought to be caused by interactions between ions with the polymer and the hydration shell surrounding the polymer

chains.³⁷ Firstly, by the destabilisation of hydrogen bonding between the amide groups and water due to the polarisation caused by the anion. Secondly, by an increasing interfacial tension of the PNIPAM/water molecules due to a high anion concentration. It was also noted that in the absence of acetate ions, the phase transitions of the copolymers were not smooth probably due to the polyampholyte nature of the DM_x macro-CTAs. This suggests that the presence of acetate anions as cosolute provides a more stable phase transition with increasing temperature when using a polyampholyte as shell-forming block. Hence, it is expected that for nanogel formation the presence of acetate ions as cosolute will affect the critical chain length at which the copolymer self-assembles.

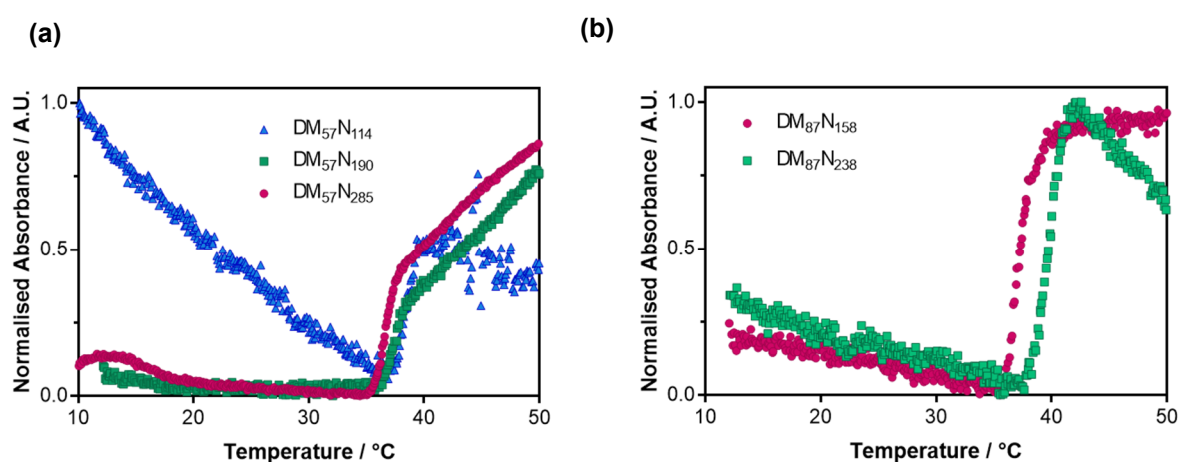


Figure 4.9: Turbidimetry experiments of purified DM_xN_y diblock copolymers in salt-free aqueous solutions at pH 7. Copolymers synthesised from (a) DM_{57} and (b) DM_{87} , where y corresponds to the DP of the PNIPAM block. The cloud points were determined from the inflection point of the normalised absorbance curve at 550 nm on a heating rate of $0.12 \text{ }^\circ\text{C min}^{-1}$.

4.3.2.2. The self-assembly of P(DMAEMA-*co*-MAA)-*b*-PNIPAM copolymers

At pH 5.2, the DMAEMA units are >99% protonated and the MAA units are 83% deprotonated, whereas at pH 7, the protonation of the DMAEMA units is reduced to 94% while the deprotonation of MAA is increased to >99%. Hence, it is expected that the self-assembly of the copolymers is influenced by the higher degree of protonation of the dimethylamino group at pH 5.2 than at pH 7, thus affecting the packing parameter. Additionally, the presence of acetate ions is expected to affect the phase transition of PNIPAM. As judged by DLS, the hydrodynamic size of the self-assembled copolymers was smaller in acetate buffer than in salt-free aqueous solutions for copolymers made from DM₅₇ (Table 4.2 and Figure 4.10). Considering the DM₅₇N₁₉₀ copolymer as an example, this had a narrow size distribution (PDI=0.03) centred at 82 nm in acetate buffer at 50 °C, whilst in water the same copolymer had a broader size distribution (PDI=0.18) and a D_h of 145 nm. As previously discussed, this difference may be attributed to the anion concentration and the overall charge of DM₅₇ at the different pH. Acetate ions shift the PNIPAM LCST to lower temperatures due to the salting-out effect, additionally, counterions can screen the charges present from the acid and basic groups at pH 5.2, which in turn can decrease the shell thickness. In a salt-free aqueous solution, the unscreened charges present at pH 7 can apparently increase the shell thickness, hence particles with larger sizes were estimated by DLS. It is observed from Figure 4.10b that the DM₅₇N₁₁₄ copolymer showed poor self-assembly in a salt-free aqueous solution at pH 7, where two peaks were observed approximately at 50 and 180 nm. Moreover, it is noted that the correlation function breaks up and has a non-linear baseline, which could be an indication of some different aggregation of polymer chains. These results suggest that the length of the PNIPAM block of the DM₅₇N₁₁₄ was not sufficient to stabilise the self-assembled structure in the absence of counterions. Nevertheless, stable aggregated chains were observed as the volume fraction of PNIPAM increased with DM₅₇N₁₉₀ and DM₅₇N₂₈₅ copolymers having monomodal size distributions. Although polyelectrolyte complex formation was feasible due to the presence of deprotonated MAA and protonated DMAEMA units at pH 7, it is noted that indeed the degree of ionisation of PDMAEMA greatly exceeded the small amount of ionised MAA units thus allowing the formation of stable micelles in salt-free aqueous solution. Consequently, it was anticipated that nanogels made from DM₅₄ would be colloidally stable in the absence of a salt at pH 7.

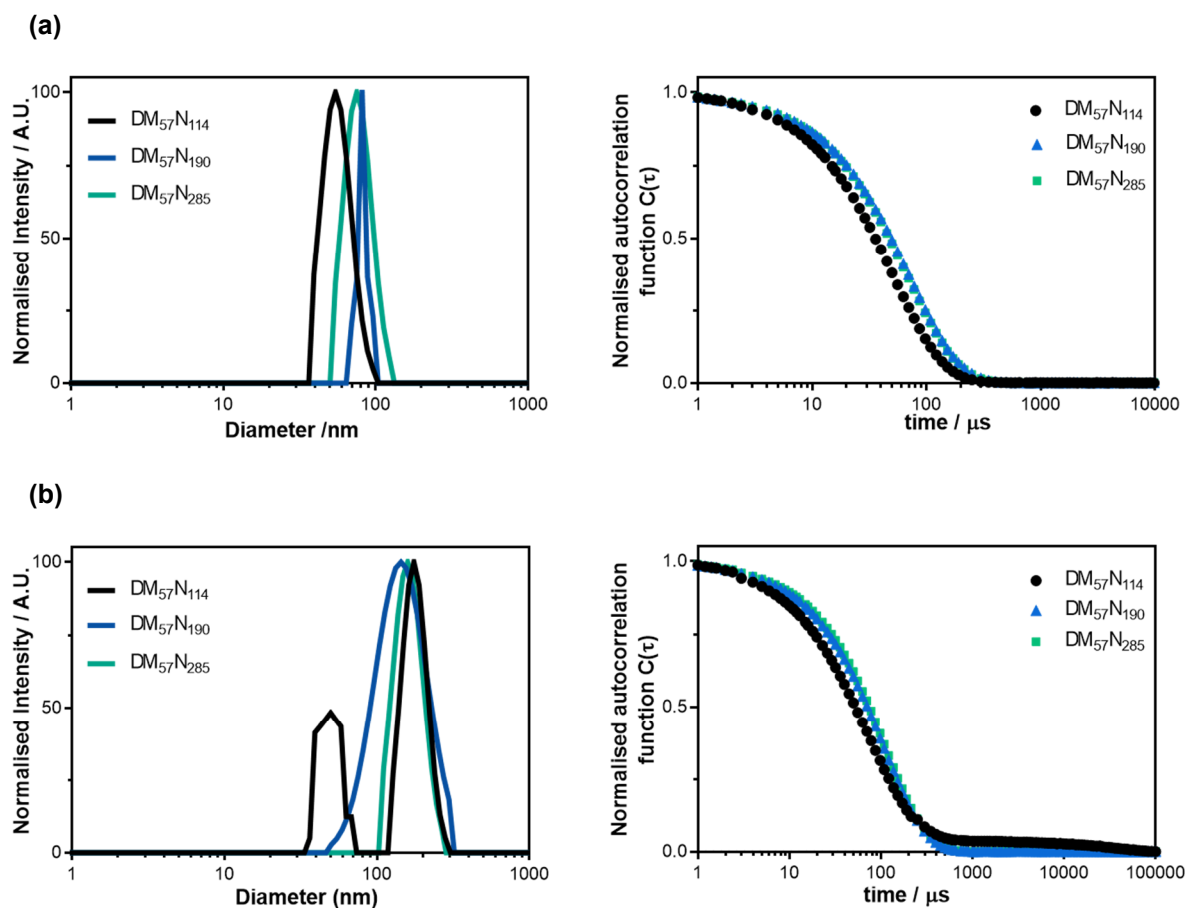


Figure 4.10: MSD size determination studies of the self-assembled $DM_{54}N_y$ diblock copolymers in (a) acetate buffer (1 M, pH 5.2) at 50 °C and (b) DI water at pH 7 and 62.5 °C, where y corresponded to the DP of the PNIPAM block.

Interestingly, the copolymers synthesised from DM_{87} (larger solvophilic block) had a smaller hydrodynamic size when self-assembled in water than in acetate buffer solution (Table 4.2 and Figure 4.11). For instance, the $DM_{87}N_{238}$ copolymer had a narrow size distribution (PDI=0.05) centred at 106 nm in acetate buffer, whereas in a salt-free aqueous solution at pH 7 the same copolymer had a D_h of 57 nm and PDI=0.10. Additionally, this difference in size can be observed clearly in the correlation functions, where the correlation function of the aggregates of smaller size decays quicker than the bigger aggregated particles. An explanation can be found in the different packing parameter of the copolymer chains in a buffer solution at pH 5.2 than in a salt-free aqueous solution at pH 7. Due to the screening of charges, more copolymer chains can aggregate into micelles in an acetate buffer solution. However, the shell-stabiliser block should have a greater area in a salt-free solution due to the unscreened Coulomb repulsion mainly from the protonated DMAEMA units. Considering that DM_{87} is longer than DM_{57} , a greater electrostatic contribution can influence the self-assembly process. Generally, as the electrostatic repulsions are increased, fewer copolymer chains aggregate into micelles thus forming smaller particles.^{39,40}

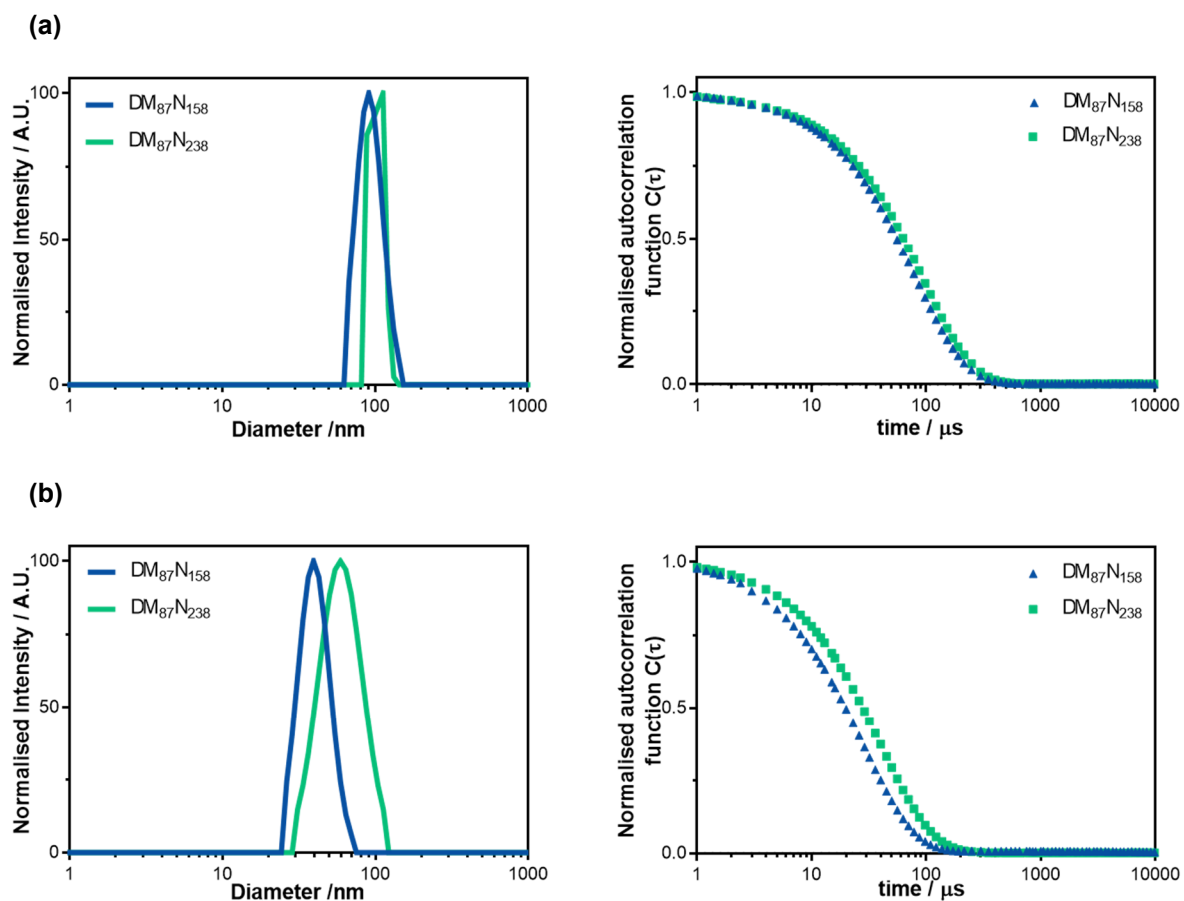
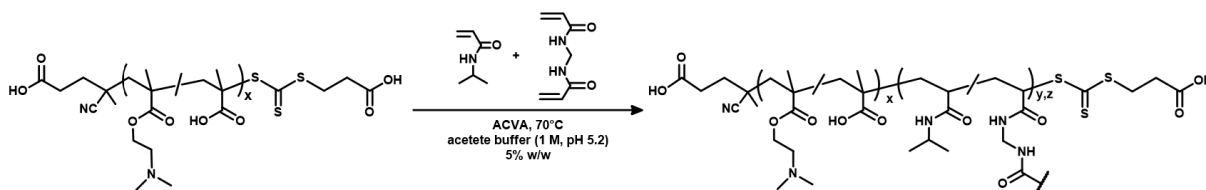


Figure 4.11: MSD size determination studies of the self-assembled DM_{87}N_y diblock copolymers in (a) acetate buffer (1 M, pH 5.2) at 50 °C and (b) DI water at pH 7 and 62.5 °C, where y corresponded to the DP of the PNIPAM block.

These preceding observations served as reference for understanding the nanogel formation using a polyampholyte macro-CTA as it will be shown below.

4.3.3. Synthesis of P(DMAEMA-*co*-MAA)-*b*-P(NIPAM-*st*-BIS) nanogels

Similar to the synthesis of diblock copolymers, P(DMAEMA-*co*-MAA)-*b*-P(NIPAM-*st*-BIS) nanogels were synthesised *via* RAFT dispersion polymerisation of NIPAM but in the presence of BIS as a crosslinker. The DM₅₇ macro-CTA was chain-extended with NIPAM and BIS in an acetic acid/acetate buffer solution (1 M, pH 5.2) in a one-step synthesis (Scheme 4.2). The reactions were stopped after approximately 18 hours and high monomer conversion (>92%) was achieved on average as estimated by gravimetric analysis. The full list of the properties of the synthesised nanogels can be found in Table 4.3 and these results will be discussed in detail in Section 4.3.3.1 and 4.3.3.2. After purification, the size and shape of the nanogels was investigated by DLS and TEM studies. At a neutral pH, all the nanogels had an overall positive charge as determined by ζ -potential measurements.



Scheme 4.2: The synthesis of P(DMAEMA-*co*-MAA)_x-*b*-P(NIPAM-*st*-BIS)_{y,z} nanogels *via* RAFT aqueous dispersion polymerisation. Note: Under the reaction conditions, the amino groups are mainly protonated, and the carboxylic groups are minorly deprotonated.

A notation is used henceforth to symbolise the nanogel composition (DM_xN_yB_z). Hence, DM_x, N_y and B_z symbolises P(DMAEMA-*co*-MAA)_x-*b*-P(NIPAM-*st*-BIS)_{y,z}, where x, y and z are the DP of each monomer.

Table 4.3: Summary of the synthesis and properties of the DM_xN_yB_z nanogels.

Target composition [DM _x]:[NIPAM]:[BIS] ^a	Conversion ^b %	DP _{,theo} ^c	$\bar{M}_{n,theo}$ ^d kDa	D_h / nm (PDI) ^e	ζ - Potential ^f mV	
x=57	[1]:[115]:[3]	96	110	21.3	72 (0.08)	22
	[1]:[191]:[3]	98	187	30.0	100 (0.05)	14
	[1]:[287]:[3]	92	265	38.9	127 (0.10)	12
x=87	[1]:[159]:[3]	77	123	26.7	49 (0.13)	19
	[1]:[238]:[3]	90	214	37.0	62 (0.14)	17

^aGeneral reaction conditions: Targeted [DM_x]/[ACVA]=5, solids content 5% w/w in acetate buffer at 70 °C for 18 h. ^bGravimetric determination by moisture analysis of solids content against predicted solids content. ^cEstimated by [NIPAM]/[DM_x] \times conversion. ^dCalculated by $\bar{M}_n = M_{CTA} + (\varphi)M_1 + (x-\varphi)M_2 + yM_3 + zM_4$, where M_{CTA} is the molar mass of the CTA end groups, φ the DP of PDMAEMA, x the DM macro-CTA DP, y and z are the DPs of NIPAM, and BIS respectively, and M_1 , M_2 , M_3 , and M_4 are the molar masses of the corresponding monomer unit. ^eDLS data obtained from 0.1% w/w nanogel aqueous dispersions at pH 7 and 25 °C. ^fMeasurements in DI water with 1 mM KCl background electrolyte at pH 7 and 25 °C.

4.3.3.1. The effect of the DP of the core-forming block on the size of the cationic nanogels

First, the DM_{57} was chain extended with varying ratios of NIPAM at a fixed molar ratio of BIS to DM_{57} of 3:1. Three nanogel dispersions were synthesised by targeting a PNIPAM DP of 115, 191 and 287. Like the PAA-*b*-P(NIPAM-*st*-BIS) nanogels, the colour of the crude dispersions of PDMAEMA-based nanogels varied accordingly to the volume fraction of PNIPAM with smaller particles seemingly produced for nanogels with a shorter PNIPAM DP (Figure 4.12a). After purification by dialysis against water, the $DM_{57}N_{187}B_3$ and $DM_{57}N_{285}B_3$ nanogel dispersions remained as heterogeneous dispersions suggesting the formation of crosslinked particles. The gradual size change with increasing DP of PNIPAM agreed with DLS and transmission electron microscopy (TEM) studies.

The average hydrodynamic particle diameter (D_h) of the purified nanogel dispersions was determined by DLS first at a constant temperature of 25 °C and at neutral pH. As judged by the size distributions and the autocorrelation curves of these nanogels (Figure 4.12b and c, respectively), nanogel formation was feasible using a polyampholyte macro-CTA. This suggests that the reaction took place within the *in situ* self-assembled growing PNIPAM chains stabilised by the highly charged and hydrophilic DM_{54} macro-CTA. During polymerisation, the presence of counterions from the acetate buffer solution helped screening both positive and negative charges along the DM_x macro-CTA, thus allowing the synthesis of defined nanogel particles. This idea is supported by the narrow size distributions of the nanogels ($PDI < 0.1$) obtained by DLS in water at pH 7. Additionally, as suggested by cloud point measurements of the DM_xN_y copolymers, the decreased solubility of the growing PNIPAM chains in the presence of acetate ions (1 M) should have influenced the nucleation process and assist in the formation of crosslinked particles with an apparently PNIPAM core. It is noted from Figure 4.12b that the D_h of the nanogels gradually increased from 72 to 127 nm with increasing DP of the PNIPAM block and therefore a larger volume fraction of the presumably core of the particles. From the correlogram, it is clearly observed that the single correlation function decays quicker for the smaller particles ($DM_{57}N_{110}B_3$) than those with greater size ($DM_{57}N_{265}B_3$) (Figure 4.12c). The particle sizes are shown in a lognormal plot in Figure 4.12b. However, examples of size distributions by intensity, volume, and by number of this series of nanogels is shown in Appendix C (Figure 4C.9), where it is seen that the D_h size as determined by intensity, volume, and number was similar and that the average size distributions were monomodal.

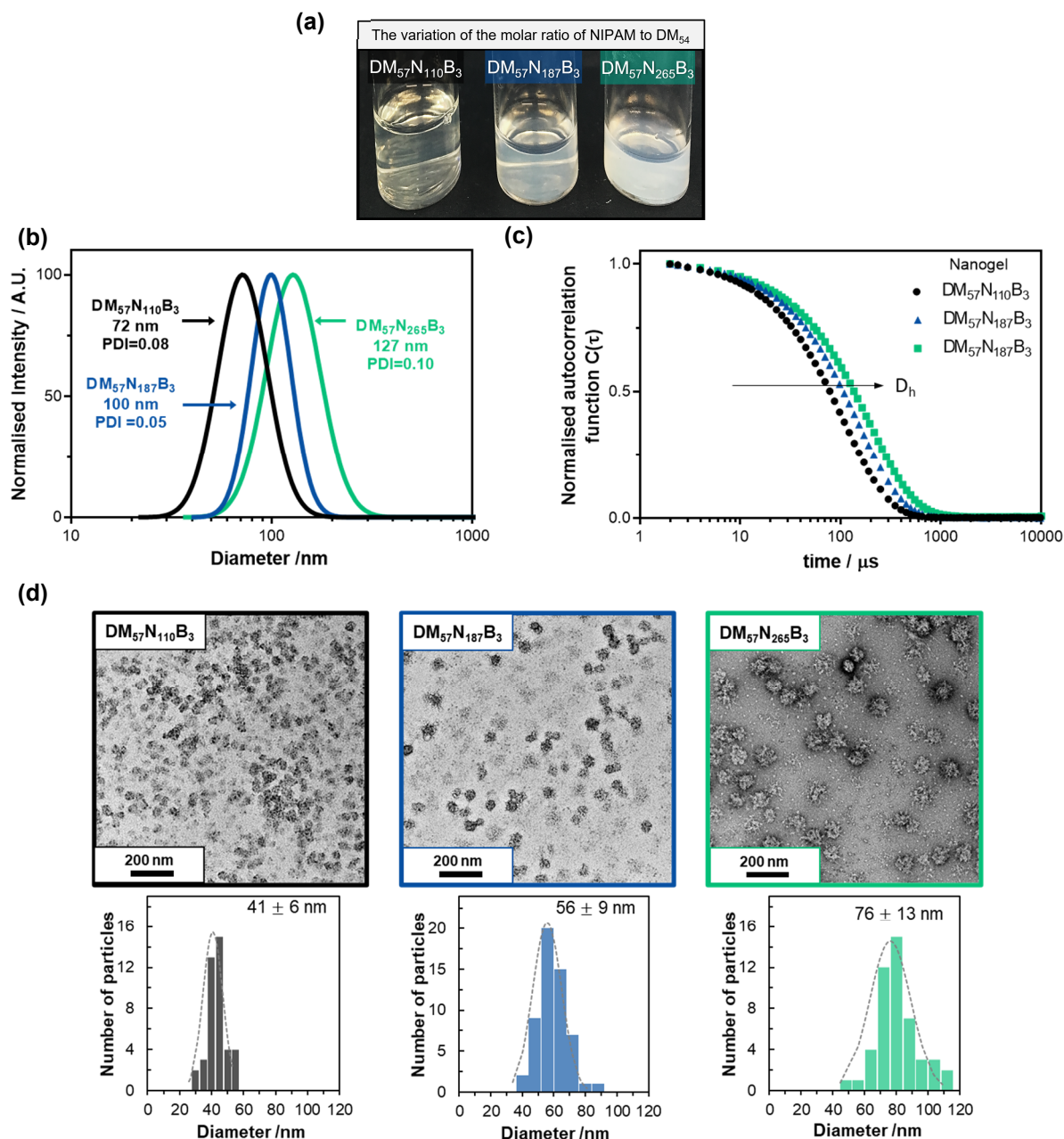


Figure 4.12: Size determination of the $DM_{57}N_yB_3$ nanogels. (a) Digital photograph of the crude nanogel dispersions. (b) Intensity average lognormal size distribution curves ($n=4$) and (c) their respective autocorrelation functions with time at 25 °C, and (d) TEM micrographs of the purified nanogels with their number particle size distributions. Data obtained from 0.1% w/w purified nanogel dispersions in DI water at pH 7 and 25 °C. Uranyl formate (0.75% w/v) was used as the TEM stain.

In agreement with DLS data, a correlation between the dehydrated mean TEM diameter (D_{TEM}) and the target PNIPAM block DP was observed as determined by TEM studies. For example, the $DM_{57}N_{110}B_3$ nanogel had a D_{TEM} of 41 ± 6 nm whereas the $DM_{57}N_{265}B_3$ had D_{TEM} of 76 ± 13 nm. In terms of shape, it was noted that these were semi-spherical despite the increasing volume fraction of PNIPAM in the core of the nanogels, analogously to the anionic PAA-*b*-P(NIPAM-*st*-BIS) nanogels. As stated in Chapter 2, an early crosslinking could prevent the reorganisation of the

growing chains, which can lead to kinetically trapped micellar spheres. However, a highly charged macro-CTA solvated by counterions can also influence the packing parameter thus forming spheres with increasing volume fractions of PNIPAM.^{41,42} In the case of the $DM_{57}N_{265}B_3$ nanogel, analysis of TEM micrographs suggests some inter-particle crosslinking between the growing micellar aggregates during polymerisation.

It is worth mentioning that the surface of the nanogels looked patchy, which could suggest nanoscale phase separation (Figure 4.13). This may be attributed to the presence of two oppositely charged polyelectrolytes within the shell of the particles at pH 7. Müller *et al.*⁴³ showed that a variety of micellar aggregates with a compartmentalised shell can be formed after modification by hydrolysis or quaternisation of polybutadiene-*b*-poly(*tert*-butyl methacrylate)-*b*-poly(2-(dimethylamino)ethyl methacrylate) (PB-*b*-PtBMA-*b*-PDMAEMA) ABC triblock terpolymers. Using cryo-TEM, they identified the formation of intramicellar interpolyelectrolyte complexes (*im*-IPECs) formed between PMAA and quaternised PDMAEMA in the shell of the particles. Although, the length of PDMAEMA (DP 285) and PMAA (DP 200) of their terpolymers was considerably greater than the one used in this work, some compartmentalisation in the shell could have been feasible herein due to the asymmetric gradient-like macro-CTA. A continuous change in composition along the chains in gradient copolymers leads to the formation of various microphase domains.⁴⁴ However, another technique such as small angle X-ray scattering could provide more information about the actual structure of these nanogels.

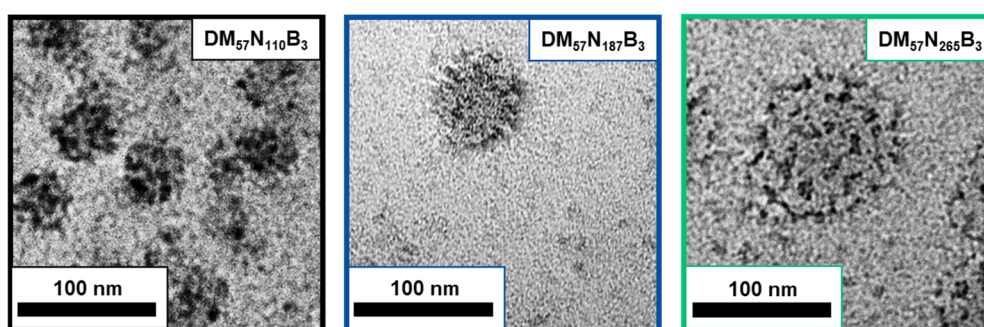


Figure 4.13: Enlargement of TEM micrographs of the $DM_{57}N_yB_3$ nanogels.

4.3.3.2. The effect of the length of the shell stabilizer block on the size of the cationic nanogels

The formation of nanogels using the DM₈₇ macro-CTA was conducted at 5% w/w in acetate buffer (1 M, pH 5.2), by following the chain extension reaction of DM₈₇ with NIPAM and BIS shown in Scheme 4.2. The comparison of nanogel size measurements of nanogels prepared from DM₅₇ and DM₈₇ with similar PNIPAM volume fraction is shown in Figure 4.14. It is observed that nanogels with smaller sizes were obtained when using DM₈₇ than with the shorter macro-CTA (DM₅₇). For instance, the DM₈₇N₁₂₃B₃ had a D_h of 49 nm at an aqueous dispersion pH of 7, whilst the DM₅₇N₁₁₀B₃ nanogel had a D_h of 72 nm under similar conditions (Figure 4.14a and b). However, the DM₈₇N₁₂₃B₃ nanogel displayed a broader size distribution (PDI=0.13) than the DM₅₇N₁₁₀B₃ nanogel (PDI=0.08).

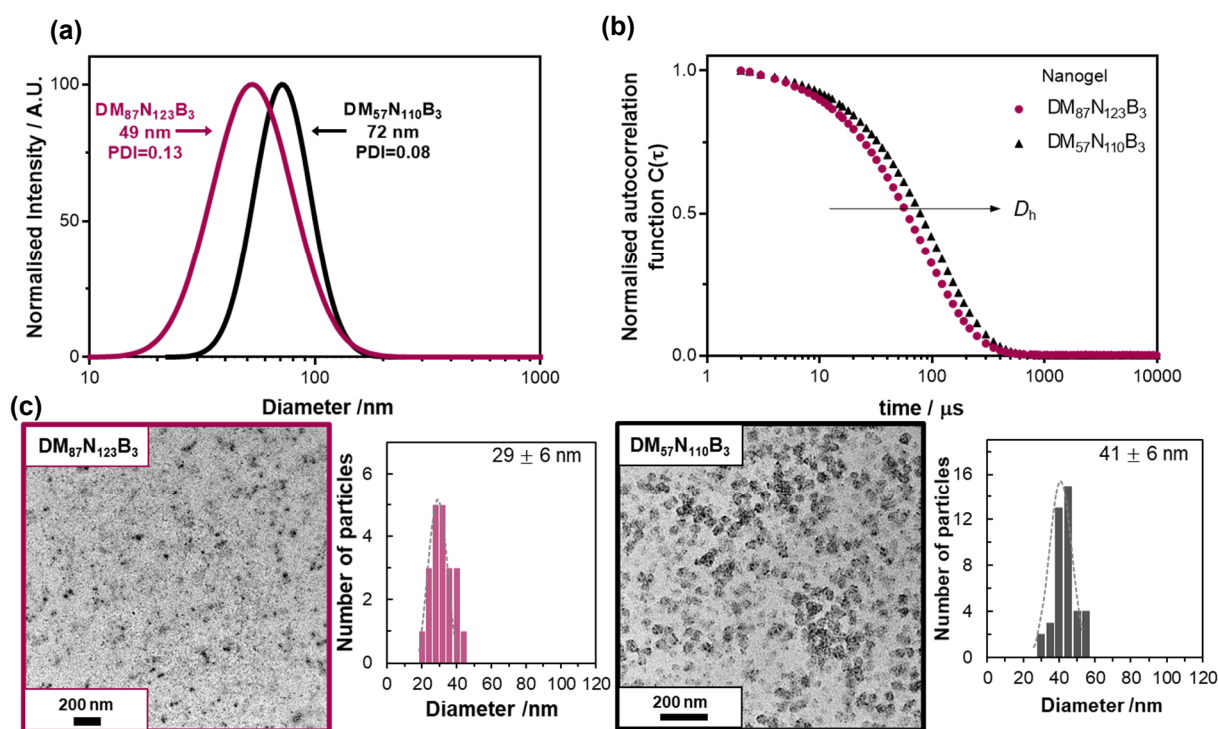


Figure 4.14: Size determination of the DM₈₇N₁₂₃B₃ and DM₅₇N₁₁₀B₃ nanogels. (a) Intensity average lognormal size distribution curves ($n=4$) and (b) their respective autocorrelation functions with time at 25 °C, and (c) TEM micrographs of the purified nanogels with their number particle size distributions. Data obtained from 0.1% w/w purified nanogel dispersions in DI water at pH 7 and 25 °C. Uranyl formate (0.75% w/v) was used as the TEM stain.

TEM studies showed the same decrease in size between the DM₈₇N₁₂₃B₃ and the DM₅₇N₁₁₀B₃ nanogel (Figure 4.14c). This is a striking difference from the PAA-*b*-P(NIPAM-*st*-BIS) nanogels presented in Chapter 2, where the use of a longer macro-CTA gave larger particles. This difference could be attributed to the different formulation, e.g. solvent, chemical nature of the

macro-CTA, ionic strength, which influences the packing parameter.⁴⁵ In this series of nanogels, it appears that an interplay between the length of the macro-CTA and the effect of the counterions on both the macro-CTA and the growing PNIPAM chains affected the packing parameter. Considering that the DM_xN_y copolymers had cloud points around 15-17 °C in acetate buffer solution (1 M, pH 5.2), the critical length at which self-assembly occurred would have been reached early in the polymerisation. Additionally, the counter-ion cloud surrounding the macro-CTA chain would subtly increase the volume fraction of the solvophilic DM_{87} block compared to the solvophobic block, which could have affected the aggregation of the copolymer chains. A large electrostatic contribution can lead to the aggregation of fewer copolymer chains into micelles thus forming smaller particles.^{39,40}

A similar decrease in size was noted between the DM_{87} and DM_{57} -nanogels synthesised targeting a greater volume fraction of NIPAM (Figure 4.15a and b). For example, the D_h decreased from 100 nm for $DM_{57}N_{187}B_3$ to 62 nm for $DM_{87}N_{214}B_3$. As Figure 4.15c shows, size studies by TEM analysis showed a similar size reduction trend as DLS studies, where the D_{TEM} decreased from 56 ± 9 nm for $DM_{57}N_{187}B_3$ to 44 ± 7 nm for $DM_{87}N_{214}B_3$.

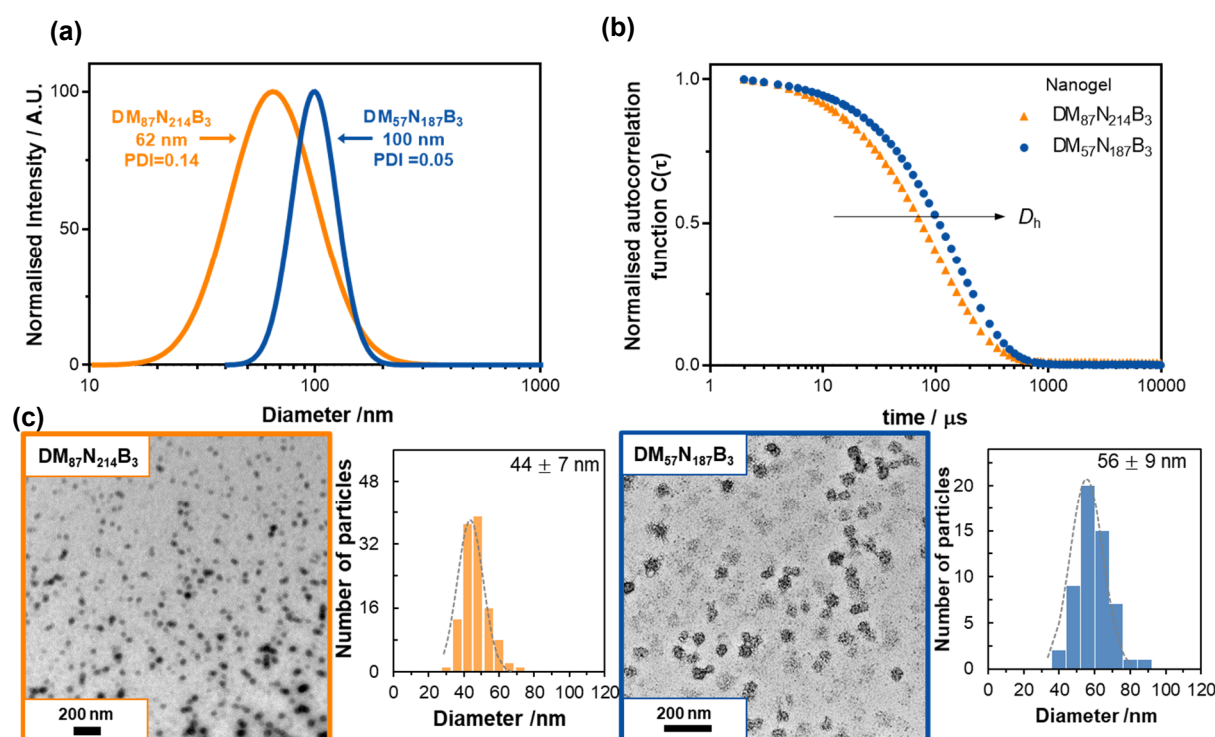


Figure 4.15: Size determination of the $DM_{87}N_{214}B_3$ and $DM_{57}N_{187}B_3$ nanogels. (a) Intensity average lognormal size distribution curves ($n=4$) and (b) their respective autocorrelation functions with time at 25 °C, and (c) TEM micrographs of the purified nanogels with their number particle size distributions. Data obtained from 0.1% w/w purified nanogel dispersions in DI water at pH 7 and 25 °C. Uranyl formate (0.75% w/v) was used as the TEM stain.

4.3.4. The temperature behaviour of cationic nanogels

As presented in Chapter 3, PAA-*b*-P(NIPAM-*st*-BIS) nanogels normally exhibit a volume phase transition temperature (VPTT) which depends on a fine balance between hydrophilic and hydrophobic contributions. Herein, the temperature-dependent size changes of the $DM_xN_yB_z$ nanogels was investigated by DLS experiments over the temperature range of 12.5 to 60 °C. The D_h of the nanogels was determined in salt-free aqueous nanogel dispersions (0.1% w/w) at pH 7. First, the temperature phase transitions of the $DM_{57}N_yB_3$ nanogels were determined (where $y=110, 187$ and 265) to observe the effect of the volume fraction of PNIPAM on the VPTT. Estimated VPTT values were determined using Equation 3.1, where the shrunken size was the lowest D_h value measured during the heating up ramp. Figure 4.16a, and b shows the temperature-dependent DLS experiments where, in all cases a reduction in the nanogel size was observed as the temperature increased up to around the VPTT.

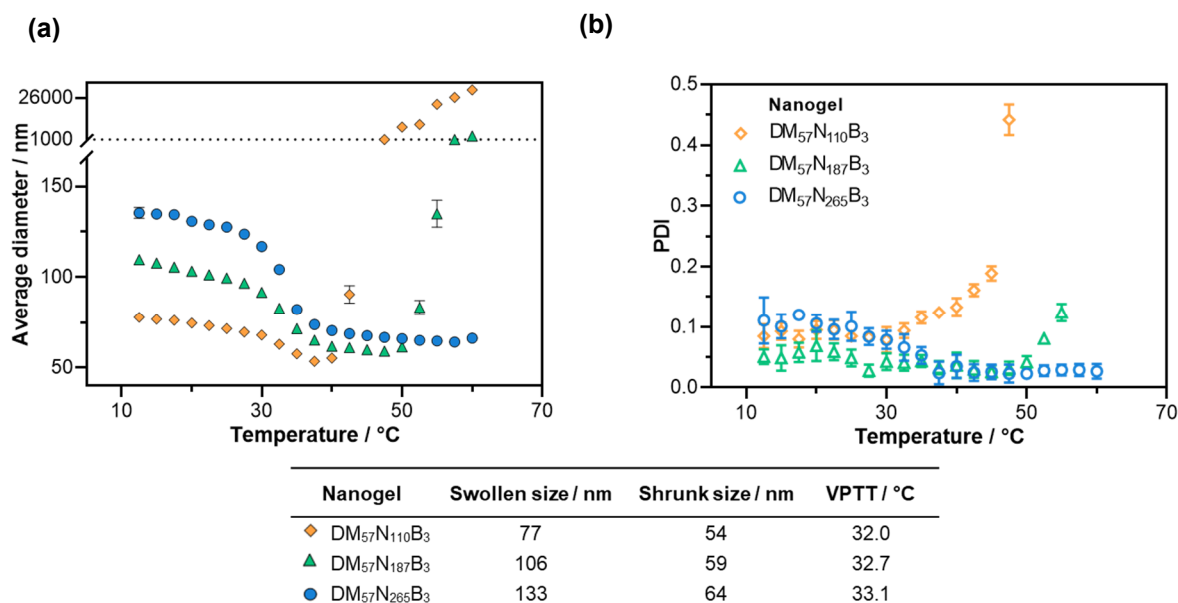


Figure 4.16: DLS studies on the deswelling behaviour of $DM_{57}N_yB_3$ nanogels where $y=$ (◇) 110, (▲) 187, and (●) 265. (a) The hydrodynamic diameter as a function of temperature, (b) their corresponding PDI values versus temperature ($n=3$). Data obtained from 0.1% w/w nanogels dispersions in DI water at pH 7.

In contrast to the observations presented in Chapter 2, the presence of the hydrophilic block did not shift the VPTT values considerably, which were similar to the reported values of the VPTT of PNIPAM at around 32 °C.⁴⁶ It was noted that nanogels with lower PNIPAM volume fractions apparently increased in size upon further heating. For instance, the nanogel with the lowest PNIPAM volume fraction ($DM_{57}N_{110}B_3$) became very unstable above the VPTT with a sharp size

increase above 38 °C indicative of flocculation. The $DM_{57}N_{187}B_3$ nanogel showed similar behavior but did not start to flocculate until above 50 °C. Conversely, the nanogel with the highest PNIPAM volume fraction ($DM_{57}N_{265}B_3$) remained colloiddally stable within the temperature range tested. Since the temperature-responsive behaviour of the nanogels at neutral pH varied for all the samples, the deswelling ratio was not determined here as it was for the PAA-*b*-P(NIPAM-*st*-BIS) nanogels.

The instability seen with lower volume fractions of PNIPAM could be attributed to the corona of the nanogels, since PDMAEMA is also a thermoresponsive polymer. This behaviour, however, was unexpected since at 25 °C and pH 7 ζ -potential measurements showed that the nanogel particles had an overall positive charge (ζ -potentials of 22-12 mV; Table 4.3). Thus, some stability from charge repulsion was expected. An explanation can be found in the greater surface area that smaller particles have per unit volume. Hence, a greater effect of the DM_{57} macro-CTA possibly affected the stability of the particles due to an enhanced concentration effect. In the literature, it is reported that at a fixed pH, as the PDMAEMA concentration increases the cloud point decreases.⁴⁷ To prove this, UV-vis spectroscopy experiments were conducted to show that an increasing concentration from 1 to 10 w/w% of the DM_{57} macro-CTA in aqueous solutions (pH 8.9 > pK_{a2}) can shift the cloud point temperature from 60 to 54 °C, respectively (Figure 4.17). Hence, at higher concentrations, the DM_{57} macro-CTA becomes insoluble at lower temperatures.

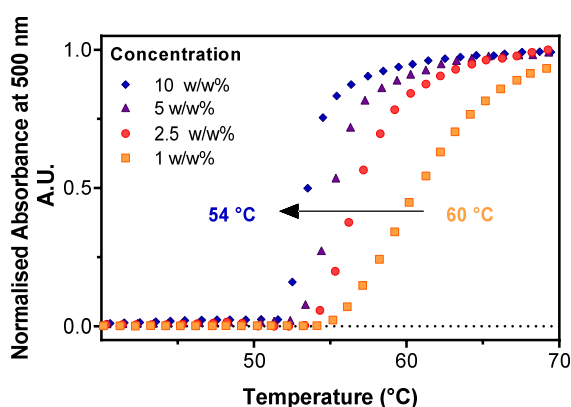


Figure 4.17: Effect of the copolymer concentration on the cloud point of DM_{57} copolymer at pH 8.9. The cloud points were determined from the inflection point of the normalised absorbance curve at 500 nm on a heating rate of 0.12 °C min⁻¹.

The effect of a higher volume fraction of the solvophilic block on the temperature behaviour of $DM_{87}N_yB_3$ nanogels was also investigated, where $y=123$ and 214 . Figure 4.18a, and b shows the temperature-dependent DLS studies. Overall, the same trend was observed with the nanogels becoming colloiddally unstable and flocculating above the VPTT due to the thermoresponsive behaviour of PDMAEMA. However, due to the small size of this series of nanogels smaller flocs were formed than those nanogels prepared with the shorter DM_{57} macro-CTA. In contrast to the DM_{57} -based nanogels, the VPTT was apparently shifted to higher temperatures when using the DM_{87} macro-CTA probably due to a higher hydrophilic contribution of the longer DM_{87} block. For instance, the $DM_{87}N_{123}B_3$ had a VPTT of $36\text{ }^\circ\text{C}$ in an aqueous solution (pH 7), whereas at a higher PNIPAM volume fraction ($DM_{87}N_{214}B_3$) a lower VPTT of $34\text{ }^\circ\text{C}$ was determined.

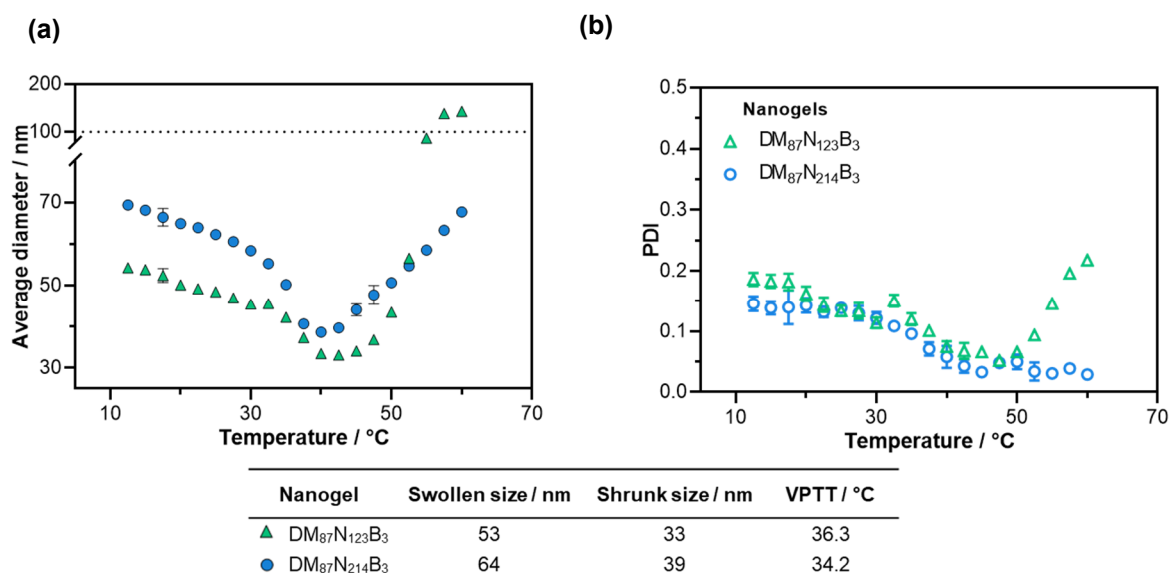


Figure 4.18: DLS studies on the deswelling behaviour of $DM_{87}N_yB_3$ nanogels where $y= (\blacktriangle)$ 123 and (\bullet) 214. (a) The hydrodynamic diameter as a function of temperature, (b) their corresponding PDI values versus temperature ($n=3$). Data obtained from 0.1% w/w nanogels dispersions in DI water at pH 7.

4.3.5. The pH responsive behavior of the cationic nanogels

As has been described above, the P(DMAEMA-*co*-MAA) macro-CTA is both pH and temperature responsive and, hence, nanogels made from it should inherit this dual response. The effect of the pH on the size and ζ -potential was investigated for the DM₅₇N₂₆₅B₃ nanogel, as it was shown to be the more stable of the synthesised nanogels under neutral pH conditions. Considering that the nanogel possesses a core that is merely sensitive to temperature and not to pH, changes in size at the same temperature but different pH can be attributed to conformational changes of the polyampholyte, which is presumably on the shell of the nanogels. The feasibility for deprotonation of the methacrylic acid and the protonation of the dimethylamino groups gives the opportunity to create both positive and negative charges along the shell depending on the specific pH. Hence, at $\text{pH} < \text{p}K_{\text{a}1}$ the DM₅₇ polyampholyte would have a net positive charge from the protonated amine group, e.g. at pH 3 the DMAEMA units are fully protonated and the MAA units are 3% deprotonated. When the pH is between $\text{p}K_{\text{a}1}$ and $\text{p}K_{\text{a}2}$ both positive and negative charged groups would coexist, but an overall net positive charge would be present due to the much higher concentration of DMAEMA in the polymer, e.g. at pH 7 the DMAEMA units are 94.1% protonated and the MAA units are >99% deprotonated. However, at highly basic pH ($\text{pH} \gg \text{p}K_{\text{a}2}$) the amine group is considerably less protonated, and the carboxylate groups would likely provide a net negative charge to the particles, e.g. at pH 10 the DMAEMA units are 6% protonated and the MAA units are fully deprotonated.

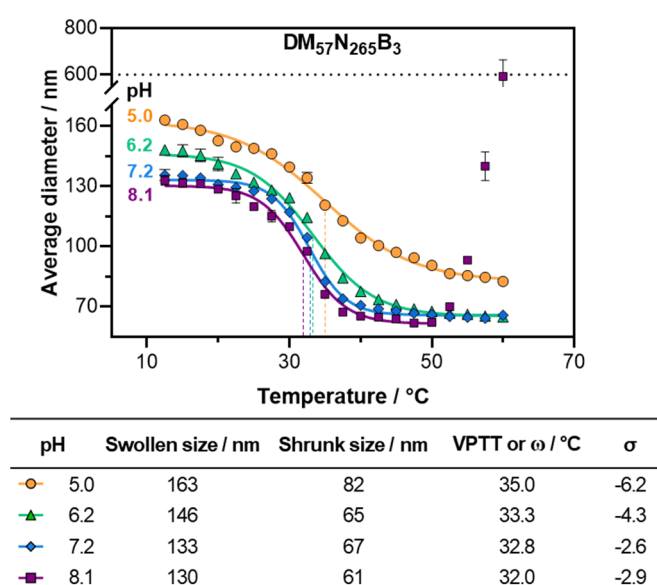


Figure 4.19: DLS studies on the deswelling behaviour of DM₅₄N₂₅₂B₃ nanogel with pH. Data obtained from 0.1% w/w nanogels aqueous dispersions at pH 7.

Figure 4.19 shows the effect of the temperature and pH on the deswelling behaviour of the $DM_{57}N_{265}B_3$ nanogel. Similar to the PAA-*b*-P(NIPAM-*st*-BIS) nanogels, when the $DM_{57}N_{265}B_3$ nanogel was fully ionised the VPTT was shifted to higher temperatures. For example, the VPTT was shifted from 32 °C at pH 8.1 (55.7% protonation of DMAEMA units) to 35 °C at pH 5.0 (99.4% protonation of DMAEMA units). An explanation can be found in the higher hydrophilicity and increased osmotic pressure that ionised groups provide to the nanogel. Consequently, in a more acidic pH, the $DM_{57}N_{265}B_3$ nanogel had a lower hydrophobic contribution (higher VPTT) and the phase transition was less sharp (i.e. higher σ values). It is also noted from Figure 4.19 that in the swollen state ($T < VPTT$) the D_h gradually increases as the pH is decreased. For instance, the nanogels have an apparent swollen size of 163 nm at pH 5.0, whilst in a basic pH of 8.1 it had a compacted size of 130 nm. Upon heating, these nanogels deswell in all the pH tested. However, the colloidal stability of the $DM_{57}N_{265}B_3$ nanogel at pH 8.1 was lost above 50 °C, where flocculation occurred. It is important to highlight that a dispersion pH of 8.1 is around the apparent pK_{a2} of 8.2, i.e. 55.7% DMAEMA units were protonated and the MAA units were 99.8% deprotonated. At this basic pH, ζ -potential was near the net zero charge (isoelectric point) (Figure 4.20b). This suggests the interchain electrostatic attraction from the cationic and anionic units from the polyampholyte which led to a charge-neutral shell at around pH 8.1. Since the nanogel was colloidally stable when swollen and shrank up to 50 °C, it is suggested that flocculation occurred due to the temperature-responsive nature of PDMAEMA.

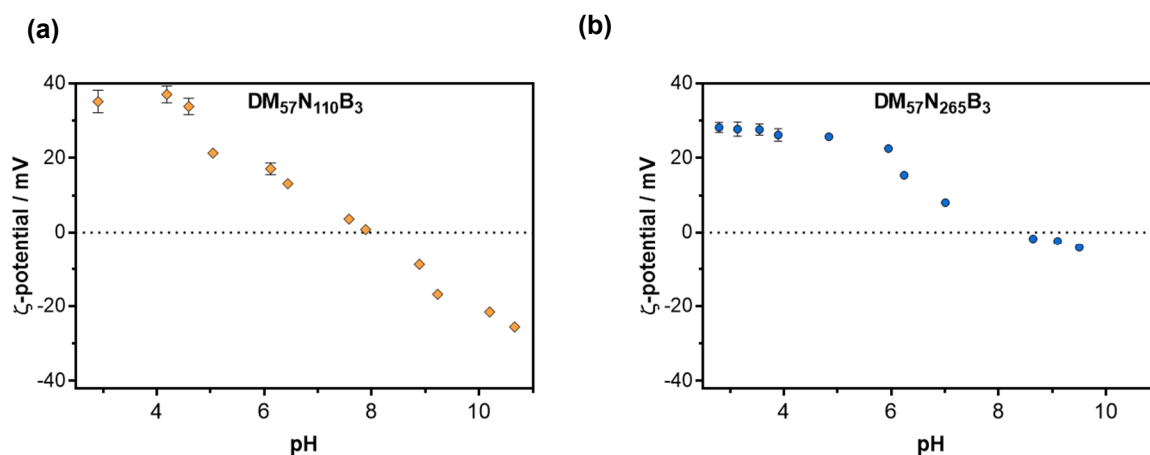


Figure 4.20: Effect of the pH on the ζ -potential of the (a) $DM_{57}N_{110}B_3$ and (b) $DM_{57}N_{265}B_3$ nanogels. Data obtained from 0.1% w/w nanogels dispersions in DI water at 1 mM KCl background electrolyte at 25 °C.

The pH-dependent electrophoretic mobility of the DM_{57} -based nanogels was investigated at 25 °C using 1 mM KCl as the background electrolyte and the ζ -potential was derived from the Smoluchowski approximation. Figure 4.20 shows the effect of the pH on the ζ -potential of

nanogels with different PNIPAM volume fractions ($DM_{57}N_{110}B_3$ and $DM_{57}N_{265}B_3$). It is evident from the plots that pH had a significant effect on the charge of the nanogels. In both cases, the ζ -potential of the nanogels was positive in acidic pH but became negative at a dispersion pH above the apparent pK_{a2} of 8.2 of the DM_{57} macro-CTA. In the range of pH 2.4 to 4.8, ζ -potentials were approximately constant with values of 35 mV for $DM_{57}N_{110}B_3$ and 27 mV for $DM_{57}N_{265}B_3$. Hence in acidic pH, as previously stated, the overall net charge is given by the protonated amine groups over the deprotonated carboxylate groups from MAA. With increasing pH, ζ -potentials became less positive due to the deprotonation of the amine groups and reached the net zero charge (isoelectric point) at pH 7.9 for $DM_{57}N_{110}B_3$ and pH 8.4 for $DM_{57}N_{265}B_3$. Above the isoelectric point, ζ -potentials became progressively negative with increasing pH reaching a value of around -17 mV for $DM_{57}N_{110}B_3$ and -3 mV for $DM_{57}N_{265}B_3$ at around pH 9.2. The negative ζ -potentials were likely to be due to the presence of the deprotonated carboxylate moieties, since at this pH MAA units are fully deprotonated and DMAEMA units are 9.1% protonated. Interestingly, much larger ζ -potentials were obtained for nanogels with lower PNIPAM volume fractions, which may be related to a greater charge build-up on the surface of the nanogels with lower PNIPAM content. In the case of the intermediate size nanogel ($DM_{57}N_{187}B_3$), ζ -potentials were in between the values of the other two samples, e.g. 31 mV in the pH range of 2.4 to 4.8, and -7 mV at pH 9.2 (Appendix C; Figure 4C.10).

4.3.6. Effect of solution ionic strength on the properties of cationic nanogels

As previously shown, the cloud point temperature of the P(DMAEMA-*co*-MAA)-*b*-PNIPAM copolymers was shifted to lower temperatures in the presence of acetate ions. To investigate the effect of the ionic strength of the solution on the crosslinked analogue, the $DM_{57}N_{265}B_3$ nanogels were redispersed in the acetate buffer solution used during its synthesis. Figure 4.21 shows the effect that the ionic strength had on the same nanogel in mildly acidic pH at 25 °C. Overall, it can be seen that the nanogel seemingly reduces in size in the presence of acetate ions. For instance, in a salt free/low ionic strength solution the nanogel had a D_h of 149 nm, whilst in acetate buffer a D_h of 96 nm was determined. Figure 2.21b shows the correlation function single decay of the correlation functions of $DM_{57}N_{265}B_3$ nanogel in different media, where in acetate buffer the signal decays quicker than in water due to reduction of the nanogel size in the presence of acetate ions. Moreover, a narrower size distribution was observed in acetate buffer (PDI of 0.047 versus 0.124) probably due to the “salting out” effect which excludes water also from the PNIPAM core and,

thus compacting the nanogel structure.

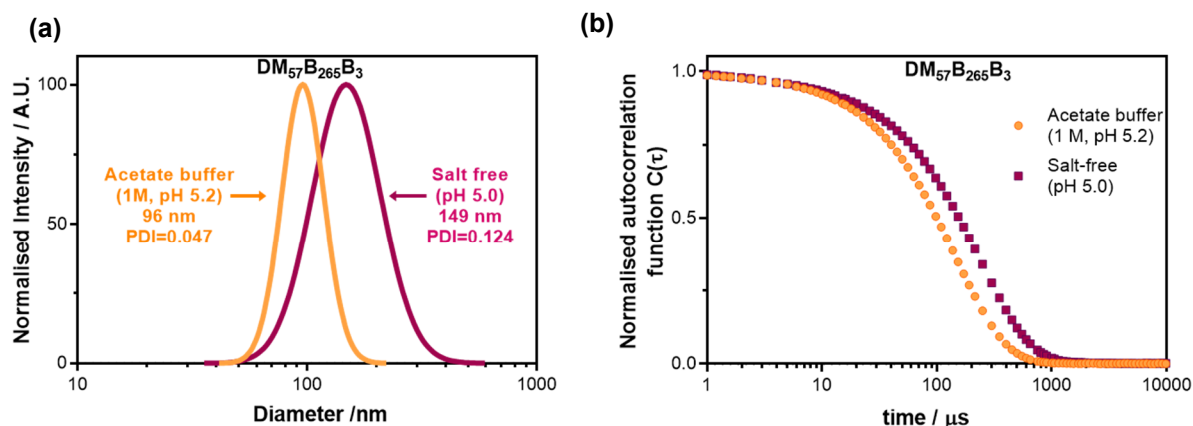


Figure 4.21: DLS studies on the effect of dispersions ionic strength of $DM_{57}B_{265}B_3$ nanogel in (●) acetate buffer (1 M, pH 5.2) and (■) salt-free aqueous dispersion (pH 5.0).

Since the addition of a kosmotropic anion at relatively high concentrations can also affect the solubility of the PNIPAM core, the sensitivity of the polyampholyte to salts was assessed under milder conditions. Given that DMAEMA-based materials as well as PMAA polymers are sensitive to salts,^{48–51} the effect of adding NaCl or CaCl₂ to an aqueous nanogel dispersion was investigated at the same ionic strength ($\mu=45$ mM) at pH 7. It is evident from Figure 4.22 that, in the swollen state, the size of the nanogels was almost unaffected by the salt addition. An explanation can be found in the reduced net charge of the nanogel at pH 7, as seen in the ζ -potential measurements, meaning that the charge screening from the salt has minimal effect. For example, when no salt was added the nanogel had a D_h of 128 nm, while in CaCl₂ a D_h of 124 nm and in NaCl a D_h of 120 nm at 25 °C. The results also indicate that the screening of charges by salt addition led to flocculation of the nanogels upon heating. However, a greater disruption of the colloidal stability of the nanogels was achieved with NaCl than CaCl₂.

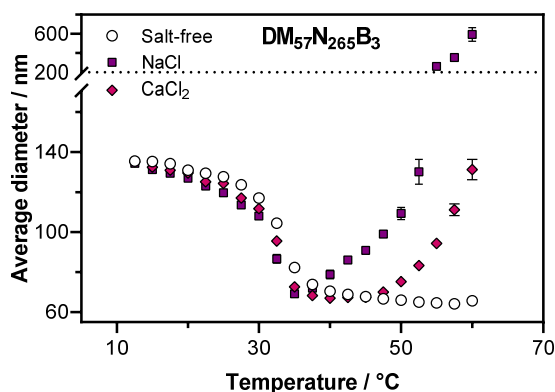


Figure 4.22: DLS studies on the addition of NaCl and CaCl₂ to $DM_{57}N_{265}B_3$ nanogel at 45 mM ionic strength. Data obtained from 0.1% w/w nanogels dispersion in DI water at pH 7.2.

4.4. Conclusions

In this chapter, it has been highlighted the synthesis and properties of cationic nanogels formed *via* RAFT dispersion polymerisation. During the synthesis of the PDMAEMA-based macro-CTA using RAFT solution polymerisation in acetate buffer, it was found that DMAEMA monomer was converted into polymer and hydrolysed into DMEA and MAA. Kinetic studies showed that MAA was gradually incorporated into the copolymer; however, it was mainly composed of DMAEMA with a minor amount of MAA thus forming a polyampholyte with a gradient-like composition. The acid titration of a DM₅₇ macro-CTA showed that the copolymer had two pK_a values at 4.5 and 8.2 corresponding to the anionic and cationic units, respectively. The characterisation of the polyampholyte macro-CTAs by UV-vis spectrophotometry demonstrated that these copolymers displayed a phase separation upon heating in solution above pH 8.5, thus also proving the minor composition of MAA in the copolymer.

In order to assess the use of the DM_x macro-CTAs for nanogel formation, these were first chain extended with NIPAM without crosslinker to form amphiphilic copolymers in an acetate buffer solution at pH 5.2. NMR spectroscopy studies demonstrated the chain extension of the polyampholyte, which was stable under the polymerisation conditions since no hydrolysis products (i.e. DMEA) were observed. In the acetate buffer solution at pH 5.2, the P(DMAEMA-*co*-MAA)_x-*b*-NIPAM_y (DM_xN_y) copolymers exhibited a phase transition corresponding to the PNIPAM block at around 15-17 °C depending on the composition of the copolymer. The acetate anions had a salting-out effect, thus lowering the cloud points of the DM_xN_y solutions when compared to salt-free DM_xN_y solutions which displayed higher cloud points at pH 7. Additionally, self-assembly studies at 50 °C suggested that the DM_xN_y copolymers form aggregates with narrower size distributions in acetate buffer than in salt-free solutions. Since the use of an acetate buffer solution appeared to be beneficial for the self-assembly of DM_xN_y copolymers, the same synthetic conditions were used to produce nanogels *via* a dispersion process.

Similar to the work presented in previous chapters, the investigation of the effect of length of the shell-stabiliser block and the volume fraction of the PNIPAM core showed an effect on the size of the nanogels. Overall, nanogels had narrow size distributions and their size increased with increasing volume fractions of PNIPAM. TEM studies showed that the surface of the DM_xN_y nanogels looked patchy, thus suggesting nanoscale phase separations due to the gradient-like

composition of the DM₅₇ block. Nevertheless, the nanogels showed a dual response to temperature and pH despite the complex behaviour of charged polyelectrolytes on the shell block as judged by ζ -potential experiments. However, nanogels with smaller PNIPAM cores were less stable at neutral pH and a temperature above the VPTT of 32 °C, where flocculation was observed due to the temperature response of PDMAEMA. Lastly, the nanogels lost their colloidal stability in the presence of NaCl and CaCl₂ upon heating at neutral pH. However, these do not form macroscopic aggregates in the presence of salt at the concentrations tested. Although an only cationic nanogel was targeted, this work has demonstrated the ability of a self-assembly approach to form stimuli-responsive polyampholyte nanogels under aqueous conditions.

4.5. Experimental

4.5.1. Materials

4-((((2-carboxyethyl)thio)carbonothioyl)thio)-4-cyanopentanoic acid (CECPA, $\geq 95\%$) was purchased from Boron Molecular and used as received. 4,4'-azobis(4-cyanovaleric acid) (ACVA, 98%) was purchased from Sigma-Aldrich and used without further purification. 2-(dimethylamino)ethyl methacrylate (DMAEMA) (Sigma-Aldrich, 98%) was passed through a column of basic Al_2O_3 prior to use. *N*-isopropyl acrylamide (NIPAM) (Fluorochem) was recrystallised from *n*-hexane and dried before use. *N,N'*-methylene bisacrylamide (BIS) (Sigma-Aldrich) was recrystallised from hot methanol and dried before use. Glacial acetic acid (Fisher, 100%), sodium hydroxide pellets (Fisher), hydrochloric acid (VWR, 35%), sodium chloride (Sigma-Aldrich), calcium chloride dihydrate (VWR) were all used without further purification. SnakeSkin™ dialysis tubing (ThermoFisher scientific) of 3.5 kDa molecular weight cut-off (MWCO) was used to purify the nanogel dispersions. For nuclear magnetic resonance (NMR) experiments, samples were prepared in either D_2O or DMSO-D_6 (Sigma Aldrich).

4.5.2. Synthesis of PDMAEMA-based macro-CTA by aqueous RAFT solution polymerisation

Two macro-CTAs with different DPs were synthesised targeting different monomer to CTA molar ratios. The typical procedure used for the macro-CTA synthesis when targeting a DMAEMA to CECPA molar ratio of 62 to 1 was as follows: CECPA (0.32 g, 1.03 mmol), DMAEMA (10.01 g, 63.7 mmol), ACVA (0.03 g, 0.1 mmol) were mixed in an acetate buffer solution (10.18 g, 1 M, pH 5.2) to give a 25% w/w solids solution. The mixture was magnetically stirred and purged with nitrogen for 30 minutes. The flask was then placed onto a DrySyn® heating block preheated to 70 °C and left to react for 115 min. The reaction mixture was quenched by cooling the flask in an ice bath and opened it to air. The final DMAEMA conversion (50%) was determined by ^1H NMR spectroscopy by comparison of the oxymethylene protons area from the monomer and the polymer located at 4.26 and 4.18 ppm respectively. The product was recovered by precipitation from acetonitrile (400 mL) and collected by centrifugation. It was then redissolved in water and lyophilised to give a pale yellow solid. δH (400 MHz; D_2O , 25 °C) (ppm): 4.38 (2H, br. s, $\text{CH}_2\text{O-}$), 3.53 (2H, br. s, CH_2N), 2.95 (6H, br. s, $\text{N-(CH}_3)_2$), 2.61 (2H, s, $-\text{CH}_2-\text{COOH}$), 2.25-1.49 (2H, br. m, $-\text{CH}_2-$), 1.44-0.65 (3H, br. m, C-CH_3); δC (100 MHz; D_2O ,

25 °C): 221.3 (SC(S)S), 178.2 (C=O), 119.4 (SCCN), 52.7 (-CH₂-), 40.8 (-C-CH₂-), 31.5 (N-(CH₃)₂), 26.9 (O-CH₂-), 13.11 (-CH₂CH₂-N), 8.51 (SCCH₃); $\bar{\nu}_{\max}$ (ATR) cm⁻¹: 2997 (br. w, R-COOH), 2934 (br. w, -CH₂-) 1720 (vs, C=O), 1572 (vs, H N⁺(CH₃)₂), 1399 cm⁻¹ (vs, -R-C(O)O⁻), 1149 (w, C-O), 1043 (m, C-N). $\bar{M}_{n,\text{theo}}=8,013$ g mol⁻¹ $\bar{M}_{n,\text{GPC}}=14.2$ kDa, $\bar{M}_w/\bar{M}_n=1.27$. The final DP of the macro-CTAs was calculated by ¹H NMR spectroscopy by comparison of the two carboxymethylene protons peak area at 2.61 ppm from the CECPA RAFT CTA end groups to the total area of the methyl group attached to the ¹³C of the copolymer backbone located in the range of 1.44 to 0.65 ppm. The DP of the PDMAEMA was estimated by comparison of the oxymethylene protons total area at 4.38 ppm. The PMAA content corresponded to the difference between the DP of the macro-CTA and the DP of PDMAEMA.

4.5.3. Synthesis of P(DMAEMA-*co*-MAA)-*b*-PNIPAM copolymers

Using a targeted molar ratio of NIPAM to P(DMAEMA-*co*-PMAA)₅₇ of 191 to 1 as an example, a typical procedure for the chain extension of the macro-CTA by NIPAM *via* RAFT-mediated aqueous dispersion was as follows: P(DMAEMA-*co*-MAA)₅₄ (0.058 g, 0.007 mmol) and NIPAM (0.15 g, 1.32 mmol) were dissolved in acetate buffer solution (3.89 g, 1 M, pH 5.2) to give a 5% w/w solids solution. The mixture was then degassed under nitrogen for 30 min, followed by the addition of ACVA in acetate buffer solution (94 μL, 4.12 mg mL⁻¹). The solution was immersed into an oil bath preheated to 70 °C and left to react for 18 h. The final NIPAM conversion (>99 %) was determined by ¹H NMR spectroscopy. The crude product was dialysed against DI water and freeze-dried to give a pale yellow solid. $\bar{M}_{n,\text{theo}}=28,605$ g mol⁻¹; δH (400 MHz, D₂O, 25 °C): 7.9 (br. d, 1H, NH), 4.38 (br. s, 2H, O-CH₂-), 3.89 (br. s, 1H, -NHCH-), 3.52 (br. s, 2H, CH₂-CH₂-N), 2.95 (br.d, 6H, -N(CH₃)₂), 2.25-1.80(br. d, 1H,-CH-), 1.64 (br. t, 3H, C-CH₃), 1.14 (br. s, 6H, -CH(CH₃)₂); $\bar{\nu}_{\max}$ (ATR) cm⁻¹: 3281 (br. m, -CONH), 2972 (m, R-COOH), 2935 and 2878 (w, -CH₂-), 1726 (w, -COOH) 1626 and 1542 (s, -CON-R₂), 1459 (m, -CH₂-), 1387 and 1367 (m, -C(CH₃)₂), 1170 (w, C=S).

4.5.4. Synthesis of P(DMAEMA-*co*-MAA)-*b*-P(NIPAM-*st*-BIS) nanogels *via* RAFT aqueous dispersion polymerisation

A similar procedure for the synthesis of diblock copolymers was followed for the synthesis of nanogels. Using a targeted molar ratio of NIPAM to P(DMAEMA-*co*-MAA)₅₇ of 191 to 1 as an example, a typical procedure for the chain extension of the macro-CTA by NIPAM and BIS *via* RAFT-mediated aqueous dispersion was as follows: P(DMAEMA-*co*-MAA)₅₇ (0.039 g, 0.005 mmol), NIPAM (0.10 g, 0.884 mmol) and BIS (0.002 g, 0.013 mmol) were dissolved in acetate buffer solution (2.63 g, 1 M, pH 5.2) to give a 5% w/w solids solution. The mixture was thoroughly purged with nitrogen for 30 min, followed by the addition of ACVA in acetate buffer solution (67 μ L, 3.95 mg mL⁻¹). The mixture was then placed into an oil bath previously set at 70 °C and left to react for 18 h. The total monomer conversion (98 %) was estimated by moisture analysis. The nanogel dispersion was then purified by dialysis against DI water and freeze-dried to give a pale yellow solid. $\bar{\nu}_{\max}$ (ATR) cm⁻¹: 3278 (br. m, -CONH), 2973 (m, R-COOH), 2939 and 2878 (m, -CH₂), 1726 (w, -COOH), 1638 and 1536 (s, -CONR₂), 1455 cm⁻¹ (m, -CH₂), 1449 (m, -CH₂-), 1388 and 1361 (m, -C(CH₃)₂), 1170 (m, C=S).

4.6. Characterisation

4.6.1. NMR Spectroscopy

Nuclear Magnetic Resonance (NMR) experiments were performed at 25 °C on a 400 MHz Bruker Avance III HD spectrometer. Each collected spectrum was calibrated using the residual solvent peak as reference. ^1H NMR spectra were collected over 64 scans averaged per spectrum. NMR data was analysed using the MNova software from Mestrelab Research.

4.6.2. Aqueous gel permeation chromatography (GPC)

Molar masses and polydispersities of PDMAEMA-based macro-CTAs were measured using an Agilent 1260 Infinity series degasser and pump GPC/SEC system fitted with 2 \times PL aquagel-OH 30 8 μm (300 \times 7.5 mm) columns. An acidic aqueous buffer (pH 2) containing 0.5 M acetic acid, 0.3 M NaH_2PO_4 was used as eluent at a flow rate of 1 mL min^{-1} at 30 °C. The equipment was calibrated with near-monodisperse poly(ethylene oxide) (PEO) and poly(ethylene glycol) (PEG) standards (molar mass range between $4.12 \times 10^3 - 1.06 \times 10^5 \text{ g mol}^{-1}$). Analyte samples were prepared at a concentration of 2 mg mL^{-1} in the acidic aqueous buffer and filtered through a 0.45 μm polytetrafluoroethylene (PTFE) filter before injection (100 μL).

4.6.3. Fourier transform infrared spectroscopy (ATR-FTIR)

IR spectra were recorded on a PerkinElmer SpectrumTM 100 FT-IR spectrometer using a universal diamond ATR (UATR) accessory. Data was collected over 5 scans in the 450 to 4000 cm^{-1} region. The IR data was recorded on a Bruker software and further processed in Microsoft Excel.

4.6.4. Gravimetric analyses

The final monomers conversion for the nanogel preparation was estimated gravimetrically using a KERN DAB 100-3 electronic moisture analyser. Samples were weighed and heated up to 190 °C to determine their solids content.

4.6.5. Dynamic light scattering (DLS)

The hydrodynamic particle diameter of the purified nanogels (0.1% w/w) was obtained using a NanoBrook Omni particle analyser using a 35 mW diode laser with a nominal 640 nm wavelength. Data was obtained at a scattering angle of 173°. Each DLS measurement consisted on 4 or 5 runs of 3 minutes at count rates between 440-550 kcps. Temperature dependent DLS experiments were performed from low to high temperatures with increments of 2.5 °C with 8 minutes in-between intervals to allow thermal stabilisation. The pH of the dispersions was manually adjusted by addition of NaOH or HCl solutions using a Hach H160 ISFET probe. The method of the constrained regularization method for inverting data (CONTIN) was used to obtain the size distribution from the autocorrelation function.

4.6.6. Aqueous electrophoresis

ζ -potential measurements for the aqueous nanogel dispersions (0.1% w/w) containing KCl (1 mM) as background were determined on a Malvern Zetasizer Nano-ZS instrument at 25 °C. The smoluchowski relationship was used to determine the ζ -potential from the electrophoretic mobility. The pH of the solutions was manually adjusted by addition of NaOH or HCl solutions using a Hach H160 ISFET probe.

4.6.7. Transmission electron microscopy (TEM)

TEM images were collected using a Phillips CM100 microscope adapted with a Gatan CCD camera. Nanogel dispersions (0.1% w/w, 10 μ L) were placed onto freshly glow discharged carbon-coated grids for 1 min and then blotted with filter paper. Uranyl formate (0.75% w/w, 5 μ L) stain was then placed onto the sample and left for 20 s to finally blot it again with filter paper to remove the excess of stain. The grid was then dried with an adapted vacuum hose.

4.7. References

1. Emileh, A., Vasheghani-Farahani, E. & Imani, M. Swelling behavior, mechanical properties and network parameters of pH- and temperature-sensitive hydrogels of poly((2-dimethyl amino) ethyl methacrylate-co-butyl methacrylate). *Eur. Polym. J.* **43**, 1986–1995 (2007).
2. Molina, M., Giubudagian, M. & Calderón, M. Positively charged thermoresponsive nanogels for anticancer drug delivery. *Macromol. Chem. Phys.* **215**, 2414–2419 (2014).
3. Gao, D. *et al.* Preparation of thermo/redox/pH-stimulative poly(*N*-isopropylacrylamide-co-*N,N'*-dimethylaminoethyl methacrylate) nanogels and their DOX release behaviors. *J. Biomed. Mater. Res. Part A* **107**, 1195–1203 (2019).
4. Shakoori, Z. *et al.* Fluorescent multi-responsive cross-linked P(*N*-isopropylacrylamide)-based nanocomposites for cisplatin delivery. *Drug Dev. Ind. Pharm.* **43**, 1283–1291 (2017).
5. Moselhy, J., Vira, T., Liu, F.-F. & Wu, X. Y. Characterization of complexation of poly(*N*-isopropylacrylamide-co-2-(dimethylamino) ethyl methacrylate) thermoresponsive cationic nanogels with salmon sperm DNA. *Int. J. Nanomedicine* **4**, 153–64 (2009).
6. Shen, Z., Mellati, A., Bi, J., Zhang, H. & Dai, S. A thermally responsive cationic nanogel-based platform for three-dimensional cell culture and recovery. *RSC Adv.* **4**, 29146 (2014).
7. Rawlinson, L.-A. B. *et al.* Antibacterial effects of poly(2-(dimethylamino ethyl)methacrylate) against selected gram-positive and gram-negative bacteria. *Biomacromolecules* **11**, 443–453 (2010).
8. Layman, J. M., Ramirez, S. M., Green, M. D. & Long, T. E. Influence of polycation molecular weight on poly(2-dimethylaminoethyl methacrylate)-mediated DNA delivery in vitro. *Biomacromolecules* **10**, 1244–1252 (2009).
9. Qiao, Y. *et al.* The use of PEGylated poly[2-(*N,N*-dimethylamino) ethyl methacrylate] as a mucosal DNA delivery vector and the activation of innate immunity and improvement of HIV-1-specific immune responses. *Biomaterials* **31**, 115–123 (2010).
10. Zhu, C. *et al.* Cationic methacrylate copolymers containing primary and tertiary amino side groups: Controlled synthesis *via* RAFT polymerization, DNA condensation, and in vitro gene transfection. *J. Polym. Sci. Part A Polym. Chem.* **48**, 2869–2877 (2010).
11. Lee, S. B. *et al.* Permanent, nonleaching antibacterial surfaces. 1. Synthesis by Atom Transfer Radical Polymerization. *Biomacromolecules* **5**, 877–882 (2004).
12. Murata, H., Koepsel, R. R., Matyjaszewski, K. & Russell, A. J. Permanent, non-leaching antibacterial surfaces. 2: How high density cationic surfaces kill bacterial cells. *Biomaterials* **28**, 4870–4879 (2007).
13. Yancheva, E. *et al.* Polyelectrolyte complexes based on (quaternized) poly[(2-dimethylamino)ethyl methacrylate]: behavior in contact with blood. *Macromol. Biosci.* **7**, 940–954 (2007).
14. Yan, L. & Tao, W. One-step synthesis of pegylated cationic nanogels of poly(*N,N'*-dimethylaminoethyl methacrylate) in aqueous solution *via* self-stabilizing micelles using an amphiphilic macroRAFT agent. *Polymer (Guildf)*. **51**, 2161–2167 (2010).

15. Fournier, D., Hoogenboom, R., Thijs, H. M. L., Paulus, R. M. & Schubert, U. S. Tunable pH- and temperature-sensitive copolymer libraries by reversible addition–fragmentation chain transfer copolymerizations of methacrylates. *Macromolecules* **40**, 915–920 (2007).
16. Jana, S., Rannard, S. P. & Cooper, A. I. Structure–LCST relationships for end-functionalized water-soluble polymers: an “accelerated” approach to phase behaviour studies. *Chem. Commun.* 2962–2964 (2007).
17. An, X., Tang, Q., Zhu, W., Zhang, K. & Zhao, Y. Synthesis, thermal properties, and thermoresponsive behaviors of cyclic poly(2-(dimethylamino)ethyl methacrylate)s. *Macromol. Rapid Commun.* **37**, 980–986 (2016).
18. Jung, S.-H. & Lee, H.-I. Well-Defined Thermoresponsive copolymers with tunable LCST and UCST in Water. *Bull. Korean Chem. Soc.* **35**, 501–504 (2014).
19. Yañez-Macias, R. *et al.* Effect of the degree of quaternization and molar mass on the cloud point of poly[2-(dimethylamino)ethyl methacrylate] aqueous solutions: A systematic investigation. *Macromol. Chem. Phys.* **218**, 1700065 (2017).
20. Plamper, F. A. *et al.* Tuning the thermoresponsive properties of weak polyelectrolytes: aqueous solutions of star-shaped and linear Poly(*N,N*-dimethylaminoethyl methacrylate). *Macromolecules* **40**, 8361–8366 (2007).
21. Vamvakaki, M. *et al.* Effect of partial quaternization on the aqueous solution properties of tertiary amine-based polymeric surfactants: unexpected separation of surface activity and cloud point behavior. *Macromolecules* **34**, 6839–6841 (2001).
22. Wang, B. *et al.* Synthesis and properties of pH and temperature sensitive p(NIPAAm-co-DMAEMA) hydrogels. *Colloids Surfaces B Biointerfaces* **64**, 34–41 (2008).
23. Brassinne, J., Poggi, E., Fustin, C.-A. & Gohy, J.-F. Synthesis and self-assembly of terpyridine end-capped poly(*N*-Isopropylacrylamide)-block-poly(2-(dimethylamino)ethyl methacrylate) diblock copolymers. *Macromol. Rapid Commun.* **36**, 610–615 (2015).
24. Huang, Y. *et al.* Micellization and gelatinization in aqueous media of pH- and thermo-responsive amphiphilic ABC (PMMA₈₂-*b*-PDMAEMA₁₅₀-*b*-PNIPAM₆₅) triblock copolymer synthesized by consecutive RAFT polymerization. *RSC Adv.* **7**, 28711–28722 (2017).
25. Li, Q., Gao, C., Li, S., Huo, F. & Zhang, W. Doubly thermo-responsive ABC triblock copolymer nanoparticles prepared through dispersion RAFT polymerization. *Polym. Chem.* **5**, 2961–2972 (2014).
26. Van de Wetering, P. *et al.* A Mechanistic study of the hydrolytic stability of poly(2-(dimethylamino)ethyl methacrylate). *Macromolecules* **31**, 8063–8068 (1998).
27. Bevington, J. C., Eaves, D. E. & Vale, R. L. Tests on the hydrolysis of certain synthetic polymers. *J. Polym. Sci.* **32**, 317–322 (1958).
28. Zheng, P. *et al.* Deep insights into the hydrolysis of *N,N*-dialkylaminoethyl methacrylates in aqueous solution with ¹H NMR spectroscopy. *J. Polym. Sci. Part B Polym. Phys.* **56**, 914–923 (2018).
29. Carlsson, L. *et al.* Modification of cellulose model surfaces by cationic polymer latexes prepared by RAFT-mediated surfactant-free emulsion polymerization. *Polym. Chem.* **5**, 6076–6086 (2014).

-
30. Samsonova, O., Pfeiffer, C., Hellmund, M., Merkel, O. M. & Kissel, T. Low molecular weight pdmaema-block-phema block-copolymers synthesized *via* raft-polymerization: potential non-viral gene delivery agents? *Polymers (Basel)*. **3**, 693–718 (2011).
 31. Penfold, N. J. W., Ning, Y., Verstraete, P., Smets, J. & Armes, S. P. Cross-linked cationic diblock copolymer worms are superflocculants for micrometer-sized silica particles. *Chem. Sci.* **7**, 6894–6904 (2016).
 32. Rojas-Hernández, A., Ibarra-Montaña, E. L., Rodríguez-Laguna, N. & Aníbal Sánchez-Hernández, A. Determination of pK_a values for acrylic, methacrylic and itaconic acids by ^1H and ^{13}C NMR in deuterated water. *J. Appl. Solut. Chem. Model.* **4**, 7–18 (2015).
 33. Manouras, T., Koufakis, E., Anastasiadis, S. H. & Vamvakaki, M. A facile route towards PDMAEMA homopolymer amphiphiles. *Soft Matter* **13**, 3777–3782 (2017).
 34. Gibson, M. I. & O'Reilly, R. K. To aggregate, or not to aggregate? Considerations in the design and application of polymeric thermally-responsive nanoparticles. *Chem. Soc. Rev.* **42**, 7204–7213 (2013).
 35. Gibb, B. C. Supramolecular assembly and binding in aqueous solution: useful tips regarding the hofmeister and hydrophobic effects. *Isr. J. Chem.* **51**, 798–806 (2011).
 36. Liu, L. *et al.* Insight into the amplification by methylated urea of the anion specificity of macromolecules. *Soft Matter* **10**, 2856 (2014).
 37. Zhang, Y., Furyk, S., Bergbreiter, D. E. & Cremer, P. S. Specific ion effects on the water solubility of macromolecules: PNIPAM and the Hofmeister series. *J. Am. Chem. Soc.* **127**, 14505–14510 (2005).
 38. Humphreys, B. A., Willott, J. D., Murdoch, T. J., Webber, G. B. & Wanless, E. J. Specific ion modulated thermoresponse of poly(*N*-isopropylacrylamide) brushes. *Phys. Chem. Chem. Phys.* **18**, 6037–6046 (2016).
 39. Borisov, O. V. & Zhulina, E. B. Effect of salt on self-assembly in charged block copolymer micelles. *Macromolecules* **35**, 4472–4480 (2002).
 40. Lee, A. S. *et al.* Structure of pH-dependent block copolymer micelles: charge and ionic strength dependence. *Macromolecules* **35**, 8540–8551 (2002).
 41. Lovett, J. R., Warren, N. J., Ratcliffe, L. P. D., Kocik, M. K. & Armes, S. P. pH-Responsive non-ionic diblock copolymers: ionization of carboxylic acid end-groups induces an order-order morphological transition. *Angew. Chemie Int. Ed.* **54**, 1279–1283 (2015).
 42. Jones, E. R., Semsarilar, M., Wyman, P., Boerakker, M. & Armes, S. P. Addition of water to an alcoholic RAFT PISA formulation leads to faster kinetics but limits the evolution of copolymer morphology. *Polym. Chem.* **7**, 851–859 (2016).
 43. Betthausen, E., Drechsler, M., Förtsch, M., Schacher, F. H. & Müller, A. H. E. Dual stimuli-responsive multicompartiment micelles from triblock terpolymers with tunable hydrophilicity. *Soft Matter* **7**, 8880–8891 (2011).
 44. Alam, M. M., Jack, K. S., Hill, D. J. T., Whittaker, A. K. & Peng, H. Gradient copolymers – Preparation, properties and practice. *Eur. Polym. J.* **116**, 394–414 (2019).
 45. Rieger, J. Guidelines for the synthesis of block copolymer particles of various morphologies by RAFT dispersion polymerization. *Macromol. Rapid Commun.* **36**, 1458–1471 (2015).
-

-
46. Halperin, A., Kröger, M. & Winnik, F. M. Poly(*N*-isopropylacrylamide) Phase diagrams: fifty years of research. *Angew. Chemie Int. Ed.* **54**, 15342–15367 (2015).
 47. Mohammadi, M., Salami-Kalajahi, M., Roghani-Mamaqani, H. & Golshan, M. Effect of molecular weight and polymer concentration on the triple temperature/pH/ionic strength-sensitive behavior of poly(2-(dimethylamino)ethyl methacrylate). *Int. J. Polym. Mater. Polym. Biomater.* **66**, 455-461 (2017).
 48. Xu, Y. *et al.* pH and salt responsive poly(*N,N*-dimethylaminoethyl methacrylate) cylindrical brushes and their quaternized derivatives. *Polymer (Guildf)*. **49**, 3957–3964 (2008).
 49. Lee, H., Son, S. H., Sharma, R. & Won, Y.-Y. A Discussion of the pH-dependent protonation behaviors of poly(2-(dimethylamino)ethyl methacrylate) (PDMAEMA) and poly(ethylenimine-*ran*-2-ethyl-2-oxazoline) (P(EI-*r*-EOz)). *J. Phys. Chem. B* **115**, 844–860 (2011).
 50. Orakdogan, N. & Celik, T. Ion-stimuli responsive dimethylaminoethyl methacrylate/hydroxyethyl methacrylate copolymeric hydrogels: mutual influence of reaction parameters on the swelling and mechanical strength. *J. Polym. Res.* **23**, 57 (2016).
 51. Zhang, H. & Rühle, J. Swelling of Poly(methacrylic acid) Brushes: Influence of Monovalent Salts in the Environment. *Macromolecules* **38**, 4855–4860 (2005).

Appendix C

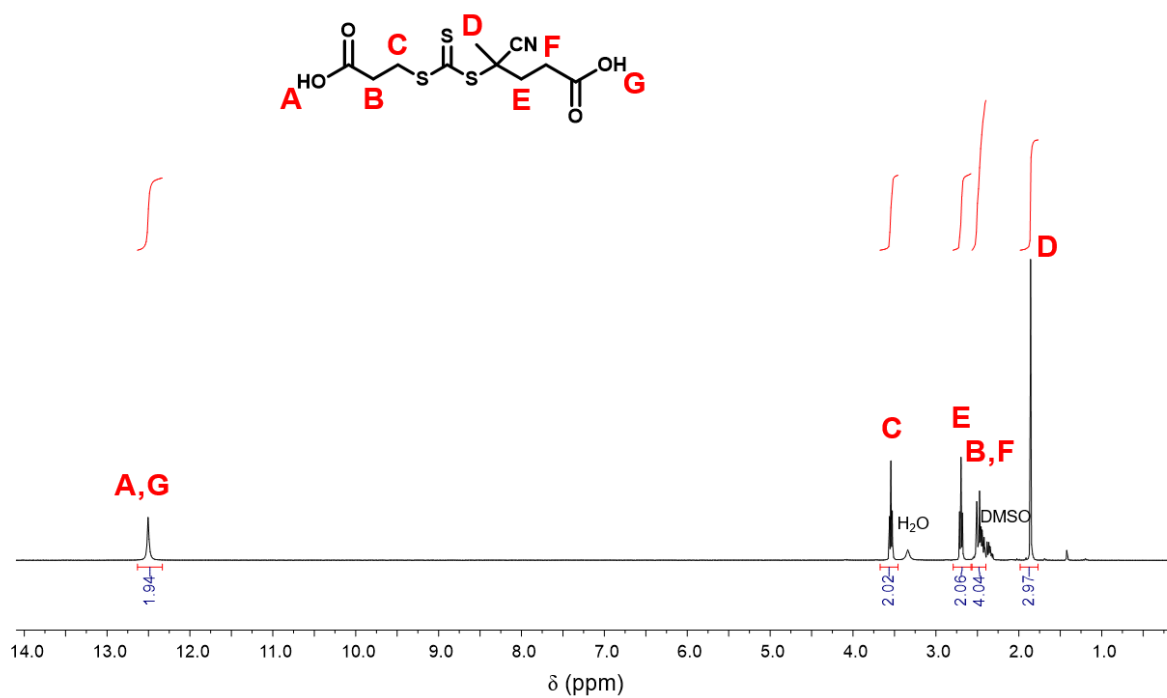


Figure 4C.1: ¹H NMR spectrum of commercially available CECPA CTA.

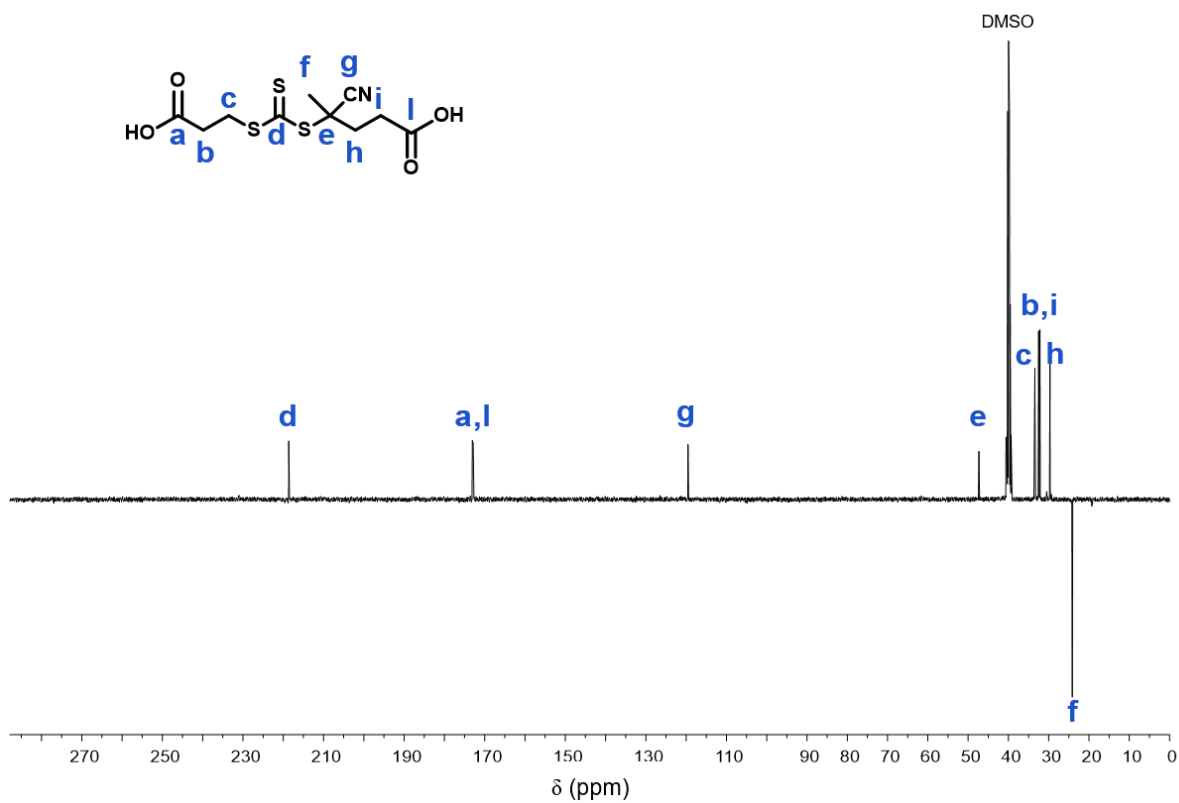


Figure 4C.2: ¹³C NMR spectrum of commercially available CECPA CTA.

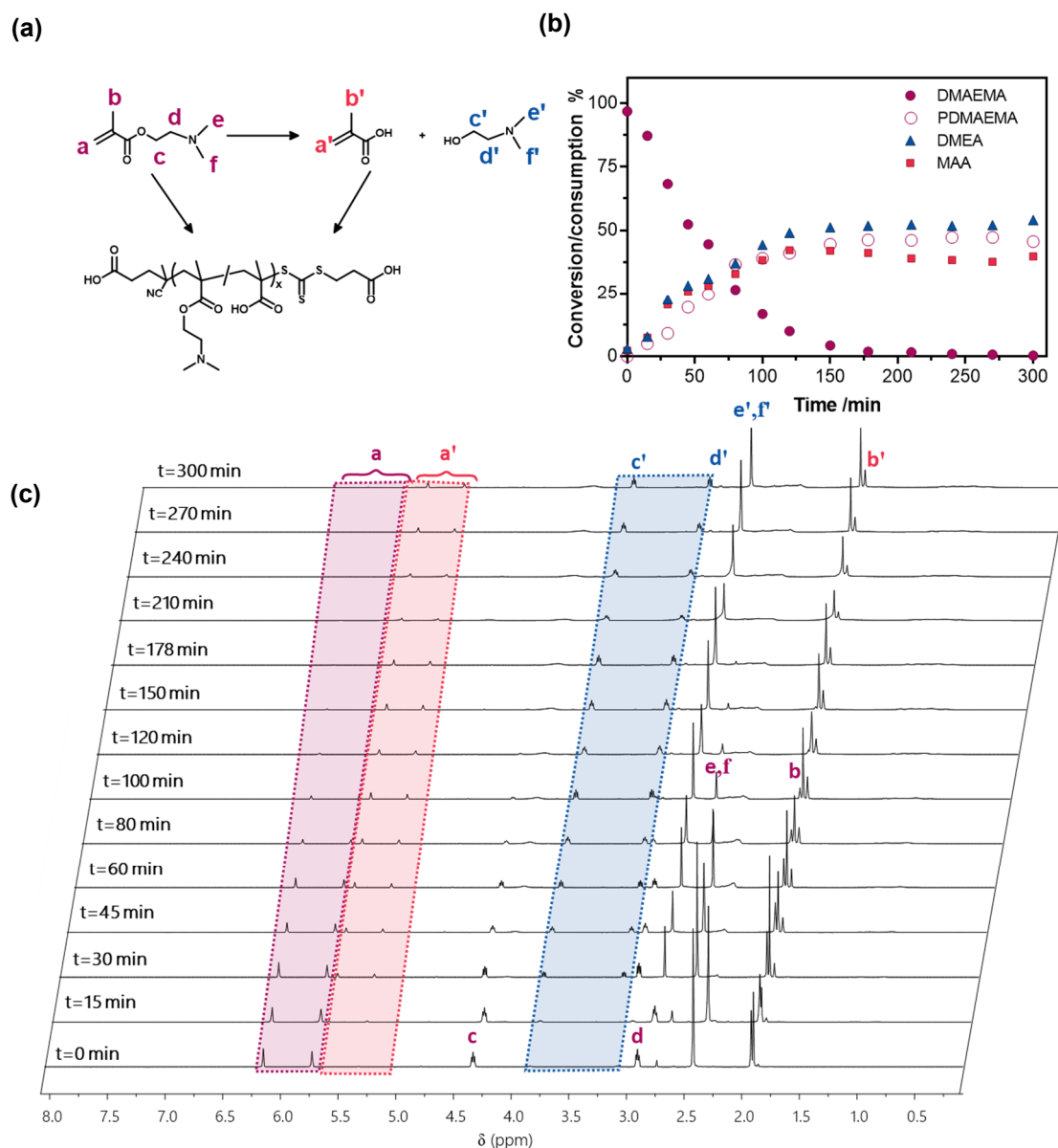


Figure 4C.3: The conversion of DMAEMA with time for target DP of 126. (a) Reaction scheme of the polymerisation and hydrolysis of DMAEMA, (b) Conversion of (●) DMAEMA into (○) PDMAEMA (▲) DMEA and (■) MAA vs time curves and (c) stacked ^1H NMR spectra recorded in D_2O of the reactions of DMAEMA. Target composition of $[\text{DMAEMA}]:[\text{CECPA}]:[\text{ACVA}]$ of 126:1:0.1 at 25% w/w and 70°C in an acetate buffer solution (1 M, pH 5.2). The H_2O residual solvent signal was suppressed to improve the resolution of the spectra.

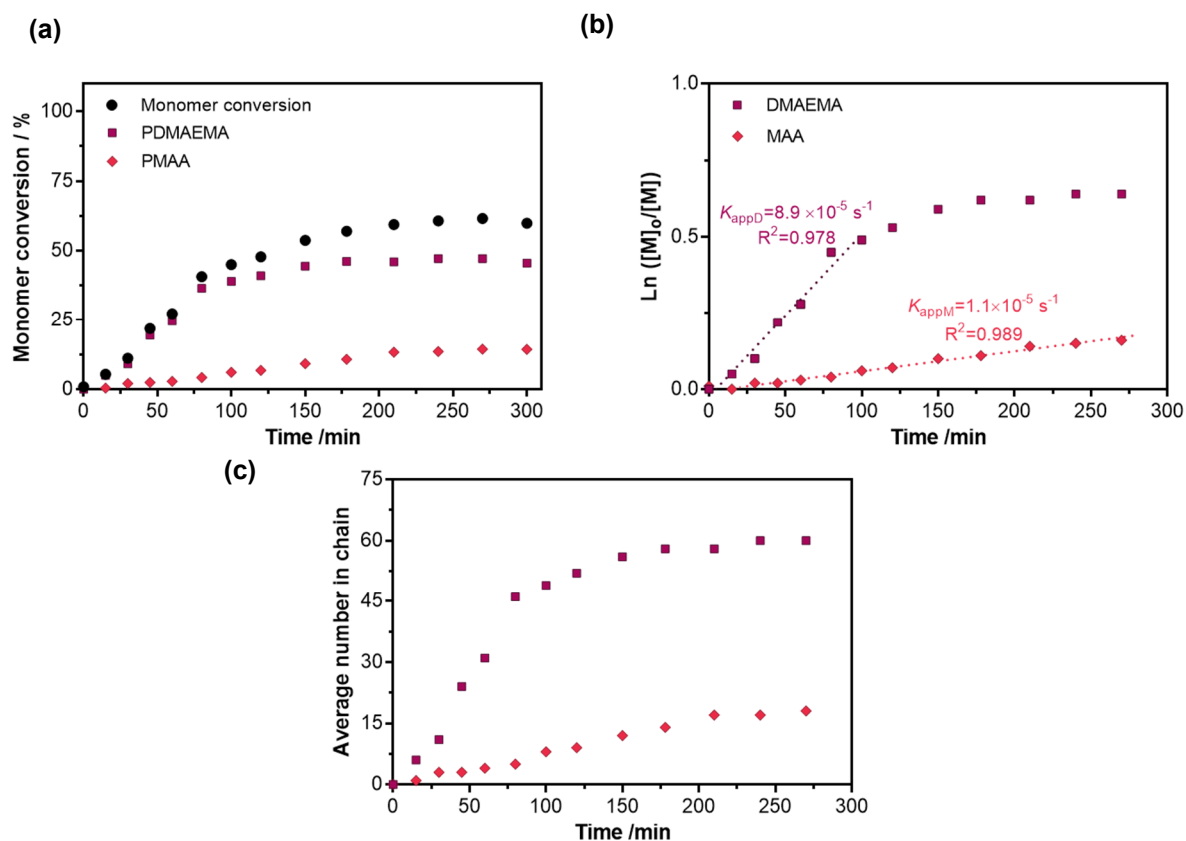
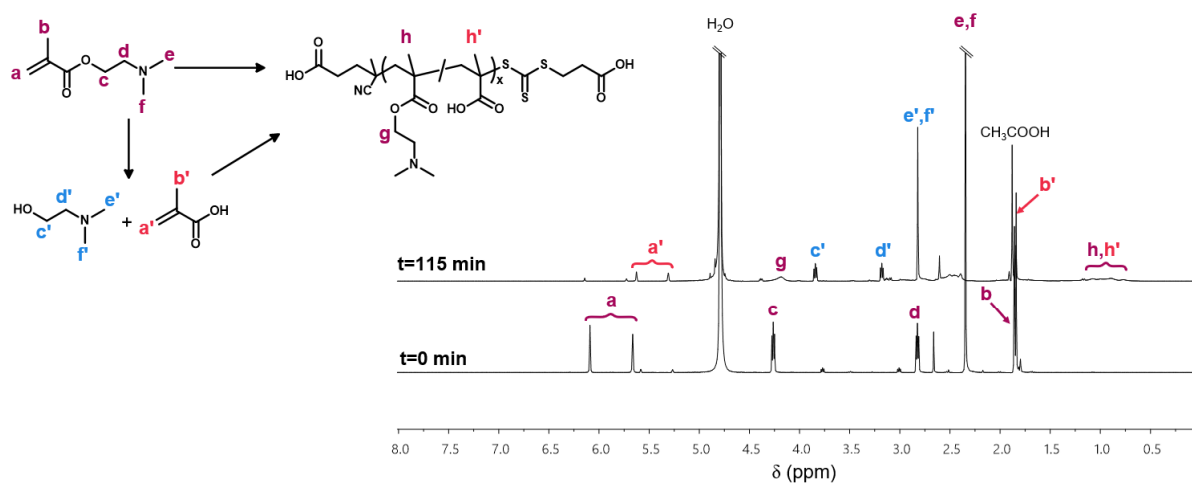
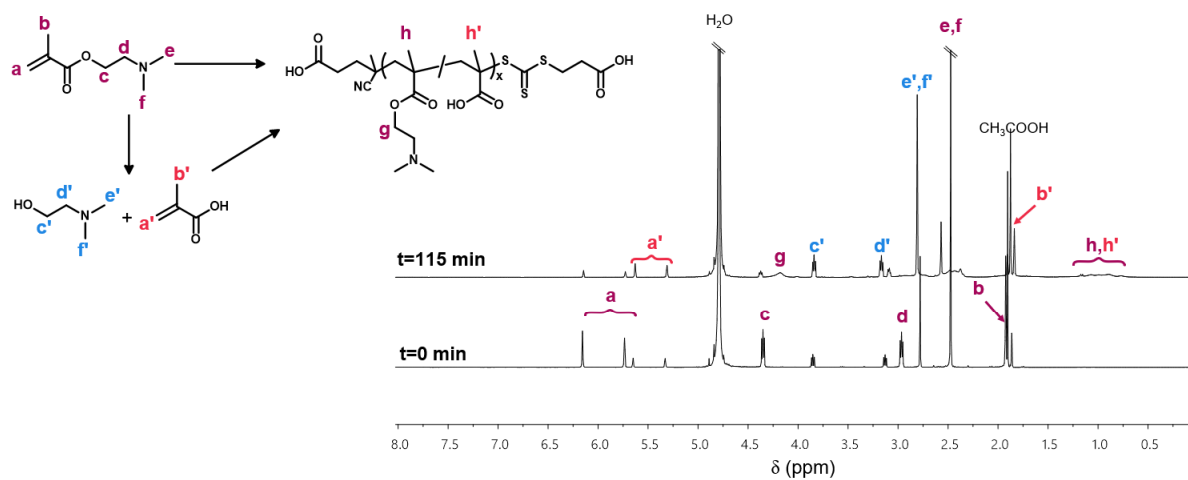


Figure 4C.4: Kinetic studies of the RAFT polymerisation of DMAEMA and MAA as determined by ^1H NMR spectroscopy. (a) DMAEMA (■), MAA (◆) and the total monomer (●) conversion vs time curves. (b) the semi-logarithmic plot of each monomer conversion over time curves, and (c) the average number of each monomer in the polymer with time. Target composition of [DMAEMA]:[CECPA]:[ACVA] of 126:1:0.1.



Time min	Area			Conversion %			
	C 4.26 ppm	C' 3.76 ppm	g 4.18 ppm	DMEA	DMAEMA	MAA	Total
0	90.21	6.07	0	6	0	0	0
115	6.83	35.77	43.41	42	50	6	56

Figure 4C.5: ^1H NMR study for the determination of the DMAEMA conversion and its degradation into dimethylethanolamine for the target composition of [DMAEMA]:[CECPA]:[ACVA] of 60:1:0.1 at 25% w/w.



Time min	Area			Conversion %			
	C 4.26 ppm	C' 3.76 ppm	g 4.18 ppm	DMEA	DMAEMA	MAA	Total
0	95.80	3.09	0	4	0	0	0
120	12.38	38.63	35.59	45	41	9	50

Figure 4C.6: ^1H NMR study for the determination of the DMAEMA conversion and its degradation into dimethylethanamine for the target composition of [DMAEMA]:[CECPA]:[ACVA] of 124:1:0.1 at 25% w/w.

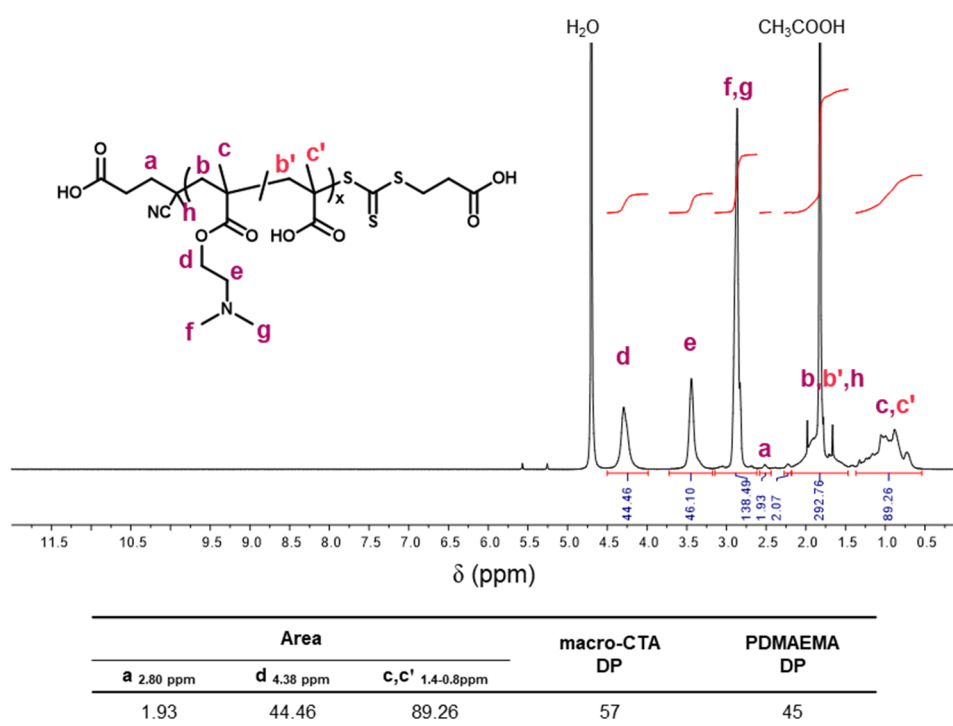


Figure 4C.7: ^1H NMR spectrum of purified DM_{57} for the determination of the macro-CTA DP.

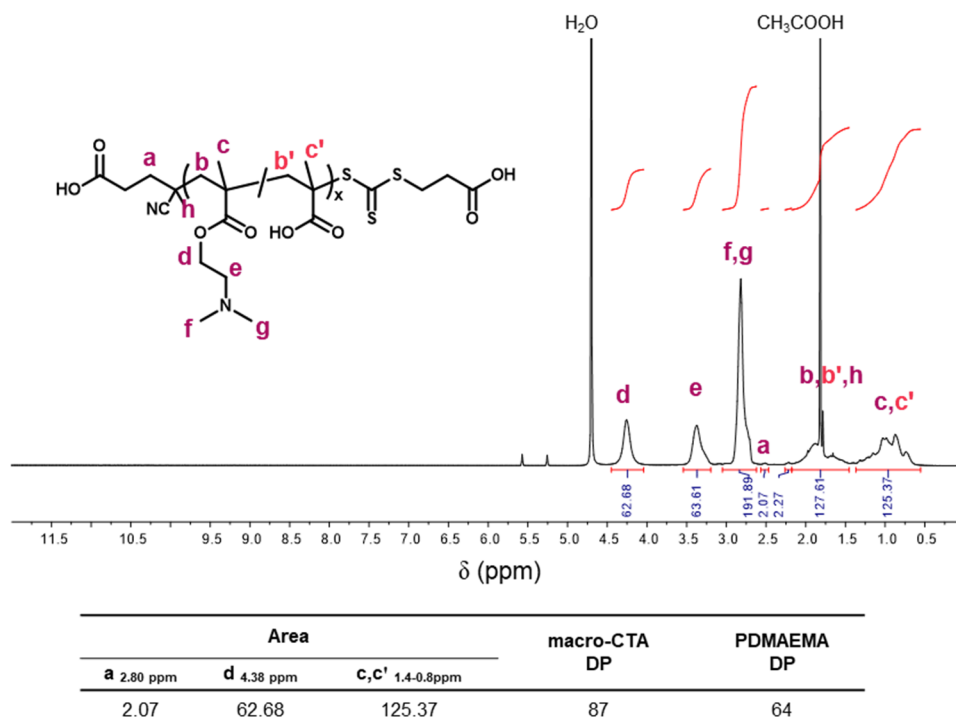


Figure 4C.8: ^1H NMR spectrum of purified DM_{87} for the determination of the macro-CTA DP.

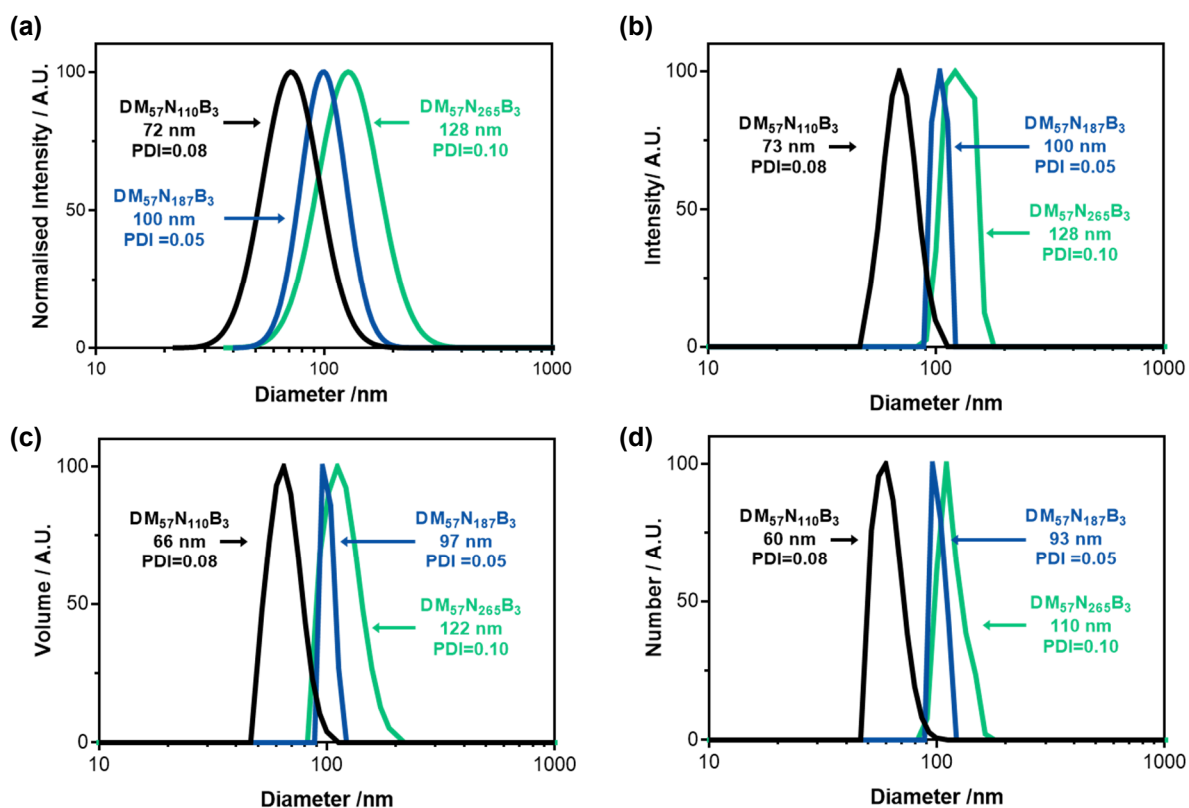


Figure 4C.9: Size distributions obtained from DLS of the $\text{DM}_{57}\text{N}_y\text{B}_3$ nanogels. (a) Intensity average log-normal size distribution, (b) intensity size distribution curves, (c) volume size distribution, and (d) number size distribution. Data obtained from 0.1% w/w nanogels dispersions in DI water at neutral pH at 25 °C.

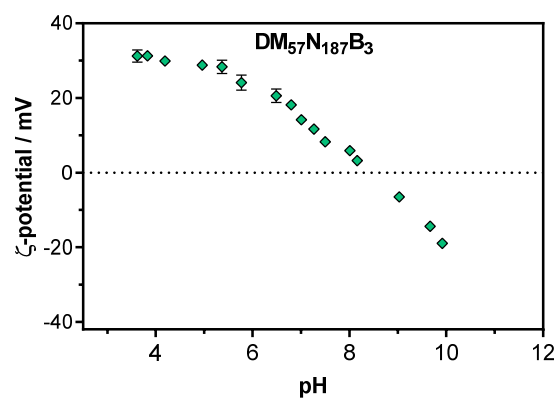


Figure 4C.10: Effect of the pH on the ζ -potential of the DM₅₇N₁₈₇B₃ nanogel. Data obtained from 0.1% w/w nanogels dispersions in DI water at 1 mM KCl electrolyte background at 25 °C.

CHAPTER 5

Concluding remarks and
future work

5.1. Concluding remarks

This thesis aimed to study the synthesis and the properties of stimuli-responsive ionic nanogels prepared from weak polyelectrolytes using a RAFT dispersion polymerisation approach. Initially, it was of particular interest to prepare two classes of ionic nanogels, which were to be synthesised from the chain extension of PAA or PDMAEMA macro-CTAs with NIPAM and BIS to form pH and thermo-responsive nanogels. Throughout this thesis, it has been demonstrated the feasibility to form ionic nanogels through the RAFT dispersion of NIPAM/BIS in a one-pot synthesis under specific conditions. Both sets of synthesised nanogels exhibited changes in their properties as a response to variations in temperature, pH, and ionic strength irrespective of their monomer composition but to different extents. Results showed that the variation of the DP of the core-forming PNIPAM/BIS block and the DP of the shell-stabiliser polyelectrolyte block not only influences the extent of the stimuli-response but also the size and the morphology of the nanogels.

Additionally, this work aimed to evaluate the effects of synthesis cononsolvent composition on the properties of the anionic nanogels to better understand the addition of ethanol as minor cononsolvent with water during the RAFT-mediated PISA of NIPAM. This thorough investigation was presented in Chapter 2 and 3, and results suggest that the addition of small quantities of ethanol to water as cononsolvent pair for the polymerisation of NIPAM, not only affects the nanogel particle formation but also their size, tacticity and the VPTT of nanogels with similar composition. Results showed in Chapter 2 revealed a gradual decrease in nanogel size with increasing ethanol content used in the synthesis of nanogels with the same target monomer composition as evaluated by DLS and TEM measurements. Moreover, the addition of ethanol as cononsolvent pair with water was found to allow the synthesis of nanogel particles with more uniform sphericity at higher volume fractions of PNIPAM and larger crosslinking densities depending on the DP of the PAA block. Characterisation studies of a series of PAA-*b*-PNIPAM diblock copolymers suggested changes in the stereochemistry of the copolymers synthesised in different cononsolvents compositions, where the copolymers synthesised only in water resulted meso-richer than the ones synthesised in a relatively higher ethanol composition. Hence, it is proposed that the synthesis cononsolvent composition for the *in situ* formation of PNIPAM nanogels greatly affects the nucleation of particles and thus the constrained chain growth influences the monomer insertion resulting in different chain packing. The effects of the stereosequence of NIPAM-nanogels on the temperature response (i.e. VPTT) was showed in Chapter 3. Overall, nanogels with similar composition but synthesised in cononsolvents displayed

a higher VPTT than the nanogels synthesised in only water, which suggested that these were relatively more hydrophilic. The shift in the VPTT is suggested to be related to the decrease in the meso diads content derived from the synthesis in higher X_e compositions, which could influence the local hydrogen bonding between the amide groups from PNIPAM and the water molecules. An increase in racemic diads generates an alternating chirality where geometric constraints make the formation of local hydrogen bonding difficult between amide groups from PNIPAM and hence water molecules interact stronger, thus more energy is needed to release these upon heating (i.e. greater VPTT).

The work presented in Chapter 4 aimed to expand upon the understanding of nanogel formation from weak polyelectrolytes under a RAFT dispersion process, specifically from a cationic polyelectrolyte such as PDMAEMA. However, the use of acetate buffer for the synthesis of a PDMAEMA macro-CTA caused the simultaneous polymerisation and hydrolysis of the monomer, thus forming a polyampholyte comprising mainly of DMAEMA and minorly MAA (DM_x) with a gradient-like composition. Regardless of the polyampholyte nature of the macro-CTAs, these were evaluated for the RAFT dispersion polymerisation of block copolymers and nanogels since the DM_x copolymers were mainly composed of PDMAEMA. Results suggested that DM_x macro-CTAs were hydrolytically stable during their chain extension with NIPAM in an acetate buffer at pH 5.2 (1 M) and allowed the synthesis of defined copolymers and nanogels due to a salting-out effect of PNIPAM during synthesis. DLS and TEM studies suggested the formation of nanogels with controlled size. However, the nanogels look patchy suggesting nanoscale phase separations due to the gradient-like composition of the DM_x block. As judged by ζ -potential measurements, the nanogels were cationic in an acidic and neutral pH. Nonetheless, at a neutral pH nanogels with small PNIPAM volume fraction lost their colloidal stability above the VPTT and flocculated due to the predominant temperature-responsive behaviour of PDMAEMA.

5.2. Future work

The work presented in this thesis has potentially provided insights into the synthesis and properties of pH- and temperature-responsive ionic nanogels prepared by RAFT-dispersion polymerisation under mild conditions. However, the following further studies are proposed to increase the understanding and applicability of these materials.

If these materials were to be used for intended biomedical applications, the cytotoxicity of both classes of nanogels should be determined as a priority since this will show how safe these nanomaterials are. Initially, it is proposed that due to the antimicrobial properties of PDMAEMA,¹⁻³ the small size and the stimuli-responsive nature of these nanogels, these could potentially penetrate biofilms. Previous work by Rotello and co-workers⁴⁻⁸ have demonstrated the use of nanoparticles bearing cationic moieties as antimicrobial agents and as drug delivery vehicles to combat drug-resistant bacteria and biofilms. Cationic PDMAEMA-based nanoparticles can disrupt the bacterial cell membrane integrity by binding with the charged membrane of the bacteria, and thus aid in the minimisation or eradication of biofilms and their related infections.^{9,10} Preliminary studies on the cytotoxicity of the DM₅₇N₁₈₇B₃ polyampholyte nanogel were carried out but due to time constraints were not finished. An experiment was designed to estimate the membrane cell disruption of Gram-positive *S.aureus* and Gram-negative *P.aeruginosa* bacteria caused by the nanogels by using the metabolic assay PrestoBlue[®] (Figure 5.1). The experiment consisted of the co-incubation of the two types of bacteria with DM₅₇N₁₈₇B₃ nanogel at different concentrations for 24 h at 37 °C. The preliminary data suggested that the bacterial membrane integrity of the *S.aureus* strand was disrupted accordingly to the DM₅₇N₁₈₇B₃ nanogel concentration (1.25 to 10 mg mL⁻¹) (Figure 5.1b). In contrast, the bacterial membrane integrity of *P.aeruginosa* was only disrupted in the highest nanogel concentration (10 mg mL⁻¹) (Figure 5.1a). After establishing the dependence of the cell membrane disruption with the nanogel particle concentration, further studies on the nanogel particles biofilm penetration were planned by the treatment of biofilms with DM₅₇N₁₈₇B₃ nanogel functionalised with either fluorescein-5-Maleimide or Texas Red fluorescent dyes. However, these were not performed. These experiments could have elucidated if the DM₅₇N₁₈₇B₃ nanogel have potential use as platform for biofilm eradication. Moreover, it would have been interesting to evaluate the effects of the anionic nanogels on these bacteria, and finally test if both of these nanogels could penetrate into biofilms and serve as antimicrobials and/or as drug delivery vehicles to treat biofilm-related infections.

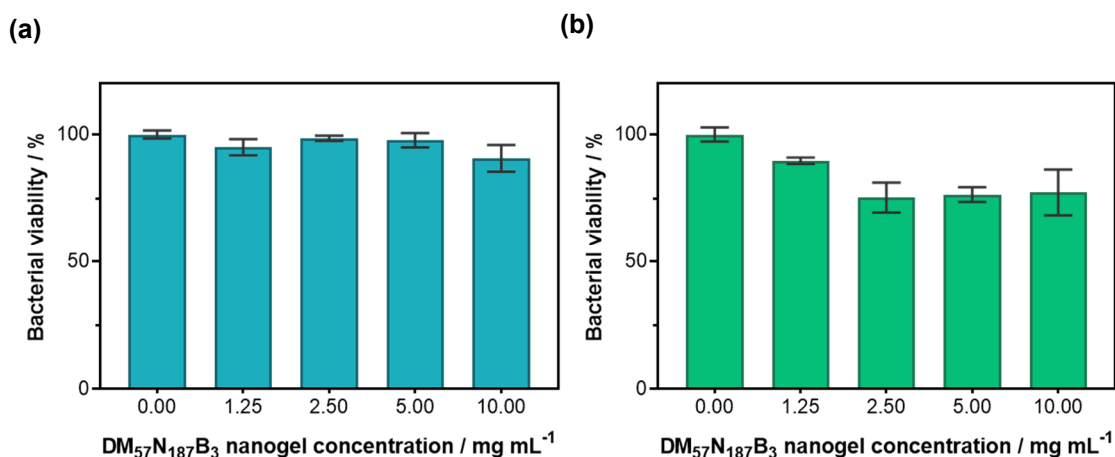


Figure 5.1: Cytotoxicity of DM₅₇N₁₈₇B₃ nanogel tested against (a) *P. aeruginosa* and (b) *S. Aureus* bacteria. Quantification of bacterial viability after 24 hours at 37 °C of co-incubation of bacteria with DM₅₇N₁₈₇B₃ nanogel at various nanogel concentrations. The percentage of bacterial viability was measured by a PrestoBlue® assay. The fluorescence was read after the bacteria were incubated for 2 hours with PrestoBlue® reagent at excitation/emission wavelengths of 560 nm/590 nm.

In the case of the anionic nanogels, the *in situ* formation of Ca²⁺-nanogel aggregates at pH 7 above the VPTT can be exploited for the formation of macroscopic hydrogel scaffolds or composite aggregates if mixed with inorganic compounds. For instance, the mixing of the PAA-*b*-P(NIPAM-*st*-BIS) with silicate glass powders (cements), which can provide the Ca²⁺ source,¹¹ could potentially serve as a new platform to form glass ionomer cements (GICs) for possibly use as dental restorative materials. If the PAA-*b*-P(NIPAM-*st*-BIS) nanogels are to be evaluated as composites materials to form GICs, the mechanical properties of these materials are to be determined such as the bond and compressive strengths. Alongside, the already commercially used PAA, and copolymers of PAA/ PNIPAM would need to be tested too as way to compare the effects of using thermo-responsive polymers and crosslinked materials for GICs.

To better understand the effects of the ethanol addition as cosolvent pair of water for the polymerisation of NIPAM on the structural changes of the anionic diblock copolymers, the characterisation of these materials by small-angle X-ray scattering (SAXS) would be needed at different temperatures. This would provide insights into the actual copolymer chains packing upon self-assembly of these copolymers.

Finally, other techniques such as microcalorimetry and temperature-dependent ¹H NMR spectroscopy are proposed to be used for the more accurate determination of the cloud point temperature of copolymers with a highly hydrophilic block and a PNIPAM block.

5.3. References

1. Rawlinson, L.A. B. *et al.* Antibacterial effects of poly(2-(dimethylamino ethyl)methacrylate) against selected gram-positive and gram-negative bacteria. *Biomacromolecules* **11**, 443–453 (2010).
2. Lee, S. B. *et al.* Permanent, nonleaching antibacterial surfaces. 1. synthesis by atom transfer radical polymerization. *Biomacromolecules* **5**, 877–882 (2004).
3. Murata, H., Koepsel, R. R., Matyjaszewski, K. & Russell, A. J. Permanent, non-leaching antibacterial surfaces. 2: How high density cationic surfaces kill bacterial cells. *Biomaterials* **28**, 4870–4879 (2007).
4. Wang, L.S., Gupta, A. & Rotello, V. M. Nanomaterials for the treatment of bacterial biofilms. *ACS Infect. Dis.* **2**, 3–4 (2016).
5. Gupta, A., Landis, R. F. & Rotello, V. M. Nanoparticle-based antimicrobials: surface functionality is critical. *F1000Research* **5**, 364 (2016).
6. Landis, R. F. *et al.* Biodegradable nanocomposite antimicrobials for the eradication of multidrug-resistant bacterial biofilms without accumulated resistance. *J. Am. Chem. Soc.* **140**, 6176–6182 (2018).
7. Gupta, A., Mumtaz, S., Li, C.H., Hussain, I. & Rotello, V. M. Combatting antibiotic-resistant bacteria using nanomaterials. *Chem. Soc. Rev.* **48**, 415–427 (2019).
8. Gupta, A. *et al.* Engineered polymer nanoparticles with unprecedented antimicrobial efficacy and therapeutic indices against multidrug-resistant bacteria and biofilms. *J. Am. Chem. Soc.* **140**, 12137–12143 (2018).
9. Rawlinson, L.A. B., O’Gara, J. P., Jones, D. S. & Brayden, D. J. Resistance of *Staphylococcus aureus* to the cationic antimicrobial agent poly(2-(dimethylamino ethyl)methacrylate) (pDMAEMA) is influenced by cell-surface charge and hydrophobicity. *J. Med. Microbiol.* **60**, 968–976 (2011).
10. Koufakis, E., Manouras, T., Anastasiadis, S. H. & Vamvakaki, M. Film properties and antimicrobial efficacy of quaternized PDMAEMA brushes: short vs long alkyl chain length. *Langmuir* **36**, 3482–3493 (2020).
11. Lohbauer, U. Dental glass ionomer cements as permanent filling materials? – Properties, limitations and future trends. *Materials (Basel)*. **3**, 76–96 (2009).